

**Atomization of dilute oil-in-water emulsions during
application of crop protection products**

Emilia Hilz

Thesis committee

Promotors

Prof. dr. M.A. Cohen Stuart
Professor of Physical Chemistry and Colloid Science
Wageningen University

Prof. dr. ir. F.A.M. Leermakers
Personal chair at the Laboratory of Physical Chemistry and Colloid Science
Wageningen University

Co-promotor

Dr. A.W.P. Vermeer
Product Development Manager
Formulation Technology
Bayer CropScience AG, Monheim, Germany

Other members

Prof. dr. D. Bonn, University of Amsterdam, The Netherlands
Dr. C. Butler Ellis, Silsoe Spray Applications Unit at NIAB, Bedford, United Kingdom
Prof. dr. ir. E.J. van Henten, Wageningen University
Prof. dr. S. Stoyanov, Unilever Food & Health Research Inst., Vlaardingen, The Netherlands

This research was conducted under the auspices of the Graduate School VLAG
(Advanced studies in Food Technology, Agrobiotechnology, Nutrition and Health)

Atomization of dilute oil-in-water emulsions during application of crop protection products

Emilia Hilz

Thesis

submitted in fulfilment of the requirements for the degree of doctor
at Wageningen University

by the authority of the Rector Magnificus

Prof. dr. M.J. Kropff,

in the presence of the

Thesis Committee appointed by the Academic Board

to be defended in public

on Monday 3 Juni 2013

at 1:30 p.m. in the Aula

Emilia Hilz

Atomization of dilute oil-in-water emulsions during application of crop protection products

PhD Thesis, Wageningen University, Wageningen, The Netherlands (2013)

With references, with summaries in English and Dutch

ISBN: 978-94-6173-541-6

Contents

1	Introduction	1
2	Spray drift review	11
3	The breakup of a liquid sheet during spray atomization	35
4	A SCF study of a hydrocarbon droplet	49
5	A SCF study to underpin trends for spray atomisation	75
6	Mechanism of perforation	99
7	Effect of hydrophobic silica added to oil	123
8	Mixtures of a polymer solution with a dilute emulsion	137
9	Formulation types with spray drift reduction potential	151
	Summary and General Discussion	177
	Samenvatting	187
	Acknowledgements	191
	List of publications	193
	Overview of completed training activities	195
	Curriculum Vitae	197

Chapter 1

General Introduction

In this Chapter, a general introduction will be given on the structure of this thesis, titled "Atomization of dilute oil-in-water emulsions during application of crop protection products". Spray atomization of dilute emulsions is central to this work. At the same time, the dissertation strongly focuses on spray drift phenomena, its origin, its definition, and ways to minimize it. The project was launched by Bayer CropScience AG, Germany, with the aim to understand the action of atomization and to develop innovative crop protection products that can contribute to spray drift reduction. The company provided facilities, chemicals and knowledge on the applied side of the project. Scientific support and guidance for this project were provided by the Laboratory for Physical Chemistry and Colloid Science at Wageningen University, the Netherlands. This collaboration merged into a more application focused project that approaches some fundamental questions of multi-phase systems.

Scope

Agrochemicals are commonly applied as water-based sprays produced by a hydraulic nozzle. During the application process, the fine spray fraction can be carried away from the application site by crosswinds. This ‘downwind movement of airborne spray droplets beyond the intended area of application originating from aerial or ground-based spraying operations’ is defined as spray drift.¹ Dislocation of agrochemicals *via* spray drift raises concern of contamination of surface water and the environment in general,^{2–4} exposure of workers, bystanders, and residents.⁵

The tendency of a spray droplet to drift off is linked to its mass and size. Very large spray drops have a sedimentation velocity that is higher than wind speeds typical of agrochemical application conditions⁶ while fine droplets adopt the velocity of the ambient air movements and can travel from the application point to distances up to several kilometres away.⁷ Based on theoretical studies and computer simulations, spray droplets with diameter $< 100 \mu\text{m}$ have been identified as the most drift-prone.^{6,8,9} Climatic conditions during the application process including air temperature, relative humidity, wind speed and direction at crop height, all influence in one or another way the spray droplet size, its velocity and trajectory, and can reinforce spray drift. Recommendations for safe and precise application of agrochemicals with regard to weather conditions are summarized in country-specific guidelines for good practice in crop protection.^{10,11} Choice of the spray equipment, driving speed of the tractor, operating pressure, spray release height, nozzle design, spacing, and size also influence deposition patterns.^{12–15}

Unintended exposure to agrochemicals *via* spray drift is not a new environmental concern and within the last decade, several risk mitigation measures have been developed to minimize it.¹⁶ No-spray buffer zones at the field edge are the most widely used mitigation measures at the European level.² The width of buffer zones is estimated according to country-specific regulations, crop type, dose rate of the applied agrochemical, and drift can often be reduced further when using drift-reducing techniques.¹² Drift reducing equipment is a more straightforward way to manipulate the spray droplet size distribution and in-flight trajectory of spray droplets. Low-drift and air-induction nozzles produce coarser sprays than conventional spray nozzles achieving a relative drift reduction of 50% to 90%.^{12,17} Next to these measures, the use of shielded sprayers designed to guide the drops to the target, end-nozzles to prevent overspray at the field edge, or application of spray-coarsening additives can reduce the risk of spray drift.³

The use of drift-reducing techniques is desirable but optional. At the same

time, a spraying process usually involves application of formulated crop protection products, and these are also known to influence spray drift. In an extensive review of exposure of agrochemicals, the FOCUS Working Group on Landscape and Mitigation Factors in Ecological Risk Assessment stated that more investigations are required to assess the influence of formulation type on spray drift and to accept it as a reliable risk mitigation measure.² Formulation type can influence drift risk by altering the physical properties of spray liquids. The relevant physical properties have been identified as shear and elongational viscosity, surface tension, and presence of inhomogeneities such as emulsion droplets.^{18,19} By modifying these properties of spray liquids it is possible to influence the spray droplet size and velocity, spray angle, and the dimensions of the spray footprint.^{20–24}

Many investigations have been carried out to assess the mode of action of different chemical compounds with respect to the nozzle design. The next challenge is to understand the interactions between physical properties induced by different formulation components in mixtures and in combination with nozzle design. The understanding of the spray formation process is important to deduce why and how different physical properties of spray liquids can influence spray characteristics.

Spray formation

The simplest and most widely used nozzle for agricultural applications is the flat fan nozzle. When spray liquid is atomized through a flat fan nozzle, it emerges as a liquid sheet (figure 1.1). The velocity of the liquid sheet is in the range of 10–25 m/s depending on the orifice dimensions and design, the operating pressure and the position in the cross section of the liquid sheet.^{25–28} Sheet length decreases with increasing operating pressure (with increasing relative velocity between the liquid and the gas).²⁶

Early investigations of sheet breakup were reported by Dombrowski and Fraser²⁵ who distinguished between two possible disintegration mechanisms: oscillation (figure 1.1a) or by perforation (figure 1.1b).

In the first mode, waves develop along the liquid sheet, grow in amplitude, and disrupt it into ligaments. The ligaments subsequently break up into spray droplets by a kind of Rayleigh's instabilities.²⁶ The ligament diameter was found to depend on the sheet thickness which is inversely proportional to the distance from the nozzle.^{26,29} When the sheet breaks up at a position closer to the nozzle orifice where it is thicker, spray so formed is coarser. In contrast, a delayed breakup leads to the formation of finer sprays.

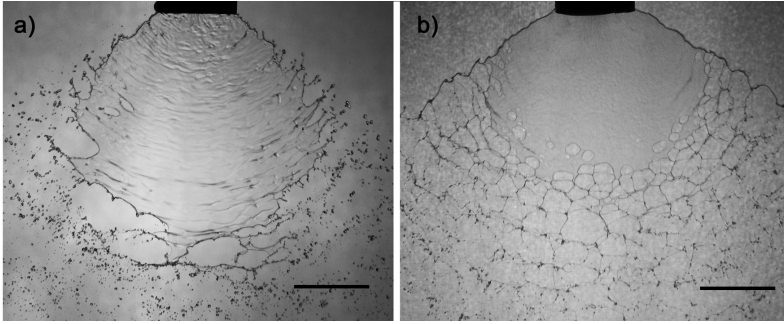


Figure 1.1: The breakup of a liquid sheet of a) water and b) 10% emulsion of sunflower oil and 0.1% w/w of Guar gum based thickener (Kelzan S) produced through a XR11003 flat fan nozzle at a pressure of 1.5 bar. The black bar is 10 mm.

A decrease in surface tension was observed to increase the growth rate of instabilities at the air/water interface.²⁵ Liquids that contain water-soluble surfactants create a liquid sheet of a similar or a greater length before breakup compared to a liquid sheet formed by water.^{21,25,30,31} The correlation between the decrease in surface tension at breakup and the decrease in mean spray droplet diameter was observed to be weaker for pure liquids than for surfactant solutions.³² Based on these observations, surface elasticity and Marangoni flows were suggested to stabilize liquid sheet that is formed by surfactant solutions because they can suppress the perturbations in the sheet.

Increased viscosity of the spray liquid suppresses wave motions of the liquid sheet and lowers the radial and contraction velocity of the sprayed liquid so that smoother sheets with a thick rim are formed that disintegrated much farther from the nozzle (compared to water).²⁵ Sprays formed by viscous liquids are, therefore, coarser. Elongational viscosity was identified as the more important property during spray formation^{33,34} so that polymer liquids that show elongational thickening increase the spray droplet size more efficiently.^{20,35,36}

The second sheet disintegration mechanism is perforation. In this mode, hole nucleation occurs closer to the nozzle outlet and induces the formation of coarser sprays with a lower fraction of fine, drift-prone droplets compared to sprays produced by water. Hole formation can be induced for pure liquid in vacuum (in the absence of air friction)²⁶ or by hot gas flow under atmospheric conditions.³⁷ Perforation mode was also observed when a solution with worm-like micelles was sprayed through a flat fan and a hollow cone nozzle.³⁸ Initially, it has been suggested that hydrophobic particles such as wax suspensions cause perforation and that

holes are nucleated at high flow turbulences.^{25,39} Further, deformability of particles was recognized as an essential property to initiate perforation onset, such as in the case of dilute oil-in-water emulsions.^{21,40,41} It was observed that emulsions based on different oils influence spray formation to a different extent.^{21,42} The concentration,²¹ the origin of the emulsified oil,⁴² its viscosity,⁴⁰ the emulsion droplet size, and number of emulsion droplets,⁴¹ all were observed to have an effect on the perforation onset and, thus, on the spray droplet size distribution. Perforation onset also depends on the dynamic surface tension at breakup.²¹ Although different hypotheses have been proposed,^{21,40,41} the nucleation mechanism of point disturbances in the sheet is not yet well understood.

Perforation onset was initially explained by a particle puncturing through the sheet connecting both interfaces.^{22,25} This hypothesis was contradicted by more recent studies whereby deformability of emulsion droplets was recognized as an important property in the spray formation mechanism.^{21,40,41} It has been suggested that rapidly stretched emulsion droplets with a temporary hydrophobic oil/water interface may initiate perforation⁴¹ *e.g.*, by diffusion to the air/water interface of the liquid sheet.²¹ These observations and conclusions construct the starting point for our investigations.

The picture becomes more complex if an air-induction nozzle is used for spray application. Air-induction nozzles were constructed specially for drift reduction purposes. They apply the Venturi principle and incorporate air bubbles into the liquid sheet and spray droplets.²² As a consequence, sprays become extremely coarse compared to sprays produced through a common flat fan nozzle. Additives, that decrease surface tension at breakup facilitate air inclusion while dilute oil-in-water emulsions inhibit it.^{43,44} Drops with air inclusion are larger but lighter than water drops of the same dimensions; both these effects alter the spray droplet size and velocity²⁴ influencing spray deposition and drift risk.

Research objectives

The research objective of this thesis is to investigate how the perforation mode is initiated by dilute oil-in-water emulsions in a liquid sheet formed by a flat fan nozzle. The aim is to increase our understanding as to why emulsions of various oils differ in their impact on the spray atomization process producing sprays with varying mean droplet sizes.

Emulsions are of a particular interest for drift reducing purposes because they can be incorporated into crop protection products at the required concentration.

Polymers, in contrast, are sensitive to salt concentration and to any pH changes in the carrier liquid and their network structures, that lead to the viscosity increase can be destroyed through shearing in the nozzle and in the sprayer pump.^{45,46} For these reasons, they are less suited to be part of a formulated product with drift reducing properties.

Formulated crop protection products contain, next to the active ingredient, a mixture of various adjuvants that have different chemical compositions and fulfil various task (*e.g.*, act as penetration enhancer, sticker, synergist *etc.*⁴⁷) An adjuvant is defined as a ‘substance added to a pesticide formulation or to the spray tank to modify pesticide activity or application characteristics’.¹ The next objective of this thesis is the characterisation of mixtures of dilute emulsions with polymers and water-soluble surfactants where polymers influence the viscosity and surfactants the dynamic surface tension of spray liquids. These investigations shall provide a picture as to what happens in more complex mixtures produced by diluted commercial products when they are sprayed.

Table 1.1: Formulation types according to the international classification scheme.⁴⁸

Term	Code	Spray liquid
Emulsifiable concentrate	EC	(micro)emulsion
Oil dispersion	OD	emulsion
Soluble concentrate	SL	liquid
Suspension concentrate	SC	suspension
Suspo-emulsions	SE	emulsion/suspension
Emulsion, oil in water	EW	(micro)emulsion
Water dispersible granules	WG	suspension
Wettable powder	WP	suspension

As shown in table 1.1, some formulation types already contain emulsifiable oils or concentrated emulsions. Without additional improvement or a new development, these formulation types may already significantly minimize the amount of fine spray droplets and contribute to drift risk reduction. A limited number of investigations describing the effect of the formulation type on the mean droplet size and the spray structure have been made with the conclusion that such a classification is not yet possible and applicable.^{3,49} There is some evidence that spray drift reduction can be achieved as a function of formulation type;⁵⁰ however, from the current state of knowledge, this effect requires further structured analysis.

In this thesis, an attempt is made to classify the most common liquid formulation types according to their ability to reduce the fine spray fraction, so as to sort

out those with drift reducing properties. This analysis is based on experimental work and literature research and covers a number of commercial products.

Outline of the thesis

The thesis begins with a more general analysis of the drift issue and then focuses on the mode of action of dilute oil-in-water emulsions with a detailed study of a sessile emulsion drop at the air/water interface of the liquid sheet.

Chapter 2 is a bibliographic review that outlines relevant aspects related to the spray drift phenomenon. By collating research studies on this topic, the influence of physicochemical properties of spray liquids influence on spray droplet size, velocity, and structure is evaluated. Furthermore, the combined effect of spray liquid and the nozzle type is discussed. The concluding part of this chapter contains a forecast of the impact of a formulation type on drift risk which is a combination of effects induced by various adjuvants.

Chapter 3 covers in a more detail the dynamics of the spray formation process induced by dilute oil-in-water emulsions. Applying Computational Fluid Dynamics (CFD) simulations, this chapter describes a discrete situation of an oil drop placed at an air/water interface of a liquid lamella. After passing through the nozzle, some emulsion droplets may be present at the air/water interfaces of the liquid sheet and, as it is shown in this chapter, these drops can induce liquid flow within the lamella leading to its necking and final breakup. Proceeding with investigations of a sessile oil droplet, a thermodynamic analysis of a system in equilibrium is provided in Chapter 4 applying the self-consistent field (SCF) approach and the molecular approximation developed by Scheutjens and Fleer.^{51,52} The model set up in Chapter 4 is further extended in Chapter 5 accounting for changes in the wetting behaviour of emulsion droplet induced by different molecular structures of the oil in presence of two types of surfactant molecules.

Based on experimental studies on dilute oil-in-water emulsions and supported by theoretical investigations in previous chapters, a spray atomization mechanism is developed in Chapter 6. This mechanism is based on spreading of emulsion droplets at the air/water interface of the liquid sheet. The mechanism also addresses interactions in mixtures of dilute emulsions with water-soluble surfactants. Modified fumed silica is sometimes added to the oil phase in a formulation, primarily to increase the oil viscosity. It has been observed that the addition of hydrophobized silica influences the spray droplet size produced by respective dilute emulsions.⁴⁰ This effect is investigated in Chapter 7 and explained applying the mechanism

proposed in Chapter 6. In Chapter 8, properties of mixtures of polymer solutions with dilute emulsions are studied. The measured droplet size spectra are related to the physical properties of spray liquids and explained by consulting the earlier proposed spray formation mechanism.

Spray droplet size distributions of several commercially available products are analysed in Chapter 9. The obtained droplet size spectra are verified by spray deposition measured in two small-scale drift trials. The results are further compared with a set of earlier published modelling data of spray deposition for different formulation types,^{53,54} which are calculated using the Silsoe arable crop drift model.⁵⁵

The final Chapter, Summary and General Discussion contains a general discussion and a summary of the outcome of the project. It provides suggestions how the observations made in this thesis can be implemented and outlines perspectives for further research.

References

- [1] G. R. Stephenson, I. G. Ferris, P. T. Holland and M. Nordberg, *Pure Appl. Chem.*, 2006, **78**, 2075–2154.
- [2] FOCUS, *Landscape And Mitigation Factors In Aquatic Risk Assessment. Volume 1. Extended Summary and Recommendations. Report of the FOCUS Working Groupon Landscape and Mitigation Factors in Ecological Risk Assessment*, 2007, EC Document Reference SANCO/10422/2005 v.2.0. pp. 1-169.
- [3] FOCUS, *Landscape And Mitigation Factors In Aquatic Risk Assessment. Volume 2. Detailed Technical Reviews. Report of the FOCUS Working Groupon Landscape and Mitigation Factors in Ecological Risk Assessment*, 2007, EC Document Reference SANCO/10422/2005 v.2.0. pp. 1-436.
- [4] Directive 2009/128/EC, *Official Journal of the European Union*, 2009.
- [5] M. C. Butler Ellis and P. C. H. Miller, *Biosystems Eng.*, 2010, **107**, 169–177.
- [6] H. Holterman, *Kinetics and evaporation of water drops in air*, 2003, IMAG Report 2003-12.
- [7] H. De Ruiter, H. J. Holterman, C. Kempenaar, H. G. J. Mol, J. J. de Vlieger and J. van de Zande, *Influence of adjuvants and formulations on the emission of pesticides to the atmosphere. A literature study for the Dutch Research Programme Pesticides and the Environment (DWK) theme C-2*, 2003, Plant Research International B.V., Wageningen, Report 59.
- [8] P. A. Hobson, P. C. H. Miller, P. J. Walklate, C. R. Tuck and N. M. Western, *J. Agr. Eng. Res.*, 1993, **54**, 293–305.
- [9] P. C. H. Miller, *Pesticide Outlook*, 2003, **14**, 205–209.
- [10] FAO, *Guidelines on Good Practice for Ground Application of Pesticides*, 2001, Food and Agriculture Organization of the United Nations, Rome.

- [11] BMELV, *Gute fachliche Praxis im Pflanzenschutz*, 2010, Bundesministerium für Ernährung, Landwirtschaft und Verbraucherschutz, Referat 512, Bonn.
- [12] SDRT, *Spray Drift Reduction Technology: A European Database*, <http://www.sdrtd.info/>, 2012, (2 October 2012).
- [13] S. D. Murphy, P. C. H. Miller and C. S. Parkin, *J. Agr. Engin. Res.*, 2000, **75**, 127–137.
- [14] J. H. Combellack, *Weed research*, 1982, **22**, 193–204.
- [15] A. J. Hewitt, *Atomization Sprays*, 1997, **7**, 235–244.
- [16] A. S. Felsot, J. B. Unsworth, J. B. H. J. Linders, G. Roberts, D. Rautman, C. Harris and E. Carazo, *J. Environ. Sci. Heal. B*, 2010, **46**, 1–23.
- [17] H. Guler, H. Zhu, H. Ozkan, R. Derksen, Y. Yu and C. Krause, *Trans. ASABE*, 2007, **50**, 745–754.
- [18] C. G. Hermansky and G. F. Krause, Proceedings of 4th International Symposium on Adjuvants for Agrochemicals (ISAA 1995), Melbourne, Australia, 1995, pp. 20–26.
- [19] A. J. Hewitt, *Environmentalist*, 2008, **28**, 25–30.
- [20] R. W. Dexter, *Atomization Spray*, 1996, **6**, 167–191.
- [21] R. W. Dexter, in *Pesticide formulations and application systems*, ed. A. K. Viets, R. S. Tann and J. C. Mueninghoff, American Society of Testing and Materials, West Conshohocken, PA, 2001, vol. 20, pp. 27–43.
- [22] M. C. Butler Ellis, C. R. Tuck and P. C. H. Miller, *Crop Prot.*, 1997, **16**, 41–50.
- [23] P. C. H. Miller and C. R. Tuck, *J. ASTM Int.*, 2005, **2**, 1–13.
- [24] P. C. H. Miller, C. R. Tuck, S. Murphy and M. da Costa Ferreira, Proceedings of 22nd European Conference on Liquid Atomization and Spray Systems (ILASS-Europe), Como Lake, Italy, 2008, pp. 1–8.
- [25] N. Dombrowski and R. P. Fraser, *Philos. T. R. Soc. S. A*, 1954, **247**, 101–130.
- [26] R. P. Fraser, P. Eisenklam, N. Dombrowski and D. Hasson, *AIChE J.*, 1962, **8**, 672–680.
- [27] M. D. Cloeter, K. Qin, P. Patil and B. Smith, Proceedings of 22nd Annual Conference on Liquid Atomization and Spray Systems (ILASS-Americas), Cincinnati, OH, USA, 2010, pp. 1–9.
- [28] H. Zhu, R. D. Braze, D. L. Reichard, R. D. Fox, C. R. Krause and A. C. Chapple, *Atomization Spray*, 1995, **5**, 343–356.
- [29] N. Dombrowski and W. R. Johns, *Chem. Engin. Sci.*, 1963, **18**, 203–214.
- [30] M. C. Butler Ellis and C. R. Tuck, *Crop Prot.*, 1999, **18**, 101–109.
- [31] M. Butler Ellis and C. Tuck, *Aspects Appl. Biol.*, 2000, **53**, 155–162.
- [32] M. C. Butler Ellis, C. R. Tuck and P. C. H. Miller, *Colloid Surface A*, 2001, **180**, 267–276.
- [33] R. P. Mun, J. A. Byars and D. Boger, *J. Non-Newton. Fluid Mech.*, 1998, **74**, 285–297.

- [34] R. P. Mun, B. W. Young and D. V. Boger, *J. Non-Newtonian Fluid Mech.*, 1999, **83**, 163–178.
- [35] A. Mansour and N. Chigier, *J. Non-Newton. Fluid Mech.*, 1995, **58**, 161–194.
- [36] G. M. Harrison, R. Mun, G. Cooper and D. V. Boger, *J. Non-Newton. Fluid Mech.*, 1999, **85**, 93–104.
- [37] N. Dombrowski, D. Hasson and D. E. Ward, The proceedings of the Brighton Crop Protection Conference - Weeds, 1989, pp. 663–668.
- [38] J. C. Thompson and J. P. Rothstein, *J. Non-Newton. Fluid Mech.*, 2007, **147**, 11–22.
- [39] R. P. Fraser and P. Eisenklam, *Imp. Coll. Chem. Eng. Soc. J.*, 1953, **7**, 52–68.
- [40] K. Qin, H. Tank, S. Wilson, B. Downer and L. Liu, *Atomization Spray*, 2010, **20**, 227–239.
- [41] M. C. Butler Ellis, C. R. Tuck and P. C. H. Miller, *Atomization Spray*, 1999, **9**, 385–397.
- [42] N. M. Western, E. C. Hislop, M. Bieswal, P. J. Holloway and D. Coupland, *Pestic. Sci.*, 1999, **55**, 640–642.
- [43] J. H. Combellack and P. C. H. Miller, Proceedings of 6th International Symposium on Adjuvants for Agrochemicals (ISAA 2001), Amsterdam, Netherlands, 2001, pp. 557–562.
- [44] O. Nicetic, G. Dorr, N. Woods and G. A. C. Beattie, Proceedings of 7th International Symposium on Adjuvants for Agrochemicals (ISAA 2004), Cape Town, South Africa, 2004, pp. 136–142.
- [45] J. Ferguson, N. E. Hudson and B. C. H. Warren, *J. Non-Newton. Fluid Mech.*, 1992, **44**, 37–54.
- [46] H. Zhu, R. W. Dexter, R. D. Fox, D. L. Reichard, R. D. Brazee and H. E. Ozkan, *J. Agric. Engineering Res.*, 1997, **67**, 35–45.
- [47] J. L. Hazen, *Weed Technol.*, 2000, **14**, 773–784.
- [48] CropLife International, *Catalogue of pesticide formulation types and international coding system*, 2008, Technical Monograph n2, 6th Edition, Brussels.
- [49] M. C. Butler Ellis and A. Bradley, *Aspects Appl. Biol.*, 2002, **66**, 251–258.
- [50] R. Stadler, *Brandenburger Bauernzeitung*, 2004, **45**, 30–31.
- [51] J. M. H. M. Scheutjens and G. J. Fleer, *J. Phys. Chem.*, 1979, **83**, 1619–1635.
- [52] J. M. H. M. Scheutjens and G. J. Fleer, *J. Phys. Chem.*, 1980, **84**, 178–190.
- [53] R. Vermeer, A. C. Chapple and R. Friessleben, *Use of oil based suspension concentrates for reducing drift during spray application*, Patent WO 2011147766.
- [54] P. C. H. Miller, C. R. Tuck, C. M. O’Sullivan and M. C. Butler Ellis, *Measurements of droplet size distributions from different designs of agricultural spray nozzle operating with different liquids*, 2009.
- [55] P. C. H. Miller and D. J. Hadfield, *J. Agric. Eng. Res.*, 1989, **42**, 135–147.

Chapter 2

Spray drift review

Mitigation of risk arising from spray drift in Europe is achieved mostly by implementation of no-spray buffer zones and the use of approved drift-reducing techniques. Although physiochemical properties of spray solutions are known to influence drift risk, they are not yet incorporated into regulatory risk assessments at the European level. This Chapter provides a systematic report on the relevant physical properties of agricultural spray liquids and how these influence spray characteristics. To complete the picture, several drift-related aspects are highlighted such as drift mitigation techniques and conditions, measuring equipment which is commonly used to characterize agricultural sprays, existing spray deposition models, and biological efficacy of sprays. In a final step, we discuss the possibility of estimating drift risk based on the physiochemical properties of spray liquids induced by different formulation types.

A shortened version of this Chapter is published as:

E. Hilz, A. W. P. Vermeer, Spray drift review: The extent to which a formulation can contribute to spray drift reduction. *Crop Protection*, **2013**, *44*, 75-83.

2.1 Introduction

The use of pesticides is an integral part of modern agriculture and contributes to the productivity and the quality of the cultivated crop. It has been estimated that the use of agrochemicals prevents a loss of up to 45% of the world food supply.¹ On the other hand, the increasing use of crop protection products is one of the rising environmental concerns.

Pesticide exposure *via* spray drift can have a negative impact on bystanders, residents, livestock, terrestrial and aquatic ecosystems. Awareness of drift risk when operating with agricultural chemicals is therefore essential in order to minimize off-target contamination and at the same time fully benefit from product efficacy. Pesticides are typically applied as sprays which are formed when the liquid is atomized through a hydraulic nozzle. Thereby, the fine spray fraction is more sensitive to off-target translocation by wind. The downwind movement of airborne spray beyond the intended area of application originating from aerial or ground-based spraying operations is defined as spray drift.² Within the last decades, it has become evident that a major contribution to environmental pollution is caused by aerial pesticide drift and that there is a need for harmonized approaches to mitigation measures at the European level.³ Although spray drift is not a new issue, some of its aspects require further investigations. Consequently, new aspects have to be considered and higher safety requirements have to be satisfied when new active ingredients or new formulations are introduced into the market.⁴

Several reviews related to drift phenomena have been published since the negative effect of spray drift has been recognized.^{5–13} A closer look into the subject reveals that the focus of each of the reviews changed over time. Early application methods and agricultural chemicals were rather simple.⁵ It was assumed that the best pest management could be achieved by a complete coverage, so that applications were wasteful and inefficient.¹⁴ First, damages of non-target and susceptible crops from drift were reported.⁵ Next after droplet drift, vapour drift of 2,4-Dichlorophenoxyacetic acid* was measured.¹⁵ Vapor drift is the dispersion of vaporized chemical to the atmosphere and areas surrounding the target area during and following application.¹⁶ Subsequently, closer attention was paid to the presence of pesticides in the atmosphere through volatilization.⁷ Exposure of rainwater and groundwater was reported.¹⁷ Vapour drift is a concern for volatile substances and applications at high temperatures. Today, many modern formulations registered for use in northern Europe have low vapour pressures.¹⁸ Surface water contamina-

*systemic active ingredient

tion and protection of aquatic life came into focus in more recent risk assessments.³ Bystander and resident exposure through airborne spray and ground deposits is a topic of current investigations.¹⁹

With the increasing awareness about the potential risk of pesticides, numerous mitigation measures for pesticide exposure *via* spray drift have been developed. An extensive overview of the state-of-the-art in risk mitigation is given in the EU report ‘Landscape and mitigation factors in aquatic risk assessment’.^{3,12} The three types of mitigation measure recommended there are: 1) the use of no-spray buffer zones; 2) the application of drift reducing techniques, and 3) the use of windbreaks. For surface water assessment FOCUS uses tables based on the basic drift values developed by the BVL (Bundesamt für Verbraucherschutz und Lebensmittelsicherheit, former BBA[†]). These tables are based on two set of experiments for applications in field and orchards, carried out in 1989-1992²⁰ and in 1996-1999 with improved analytical methods and extended deposition distances.²¹ Buffer zone widths are estimated based on these experimental data (95th percentile). Moreover, such parameters as dose rate, cultivated crop and number of applications have to be also considered. The width of buffer zones differs from country to country and can be reduced when accepted drift mitigation equipment or operating conditions are used. The Spray Drift Reduction Technology Database (SDRT)²² gives a current update of drift mitigation techniques and developments in Europe.

In some European countries such as UK and since recently the Netherlands,^{12,22} it is allowed to use drift control spray-additives. At the same time, the effect of pesticide formulations is not yet well evaluated and, therefore, not implemented into drift mitigation scenarios.³ In this review, we make an attempt to classify the most common pesticide formulation type according to their spray drift reduction potential. We start the approach with evaluation of relevant physicochemical properties of spray liquids, that influence the spray formation, followed by an analysis of how these properties can be induced by spray additives and formulation(types). Spray droplet size also influences biological efficacy and is an important input for spray deposition models. Therefore, this aspect will be discussed as well as different methods of determining droplet size distributions, droplet velocities and other spray characteristics.

[†]Biologische Bundesanstalt für Land- und Forstwirtschaft

2.2 Factors that influence spray drift

Spray drift is influenced by environmental and meteorological conditions, the spray technique and the crop. Wind speed and wind direction are meteorological factors that influence the trajectory and the velocity of airborne drops.^{23–25} Evaporation of the carrier liquid (mostly water) that depends on relative humidity and temperature can lead to a decrease of the droplet size, particularly in the case of finer spray droplets.²⁶ The fate of spray droplets is influenced by operating conditions such as application height, driving speed of sprayer, and nozzle spacing.^{27–29} Air assisted sprayer and use of shielded sprayers can reduce spray drift.^{30,31} The use of an end nozzle at the edge of the field prevents overspray of pesticides.³¹

The risk of spray drift is closely related to the spray droplet size.^{6,23,32–34} At the same time droplet velocities,³⁵ trajectories⁶ and porosity of the spray plume²⁷ influence droplet deposition. Nozzle design, orifice size, operating pressure and the entrained air-currents influence the size and the velocity of spray droplets.^{36,37} The exiting variety of nozzle designs evolves through the variety of situations for different applications and effort to minimize drift risk by increasing the spray droplet size. Drift reduction for low-drift and air-induction nozzles is defined as the reduction in the airborne portion compared to a standard nozzle according to the classification scheme described in ISO Standard 22369-1³⁸. Air-induction nozzles incorporate air bubbles into spray liquid and spray droplets and thus produce coarser sprays as compared to a conventional flat fan nozzle. Several methods exist to estimate the quantity of the air intake for air-induction nozzles.^{39,40}

Moreover, drift control additives designed to increase spray droplet size are available for use in some European countries.^{12,22}

2.3 Evaluation of spray drift

The established standard principles to measure spray drift are field trials engaging full spraying equipment, when working at typical weather and operating conditions.⁴¹ A tracer dye is usually used to track the airborne spray. It is recommended that the representative spray liquids shall contain water-soluble surfactants as *e.g.* Agral[®] at typical application rates of *e.g.*, 0.1% w/w. The choice of the sampling techniques is important to measure the ground sedimentation as well as the airborne concentration of spray droplets.¹⁸

Wind tunnels have been developed for comparison of experimental data because field trials carried out with varying weather parameters and for different crops

lack in direct repeatability. As recommended by the International Organization for Standardisation, the measurements of spray drift can be preformed in wind tunnels by tracing spray droplets displaced by the wind flow. The spraying conditions, along with the allowed test equipment, sampling techniques, and recommendations on the calculation of the results are collected in the ISO 22856 standard.⁴² However, it is agreed on that wind velocity and turbulence profiles in the field can not be reproduced in wind tunnels.¹⁸ Therefore, wind tunnel are used to compare spray nozzles and to estimate relative drift risk but cannot replace field experiments.

2.4 Modeling

Many drift risk assessments use computational model to predict the environmental fate of airborne spray droplets as well as the bystander and resident exposure.¹³ Spray drift models have been developed over last 30 years.¹⁹ Only some will be mentioned in this paragraph.

The *via* internet accessible model AgDrift⁴³ for example is part of drift assessment programs in US, Canada and Australia. IDEFICS model has been developed in the Netherlands by IMAG (presently Plant Research International), in close cooperation with local authorities.⁴⁴ This model is adjusted to special environmental conditions in the Netherlands because the coexistence of numerous surface water ditches along with smaller fields requires special attention and different standards for spray drift mitigation. A Bystander and Residential Exposure Assessment Model (BREAM) was developed in cooperation with the governmental department for Environment, Food and Rural Affairs (Defra) and covers scenarios currently relevant in UK.¹⁹ It estimates the potential exposure to pesticides of bystanders and residents by airborne spray droplets and ground deposits.

The required input parameters for these droplet tracking models are droplet size distribution and evaporation rate, and also droplet velocity distribution, distance from nozzle of droplet origin, spray angle, velocity of the liquid sheet.

Although, the droplet size spectrum is difficult to predict with modeling, the effect of physical properties of spray liquid on the droplet size distribution can be empirically calculated using the DROPKICK model.⁴⁵ This model was developed for aerial application and is based on physical properties of spray liquids such as dynamic surface tension, shear and extensional viscosity.⁴⁶

The main advantages of computational and mathematical models are that they present an alternative to expensive drift trials. They can be performed in a reasonable time, require lower costs and allow to vary the application parameters.

However, it is often stressed that models simplify complex field conditions and predictions require verification through experimental studies.^{10,13}

2.5 Spray droplet size

Agricultural sprays are often characterized by a mean droplet diameter. According to American Society of Agricultural Engineers S-572 Standard classification,⁴⁷ nozzles can be classified as very fine ($< 100 \mu\text{m}$), fine ($100 - 175 \mu\text{m}$), medium ($175 - 250 \mu\text{m}$), coarse ($250 - 375 \mu\text{m}$), very coarse ($375 - 450 \mu\text{m}$), or extremely coarse ($> 450 \mu\text{m}$). A similar classification scheme is published by the British Crop Protection Council.⁴⁸

The amount of spray drift is usually related to the percentage of fine spray droplets. The smaller a spray droplet, the longer it remains airborne and the higher the possibility for it to be carried away by crosswind.⁸ Droplets with diameter $< 100 \mu\text{m}$ contribute significantly to drift losses.^{18,23,26} Other researchers consider droplets with diameter $< 50 \mu\text{m}$,⁴⁹ $< 150 \mu\text{m}$ ^{24,50} or $< 200 \mu\text{m}$ ⁵¹ to be most drift-prone. Moreover, spray droplets of a few microns in size can evaporate before sedimentation.

It is fundamentally important to measure droplet size and the size distribution to understand the environmental and the biological fate of spray droplets.

Passive collectors with suitable surface can be used to collect the deposits. The droplet diameter can be subsequently calculated from the deposit size with a known spread factor on the target surface.^{49,52} Droplets in flight are often measured using laser-based spatial (number-density weighted) and temporal (number-flux weighted) techniques. The later allows to measure both droplet size and velocity. Measurements of droplets velocities and trajectories are required for spray deposition modeling.¹⁹ The most common measuring systems used for agricultural sprays are Particle Measuring Systems (PMS) spectrometers, phase Doppler particle analyser (PDA), particle imaging systems *e.g.* Oxford Lasers VisiSizer, and Malvern laser diffractometer.⁵²

Comparative studies have been performed on different measuring systems. It was outlined that obtained data differ, sometimes significantly, when measured with different techniques,⁴⁹ especially in the case of coarse and very coarse sprays.⁵³ Spatial sampling techniques tend to overestimate the small spray fraction.^{49,54} A high density of internal interfaces in spray droplets due to the presence of emulsion droplets or air bubbles can cause measurement inaccuracies in techniques based on refraction and diffraction.⁵⁵ Therefore, it has been suggested that a reference

system should be used to compare data obtained with different measuring techniques.⁵³

2.6 Biological efficacy

Coarser sprays produced by low-drift and air-induction nozzles or by adding spray additives, which shift the droplet spectra to higher values, may reduce biological efficacy of an agrochemical application. Fine droplets contribute to off-target losses *via* spray drift, whereas large droplets with a high volume achieve a relatively low degree of coverage and may rebound or scatter. As outlined by Göhlich,⁵⁶ a narrow droplet size spectrum is thus required for an optimized application. Other researchers stress that narrowing the droplet size distribution is not sufficient to improve the efficacy and further information on the biological requirements is essential.^{57,58} These biological requirements might be *e.g.*, the wetting properties and the orientation of the leaves, pest or disease location, or the mode of action of the pesticide.

Pesticide efficacy, or dose received by the target site or organism, can be described as a function of deposition and retention of spray droplets considering the uptake and the translocation of the active ingredient (a.i.).^{59,60} Impaction and retention depend on the spray properties such as droplet size distribution, sedimentation velocity, surface tension of the spray droplet and to a smaller extent on its viscous properties.⁶ The impaction efficacy is also influenced by aerodynamic forces as well as by orientation, size, and surface properties of the target.⁶¹ The impaction efficacy increases with increasing droplet size and wind speed. Retention generally increases with decreasing droplet size and decreasing dynamic surface tension.

As reviewed by Knoche⁶², a decrease in droplet size generally increases the performance of contact-acting and more frequently of systemic herbicides at constant carrier volume. In 20% of the reviewed experiments for foliar-applied herbicides, droplet size did not change herbicide performance and in 9% of cases the performance decreased with decreasing droplet size. Uptake was found to be rather independent of droplet size and can increase with increasing dose of a.i. on the target surface which can be achieved by increasing the droplet size or by increasing the a.i. concentration per droplet. A decrease in spray droplet size may also improve the efficacy of herbicides with limited mobility.

It has often been suggested that a larger number of fine spray droplets results in a more uniform coverage and an improved efficacy of contact fungicides and in-

secticides.^{14,63} As outlined by Ebert *et al.*,⁶⁴ uniform coverage does not necessarily achieve a better efficacy of ingested insecticides. These observations were explained by sub-lethal exposure through application of fine, uniform distributed sprays. The results imply that a non-uniform deposition over the leaf and a uniform coverage over the application area are required to improve insecticide efficacy.

Spray quality and application parameters were found to have a smaller effect on the biological efficacy of systemic fungicides.^{50,65} However, a tendency towards reduced biological efficacy of coarser sprays was reported in both studies.

2.7 Physical properties of spray liquids

Spray formation through a hydraulic nozzle is a highly dynamic and complex process. Therefore, many experimental investigations, especially in the case of viscous liquids, have been performed on liquid jets.⁶⁶⁻⁶⁸ In a simplest case, when the liquid is atomized through a conventional flat fan nozzle, it is ejected as a liquid sheet. The subsequent development of the sheet and its atomization into spray droplets depend on the ejecting velocity, the design of the nozzle, the size of the orifice, and physical properties of the spray liquid and the ambient gas.⁶⁹ The outcome of previous research on agricultural sprays shows that there are essentially three relevant physical properties of spray liquids that influence the mechanism of spray formation.^{12,70,71} These properties are 1) shear and extensional viscosity, 2) surface tension, and 3) the presence of inhomogeneities in the spray liquid such as emulsion droplets or solid particles.

2.7.1 Viscosity

Polymer-based drift control additives are commonly used in US and Australia to decrease spray drift.^{12,72} The general mode of action of polymeric material is based on the increase in viscosity of the spray liquid. The viscosity increase leads to the formation of coarse sprays by shifting the droplet size distribution to a larger size.^{70,73-75}

High-speed photographs of sheet breakup reveal that, under atmospheric conditions, spray liquids without inhomogeneities disrupt through oscillation.⁶⁹ In this disintegration mode waves develop, grow in amplitude and subsequently disrupt the sheet into ligaments and finally into spray droplets. Viscous liquids can sustain high stretching before they break up, suppress formation of perturbations at the interface and oscillation growth.

The viscosity of a fluid in the shear flow can be Newtonian (that is independent of shear rate or shear stress), shear thinning (decreasing with shear rate) or shear thickening (increasing with shear rate).⁷⁴ However, many polymers used for agricultural applications exhibit shear-thinning behavior.⁵¹ Therefore, a substantial increase of the shear viscosity is required to compensate for the loss of viscosity due to shear forces in the nozzle or in the sprayer pump. This can be achieved only at high polymer concentrations. Shear viscosity of polymer liquids used for spray drift control is typically much smaller than their extensional viscosity.⁷⁶ Substantially smaller amounts of polymer are required to produce coarser sprays if the polymer increases the extensional viscosity of the spray liquid.⁷⁷

The extensional viscosity is the resistance of a fluid to stretching forces in an extensional flow that determines the resistance of a fluid to form a new interface.⁷⁸ It is defined as $\eta_e = (\sigma_{xx} - \sigma_{yy}) / \dot{\epsilon}$, where $\dot{\epsilon}$ is the elongational rate. The difference in stress in the flow direction σ_{xx} and the direction normal to it σ_{yy} is the first normal stress difference N_1 that is often used to describe polymer chain stretching.^{67,79}

In the case of Newtonian liquids, the elongational viscosity η_e is three times higher than the shear viscosity η_s . This ratio of elongational viscosity to shear viscosity is known as the Trouton ratio. The elongational viscosity (and the Trouton ratio) of polymer liquids can remain constant, increase or decrease as a function of the elongational rate.^{80,81}

Polymer liquids that show elongational thickening, increase most efficiently the spray droplet size. Three parameters have been outlined that influence the elongational viscosity of spray liquids:^{76,81} 1) the rigidity of the polymer chain, 2) molecular weight of the polymer and 3) its concentration. The elongational viscosity of rigid and low molecular weight polymers is constant as a function of elongational rate. In the case of high molecular weight flexible polymers, the elongational viscosity strongly increases with the increasing strain rate due to the recoiling of the polymer chain. The elongational viscosity of a semi-rigid polymer increases and reaches a plateau as a function of the elongational rate. Highly flexible but compact polymers that cannot recoil their chains in the solvent exhibit a similar behavior to the semi-rigid polymer solutions. There is a critical elongational rate above which the extensional viscosity of the polymer solution begins to increase. This critical value is smaller for polymer of high molecular weight and at high concentrations.

Increasing concentration of the polymer decreases the spray cone angle^{81,82} and the fan width compared to water.⁸³ As a consequence, the footprint produced by this spray is smaller in dimensions, so that in an extreme case, the nozzle spacing has to be readjusted.

Various stretching rheometers are successfully used for testing high viscosity materials while measurements of the extensional viscosity for diluted polymer solutions at high elongational rates are difficult. These are some of the approaches: the relaxation of elastic forces leads to the phenomenon of die-swell in free jets. Digital die-swell measurements have been used to obtain the first normal stress difference.⁶⁷ Elongational viscosity of dilute polymer solutions can be calculated from the neck thinning during droplet fission.⁸⁴ The opposite jet viscometer is often used to measure low viscosity samples. The experimental data obtained with this type of equipment are sometimes not consistent and it has been shown that a shear component is measured along with extensional forces.^{85,86} Furthermore, extensional properties of diluted polymer solutions can be obtained from the measurements of flow through a porous material^{76,87,88} or through a screen pack.⁸⁹ Based on these techniques a 'screen viscometer' was introduced by the American Society for Testing and Materials as a test method to obtain "relative extensional viscosity of agricultural spray tank mixes".⁷⁸ In this standard test method the relative extensional viscosity (or screen factor) is defined as the ratio of the flow time of a test fluid to the flow time of water through the 'screen viscometer'. A good correlation between an increase of the screen factor and spray coarsening was reported for some commercial polymers.⁵¹

As discussed above, polymers are sensitive to shear stress in the nozzle and in the tank. The sheet velocity ranges between 10 – 25 m/s depending on the orifice dimensions and design, the operating pressure and the position in the cross section of the liquid sheet.^{69,90–92} The shear rates in a flat fan nozzle were estimated to range between $\dot{\gamma} = 1.6 \times 10^4 \text{ s}^{-1}$.⁹³ and $\dot{\gamma} = 1.2 \times 10^5 - 7.0 \times 10^5 \text{ s}^{-1}$.⁹² The shear rates in the tank are typically 50 s^{-1} .⁸ Intensive recirculation, especially at the end of a spray session, can easily destroy weak polymeric structures, decrease the viscosity of the spray liquid, and consequently can induce formation of finer sprays compared to the situation before shearing. Long-chain polymers were found to be highly sensitive to recirculation because their polymeric structures can break down, while stiffer polysaccharides are less sensitive to shear forces. It has been observed that non-ionic polyacrylamides and polyethylenes are often more strongly affected by recirculation than polysaccharides and anionic polyacrylamides.^{51,94,95}

The viscosity of polymer liquids is also influenced by the salt concentration and the pH of the spray liquid when *e.g.*, fertilizer is added into the tank. The viscosity increase is attributed to the stretching of polymer chains in the flow. An increase of the pH was suggested to increase the degree of neutralization of the polyelectrolyte chains, causing them to contract;⁷⁴ consequently the viscosity of a spray liquid can

decrease with changes in pH.

2.7.2 Surface tension

The effect of the surface tension on the spray droplet size depends on the nozzle type. A decrease in the dynamic surface tension generally leads to the formation of finer sprays for flat fan and hollow cone nozzles.^{69,70,96} The degree of reduction in spray droplet size was observed to differ for different nozzles.⁹⁷ On the other hand, spray additives that decrease the surface tension often produce coarser sprays than water when atomized through an air-induction nozzle.⁹⁸

Dyes that are used to trace spray droplets in drift experiments can decrease the surface tension of the spray liquid.⁷³ Polymers have little effect on the surface tension of spray solutions so that it is often controlled by surfactants. A wide range of surfactants and surfactant blends are part of commercial pesticide formulations and additives. Additives such as spreader and wetting agents contain surfactants that promote the wetting and the coverage of the target surface.⁹⁹ This effect is correlated with a decrease in the dynamic surface tension of the spray liquid at the moment of droplet impact on the leaf surface.^{100,101} The relevant surface age at impact was estimated to fall in the range 60 – 2500 ms.¹⁰² The atomization of the liquid sheet into spray droplets happens within a few milliseconds,^{83,97} so that the dynamic surface tension at much shorter times is relevant for the spray formation process. This implies that additives that decrease the dynamic surface tension sufficiently to improve the retention and the wetting properties of spray droplets will not necessarily influence spray formation.

Very short measuring times are required to estimate the dynamic surface tension at sheet breakup. A bubble pressure tensiometer is often the method of choice for measuring the dynamic surface tension of agricultural spray liquids. The limitation of this technique is that it provides reliable result at surface ages that are greater than the surface ages at the moment of sheet breakup. The surface tension at a shorter surface lifetime can be estimated by interpolation as described by Butler Ellis *et al.*⁹⁷

Moreover, the interfacial rheology of the liquid sheet was suggested to influence the spray formation process.¹⁰³ The statement that the dynamic surface tension is not the only surface property that influences spray atomization is supported by the observation that the correlation between the decrease in dynamic surface tension and the decrease in mean spray droplet diameter is weaker for pure liquids than for surfactant solutions.⁹⁷ In the same study, surfactant solutions were observed to

reduce the oscillation of the sheet and to increase the sheet length, whereas pure liquids showed no effect either on the length of the liquid sheet or on the oscillation growth. Surface elasticity and Marangoni flows were suggested to stabilize the liquid sheet formed by surfactant solutions and to suppress surface perturbations. The breakup length of the liquid sheet of a spray liquid that contains water-soluble surfactants may increase or remain similar as the length of the liquid sheet produced by water.^{83,97}

The surface tension of water decreases with increasing temperature. This effect has to be considered because water is mostly the carrier liquid in agricultural spray applications. The effect of temperature on the spray droplet size was studied for typical agricultural additives and blank formulations when atomized through a flat fan nozzle by Downer *et al.*¹⁰⁴ It was observed that the spray droplet size decreases with increasing temperature and decreasing surface tension for all spray liquids but a blank WP formulation and spray liquids that contain organosilicones. Furthermore, a decrease of the spray droplet size with increasing temperature was reported for tap water sprays produced through a flat fan and an air-induction nozzle.³³ However, these measurements were not correlated with the dynamic surface tension of the spray liquid.

Other aspects related to changes in the dynamic surface tension are the shape of the spray footprint, changes in the vertical velocity of spray droplets and their internal structure. Water-soluble surfactants and pure water were found to produce spray fans with a similar footprint.^{83,103} These footprints are thicker and shorter than those produced by dilute emulsions. Surfactants were shown to facilitate inclusion of air bubbles into spray droplets when sprayed through an air-induction nozzle.^{24,103} This effect was also related to the decrease in surface tension. Moreover, spray liquids that contain surfactants, produce droplets of lower velocity than water when sprayed through a flat fan¹⁰³ or an air-induction nozzle.³⁶ Thereby, droplets with a diameter $< 200 \mu\text{m}$ have similar vertical velocities (about 2 m/s in this particular example) and are less influenced by the changes in physical properties of the spray liquid.³⁶

2.7.3 Inhomogeneities

Agricultural sprays that contain solid particles such as crystals of active ingredient, dilute oil-in-water emulsions, or both are described in this review as liquid systems with inhomogeneities.

Drift reduction achieved by incorporated emulsions is not affected by recir-

ulation in the tank but is nozzle-type dependent. It has been observed that spray liquids that contain emulsified oils increase the spray droplet size and at the same time decrease the fine spray fraction compared to water sprays when atomized through a flat fan, a hollow cone or a twin fluid nozzle. This was described for emulsions that are based on vegetable oils,^{24,93,103,105-110} mineral oils,^{24,83,98,103,105,106,108,110,111} organosilicones,^{83,98,103,104,106,107,110} and water insoluble surfactants.^{33,83} Further studies on the ability of emulsified oils to influence spray characteristics with regard to spray drift are collected by Spanoghe *et al.*¹¹².

The induced spray coarsening effect can be explained by the mode of spray formation induced by emulsions. The thickness of the liquid sheet, which is formed by a flat fan nozzle, is inversely proportional to the distance from the nozzle outlet.^{90,113} Compared to water, dilute emulsions perforate the liquid sheet at an early stage, decrease the sheet length at breakup and thus produce coarser sprays and sometimes significantly decrease the fine spray fraction when atomized through a flat fan, a hollow cone or a twin fluid nozzle.^{24,33,34,98,106,109,111} However, it was observed that emulsions can reduce the mean droplet size compared to water when sprayed through an air-induction nozzle. In this case, the fine spray fraction can increase, as expected, or remains unchanged compared to the water spray sprayed at same operating conditions.^{34,111}

For a flat fan nozzle, the onset of spray coarsening occurs when the emulsion concentration is in the range of 2×10^{-3} - $5 \times 10^{-2}\%$ w/w.⁸³ It was observed that with increasing emulsion concentration the mean spray droplet size increases. After reaching a maximum, the spray droplet size was found to decrease. The decrease in spray droplets size at higher emulsion concentrations goes along with the decrease in the dynamic surface tension. Apparently, dynamic surface tension controls spray formation by counteracting the spray coarsening effect induced by emulsion droplets. Formation of finer sprays and an increase in airborne drift were also observed for mixtures of a surfactant and a dilute emulsion when sprayed through different nozzle designs in a wind tunnel experiment.¹¹⁴ Probably, the decrease in the dynamic surface tension in such mixtures controls spray formation in a similar way as for emulsions at high concentrations.

A casual relation was observed between the initial emulsion droplet size and the emulsion concentration at the onset of spray coarsening.⁸³ However, larger emulsion droplets may split in the nozzle, so that the initial emulsion droplet size might not necessarily represent the emulsion droplet size distribution during spray formation. Furthermore, it was suggested that the breakup length of the liquid sheet and the spray droplet size are influenced by the number of emulsion droplets.¹⁰⁷ A larger

number of emulsion particles was suggested to induce formation of coarser sprays.

Dilute emulsions were also observed to increase the spray angle, increase the width of the spray fan and to reduce its breadth compared to water sprays.^{83,103} The reduction of the fan breadth was explained by the absence of the wave motions during perforation so that more spray droplets stay in plane of the nozzle. A thinner and wider spray fan produced by emulsions corresponds to higher spray droplet velocities.^{103,105} With the increase of the droplet size in the fan center, the droplet size distribution of dilute emulsion becomes narrower compared to droplet size distributions produced by water, surfactant solutions or viscous liquids.

When atomized through an air-induction nozzle, dilute emulsions, that contain emulsion droplets of some μm in diameter, prevent air intake, whereas microemulsions can enhance air inclusion.¹¹⁵ The high surfactant concentration that is required to stabilize microemulsions might be responsible for the increased air intake.

An increase in the mean spray droplet size and a reduction of the fine spray fraction were measured when an emulsifiable additive was added to a formulation of glyphosate (Roundup).¹¹⁶ A good correlation was reported in this study between the effect of the additive on the spray droplet size and spray drift.

Many pesticide formulations contain a crystalline active ingredient of a few microns in size. These crystals are homogeneously distributed throughout the bulk liquid by means of dispersing additives. In several experiments reported in literature, solid dispersions were shown not to influence either the spray droplet size spectra or the spray disruption patterns.^{83,93,117} However, some experiments have been performed where spray liquids with solid particles coarsen the spray droplet size.^{34,69,104}

2.8 Formulations with drift reduction potential

The use of tank-mix additives for improving the properties of spray liquids and among others for controlling spray drift is not common in most European countries.⁸ To be approved, tank mix additives have to be tested in combination with a pesticide formulation because they do not lead necessarily to the same results with different products.¹² At the same time, the registration process of an additive can be expensive and time consuming. This implies higher demands on ready-to-use agrochemicals and a tendency to develop formulations that show drift reducing properties. Strict European drift values and regulations on pesticide exposure lead to posing the question if formulation types can be accepted as a measure for drift

Table 2.1: Pesticide formulation types¹¹⁹ and spray liquids.

Term	Code	Solvent of the a. i.	Spray liquid
Emulsifiable concentrate	EC	organic	(micro)emulsion
Oil dispersion	OD	organic	emulsion
Soluble concentrate	SL	water	liquid
Suspension concentrate	SC	water	suspension
Suspo-emulsions	SE	water/organic	emulsion/suspension
Emulsion, oil in water	EW	organic	(micro)emulsion
Water dispersible granules	WG	-	suspension
Wettable powder	WP	-	suspension

risk reduction.

Although the effect of formulated products on spray drift is evident, it is a non-trivial task to evaluate and to model it. Formulated products influence the physical properties of spray liquids^{12,73} and differences in droplet drift have been observed for different formulated products in field experiments.¹¹⁸ A generally good correlation between the spray droplet size and the amount of drift was found in wind tunnel experiments^{24,34,116} and a small-scale drift trial.¹¹⁷ In another set of experiments, it was observed that there is not an absolute correlation between the spray droplet size distribution and the total airborne spray, and that this correlation depends on methods that are chosen to measure spray drift and on the nozzle design.¹¹⁴

Next to the droplet size, other physical properties have to be evaluated to measure drift. Wind tunnel experiments performed by Nicetic *et al.*¹¹¹ showed that drift reduction for agricultural mineral oil emulsions when sprayed through an air-induction nozzle does not correlate with the measured spray droplet size distribution. It was suggested that an increased spray droplet weight can be the reason for the drift reduction rather than the droplet size. Besides the droplet size and weight, droplet's velocities, trajectories and spray porosity have to be taken into account to calculate the downwind deposition during an application process.

Based on the physical properties of spray liquids and their effect on spray performance, a rough prediction can be made about the formulation types that will influence spray characteristics and thus spray deposition and drift. The most common formulation types are summarized in table 2.1

Polymers in formulated product are present at a low concentration that probably won't be sufficient to influence the properties of spray liquids. The effect of the dynamic surface tension induced by surfactants and the presence of inhomogeneities such as emulsion droplets or solid particles need to be considered in more

detail.

OD and SE formulations that contain a high concentration of emulsifiable oil can be expected to influence spray performance by reducing the fine spray fraction what directly decreases drift risk, and by increasing the spray angle that has an effect on spray plume porosity. Dilute emulsions produced by these formulation types will also increase droplet velocities, which increases the probability of impact of spray droplet on the target surface. In a second consequence emulsions narrow the spray droplet size distribution, which can be desirable for certain applications.⁵⁶ All these effects occur when dilute emulsions are sprayed through a flat fan nozzle. When sprays are produced through an air-induction nozzle, emulsions often decrease the mean droplet size, although not all air-induction nozzles respond in the same way.^{98,120} At the same time, under these application conditions, the increase of the fine spray fraction induced by emulsions is small and will not necessarily result in higher spray drift compared to water sprayed through the same nozzle.¹¹¹

Spray characteristics also depend on the concentration and the chemical composition of the oil and other co-formulants. Thus, deviation in absolute values of spray droplet size and the degree of drift reduction are possible for different products of the same formulation type. Thereby, the concentration and the composition of the oil appear to be most important. Emulsions of vegetable oils were observed to be more effective at drift reduction than an emulsion of mineral oil when sprayed through a flat fan nozzle.¹⁰⁸ The emulsion concentration required to induce spray coarsening depends on the oil type and probably on the emulsion droplet size.⁸³ Additional spray coarsening can be achieved by adding modified fumed silica to the oil phase.⁹³

There can be a measurable decrease in the dynamic surface tension at high emulsion concentrations which counteracts the effects induced by emulsion droplets with respect to the spray droplet size and also with respect to other spray characteristics. However, emulsion concentrations at typical application rates are low. Oil-based additives improve the uniformity of the spray when atomized through an air-induction nozzle producing spray droplets with a low amount of the inducted air.³⁹ Reduction of air inclusion showed a minimal effect on spray drift in a wind tunnel experiment²⁴ which might contribute to an increased droplet weight.¹¹¹ On the other hand, spray retention and efficacy can be compromised by reduced air intake.¹¹⁵

EC and EW formulations contain an emulsifiable oil or a concentrated emulsion and might also contribute to spray drift reduction for sprays produced through a

flat fan nozzle. On the other hand, high surfactant concentration in these formulation types might induce a sufficient decrease in the dynamic surface tension and overcome the drift-reducing effect induced by emulsion droplets. Drift mitigation is possible only if a macroscopic emulsion is formed by these formulation types which is not always the case. There might be a finite emulsion droplet size required to influence the spray characteristics so that microemulsions will perform in a completely different way with respect to spray atomization. Some evidence of such behavior is provided by the observation that microemulsions facilitate air intake when applied with air-induction nozzles in contrast to macroscopic emulsions.¹¹⁵

An SL formulation usually contains a high load of surface active material. A high surfactant concentration generally tends to increase the fine spray fraction when sprayed through a flat fan as well as through an air-induction nozzle.³⁶ This indicates that this formulation type will either have no influence on the spray performance when applied at low product concentrations or might even increase spray drift by increasing the fine spray fraction.

WG, WP and SC formulations can be expected to perform in the same way as pure water sprays because dispersions that contain non-deformable particles typically do not influence the spray formation process.^{83,93,107,110} At the same time, if an emulsifiable component is part of an SC formulation, this will change the droplet size distribution in a similar way as in case of a dilute oil-in-water emulsion. An SC formulation was shown to decrease spray drift more efficiently than a formulation containing emulsified oil in a wind tunnel experiment.³⁴ The composition of this formulation indicates that the drift-reducing effect was more likely to have been induced by an oil-based co-formulant than by the crystalline active ingredient. In another study a WP blank formulation was reported to reduce spray drift more efficiently than an EC blank formulation.¹⁰⁴ Again, here it is necessary to know the composition of the product to understand its impact on the droplet size distribution.

Formulation types that contain a high concentration of emulsifiable oil will certainly produce coarser sprays than water when sprayed through a conventional nozzle. For other formulation types, the knowledge of the composition is required to evaluate its impact on spray characteristics. The potential of a formulated product to reduce spray drift can be identified at early development stage when measuring the spray droplet size spectra at relevant concentrations. Droplet velocity, spray patterns, and air intake greatly depend on the physical properties of spray liquids and have to be evaluated for more detailed spray drift predictions or

as input for spray deposition modeling.

It is often stated that drift reduction with an appropriate nozzle is greater than those achieved by a formulated product or a spray additive. The combined effect of nozzle type and physical properties of spray liquids has been explored in different studies and it appears that physical properties of spray liquids can be used in addition to accepted drift reducing application technologies or when these technologies are not available for use. In some cases significant spray drift reduction can be achieved with commercial products that do not need further optimization. Although the main trends can be anticipated from previous extensive studies, further research is required to quantify the drift reduction effect induced by a certain formulation type.

2.9 Conclusions

New technical equipment and improved application methods have been developed during the last decades to reduce environmental contamination and to minimize spray drift emission. Many of these improvements *e.g.*, low-drift nozzles are widely used in modern agricultural practice; others *e.g.*, air-assisted spraying equipment, may experience lack of acceptance due to application limitations or the costs involved. The use of formulated products is part of agricultural applications. Improvements by means of formulation benefit everyone and do not require special technical equipment. Consequently, formulation effect can be included in the development of drift mitigation scenarios accounting for the combined effects of nozzle design and formulation type. Changes in the droplet size spectrum induced by a formulation type can contribute to an improved biological efficacy of a product.

Drift risk is often correlated with spray droplet size, in particular with the percentage of fine spray droplets. To identify formulations that can contribute to spray drift reduction, the droplet size distribution can be measured at an early development stage when the product is sprayed in a relevant concentration range using common application techniques. The obtained droplet size spectra in combination with further relevant spray characteristics can then be included in an appropriate modeling program which gives a prediction for the most probable downwind deposition and airborne spray. These modeling data can help to estimate the drift risk and bystander exposure as a first approximation method. Certainly, the final data have to be approved by field trials or more extensive experiments creating a database that include the formulation effects. Such a database could help in the reevaluation of the width of existing buffer zones towards a more realistic value ac-

ording to the applied product. Finally, it has to be emphasized that the described scenario is possible only in the case of a close cooperation of regulatory bodies and operators.

It is well known that spray atomization is greatly influenced by the physical properties of spray liquids such as extensional and shear viscosity, dynamic surface tension and the presence of emulsion droplets. As outlined in this review, numerous research studies have been published on this topic. These studies are a starting point in the evaluation of the effect of a formulation type on spray drift. Rough predictions can be made from the current state of knowledge. Evidently, more research is required to develop a classification scheme based on drift-reducing properties of formulation types. Lack of acceptance in several application-related areas yet hampers development of such a classification scheme. With argumentation provided in this review, we hope to have highlighted well enough benefits that such a development can bring for operators, consumers and industry, without harming the environment.

References

- [1] E. C. Oerke, *J. Agr. Sci.*, 2006, **144**, 31–43.
- [2] G. R. Stephenson, I. G. Ferris, P. T. Holland and M. Nordberg, *Pure Appl. Chem.*, 2006, **78**, 2075–2154.
- [3] FOCUS, *Landscape And Mitigation Factors In Aquatic Risk Assessment. Volume 1. Extended Summary and Recommendations. Report of the FOCUS Working Group on Landscape and Mitigation Factors in Ecological Risk Assessment*, 2007, EC Document Reference SANCO/10422/2005 v.2.0. pp. 1-169.
- [4] R. J. Hillocks, *Crop Prot.*, 2012, **31**, 85–93.
- [5] N. B. Akesson and W. E. Yates, *Annu. Rev. Entomol.*, 1964, **9**, 285–318.
- [6] J. H. Combellack, *Weed research*, 1982, **22**, 193–204.
- [7] F. van den Berg, R. Kubiak, W. G. Benjey, M. S. Majewski, S. R. Yates, G. L. Reeves, J. H. Smelt and A. M. A. van der Linden, *Water Air Soil Poll.*, 1999, **115**, 195–218.
- [8] H. De Ruiter, H. J. Holterman, C. Kempenaar, H. G. J. Mol, J. J. de Vlieger and J. van de Zande, *Influence of adjuvants and formulations on the emission of pesticides to the atmosphere. A literature study for the Dutch Research Programme Pesticides and the Environment (DWK) theme C-2*, 2003, Plant Research International B.V., Wageningen, Report 59.
- [9] A. M. Bozdogan and N. Y. Bozdogan, Proceedings of 7th International Symposium on Adjuvants for Agrochemicals (ISAA 2004), Cape Town, South Africa, 2004, pp. 92–98.
- [10] Y. Gil and C. Sinfort, *Atmos. Environ.*, 2005, **39**, 5183–5193.

- [11] S. Reichenberger, M. Bach, A. Skitschak and H. G. Frede, *Sci. Total Environ.*, 2007, **384**, 1–35.
- [12] FOCUS, *Landscape And Mitigation Factors In Aquatic Risk Assessment. Volume 2. Detailed Technical Reviews. Report of the FOCUS Working Group on Landscape and Mitigation Factors in Ecological Risk Assessment*, 2007, EC Document Reference SANCO/10422/2005 v.2.0. pp. 1-436.
- [13] A. S. Felsot, J. B. Unsworth, J. B. H. J. Linders, G. Roberts, D. Rautman, C. Harris and E. Carazo, *J. Environ. Sci. Heal. B*, 2010, **46**, 1–23.
- [14] G. A. Matthews, *Pestic. Sci.*, 1977, **8**, 96–100.
- [15] R. Grover, J. Maybank and K. Yoshida, *Weed Sci.*, 1972, **20**, 320–324.
- [16] ASABE, *Terminology and Definitions for Agricultural Chemical Application*, 2006, ASAE S327.2 FEB03.
- [17] T. D. Bucheli, S. R. Müller, S. Heberle and R. P. Schwarzenbach, *Environ. Sci. Technol.*, 1998, **32**, 3457–3464.
- [18] P. C. H. Miller, *Pesticide Outlook*, 2003, **14**, 205–209.
- [19] M. C. Butler Ellis and P. C. H. Miller, *Biosystems Eng.*, 2010, **107**, 169–177.
- [20] H. Ganzelmeier, D. Rautmann, R. Spagenberg, M. Streloke, M. Hermann, H. J. Wenzelburger and H. F. Walter, *Mitt. Biol. Bundesanst. Land Forstwirtsch., Berlin-Dalem*, 1995, **305**, 1–111.
- [21] D. Rautmann, M. Streloke and R. Winkler, *Mitt. Biol. Bundesanst. Land Forstwirtsch.*, 2001, **383**, 133–141.
- [22] SDRT, *Spray Drift Reduction Technology: A European Database*, <http://www.sdrt.info/>, 2012, (2 October 2012).
- [23] P. A. Hobson, P. C. H. Miller, P. J. Walklate, C. R. Tuck and N. M. Western, *J. Agr. Eng. Res.*, 1993, **54**, 293–305.
- [24] J. H. Combellack, N. M. Westen and R. G. Richardson, *Crop Prot.*, 1996, **15**, 147–152.
- [25] K. Baetens, D. Nuyttens, P. Verboven, M. De Schampheleire, B. Nicolai and H. Ramon, *Comput. Electron. Agr.*, 2007, **56**, 161–173.
- [26] H. Holterman, *Kinetics and evaporation of water drops in air*, 2003, IMAG Report 2003-12.
- [27] S. D. Murphy, P. C. H. Miller and C. S. Parkin, *J. Agr. Engin. Res.*, 2000, **75**, 127–137.
- [28] J. van de Zande, H. Stallinga, J. M. G. P. Michielsen and P. van Velde, Proceedings of the International Conference on Pesticide Application for Drift Management, Waikoloa, Hawaii, 2004, pp. 339a–339j.
- [29] D. Nuyttens, M. De Schampheleire, K. Baetens and B. Sonck, *T. ASABE*, 2007, **50**, 1129–1140.

- [30] A. H. J. Porskamp, J. M. G. P. Michielsen and J. van de Zande, *Emission-reducing pesticide application in flowerbulb growing. Drift deposition of an air-assisted field sprayer, a sprayer with shielded sprayer boom and a tunnel sprayer*, 1997, Institute of Agricultural and Environmental Engendering, Wageningen, IMAG-DLO Report 97-08, (in Dutch with English summary).
- [31] J. van de Zande, J. M. G. P. Michielsen and H. Stallinga, *Spray drift and off-field evaluation of agrochemical in the Netherlands*, 2007, Plant Research International B.V., Wageningen, Report 2007-149.
- [32] A. J. Hewitt, *Atomization Sprays*, 1997, **7**, 235–244.
- [33] P. C. H. Miller and C. R. Tuck, *J. ASTM Int.*, 2005, **2**, 1–13.
- [34] C. Stainier, M. F. Destain, B. Schiffers and F. Lebeau, *Crop Prot.*, 2006, **25**, 1238–1243.
- [35] P. C. H. Miller, Proceedings of the North American Conference on Pesticide Spray Drift Management, Portland, Maine, 1998, pp. 229–244.
- [36] P. C. H. Miller, C. R. Tuck, S. Murphy and M. da Costa Ferreira, Proceedings of 22nd European Conference on Liquid Atomization and Spray Systems (ILASS-Europe), Como Lake, Italy, 2008, pp. 1–8.
- [37] H. Guler, H. Zhu, H. Ozkan, R. Derksen, Y. Yu and C. Krause, *Trans. ASABE*, 2007, **50**, 745–754.
- [38] ISO Standard 22369-1, *Crop protection equipment - Drift classification of spraying equipment - Part 1: Classes*, 2006, Switzerland.
- [39] J. H. Combellack and P. C. H. Miller, Proceedings of 6th International Symposium on Adjuvants for Agrochemicals (ISAA 2001), Amsterdam, Netherlands, 2001, pp. 557–562.
- [40] M. C. Butler Ellis, T. Swan, P. C. H. Miller, S. Waddelow, A. Bradley and C. R. Tuck, *Bios. Eng.*, 2002, **82**, 289–296.
- [41] ISO Standard 22866, *Equipment for crop protection - Methods for field measurement of spray drift*, 2005, Switzerland.
- [42] ISO Standard 22856, *Equipment for crop protection - Methods for the laboratory measurement of spray drift - Wind tunnels*, 2008, Switzerland.
- [43] M. E. Teske, S. L. Bird, D. M. Esterly, T. B. Curbishley, S. L. Ray and S. G. Perry, *Environ. Toxicol. Chem.*, 2002, **21**, 659–671.
- [44] H. J. Holterman, J. van de Zande, H. A. J. Porskamp and J. F. M. Huijsmans, *Comput. Electron. Agri.*, 1997, **19**, 1–22.
- [45] D. M. Esterly, *Neural network analysis of spray drift task force DROPKICK IITM*, 1998, ASAE Paper No. 981014.
- [46] A. J. Hewitt, *Australian J. Ecotox.*, 2002, **8**, 7–19.
- [47] ASAE, *S-572 Spray Tip Classification by Droplet Size*, 2009, Developed by the Pest Control and Fertilizer Application Committee; approved by the Power and Machinery Division Standards Committee; adopted by ASAE PM41.
- [48] BCPC, *X-572 spray nozzle classification adopted by the ASAE*, 1998, (British Crop Protection Council).

- [49] A. C. Arnold, *Aerosol Sci. Tech.*, 1990, **12**, 431–445.
- [50] O. Permin, L. N. Jørgensen and K. Persson, *Crop Prot.*, 1992, **11**, 541 – 546.
- [51] H. Zhu, R. W. Dexter, R. D. Fox, D. L. Reichard, R. D. Brazee and H. E. Ozkan, *J. Agric. Engineering Res.*, 1997, **67**, 35–45.
- [52] C. S. Parkin, in *Application Technology for Crop Protection*, ed. G. A. Matthews and E. C. Hislop, CAB International, 1993, pp. 57–84.
- [53] A. Herbst, Proceedings of 17th Annual Conference on Liquid Atomization and Spray Systems (ILASS-Europe), Zürich, Switzerland, 2001.
- [54] W. C. Hoffmann, A. J. Hewitt, J. B. Ross, W. E. Bagley, D. E. Martin and B. K. Fritz, *J. ASTM Int.*, 2008, **5**, year.
- [55] C. R. Tuck, M. C. Butler Ellis and P. C. H. Miller, *Crop Prot.*, 1997, **16**, 619–628.
- [56] H. Göhlich, *Gesunde Pflanzen*, 1980, **32**, 25–31.
- [57] S. Uk, *Pestic. Sci.*, 1977, **8**, 501–509.
- [58] J. H. Combellack, *Crop Prot.*, 1984, **3**, 9–34.
- [59] F. R. Hall, A. C. Chapple, R. A. Downer, L. M. Kirchner and J. R. M. Thacker, *Pestic. Sci.*, 1993, **38**, 123–133.
- [60] J. A. Zabkiewicz, *Crop Prot.*, 2007, **26**, 312–319.
- [61] J. J. Spillman, *Pest. Sci.*, 1984, **15**, 97–106.
- [62] M. Knoche, *Crop Prot.*, 1994, **13**, 163 – 178.
- [63] D. C. Munthali, *Crop Prot.*, 1984, **3**, 327 – 334.
- [64] T. A. Ebert, R. A. J. Taylor, R. A. Downer and F. R. Hall, *Pestic. Sci.*, 1999, **55**, 783–789.
- [65] P. K. Jensen, L. N. Jørgensen and E. Kirknel, *Crop Prot.*, 2001, **20**, 57–64.
- [66] A. H. Lefebvre, *Atomization and Sprays*, Hemisphere publishing corporation, 1989.
- [67] A. Mansour and N. Chigier, *J. Non-Newton. Fluid Mech.*, 1995, **58**, 161–194.
- [68] R. P. Mun, J. A. Byars and D. Boger, *J. Non-Newton. Fluid Mech.*, 1998, **74**, 285–297.
- [69] N. Dombrowski and R. P. Fraser, *Philos. T. R. Soc. S. A*, 1954, **247**, 101–130.
- [70] C. G. Hermansky and G. F. Krause, Proceedings of 4th International Symposium on Adjuvants for Agrochemicals (ISAA 1995), Melbourne, Australia, 1995, pp. 20–26.
- [71] A. J. Hewitt, *Environmentalist*, 2008, **28**, 25–30.
- [72] N. B. Akesson, W. E. Steinke and W. E. Yates, *J. Environ. Sci. Health, B.*, 1994, **29**, 785–814.
- [73] M. Schmidt, *Grundl. Landtechnik*, 1980, **30**, 126 –134.
- [74] J. Ferguson, N. E. Hudson and B. C. H. Warren, *J. Non-Newton. Fluid Mech.*, 1992, **44**, 37–54.

- [75] J. L. Hazen, Proceedings of 7th International Symposium on Adjuvants for Agrochemicals (ISAA 2004), Cape Town, South Africa, 2004, pp. 105–114.
- [76] R. W. Dexter, *Atomization Spray*, 1996, **6**, 167–191.
- [77] P. A. Williams, R. J. English, R. L. Blanchard, S. A. Rose, L. Lyons and M. Whitehead, *Pest Manag. Sci.*, 2008, **64**, 497–504.
- [78] ASTM International, *Designation: E2408 - 04. Standard test method for relative extensional viscosity of agricultural spray tank mixes*, 2006.
- [79] A. Lindner, J. Vermant and D. Bonn, *Physica A*, 2003, **319**, 125–133.
- [80] S. L. Ng, R. P. Mun, D. V. Boger and D. V. James, *J. Non-Newton. Fluid Mech.*, 1996, **65**, 291–298.
- [81] G. M. Harrison, R. Mun, G. Cooper and D. V. Boger, *J. Non-Newton. Fluid Mech.*, 1999, **85**, 93–104.
- [82] R. P. Mun, B. W. Young and D. V. Boger, *J. Non-Newtonian Fluid Mech.*, 1999, **83**, 163–178.
- [83] R. W. Dexter, in *Pesticide formulations and application systems*, ed. A. K. Viets, R. S. Tann and J. C. Mueninghoff, American Society of Testing and Materials, West Conshohocken, PA, 2001, vol. 20, pp. 27–43.
- [84] Y. Amarouchene, D. Bonn, J. Meunier and H. Kellay, *Phys. Rev. Lett.*, 2001, **86**, 3558–3561.
- [85] P. Dontula, M. Pasquali, L. E. Scriven and C. W. Macosko, *Rheol. Acta*, 1997, **36**, 429–448.
- [86] J. R. Eastman, J. W. Goodwin and A. M. Howe, *Colloid Surface A*, 2000, **161**, 329–338.
- [87] D. F. James and D. R. McLaren, *J. Fluid Mech.*, 1975, **70**, 733–752.
- [88] F. Durst and R. Haas, *Rheol. Acta*, 1981, **20**, 179–192.
- [89] T. Lim, J. T. Uhl and R. K. Prud'homme, *SPE Reservoir Eng.*, 1986, **16**, 272–276.
- [90] R. P. Fraser, P. Eisenklam, N. Dombrowski and D. Hasson, *AIChE J.*, 1962, **8**, 672–680.
- [91] M. D. Cloeter, K. Qin, P. Patil and B. Smith, Proceedings of 22nd Annual Conference on Liquid Atomization and Spray Systems (ILASS-Americas), Cincinnati, OH, USA, 2010, pp. 1–9.
- [92] H. Zhu, R. D. Brazee, D. L. Reichard, R. D. Fox, C. R. Krause and A. C. Chapple, *Atomization Spray*, 1995, **5**, 343–356.
- [93] K. Qin, H. Tank, S. Wilson, B. Downer and L. Liu, *Atomization Spray*, 2010, **20**, 227–239.
- [94] D. L. Reichard, H. Zhu, R. A. Downer, R. D. Fox, R. D. Brazee, H. E. Ozkan and F. R. Hall, *T. ASAE*, 1993, **36**, 1993–1999.
- [95] R. A. Downer, T. M. Wolf, A. C. Chapple, F. R. Hall and J. L. Hazen, Proceedings of 4th International Symposium on Adjuvants for Agrochemicals (ISAA 1995), Melbourne, Australia, 1995, pp. 138–143.

- [96] A. J. Hewitt, Proceedings of 5th International Symposium on Adjuvants for Agrochemicals (ISAA 1998), Memphis, Tennessee, 1998, pp. 451–462.
- [97] M. C. Butler Ellis, C. R. Tuck and P. C. H. Miller, *Colloid Surface A*, 2001, **180**, 267–276.
- [98] M. Butler Ellis and C. Tuck, *Aspects Appl. Biol.*, 2000, **53**, 155–162.
- [99] J. L. Hazen, *Weed Technol.*, 2000, **14**, 773–784.
- [100] N. H. Anderson, D. J. Hall and D. Seaman, *Aspects Appl. Biol.*, 1987, **14**, 233–243.
- [101] N. H. Anderson and D. J. Hall, in *Adjuvants and Agro-chemicals*, ed. P. N. P. Chow, C. A. Grant, A. M. Hinshalwood and E. Simundsson, CRC Press, Boca Raton, FL, 1989, vol. 2, pp. 51–62.
- [102] P. J. G. Stevens, M. O. Kimberley, D. S. Murphy and G. A. Policello, *Pestic. Sci.*, 1993, **38**, 237–245.
- [103] M. C. Butler Ellis, C. R. Tuck and P. C. H. Miller, *Crop Prot.*, 1997, **16**, 41–50.
- [104] R. A. Downer, F. R. Hall and R. S. Thompson, *Atomization Spray*, 1998, **8**, 241–254.
- [105] P. C. H. Miller, M. C. Butler Ellis and C. R. Tuck, Proceedings of 4th International Symposium on Adjuvants for Agrochemicals (ISAA 1995), Melbourne, Australia, 1995, pp. 95–102.
- [106] M. C. Butler Ellis and C. R. Tuck, *Crop Prot.*, 1999, **18**, 101–109.
- [107] M. C. Butler Ellis, C. R. Tuck and P. C. H. Miller, *Atomization Spray*, 1999, **9**, 385–397.
- [108] N. M. Western, E. C. Hislop, M. Bieswal, P. J. Holloway and D. Coupland, *Pestic. Sci.*, 1999, **55**, 640–642.
- [109] P. C. H. Miller and M. C. Butler Ellis, *Crop Prot.*, 2000, **19**, 609 – 615.
- [110] E. Hilz, A. W. P. Vermeer, F. A. M. Leermakers and M. A. Cohen Stuart, *Aspects Appl. Biol.*, 2012, **114**, 71–78.
- [111] O. Nicetic, G. Dorr, N. Woods and G. A. C. Beattie, Proceedings of 7th International Symposium on Adjuvants for Agrochemicals (ISAA 2004), Cape Town, South Africa, 2004, pp. 136–142.
- [112] P. Spanoghe, M. De Schampheleire, P. Van der Meeren and W. Steurbaut, *Pest Manag. Sci.*, 2007, **63**, 4–16.
- [113] N. Dombrowski and W. R. Johns, *Chem. Engin. Sci.*, 1963, **18**, 203–214.
- [114] M. C. Butler Ellis and A. Bradley, *Aspects Appl. Biol.*, 2002, **66**, 251–258.
- [115] P. McMullan, S. Thurman, G. McManic and M. Brigance, *J. ASTM Int.*, 2006, **3**, 1–6.
- [116] M. C. Butler Ellis, P. C. H. Miller, D. E. Baker, J. D. Lane and C. R. Tuck, Proceedings of 5th International Symposium on Adjuvants for Agrochemicals (ISAA 1998), Memphis, Tennessee, 1998, pp. 389–394.
- [117] E. Hilz and A. W. P. Vermeer, *Aspects Appl. Biol.*, 2012, **114**, 445–450.
- [118] S. C. K. Carlsen, N. H. Spliid and B. Svensmark, *Chemosphere*, 2006, **64**, 778–786.

- [119] CropLife International, *Catalogue of pesticide formulation types and international coding system*, 2008, Technical Monograph n2, 6th Edition, Brussels.
- [120] M. C. Butler Ellis and C. R. Tuck, *Aspect. Appl. Biol.*, 1997, pp. 105–112.

Chapter 3

The breakup of a liquid sheet during spray atomization

Perforation is the typical spray formation mechanism initiated by dilute oil-in-water emulsions which is associated with the formation of coarser sprays compared to sprays produced with water when using a conventional flat fan nozzle. In this Chapter the nucleation of holes is investigated along with processes that precede the perforation onset in dilute emulsions. Investigations are carried out with Computational Fluid Dynamics (CFD) modelling using ANSYS FLUENT software to simulate the fate of an emulsion drop in a liquid sheet close before breakup. Furthermore, microscopic observations of dilute emulsions are carried out under static conditions. Both computational and experimental studies show that an emulsion droplet, when merging with the air/water interface, induces perturbations within the bulk liquid and at its interface. These observations imply that perforation is closely linked to the entering of emulsion droplets at the interface of the liquid sheet.

3.1 Introduction

During spray applications fine spray droplets can be carried from the application site by crosswind and cause off-target contamination with agrochemicals. This downwind movement of airborne spray beyond the intended area of application originating from aerial or ground-based spraying operations is defined as spray drift.¹ Spray drift is usually correlated with the fine spray fraction that contains droplets with diameter $< 100 \mu\text{m}$.²⁻⁴ Therefore, spray drift reduction can be achieved by reducing the fraction of fine spray droplets.⁵

When spray liquid is atomized through a flat fan nozzle, it forms a liquid sheet which subsequently breaks up into filaments. In a next step, these filaments disrupt into spray droplets. The development of the liquid sheet and its breakup, both depend on the ejecting velocity, the size of the orifice, the nozzle design, physical properties of the spray liquid and the ambient gas.⁶ The physical properties can be modified through tank-mix additives and through formulated "ready-to-use" products. To be able to develop such products, it is important to understand the effects and interactions induced by different compounds.

During a spray application, spray liquid is pressed under pressure through the atomizer which is often a hydraulic flat fan nozzle. Spray liquid exits the nozzle in form of a sheet that expands below the nozzle outlet due to ejecting velocity. Surface tension counteracts this process by holding the sheet together.⁶ At a point when the aerodynamic forces exceed the interfacial forces, sinuous waves are formed that propagate with increasing amplitude. The sheet breaks up when the instability wave length is larger than the minimal disturbance wave length $\lambda_{\text{min}} = (2\pi\gamma)/(\rho_a\nu^2)$; with γ the surface tension of the applied liquid, ρ_a the air density and ν the relative velocity between liquid and air. On the other hand, turbulences below certain Reynolds and Weber numbers can reduce the growth of capillary waves at the interface, exerting a stabilizing effect.⁷

The typical exit velocity of the sheet ranges between 10 – 25 m/s depending on the orifice dimensions and design, the operating pressure and the position in the cross section of the liquid sheet.⁸⁻¹¹ The sheet length decreases with increasing relative velocity between the liquid and the gas (or with increasing operating pressure).⁹

The modes of sheet breakup were studied with flash photography by Dombrowski and Fraser.⁸ They outlined that the most stable and resistant sheets are formed by liquids with high surface tension, high viscosity, low density and at low flow turbulences. The spray droplet size was observed to decrease with increasing

spray pressure and increasing density of the ambient gas. However, the effect of the liquid density was reported to be small. Photographs showed that the sheet disintegrates either through oscillation that is caused by air friction or by perforation.

Sheet breakup caused by oscillation of the liquid sheet is greatly affected by the surface tension and by the viscosity of the liquid. The decrease of the surface tension was observed to increase the growth rate of instabilities at the interface of a liquid.^{8,12} A lower surface tension allows the sheet to expand and antennae-like structures are formed at its rim. With increasing viscosity of the spray liquid, a more placid sheet emerges that can sustain the wave motions and lower the contraction velocity.⁸ In an air-blast atomizer, the film thickness at the atomizing edge was estimated to increase with the increase in the viscosity of spray liquid.¹³

The perforation mechanism can be induced by dilute oil-in-water emulsions.⁵ In this breakup mode point disturbances in the sheet lead to the development of holes that grow in size and form a network of unstable ligaments that subsequently disrupt into spray droplets. It has been shown that perforation can be induced for a pure liquid in vacuum, in the absence of air/liquid friction⁹ or by a hot gas atmosphere.¹⁴ The growth of the perforation radius was investigated⁹ as well as the length of the sheet formed in the perforation mode.¹⁵ Perforation occurs at shorter distances from the nozzle where the thickness of the liquid sheet is higher and, therefore, sprays created by perforation are typically coarser than those produced with water alone. Perforation was also observed when worm-like micelle solutions are atomized through a flat fan and a hollow cone nozzle.¹⁶ Thereby, the number of perforation holes increased with increasing Weber number and increasing spray angle.

Initially, it has been suggested that hydrophobic particles such as wax suspensions cause perforation and that hole formation is induced at high flow turbulences.^{8,17} The origin of hole formation was explained by the puncture of a particle through the liquid sheet when its diameter equals to the sheet thickness.⁸ This hypothesis was contradicted by more recent studies on dilute emulsions.^{15,18} On the contrary, only deformable emulsion droplets were observed to induce perforation. It was hypothesised that if an emulsion droplet deforms in the flow, its water/oil interface becomes temporary hydrophobic. This hydrophobic region may interact with the local sheet perturbations and induce hole formation.¹⁵ It was also suggested that emulsion droplets with a temporary hydrophobic interface may diffuse to the air/water interface of the liquid sheet acting there as weak points and, thus, inducing perforation onset.¹⁸ It was further observed that the breakup length of the

liquid sheet decreases and the spray droplet size increases with increasing number of emulsion droplets.¹⁵

Dilute oil-in-water emulsion produce coarser sprays than water when atomized through a conventional flat fan nozzle.¹⁹ Therefore, it is of a particular interest to comprehend what parameters and properties of dilute emulsions regulate an early atomization onset and the associated spray coarsening. The breakup of the liquid sheet is a highly dynamic process and it is not yet possible to perform experiments at such dynamic conditions. One way to investigate these systems is by executing experimental studies under static or less dynamic conditions or by using computational modelling.

Here, we apply the Computational Fluid Dynamics to simulate processes at sheet breakup in the presence of an emulsion droplet. Based on the conclusions from investigations described in literature, we want to set up a possible scenario at perforation onset by placing an oil droplet with a hydrophobic oil/water surface at the interface of a liquid sheet. In this set-up it is possible to observe interfacial perturbations caused by an oil droplet and to study if these perturbations may induce the nucleation of perforation.

Further, we performed experiments under static conditions observing emulsion droplets entering an air/water interface. The entering event is accompanied by a fast spreading of the emulsion droplet at the interface from the bulk liquid phase. Microscopic observations allow tracking the movements of a satellite droplet in the bulk liquid phase during entering and spreading processes at the interface and tell more about the consequences implicated by these processes.

3.2 Material and Methods

3.2.1 Modelling

Computational Fluid Dynamics (CFD) are performed using the flow modelling simulation software ANSYS FLUENT 13.0 applying the Volume of Fluid (VOF) model theory.²⁰ VOF model is dominated by the surface tension effects and allows to observe movements of different volume fraction through the lattice in a multi-phase regime. One of the typical application of this model is the calculation of jet breakup.

A sessile oil droplet was modelled in a two-dimensional lattice without influence of the gravitational force, analysing a liquid sheet with an equal thickness without an initial subphase flow. The lattice is divided in sites of $7.8 \times 5.0 \mu\text{m}$ at the edge

and has a finer structure in the vicinity of the oil drop with cells of $1.56 \times 1.56 \mu\text{m}$. In this set-up, the water sheet has a thickness of $100 \mu\text{m}$ and a length of 2 mm . The oil drop diameter was set as $10 \mu\text{m}$, an order of magnitude smaller than the sheet thickness. Focusing on one small section, the model simplifies experimental conditions and provides a rather qualitative description of the system.

Parameters that were chosen to set up the system are collected in table 3.1. The interfacial tension at the air/water interface was set as $\gamma_{AW} = 72 \text{ mN/m}$. Oil 1 has interfacial tensions of $\gamma_{OW} = 28 \text{ mN/m}$ at the oil/water and $\gamma_{AO} = 44 \text{ mN/m}$ at the air/oil interfaces. Oil 2 has interfacial tensions of $\gamma_{OW} = 33 \text{ mN/m}$ and $\gamma_{AO} = 22 \text{ mN/m}$. The classical spreading coefficient $S = \gamma_{AW} - \gamma_{OW} - \gamma_{AO}$ ²¹ describes the tendency of the oil to spread over the air/water interface. The interfacial tensions were chosen such that oil 2 has a positive initial spreading coefficient. The spreading coefficient of oil 1 is zero. When $S > 0$, the oil will wet the interface until it reaches equilibrium conditions. $S = 0$ implies that this oil will stay at the interface in the form of a lens.

Table 3.1: Parameters for the CFD modelling.

	air	water	oil 1	oil 2
$\rho \text{ [kg/m}^3\text{]}$	1.2	1000	830	920
$\eta \text{ [mPas]}$	0.018	1	6	61

3.2.2 Experiments

A cell was constructed to observe the behaviour of emulsion droplets which move close to an air/water interface. As shown in figure 3.1, the cell consists of two cover slips $15 \times 15 \text{ mm}$ attached to glass capillary tubes with a diameter of 1 mm . The cell was filled with 0.001% w/w solution of anionic surfactant (sodium C8-ether sulphate supplied by AkzoNobel) before emulsion was added to inside. One cell was used for one experiment.

The emulsion was prepared from a stock solution of a (1/10) mixture of sunflower oil (purchased by John L. Seaton & Co. Ltd.) with Arlatone TV emulsifier (purchased by Croda). The emulsion was diluted in pure water and homogenized by shaking. The emulsion concentration was chosen such that single emulsion droplets are clearly visible under the microscope.

Digital Microscope Keyence VHX 600 with a VH-Z 100R (100-1000x zoom) objective was used to observe the entering process at the air/water interface. After

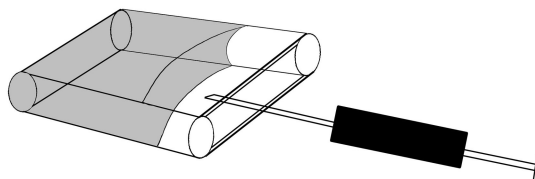


Figure 3.1: A schematic picture of the microscopy cell filled with surfactant solution. A dilute emulsion is added through the open side of the cell with a syringe.

the focus was set at the interface, the dilute oil-in-water emulsion was added with a syringe through the open cell side as shown in figure 3.1. The system was recorded with a frequency of 27 frames per second and the film was subsequently cut into snapshots.

The interfacial tension at the air/water interface of the 0.001% w/w surfactant solution was measured as 64.5 mN/m with a Prozessor-Tensiometer K100 (Krüss GmbH) using the Wilhelmy plate method.

3.3 Results and Discussion

3.3.1 Modelling

A dilute oil-in-water emulsion used in agricultural applications contains a large number of emulsion droplets. Most of these droplets will remain submerged in the bulk liquid of the formed sheet during the spraying process. Being surrounded by the bulk liquid, emulsion droplets can elongate in the shear flow induced in the nozzle.^{11,22} It is known that emulsion droplets have an effect on the stability of multiphase systems when they are located at the air/water interface.^{23,24} Being at the interface, these droplets will behave in a complete different way as those in the bulk. This scenario is also plausible for the situation, when spray liquid emerges from the nozzle. A limited number of entering events might suffice to alter the behaviour of the liquid sheet and to induce perforation. Thus, Computational Fluid Dynamic simulations have been applied to analyse changes in dynamic behaviour of a liquid film induced by a sessile oil droplet.

The lattice used in CFD simulations contains a water film which represents a sheet of a spray liquid. The water film is placed horizontally in the middle of the lattice, encompassed by two air phases. First, the situation without an oil droplet was studied. As is illustrated in figure 3.2, a disturbance is slowly growing at the

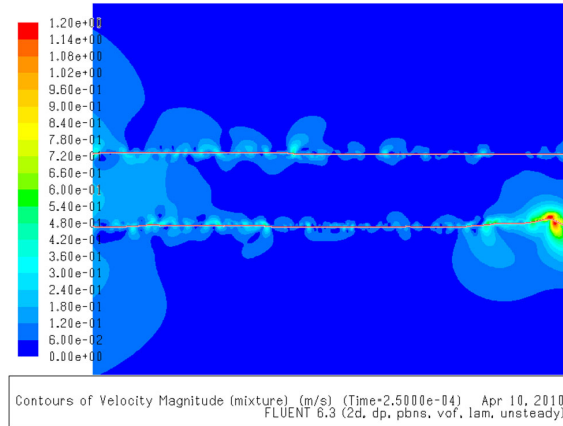


Figure 3.2: Interfacial distortions of a liquid sheet after a simulation time of $250 \mu\text{s}$.

edge of the liquid film with elapsing time. Figure 3.2 shows a contour plot of the velocity magnitude in the oil-free system after a simulation time of $250 \mu\text{s}$. The simulation lattice is subdivided in cells of a different size and dimension and the relationship between both sites of a cell is the highest at the edge of the grid. This might facilitate the disturbance growth of the liquid film close to the edge.

Figure 3.3 shows a velocity contour plot with disturbances developing when a droplet of oil 1 is placed at the interface. As illustrated in figure 3.3a, the interface of the liquid film begins to deform after a few μs . Deformations growth with time having the highest deformation magnitude at $250 \mu\text{s}$ (figure 3.3c).

Figure 3.4 illustrates perturbations of the liquid film caused by a sessile droplet of oil 2. The disturbances initiated by the second oil droplet are significantly higher at each time step. The lower interface begins to deform already after $100 \mu\text{s}$ while deformations caused by the drop of oil 1 did not reach the lowest interface of the water film even after simulation time of $250 \mu\text{s}$. Deformations caused by oil 2 grow with time and two necking points occur at the edge of the lattice at $\approx 150 \mu\text{s}$. Calculations performed for a time period of $500 \mu\text{s}$ show that at $420 \mu\text{s}$ oil 2 causes a complete film disruption at one of the necking points.

The velocity vectors of the subphase liquid and the surround air caused by the oil 2 drop are depicted in figure 3.5. Vector directions indicate an inward flow within the water film from the bulk towards the oil drop with a subsequent local thinning of the underlying subphase at both sides of the droplet. The vector direction might not represent the flow direction in a real situation because of the absence of

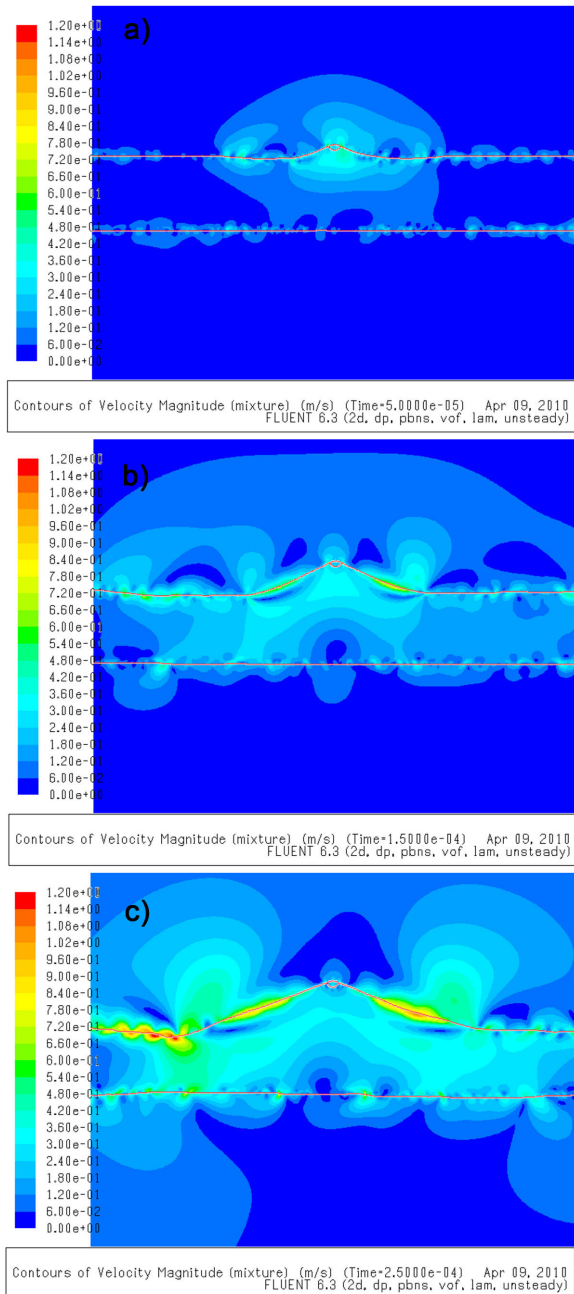


Figure 3.3: Interfacial distortions of a liquid sheet induced by the oil 1 drop after a simulation time of a) $50 \mu\text{s}$, b) $150 \mu\text{s}$, c) $250 \mu\text{s}$.

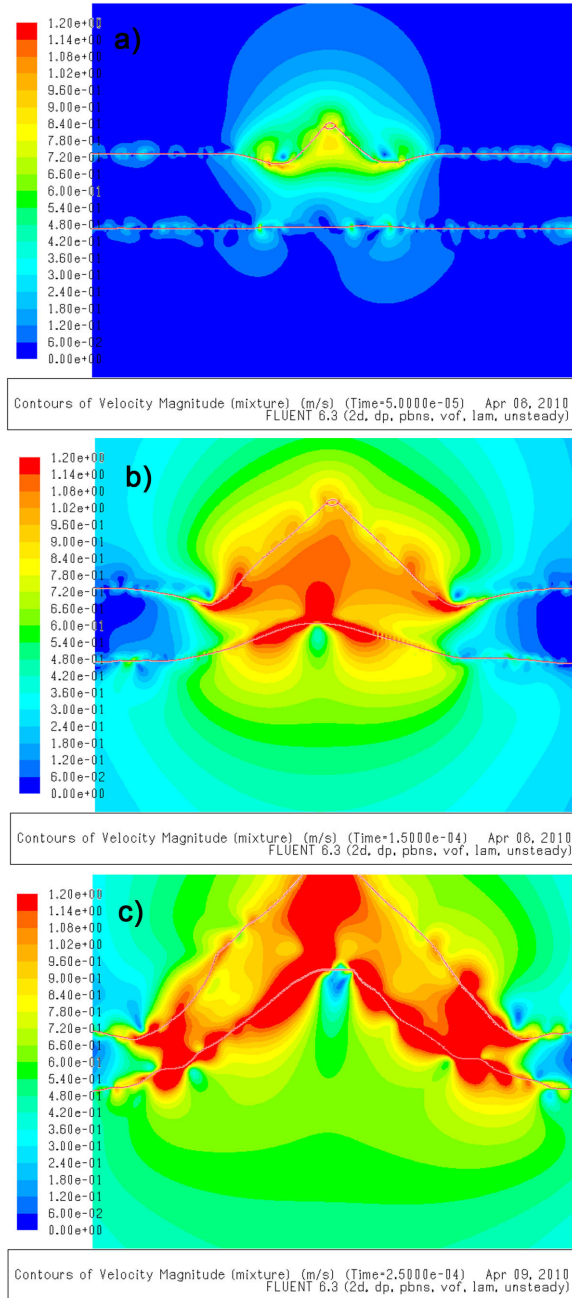


Figure 3.4: Interfacial distortions of a liquid sheet induced by the oil 2 drop after a simulation time of a) $50 \mu\text{s}$, b) $150 \mu\text{s}$, c) $250 \mu\text{s}$.

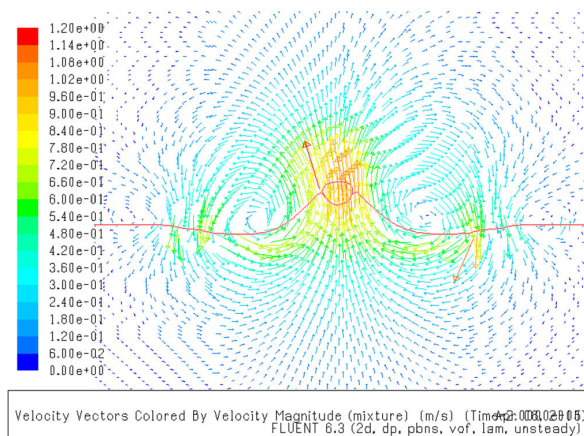


Figure 3.5: Velocity profiles around the oil 2 drop after a simulation time of $20 \mu\text{s}$. The colours indicate the magnitude of the velocity vectors.

gravitational forces in the simulation parameters. However, the calculations reveal that significant disturbances of a liquid film can be induced by an oil droplet at the interface and that the magnitude of these disturbances depends on physical properties of the oil.

A liquid sheet produced through a flat fat nozzle was observed to break up 1.7 - 2.2 ms after being formed.²⁵ The calculated time at breakup of a liquid film is shorter than the breakup times obtained experimentally. The differences might be caused by approximations used in the modelled system.

It would be expected that an oil drop placed at the air/water interface will spread due to a surface tension gradient. The spreading is not obvious in the simulation studies, however, the oil droplet that was initially placed in the lattice as a cubic structure deforms with time aiming to adapt a lens-like shape.

3.3.2 Experiments

One mechanism of the action of antifoam globules suggests that oil droplets when entering the interface of a liquid film can destroy it through spreading.²³ The spreading process induces fluid entrainment of the subsurface which can lead to film thinning and is subsequent rupture. The initiated subphase flow can be sufficiently strong to move satellite emulsion droplets from the bulk region within the liquid film towards its interface.²⁶ Moreover, emulsion droplets that enter the air/water interface may consequently spread reinforcing the entering process of

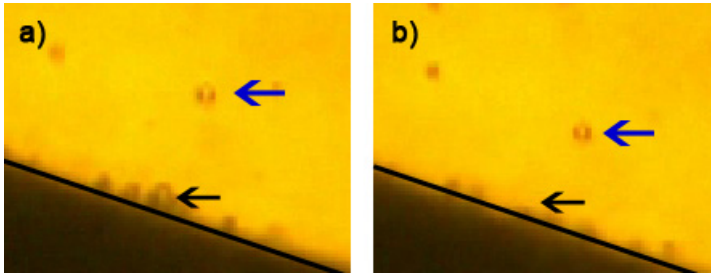


Figure 3.6: The entering of an emulsion droplet at the air/water interface causes an subphase flow that moves a satellite droplet (blue arrow) closer to the interface. Emulsion droplet diameter $\approx 2 \mu\text{m}$.

emulsion droplet from the bulk.²⁷

Inspired by the observations from earlier research studies mentioned above, the behaviour of emulsion droplets at the air/water interface was investigated under light microscope. Using the set-up illustrated in figure 3.1, it was possible to capture an entering/spreading event of an emulsion droplet at an air/water interface.

The air/water interface of the liquid is covered with surfactants that lower the surface tension down to 64.5 mN/m . Probably when 3.6a was made, some oil droplets have already spread over the interface through previous entering events that have not been captured with the camera. As shown in figure 3.6a several droplets are located in the bulk liquid close to the air/water interface. The air/water interface is marked by a black line. A black arrow points at an emulsion droplet which is close to the air/water interface shortly before entering. Upon entering the interface, this emulsion droplet spreads immediately. Figure 3.6b shows the situation 36 ms after the situation illustrated in figure 3.6a. The spreading of an emulsion droplet at the interface corresponds to a jump-like movement of the satellite drop which is indicated by the blue arrow. Within time between both snapshots, the satellite emulsion droplet moved closer to the interface.

More such events have been observed. We want to note, that it is not possible to estimate the exact time scale for the movement of the satellite droplet due to limitations set by the frame rate of the camera used.

3.4 Conclusions

Computational Fluid Dynamics simulations have been performed to study interactions that may initiate perforation during atomization of dilute emulsions. A

simplified model of the film surrounded by air with an oil droplet placed at the air/water interface was used as a system that represents a section of the liquid sheet. The simulations show that a sessile oil droplet initiates perturbations at the interface that rapidly grow over the whole liquid film resulting in its rupture. Such disturbances reinforced by the oscillation of the liquid sheet may induce perforation in sprays produced by a flat fan nozzle. It was clearly shown that the magnitude of the perturbation depends on the physical properties of the oil such as viscosity, density, and interfacial tensions between the three phases oil/water/air.

Experimental studies show that if an emulsion droplet approaches an air/water interface close enough, it will merge with it. The subphase flow, initiated by this event, can be visualized through movements of a satellite emulsion droplet in the vicinity. The entering event moves a satellite droplet in a jump-like manner closer to the interface.

Both these studies show that the presence of an oil or an emulsion droplet at the interface of a liquid film causes turbulence growth within this film which can result in its breakup. Disturbances induced by an emulsion droplet can lead to perforation when reinforced by the flow turbulences and oscillations at high liquid velocities. The magnitude of the induced disturbances depends on the physical characteristics of the oil such as the interfacial tensions with adjacent phases, viscosity, and the emulsion droplet size relative to the film thickness. The limiting step in this process appears to be the entering frequency of emulsion droplet at the air/water interface which requires further investigations.

References

- [1] G. R. Stephenson, I. G. Ferris, P. T. Holland and M. Nordberg, *Pure Appl. Chem.*, 2006, **78**, 2075–2154.
- [2] P. A. Hobson, P. C. H. Miller, P. J. Walklate, C. R. Tuck and N. M. Western, *J. Agr. Eng. Res.*, 1993, **54**, 293–305.
- [3] H. De Ruiter, H. J. Holterman, C. Kempenaar, H. G. J. Mol, J. J. de Vlieger and J. van de Zande, *Influence of adjuvants and formulations on the emission of pesticides to the atmosphere. A literature study for the Dutch Research Programme Pesticides and the Environment (DWK) theme C-2*, 2003, Plant Research International B.V., Wageningen, Report 59.
- [4] P. C. H. Miller, *Pesticide Outlook*, 2003, **14**, 205–209.
- [5] E. Hilz and A. W. P. Vermeer, *Crop. Prot.*, 2013, **44**, 75–83.
- [6] A. H. Lefebvre, *Atomization and Sprays*, Hemisphere publishing corporation, 1989.
- [7] K. Heukelbach, S. Jakirlić, R. Nakić and C. Tropea, Proceedings of 18th European Conference on Liquid Atomization and Spray Systems (ILASS-Europe).

- [8] N. Dombrowski and R. P. Fraser, *Philos. T. R. Soc. S. A*, 1954, **247**, 101–130.
- [9] R. P. Fraser, P. Eisenklam, N. Dombrowski and D. Hasson, *AIChE J.*, 1962, **8**, 672–680.
- [10] M. D. Cloeter, K. Qin, P. Patil and B. Smith, Proceedings of 22nd Annual Conference on Liquid Atomization and Spray Systems (ILASS-Americas), Cincinnati, OH, USA, 2010, pp. 1–9.
- [11] H. Zhu, R. D. Brazee, D. L. Reichard, R. D. Fox, C. R. Krause and A. C. Chapple, *Atomization Spray*, 1995, **5**, 343–356.
- [12] R. H. Rangel and W. A. Sirignano, *Phys. Fluids*, 1988, **31**, 1845–1855.
- [13] N. K. Rizk and A. H. Lefebvre, *T. ASME*, 1980, **102**, 706–710.
- [14] N. Dombrowski, D. Hasson and D. E. Ward, The proceedings of the Brighton Crop Protection Conference - Weeds, 1989, pp. 663–668.
- [15] M. C. Butler Ellis, C. R. Tuck and P. C. H. Miller, *Atomization Spray*, 1999, **9**, 385–397.
- [16] J. C. Thompson and J. P. Rothstein, *J. Non-Newton. Fluid Mech.*, 2007, **147**, 11–22.
- [17] R. P. Fraser and P. Eisenklam, *Imp. Coll. Chem. Eng. Soc. J.*, 1953, **7**, 52–68.
- [18] R. W. Dexter, in *Pesticide formulations and application systems*, ed. A. K. Viets, R. S. Tann and J. C. Mueninghoff, American Society of Testing and Materials, West Conshohocken, PA, 2001, vol. 20, pp. 27–43.
- [19] P. C. H. Miller and C. R. Tuck, *J. ASTM Int.*, 2005, **2**, 1–13.
- [20] M. Bierdel, *Zerfall einer ruhenden Wasserlamelle in Tropfen*, Bayer Technology Services, 2010.
- [21] W. D. Harkins and A. Feldman, *J. Am. Chem. Soc.*, 1922, **44**, 2665–2685.
- [22] K. Qin, H. Tank, S. Wilson, B. Downer and L. Liu, *Atomization Spray*, 2010, **20**, 227–239.
- [23] V. Bergeron, P. Cooper, J. Giermanska-Kahn, D. Langevin and A. Pouchelon, *Colloid Surface A*, 1997, **112**, 103–120.
- [24] O. E. Jensen, *J. Fluid Mech.*, 1995, **293**, 349–378.
- [25] M. C. Butler Ellis, C. R. Tuck and P. C. H. Miller, *Colloid Surface A*, 2001, **180**, 267–276.
- [26] J. Venzmer, R. Haensel and C. Penz, *Chem. unserer Zeit*, 2008, **42**, 72–79.
- [27] N. E. Hotrum, T. van Vliet, M. A. Cohen Stuart and G. A. van Aken, *J. Colloid Interf. Sci.*, 2002, **247**, 125–131.

Chapter 4

A Self-Consistent Field study of a hydrocarbon droplet at the air-water interface

In this Chapter, a molecularly detailed self-consistent field (SCF) approach is applied to describe a sessile hydrocarbon droplet placed at the air-water interface. We elaborate on this model and show that the nano-scale droplet, which is described in the SCF approach, is representative for macroscopic droplets and that the method can be used to efficiently generate accurate information on the spreading of oil droplets at the air-water interface in molecularly more complex situations.

This Chapter is published as:

E. Hilz, F. A. M. Leemakers, A. W. P. Vermeer, A self-consistent field study of a hydrocarbon droplet at the air–water interface. *Physical Chemistry Chemical Physics*, **2011**, *14*, 4917-4926.

4.1 Introduction

Three-phase colloidal systems are commonly used for commercial applications. For instance, emulsions are suitable for diverse industrial processes such as formulation and development of food, cosmetics, pharmaceutical or agricultural products. In order to gain a better understanding for such complex mixtures on a molecular level, it is of a particular interest to develop an approach that can describe the physical properties of the system by modifying the chemical structure of its single components. In the case of industrial mixtures, the content and the concentration of single components are accessible parameters rather than their detailed thermodynamic properties. Though, simulations allow a better insight into experimental findings, at the same time, they are computationally extremely expensive and it is particularly hard to compute the relevant thermodynamic quantities and/or to study large systems. In this paper we elaborate on a molecularly detailed self-consistent field (SCF) approach. The method gives accurate information on the thermodynamic quantities in a system with less computational effort compared to MD and MC simulations. With this approach we aim to improve the understanding of interfacial processes of complex multinary systems and to outline the relevant aspects of the phase behavior while providing a molecular access to its single compounds. Of a particular interest is to model emulsions and emulsion-surfactant mixtures in an environment with an existing air-water interface.

The shape of the hydrocarbon drop is typically defined by the air-liquid interface and is experimentally accessible by the macroscopic contact angles. In the case of a liquid drop on a solid substrate the air-liquid interfacial tension and the properties of the solid substrate such as roughness, molecular structure, charges if present, etcetera, influence the shape of the drop. For systems with three deformable interfaces, such as oil droplets at the air-water interface, all three interfacial tensions become relevant.^{1,2} When the oil droplet spreads completely; there are just two interfaces, namely that between water and oil and between oil and air. In contrast to this situation, partial spreading occurs when the drop adopts a lens-like shape at the air-water interface with a stable contact line where three phases with defined contact angles come together. For a sufficiently large droplet the triple (contact) line is rather straight on the molecular level and its curvature dependence can be neglected.

The situation may become more complex for nano-scale droplets, e.g. when oil droplets of an oil-in-water emulsion adsorb onto the air-water interface. Non-trivial aspects, such as interfacial forces near the triple line, have to be considered

for such sessile droplets.³ In this case a non-zero Laplace pressure exists and the interfacial tensions as well as the line tension have a certain curvature dependence. Consequently, for a highly curved contact line, the microscopic contact angle may deviate from its macroscopic value, inserting some distortion of the interface in the transition region.⁴ On the molecular level, not the interfacial tensions, but rather the molecular characteristics are the relevant parameters that logically implement interfacial phenomena. Our interest is in understanding how the droplets accommodate at the air-water interface and how the molecular composition, the molecular architectures and the interactions influence the shape and position of the droplets at the interface. Our strategy is therefore to focus on the nanoscale aspects of these systems, addressing the complications that may occur due to the finite size of the droplets.

The wetting behavior of oil droplets at liquid-liquid interface as well as calculations of the macroscopic contact angles have been performed earlier with molecular dynamics (MD).⁵ Moreover, MD and Monte Carlo (MC) simulation approaches exist that describe how fluid droplets adsorb at planar solid substrates⁶⁻⁸ or follow the wetting phenomena of three-phase systems.⁹ Some molecular simulations were dedicated to extract the line tension contribution from interfacial forces of sessile droplets.^{10,11} As shown below, it is possible to deal with all relevant aspects for nano-scale droplets at the air-water interface and evaluate the thermodynamics very accurately, albeit on a mean field level. We will show that the accuracy is comparable. The type of approximations is elaborated on in the appendix where the method is described. The discretization scheme of Scheutjens and Fler (SF) has been used to solve the SCF equations. In this scheme the molecules are segmented in such a way that each segment matches the size of a cell on the lattice.¹²⁻¹⁴ The lattice geometries can be adapted to the symmetry of the system and the problem statement which it aims to analyse. The one-gradient flat geometry is used to characterize the properties of macroscopic liquid-liquid interfaces, while two-gradient geometries are appropriate to study the curvature dependences of interfacial forces, as will be discussed in details later. The SF-SCF approach is typically used to describe self-assembly phenomena of amphiphilic molecules into association colloids, e.g. micellization or bilayer structures.¹⁵⁻²⁰ However, the SF-SCF theory has not yet been elaborated for liquid drops in between two different fluid phases. Predictions of both the macroscopic as well as nano-scale physical properties are possible from the molecularly simple system of a one-component sessile oil-droplet, placed at the air-water interface. The SCF-method which is not limited to a simple system will be evaluated, outlining its strengths (and weak-

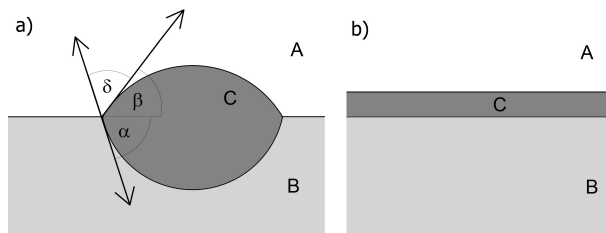


Figure 4.1: A three-phase system in (a) a partial-wetting state characterized by the three contact angles α , β , γ and (b) a complete wetting regime.

nesses). The compact SCF-model presented here is very much appropriate to study sessile liquid drops of different chemistry. It accounts for the thermodynamic properties such as interfacial tension and its curvature dependence and on the other hand provides an easy access to the molecular structure of the wetting phase. As a forecast outlining the possibilities of the developed model, we will give a short example of a four-component system that includes an oil/surfactant mixture. A non-ionic surfactant adsorbing preferable at one of the interfaces can change the shape and the thermodynamic properties of the sessile drop. Adding a new molecular component to the system is a simple way to modify the wetting behavior of the oil drop. In future work we plan to address the influence of various surfactant molecules and study how the molecular structure, composition and corresponding interactions influences the wetting characteristics of an oil drop.

4.2 Small droplets

When a liquid droplet is placed onto an air-liquid interface, it either adopts a lens-like shape with finite contact angles or covers the complete interface by a macroscopically thick film (figure 4.1).

Spreading of liquids on a fluid interface is described by the contact angles in two equilibrium states when the liquid partly wets the interface building a lens and when it spreads completely. These two equilibrium states are defined as partial wetting for $\alpha + \beta > 0$ or as complete wetting state when $\alpha + \beta = 0$, whereby the contact angles define the lens shape at the interface. The transition from partial to complete wetting is a true phase transitions, whereby an interface disappears. The case of a droplet spreading over a solid interface with $\alpha = 0$ is described by Young's equation. The Neumann's equation, which is the Young's equation for deformable surfaces, relates the surface tensions with the contact angles for droplet at a liquid

interface. Three interfacial tensions can be defined from this equation as follows:²¹

$$\gamma_{AB} = \gamma_{BC} \cos \alpha + \gamma_{AC} \cos \beta \quad (4.1)$$

$$\gamma_{AC} = \gamma_{BC} \cos \alpha + \gamma_{AB} \cos \delta \quad (4.2)$$

$$\gamma_{BC} = \gamma_{AC} \cos \beta + \gamma_{AB} \cos \delta \quad (4.3)$$

Knowing the interfacial tensions, the angles α and β are given by:

$$\cos \alpha = \frac{\gamma_{AB}^2 + \gamma_{BC}^2 - \gamma_{AC}^2}{2\gamma_{AB}\gamma_{BC}} \quad (4.4)$$

$$\cos \beta = \frac{\gamma_{AB}^2 + \gamma_{AC}^2 - \gamma_{BC}^2}{2\gamma_{AB}\gamma_{AC}} \quad (4.5)$$

The transition between the different wetting stages is typically expressed by the spreading coefficient S , which shows the difference of surface excess energy between partial and complete wetting.²²

$$S = \gamma_{AB} - \gamma_{BC} - \gamma_{AC} \quad (4.6)$$

A negative spreading coefficient corresponds to partial wetting. When the initial spreading coefficient is positive, a droplet will expand until it reaches the equilibrium state where the contact angle becomes zero (figure 4.1).²

An interfacial tension results from an imbalance of intermolecular forces for the molecules along the interfaces compared to the molecules in the bulk phase. It describes accurately the excess of free energy per unit area in the far field. However, the near field conditions of the three-phase contact line are more complex. Here, the intermolecular interactions for molecules located close to the three-phase contact line give additional contributions to the interfacial energies. As the systems tries to minimize the excess energy at the three-phase contact line this may result in a different microscopic contact angle.⁴ This microscopic deviation was described theoretically and shown experimental for droplets with radius $< 1\mu\text{m}$. The Modified Neumann's equation accounts for this effect in case of small sessile droplets introducing an additional factor. The factor is defined by the line tension contribution which is described in terms of energy excess per unit length:^{1,3}

$$\gamma_{AB} = \gamma_{AC} \cos \beta + \gamma_{BC} \cos \alpha + \frac{\tau}{R} \quad (4.7)$$

Calculated values of the line tension range between 10^{-13} and 10^{-10} N. The experimental data vary from 10^{-11} to 10^{-5} N, according to the method and the system used to perform the experiments, whereby both positive and negative values of the line tension have been reported.²³ As already mentioned, the effect of the line tension is directly linked to the curvature of the contact line: the line tension becomes negligible for macroscopic droplets, but is essential for nanoscale droplets, small bubbles and fine particles.⁴ Theoretically, negative values for the line tension are expected for systems that feature a critical wetting transition. In this wetting scenario a thin film of liquid that surrounds the droplet grows in thickness upon the approach of the wetting transition and diverges smoothly reaching the wetting transition, because of the absence of a positive line tension. A different scenario is presented upon a first-order wetting transition. In this case, the microscopically thin film around the droplet, maintains its dimensions until it approaches the wetting transition at which it jumps to a macroscopically thickness. This jump-like behavior is intimately linked to the positive value of the line tension. In the case of nanoscale hydrocarbon drops at the air-water interface, the line tension contribution is expected to be small but positive.

For a small droplet with radius R of a liquid (oil) in a solvent (water) there is interfacial tension γ between the oil and water phases. The grand potential of this system is given by:

$$\Omega = -\Delta P \left(\frac{4}{3} \pi R^3 \right) + \gamma (4\pi R^2) \quad (4.8)$$

wherein the Laplace pressure is given by ΔP .

Interfaces of macroscopic droplets are similar with flat macroscopic interfaces and the curvature of the interface may be ignored if it is investigated apart from the three-phase contact region. For very small droplets the interfacial tension may become curvature dependent due the existing Laplace pressure. This effect on the interfacial tensions is directly linked to the choice of the radius of the droplet, without changing the amount of oil in the droplet and is known as a notional change of the radius. Both the Laplace pressure and the grand potential are invariant for our choice of the radius and thus

$$\left[\frac{d\Omega}{dR} \right] = -\Delta P (4\pi R^2) + \gamma (8\pi R) + (4\pi R^2) \left[\frac{d\gamma}{dR} \right] = 0 \quad (4.9)$$

This equation indicates that the value of the interfacial tension is a function of the radius $\gamma = \gamma(R)$ which usually has a minimum. The radius at which this minimum occurs is referred to as the surface of tension (SOT). For this choice of the radius

equation 4.9 simplifies to the well-known Laplace equation

$$\Delta P = \gamma \frac{2}{R} \quad (4.10)$$

which is only valid at the SOT. The surface tension found by this equation is not necessarily identical to the surface tension of the macroscopic oil-water interface. However, the curvature corrections are typically very small. This will be verified below. Inserting the Laplace equation (equation 4.10) into equation 4.8 gives the following expression

$$\Omega = \Delta P \left(\frac{2}{3} \pi R^3 \right) = \gamma \left(\frac{4}{3} \pi R^2 \right) \quad (4.11)$$

equation 4.11 illustrates the correlation of the surface tension with the radius of curvature by the SOT. The variation of the radius, by means of adding more internal phase, gives access to the curvature dependence of the interfacial tension. The result can be analyzed using a Taylor series expansion

$$\gamma(J) = \gamma(0) + \frac{\partial \gamma}{\partial J} J + \dots \quad (4.12)$$

where $J = \frac{1}{R_1} + \frac{1}{R_2}$ is the mean curvature of the interface.

The coefficient $k_{XY} \equiv \frac{\partial \gamma_{XY}}{\partial J}$ in equation 4.12 is related to the Tolman length,²⁴ which is the distance between SOT and the Gibbs dividing plane. Theoretical studies and molecular simulations on the magnitude and the sign of the Tolman length are ambiguous.²⁵ It is widely accepted that the correction factor of the surface tension is typically small, while positive^{26,27} and negative²⁸ values have been reported in literature.

4.3 Scheutjens Fleer Self-consistent-field (SF-SCF) Theory

4.3.1 The coordinate system

The definition of a coordinate system is one the first steps to make when setting up an SF-SCF problem. The system volume is represented by a lattice of cells with a linear length b . In a simple case of one-gradient direction (flat geometry), the lattice layers are numbered $z = 1, \dots, M$. By filling the cell sites at coordinate z with segments or monomers X , its dimensionless concentration $\varphi_X(z)$ may be computed from the true local concentration multiplied by the cell volume, that is, $\varphi_X(z) = c_X(z)b^3$. As shown in the appendix, there are relatively straightforward extensions

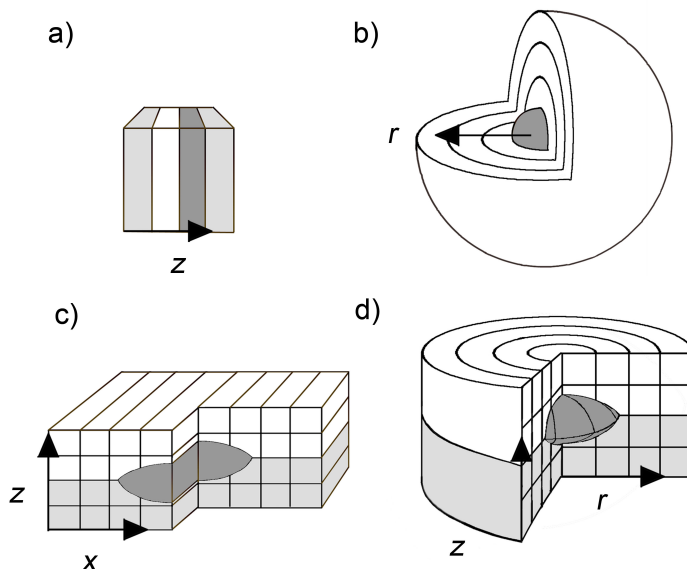


Figure 4.2: Schematic picture of (a) a one-gradient lattice which was used to compute three coexisting interfaces for the system in a complete wetting state, (b) a one-gradient spherical geometry which was used to study the curvature dependence of the interfacial tension by varying the radius of the oil droplet placed in the center of the lattice, (c) a two-gradient flat geometry which was used to analyse the curvature dependence of the line tension, (d) a two-gradient cylindrical coordinate system which was used to study the shape of the liquid drop at the air-water interface.

of the method to deal with multiple components, various lattice geometries and systems with more than one-gradient direction. Mirror-like boundary conditions are used for all systems; which means that the volume fractions of all components on either side of the boundaries are the same: $\varphi(0) = \varphi(1)$ and $\varphi(M+1) = \varphi(M)$.

To describe a system of a sessile droplet placed at the interface, the three interfacial tensions between various phases that coexist have to be defined accurately. The challenge to study the phase behaviour of many component systems is that the mutual coexistence concentrations of all components in all phases must be obeyed. Indeed, this becomes involved when in the system there are more than two phases. Here we solve this problem effectively in a single calculation using a one-gradient computation in a flat-lattice geometry (figure 4.2a). The system is filled with equal amounts of a solvent B (water), the free volume A (vapour) and a liquid C (hydrocarbon), followed by an B -rich phase, in such a way that there are AB , BC and an AC interfaces (the order of the phases is controlled by the initial guess

presented to the SCF-solver). The B -rich phase is defined as a solvent. The lattice layers are numbered as $z = 1, 2, \dots, 400$ aiming for 100 lattice layers per phase. In this geometry the mean-field averaging prevents the system to form lenses. The grand potential is straightforwardly identified by the sum of the interfacial tension of the respective interfaces. The interfacial tension for a given interface is found by summing up the grand potential density across the specified interface. Obtained macroscopic interfacial tensions can be used to predict the contact angle of a macroscopic droplet placed at the air-water interface. Below, we will use the binodal volume fractions that are found for all coexisting phases, e.g. in the evaluation of the curvature dependence of the interfacial tensions.

A one-gradient spherical coordinate system (figure 4.2b) is set up to obtain the curvature dependence of a particular interface with respect to the droplet radius aiming for the interfacial tension at SOT. For this, two series of calculations have been performed to obtain the curvature dependence of the oil-air and oil-water interface which can be computed for a spherical oil droplet in a bulk phase of air or water, respectively. The compositions of these bulk phases are constraints in these calculations and are taken consistent with the binodal values that were found earlier.

Subsequently, corresponding calculations are performed in a two-gradient cylindrical coordinate system (figure 4.2d). In the case that the contact angles are between 0° and 180° , the SC-SCF solution results in a sessile drop shape and grand potential density profiles. Inhomogeneities in densities and potentials of the volume fractions are allowed here in radial r -coordinate and vertical z -direction. The layer numbers in radial directions are given by $r = 1, 2, \dots, M_r$. Again applying mirror-like boundary conditions allows presenting results in the mirrored part with coordinates $r = -1, -2, \dots, -M_r$. The size of the cylindrical lattice is set up by $M_r = 100$ and $M_z = 50$ layers, where roughly layers $z < 25$ are occupied by the volume fraction of free volume and the layers $z > 25$ are filled by water segments. The amount of hydrocarbon monomers is approximately a factor 10 lower than those of both free volume and the solvent so that the radius of the oil lens is some orders smaller than the coordinate system size. Hereby, the oil lens is surrounded by two bulk phases of air and water. The two-gradient cylindrical geometry provides access to the grand potential density from which for example the Laplace pressure inside the drop is extracted.

Apart from the two-gradient cylindrical coordinate system, an evaluation of an oil droplet in a two-gradient flat coordinate system has been performed (figure 4.2c). In this geometry the oil drop at the air-water interface has a dike-like structure of

a channel with an endless non-curved three-phase contact line. The two-gradient flat geometry of fixed coordinates in (x, z) -direction and the mean field averaging in the y -direction is relevant for systems wherein the focus of investigations is no longer in the radial curvature of the liquid drop. Thus, the curvature dependence of the line tension can be extracted by comparing the data from the two-gradient geometries of the flat and cylindrical structures.

The lattice site length b needs to be chosen in order to convert the dimensionless quantities that follow from the computations to values with usual units. The length of the lattice site is defined by the segments that built the molecules. These are free monomer in case of vapour, CH_2 - and respectively CH_3 -groups for hydrocarbon molecules (see section below), and a segment that is part of a water cluster. The C-H bond length is about 0.1nm which leads to the Ansatz that $b \approx 0.2\text{nm}$ is an appropriate size of a lattice site when a C-atom with two hydrogens is placed inside. For the lattice site $b = 0.2\text{nm}$ and at room temperature the conversion factor is $k_B T/b^2$ for two-dimensional forces, e.g. the interfacial tension. Subsequently the factor becomes $k_B T/b$ in case of linear forces, e.g. line tension. The conversion $c_i = k\varphi$ of volume fractions φ_i to molar concentration c_i [mol/L] depends on the chain volume $N_i b^3$ and Avogadro's number N_a ; $k = 1/(N_i b^3 N_a 1000) = 1/(N_i 8 \times 10^{-30} 6 \times 10^{26}) \approx 2 \times 10^2/N_i$. In the following sections, the calculated numerical values are presented in dimensionless units in magnitude of thermal energy $k_B T$.

4.3.2 The molecules

The analyzed systems consist of three species of molecules: linear oil molecules, star-like water cluster and monomeric "free volume" units that represent the vapour phase.

Oil molecules of linear hydrocarbons consist of 16 identical segments implementing a chain containing 16 CH_2 - or CH_3 united atom groups. The CH_2 - and CH_3 -groups are equal in terms of interaction parameters of the segments and each segment fits in one lattice site of length b and volume b^3 . This approach is referred to as coarse-grained model. The freely jointed chain model is used to find the statistical weights of all possible and allowed conformations of these linear chains (see appendix for details). The alcohol ethoxylate molecules consist of a C_{12} alkane chain which contains identical segments as the oil molecules. The surfactant head group includes 5 EO-segments, whereby each CH_2 -, O- and OH-group fits in one lattice site as described above.

A simplistic W_5 -model is applied to describe water molecules as a cluster struc-

ture with one central unit that is surrounded by four similar units. Conformations of such star-like molecules are straightforwardly generated within the freely-jointed chain model.²⁹ The free volume (component A) is modeled as unoccupied lattice sites.

It is well-known that a compressible n -component lattice-gas model maps on a $n+1$ -component incompressible lattice model. Therefore, the present system can be referred to as a two-component (oil - water) compressible lattice-gas model, or to a three-component (free volume - oil - water) incompressible system. If necessary, the chemical potential of the free volume component can be converted to the pressure in the compressible system.

4.3.3 Interaction parameters

The interfacial tensions result from the definition of the interaction parameters between the segments of all integrated components. As previously described, contacts of same segments lead to interactions of $\chi = 0$. Whereby, the FH-parameters of unequal segments have been defined by considering the fact that repelling interactions implement positive χ -values while attractive interactions correspond to negative χ -values.

Bilayer formation has been studied using the SF-SCF theory and the set of interaction parameters has been defined for these systems.^{30,31} More specially, the interaction parameters $\chi_{AB} = 2.5$, $\chi_{BC} = 1.1$ and $\chi_{AC} = 2.0$, which have been fixed through previous calculations, are adapted for the present system of the oil droplet at the air-liquid interface. The hydrophobic C_{12} -tail of the surfactant molecule has the same interaction parameters as the oil segments. The interaction parameters of the oxygen with other molecular segments are defined as $\chi_{AO} = 2.5$, $\chi_{BO} = -0.6$ and $\chi_{CO} = 2.0$. Thus, surfactant head groups will be rejected by the free volume segments while attracted by water clusters. These interaction parameters give qualitatively correct values for the interfacial tensions and the proper trends for the bimodal of, *e.g.* the amount of oil in the water phase as a function of the alkyl chain length. These parameters should be considered approximate and not necessarily the best possible. We have not attempted to fine-tune the parameters in order to improve quantitative comparison with experimental data. The results section contains further details.

4.4 Results and discussion

A liquid droplet placed between two fluid phases is defined by the three interfacial tensions. To approach this system, in the first step, calculations of the respective bulk binodals and the interfacial tensions have been performed in one-gradient flat lattice (figure 4.2a). In figure 4.3a the volume fraction distribution is given in the order from left to right: a water-rich B phase, a vapour-rich A phase, an oil-rich phase C and again the terminal water-rich phase. The profile displays homogeneous volume fractions in the respective bulk regions. Only at the phase boundaries the volume fractions vary steeply, where the profile is tanh-like. The width of the interfaces is typically of two or free water molecules. As shown in figure 4.3a the bulk volume fractions of hydrocarbon within the water-rich and the vapour-rich phases are sufficiently low of 4.334×10^{-7} and 1.497×10^{-8} respectively. The bulk volume fraction of the free volume does not exceed 0.076 in the non-polar hydrocarbon phase and has a lower value of 0.048 in the water phase. The binodal values of the three components in the various phases are summarized in table 4.1.

The air-water interaction parameter of $\chi_{AB} = 2.5$ is sufficient to create a solubility gap and a sharp interface with a resulting interfacial tension of $0.665k_B T/b^2$ which converts to $\gamma_{AB} = 0.068\text{N/m}$. This numerical output is close to the experimental value of the air-water interfacial tension. The FH-parameter $\chi_{BC} = 1.1$ implements a strong demixing tendency of hydrophobic molecular segments and water cluster. The corresponding oil-water interfacial tension is found to be $0.478k_B T/b^2$ or $\gamma_{BC} = 0.049\text{N/m}$, which agrees qualitatively with experimental findings. The repulsive interactions between the oil and the free volume are set to $\chi_{AC} = 2.0$ to generate a sharp interface between these phases. Considering the fact that oil molecules have a larger molar mass than water clusters, we find that for the current parameter setting the oil molecules adsorb preferentially onto the air-water interface and that the oil-air interfacial tension is $0.537k_B T/b^2$ or $\gamma_{AB} = 0.055\text{N/m}$.

The density of the free volume is higher within the non-polar hydrocarbon phase whereby an adsorption within the two-phase region becomes evident by a close-up. The reason for this effect is that by the accumulation of free volume the number of the less favourable oil-water contacts is reduced.

Figure 4.3b shows the grand potential density profile across the interfaces. The grand potential drops to zero in-between the interfaces, and has a finite value at/or near the interfaces. As explained above, the integration of the grand potential density across a given interface gives the dimensionless interfacial tension. It is evident that the interfacial tension is highest for the air-water interface and lowest

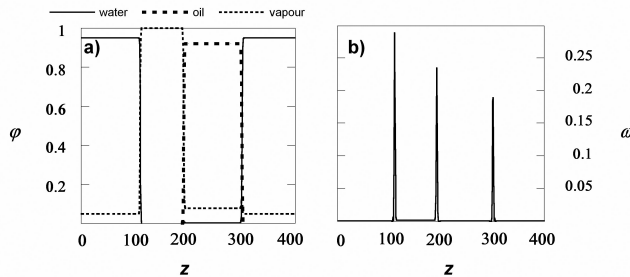


Figure 4.3: (a) Volume fraction profiles of water, oil and free volume across the three interfaces. (b) The grand potential density profile across the three interfaces.

Table 4.1: Volume densities of saturated three-component system derived from one-dimensional flat geometry calculations.

	φ_A (vapour)	φ_B (water)	φ_C (C ₁₆ oil)
vapour	0.998	1.657×10^{-4}	1.497×10^{-8}
water	0.048	0.951	4.334×10^{-7}
C ₁₆ oil	0.076	2.931×10^{-3}	0.920

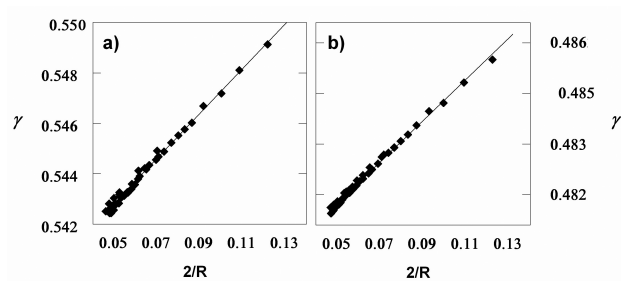


Figure 4.4: Interfacial tension as a function of the radius of an oil droplet placed in a one-dimensional spherical geometry lattice (a) in a vapour-rich phase and (b) in a water-rich phase.

for the oil-air interface consistent with the values reported above.

Calculations in a one-gradient spherical geometry (figure 4.2b) have been performed to find the SOT, to access the Laplace pressure inside the droplet, and to extract the curvature dependence of the interfacial tension. For the described system of an oil droplet placed at the air-water interface, the oil phase is always the internal phase. Figures 4.4a and b display the results for the interfacial tension as a function of the curvature $J = 2/R$ of the oil droplet embedded in a water-

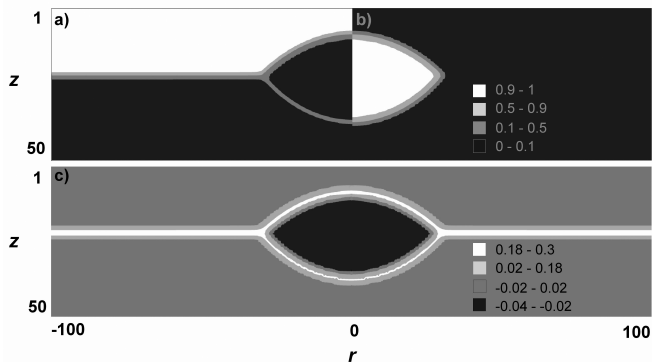


Figure 4.5: Profiles computed in a two-gradient cylindrical geometry of (a) volume fraction of the free volume units φ_A , (b) volume fraction of the hydrocarbon segments ω , (c) the grand potential density ω .

saturated vapour phase, and a vapour-saturated water-rich phase, respectively. In these calculations, the radius of the oil droplet has been varied from $R \approx 15$ to $\approx 45b$.

As anticipated, there is a linear dependency of the interfacial tension as a function of the curvature $2/R$. The values $k_{AC} \equiv \partial\gamma_{AC}/\partial J$, and correspondingly k_{AB} are given by the slopes in figures 4.4a and b, respectively. For oil droplet surrounded by vapour $k_{AC} = 0.085$ resulting in an interfacial tension of $\gamma_{AC} = 0.584k_B T/b^2$ for a droplet with a radius $R_{AC} = 47b$. Oil drops in a water phase display a similar curvature dependence, parametrized by $k_{BC} = 0.071$. As this value is of the same order of magnitude as for the oil-vapour interface, there is once again a small increase of the interfacial tension of $\gamma_{BC} = 0.513k_B T/b^2$ for a drop with radius $R_{BC} \approx 42b$ compared to the flat interface. These slightly higher interfacial energies imply that the expected contact angle of the sessile oil drop has the tendency to increase with decreasing droplet size. The resulting contact angles calculated using equation 4.4 and equation 4.5 are $\alpha = 57^\circ$ at the oil-water interface and $\beta = 47^\circ$ at the oil-vapour interface. Hence, a slightly asymmetrical lens shape with a higher contact angle towards the water phase is anticipated.

The computed interfacial tensions allow an estimate of the spreading coefficient that is a measure of how likely the oil will spread over the interface. A resulting negative value of $S = -0.044\text{N/m}$ implements partly wetting conditions under formation of a lens-like shape of oil at the interface. Measurements of the interfacial and the surface tensions performed by another group correspond to $S = -0.013\text{N/m}$.³² The magnitude of the calculated spreading coefficient is higher compared to the

experimental value but it correlates well with the wetting behaviour and the shape of the hydrocarbon drop.

Equal density contour plots for the volume fraction profiles obtained from two-gradient cylindrical geometry (figure 4.2d) give a two dimensional picture of the sessile droplet. Figures 4.5a and b illustrate the volume fraction profile in the (r, z) -plane. The volume fractions of hydrocarbon segments are given in figure 4.5b for the negative r -coordinates, whereas the volume fractions of free volume are given for the region with positive r -values in figure 4.5a. As the profiles are symmetric with respect to the change in sign of the r -coordinate, the combined viewgraph gives information on the structure of the droplet at the air-water interface. The contour of the air-water interface is straight and the sphere caps that deform the droplet shape and can be described by regular radii. As anticipated, the hydrocarbon phase sits as a lens-like drop at the air-water interface partly wetting this interface with a slightly larger volume within the water phase than in vapour. Figure 4.5c shows the grand potential density profile which is negative within the oil droplet and is close to zero in the region beneath the interface within the water-rich phase. The finite grand potential density within the oil droplet corresponds to the Laplace pressure $\omega_{drop} = -\Delta P = -0.024k_B T/b^3$. The grand potential density at interfaces has a sharp local maximum indicating repulsive interactions between different phases (compare figure 4.3b). In the water- and vapour-rich phase the grand potential density is zero according to the equal interactions between segments of the same monomer and $\chi = 0$. It is difficult to estimate from the profile what exactly happens with the grand potential density at the three-phase contact zone, e.g. it is impossible to estimate the sign of the line tension from the grand potential contour plot. A close inspection however seems to indicate that the grand potential densities that contributes to the line tension are collected from a region around the three-phase contact line that exceeds the size of the molecules.

For a sphere of identical radii of curvature ($R_1 = R_2$), one can evaluate the curvatures from the known interfacial tension and the Laplace pressure according to equation 4.10. The droplet shape of both spherical caps can be calculated from the radius of curvature as indicated in figure 4.6.

The droplet shape computed in a two-gradient cylindrical lattice is consistent with the lens-like structure predicted by experimental data. The contour plot can also be used to estimate the two contact angles, but the accuracy is, due to the small size of the droplets, not very high. Nevertheless, the estimated contact angles found from the two-gradient calculations match the predictions of the contact angles from the interfacial tensions found by one-gradient calculations. This proves that our

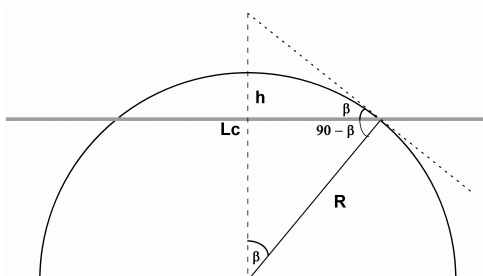


Figure 4.6: Schematic picture of the upper half sphere of a hydrocarbon lens which is in contact with vapour. The tangent that touches the sphere segment at the interface encloses the contact angle β . Thus, the angle of the tangent to the radius is 90° . The height of the spherical cap is given by $h = R - R \times \sin(90 - \beta)$ and its area by $A = 2\pi R h$. The radius of the contact line can be calculated as follows $R_a = 2 \times \cos(90 - \beta)$. L_c is the circumference of the oil droplet.

approach is internally consistent. Knowing the exact shape of the oil lens, the line tension can be estimated. As expected, there is a homogeneous curvature of the drop, both along the oil-vapour, as well as the oil-water interface. As illustrated in figure 4.6, knowing the curvatures, the height of the spherical cap that fits the droplet shape can be derived from the radius of the spherical drop and its contact angle to the interface. For the air-oil interface, the height of the spherical cap is $h_{AC} = 15b$. The height of the oil-water cap is slightly larger with $h_{BC} = 19b$. Using these results, the radius of the contact line of the oil lens is calculated as $R_a = 35b$.

When the exact shape of the oil lens has been defined, the line tension can be estimated in the following step. To extract the line tension contribution, the corresponding interfacial areas have to be calculated first. The derived area for the flat air-water interface is $A_{AB} = 299546b^2$, $A_{BC} = 5208b^2$ for the curved oil-water interface and $A_{AC} = 4771b^2$ for the interfaces of the oil lens in contact with vapour. The grand potential of the systems is the sum of interfacial tensions from each interface multiplied with the corresponding interfacial area and the line tension contribution τ for the whole length L_c of the contact line:

$$\Omega = \gamma_{AB}A_{AB} + \gamma_{BC}A_{BC} + \gamma_{AC}A_{AC} + \tau L_c \quad (4.13)$$

The overall grand potential is found to be $\Omega = 21557k_B T$, and the calculated circumference of the oil droplet is $L_c = 223b$. From this the value for the line

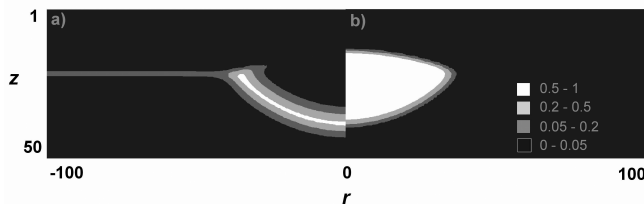


Figure 4.7: Volume fraction profiles computed in a two-gradient cylindrical geometry of (a) the non-ionic surfactant $\varphi_{C_{12}E_5}$, (b) the hydrocarbon segments φ_C .

tension $\tau \approx 71k_B T/b$ is obtained. However, this value is valid for the drop with a radial curvature $J = 1/R \approx 1/35$.

Furthermore, it is of interest to evaluate the curvature dependence of the line tension. Therefore, simulations have been repeated in a two-gradient flat geometry where the oil phase is placed in the center of the coordinate system as a channel with a curved interface in only one direction (figure 4.2c). In this case the evaluated line tension is $\tau(0) = 50k_B T/b$. The Taylor series expansion has been used to extract the line tension dependence of the drop curvature

$$\tau(J) = \tau(0) + \frac{\partial \tau}{\partial J} J + \dots = \tau(0) + k^\tau J + \dots \quad (4.14)$$

Collecting the results mentioned above, it implicates that $\tau(J) - \tau(0) = -21k_B T/b$ and thus $k^\tau \approx -700$ in units $k_B T$. The fact that $k^\tau < 0$ implies that the role of the line tension decreases with increasing interfacial areas, *i.e.* with increasing droplet size.

Converting from dimensionless units, the line tension is $\tau = 1.47 \times 10^{-9} \text{N}$ for radial curved droplets. The calculated line tension is small compared to interfacial tensions for the same droplet size, which explains why there is a little effect of the line tension on the droplet shape in two-gradient cylindrical coordinate systems. The numerical value of the line tension correlates well with experimental data of $\tau = 10^{-9} \text{N}$ reported for liquid alkanes-water-vapour systems.^{33,34} This shows that our model describes a drop placed at the air-water interface realistically.

In the next section we will illustrate how the model deals with more complex molecular situations. An example was constructed for the system described above and using a $C_{12}E_5$ non-ionic surfactant which is already known in the context of SCF simulation approach. The surfactant was added at a dimensionless concentration of $\varphi_{C_{12}E_5} = 10^{-4}$. As shown in figure 4.7a, surfactant molecules preferable

accumulate at the oil-water interface, visibly lowering the γ_{BC} and allowing the oil drop to sink further into the water phase. Thereby, the placement and the shape of the oil droplet become asymmetrical. The particular example presented in figure 4.7 will be addressed extensively in forthcoming publications.

Thus, it has been shown that the SCF-approach is suitable to simulate the wetting properties of oil droplets at the air-water interface and to extract accurately the relevant structural and thermodynamic parameters from it. More specifically, it has been shown that the parameters qualitatively describe the oil-water-vapour system and that the results allow to make a prediction for the curvature dependence of the line tension. The model is capable to deal with molecularly complex systems. This means that predictions for oil spreading at the air-water interface as a function of additives can already be estimated from the analysis of nano-scale droplets. Even though two-gradient calculations are computationally more expensive, this presents a promising opportunity. The alternative approach, that is to estimate the wetting characteristics from one-gradient calculations, becomes very involved for multi-component systems. The extensive bookkeeping of the one-gradient geometry is unnecessary in a two-gradient cylindrical coordinate system where all phases coexist mutually. Moreover, it has been shown that nano-scale droplets are already representative for droplets of larger dimensions.

4.5 Conclusions and Outlook

Based on the numerical self-consistent-field approach a model has been developed that is ideal to investigate various scenarios for droplet shapes at interfaces. Furthermore, it was shown that this approach can accurately deal with physical properties of a sessile liquid droplet. Analysing the physical properties, a closer attention has been paid to the curvature dependence of the derived microscopic parameters. It is known that the interfacial tension and especially the line tension vary with decreasing droplet size. A small curvature dependence has been calculated for the interfacial and the line tensions. A negative line tension contribution has been extracted for the described model. Those contributions have hardly a measurable effect on the final shape of the oil droplet and its wetting properties. The derived interfacial tensions are sufficiently close to the experimental data reported in literature and calculated negative spreading coefficient corresponds to partly wetting behavior of the hydrocarbon lens. The derived contact angles are qualitatively similar to the experimental data. Thus, it can be concluded that although the microscopic model presented here is simple; it can be carried over to macroscopic

systems. As has been shown in an example, that the model can be further elaborated by changing the interaction properties between both liquid phases by varying the molecular structure of the oil or by adding surfactant molecules which will occupy the interfaces and influence the wetting behavior of the oil droplet. Varying these parameters will increase the complexity of the system approaching those used for various technical applications.

4.6 Appendix A: The SCF machinery

The SF-SCF model makes use of mean-field and lattice approximations. Moreover, it is necessary to specify a chain model and thus the description naturally splits up in several sub-sections.

The start is a mean-field free energy $F = \sum_{\mathbf{r}} f(\mathbf{r})$, where the summation is over all coordinates \mathbf{r} in the system. Its implementation in various geometries is specified below. Again, the free energy is in units of the thermal energy and has four terms, with the segment volume fraction distributions $\varphi_X(\mathbf{r})$, the segment potential distributions $u_X(\mathbf{r})$ and the Lagrange field distribution $\alpha(\mathbf{r})$ as its variables:

$$f = \frac{F}{k_B T} = -\ln Q[u] - \sum_{\mathbf{r}} \sum_X u_X(\mathbf{r}) \varphi_X(\mathbf{r}) + F^{\text{int}}[\varphi] + \sum_{\mathbf{r}} \alpha(\mathbf{r}) \left(\sum_X \varphi_X(\mathbf{r}) - 1 \right) \quad (4.15)$$

The first two terms represent the translational and conformational entropy in the system. The first term features the partition function Q in potential space. The second term specifies a Legendre transformation to the classical canonical ensemble (N, V, T) . The third term introduces the interaction energy in the canonical ensemble and the fourth term implements the incompressibility constraint. It is understood that the role of the segment potentials is to give the statistical weight of (free) segments in the system. In the system discussed in the main text we use monomeric species A representing vacancies and the distribution is given by

$$\varphi_A(\mathbf{r}) = \varphi_A^b \exp -u_A(\mathbf{r}) \quad (4.16)$$

where the volume fraction of vacancies in the bulk phase is specified by φ_A^b . For monomers the partition function is just the sum of the Boltzmann factors and it is easily shown that equation 4.15 reduces to the regular solution free energy given in equation 4.16. The advantage of equation 4.15 is that it can also be used for

chains which occupy a sequence of lattice sites.

The free energy of equation 4.15 is only meaningful for particular combinations of the volume fraction distribution and the corresponding potentials. It turns out that we need to maximize the free energy with respect to the segment potentials and the Lagrange field and minimize the free energy with respect to the volume fraction distributions. In other words we need to find a saddle point of the free energy. Formally the saddle point is found when

$$\frac{\partial F}{\partial \varphi_X(\mathbf{r})} = 0 \quad (4.17)$$

$$\frac{\partial F}{\partial u_X(\mathbf{r})} = 0 \quad (4.18)$$

$$\frac{\partial F}{\partial \alpha(\mathbf{r})} = 0 \quad (4.19)$$

The extremization of the mean-field free energy leads to the so-called self-consistent field equations which are discussed in separate sub-sections.

4.6.1 Segment potentials computed from the segment volume fractions.

Equation 4.17 results in the rule that describes how to compute the segment potentials:

$$u_X(\mathbf{r}) = \alpha(\mathbf{r}) + \frac{\partial F^{\text{int}}}{\varphi_X(\mathbf{r})} \quad (4.20)$$

Depending on the model there may be various contributions to the free energy of interactions. Typically we have the contribution of short range interactions which are already outlined in the text. It can be written as

$$u_X^{\text{FH}}(\mathbf{r}) = \sum_Y \chi_{XY} (\langle \varphi_Y(\mathbf{r}) \rangle - \varphi_Y^b) \quad (4.21)$$

Here we choose to normalize the segment potentials by using the bulk volume fractions. The angular brackets specify the local average of the density and this may depend on the geometry of the lattice (to be specified in more detail below).

There may be more contributions to the segment potential. For example when there are charged components in the system one has to account for the electrostatic contribution as well. It is well-documented how the electrostatic contribution to the segment potential is computed:

$$u_X^{\text{el}}(\mathbf{r}) = \frac{e v_X \psi(\mathbf{r})}{k_B T} + \frac{1}{2} \epsilon_0 (\epsilon_X - 1) E^2(\mathbf{r}) \quad (4.22)$$

The first term is familiar for the Poisson Boltzmann theory. In this term e is the elementary charge, v_X is the valency of segment X and $\psi(\mathbf{r})$ is the electrostatic potential. The potential is computed from the Poisson equation:

$$\nabla \epsilon \nabla \psi = -q \quad (4.23)$$

With $q = q(\mathbf{r})$ is the local charge density in the system (which is computed when the volume fractions are available):

$$q(\mathbf{r}) = \sum_X v_X e \varphi_X(\mathbf{r}) \quad (4.24)$$

The second term in equation 4.22 is needed when the dielectric permittivity is not fixed but depending on the distribution of the segments. Typically we use a volume fraction weighting:

$$\epsilon(\mathbf{r}) = \epsilon_0 \sum_X \epsilon_X \varphi_X(\mathbf{r}) \quad (4.25)$$

and it is understood that $E(\mathbf{r}) = \nabla \psi$ is the local electric field.

Segment volume fractions computed from the segment potentials. From equation 4.18 the formal way to compute the volume fractions is to evaluate

$$\varphi_X(\mathbf{r}) = -\frac{\partial \ln Q}{\partial u_X(\mathbf{r})} \quad (4.26)$$

The implementation of this operation highly depends on the chain model. We choose for the freely jointed chain model for which there exists an extremely efficient propagator equation to evaluate the partition function Q and hence the segment distributions. Before outlining this method we mention that in the mean field theory, the overall partition function is split into single chain partition functions q_i .

$$Q = \prod_i \frac{(q_i)^{n_i}}{n_i!} \quad (4.27)$$

At the foundation of the freely-jointed chain model there is the Edwards diffusion equation which features the end-point distribution function $G_i(\mathbf{r}, s|s')$. Here the variable s specifies the ranking number of segments in the chain, that is, $s = 1, \dots, N$, where N is the total number of segments in the chain. Physically G includes the statistical weight of all possible and allowed conformations of chain

parts going from s' to s (at coordinate r):

$$\frac{\partial G_i}{\partial x} = \frac{1}{6} \nabla^2 G_i - U G_i \quad (4.28)$$

which is supplemented with appropriate initial conditions. The mapping of this diffusion-like equation onto the lattice results in the propagators. Here we specify two complementary propagator equations, one started at segment number $s = 1$ and the other at segment number $s = N$.

$$G_i(\mathbf{r}, s|1) = G_i(\mathbf{r}, s) \langle G_i(\mathbf{r}, s-1|1) \rangle \quad (4.29)$$

$$G_i(\mathbf{r}, s|N) = G_i(\mathbf{r}, s) \langle G_i(\mathbf{r}, s+1|N) \rangle \quad (4.30)$$

In these equations the angular brackets again define a local averaging (which depend on the geometry which is specified below). The quantity $G_i(\mathbf{r}, s) = G_i(\mathbf{r}, s|s)$ is the free segment distribution function which is given by the Boltzmann equation $G_i(\mathbf{r}, s) = \exp -u(\mathbf{r}, s)$. Here $u(\mathbf{r}, s) = u_X(\mathbf{r})$ when segment s of molecule i is of type X . As in the current problems there are no constraints on the molecules, the initiation of the propagators is straightforward $G_i(\mathbf{r}, 1|1) = G_i(\mathbf{r}, 1)$ and $G_i(\mathbf{r}, N|N) = G_i(\mathbf{r}, N)$ for equations 4.29 and 4.30, respectively. The single chain partition function is computed by $q_i = \sum_{\mathbf{r}} G_i(\mathbf{r}, 1|N)$. The volume fraction distributions follow from the composition law:

$$\varphi_i(\mathbf{r}, s) = \frac{n_i}{q_i} \frac{G_i(\mathbf{r}, s|1)G_i(\mathbf{r}, s|N)}{G_i(\mathbf{r}, s)} \quad (4.31)$$

From which the volume fraction distribution per segment type follows straightforwardly. In equation 4.31 the division by the free segment distribution function is needed because the statistical weight for segment s at coordinate \mathbf{r} should be accounted just once and both end-point distributions have accounted for this weight. The normalization of equation 4.31 is chosen such that the specified number of molecules n_i is in the system. It can be shown that

$$\frac{\varphi_i^b}{N_i} = \frac{n_i}{q_i} \quad (4.32)$$

and all bulk volume fractions are available (necessary to normalize the segment potentials).

4.6.2 Lagrange field and outline of numerical procedure.

The optimization equation as given by equation 4.19 leads to the constraint that the sum of the volume fractions over all segment types should be unity. Numerically, we adjust the value of $\alpha(\mathbf{r})$ until this is accurately the case.

We are now in the position to say in words how the so-called self-consistent field result is obtained. We typically start with a guess for the segment potentials and the value of the Lagrange field. Using this guess we can compute the volume fractions (equation 4.31). We may check for the compressibility relation and adjust the Lagrange field accordingly. We use the volume fractions to compute the charge distribution equation 4.24 and the distribution of the dielectric permittivity equation 4.25, so that we can evaluate equation 4.22. The distributions also allow us to enumerate equation 4.21 so that the total segment potential is available. We check whether the computed segment potential is identical to our guesses. If this is the case we stop the search, if not we adjust the potentials and go through the loop once again. Recalculations can be performed up to 7 significant digits.

4.6.3 Thermodynamic quantities

Once a fixed point of the SCF equations is available we can evaluate the free energy equation 4.15. For the current problem statement, the grand potential $\Omega = F - \sum_i n_i \mu_i$ is more informative. There exists a close formula for the grand potential. It can be written as the sum over the grand potential density $\Omega = \sum_{\mathbf{r}} \omega(\mathbf{r})$ with

$$\begin{aligned} \omega(\mathbf{r}) = & -\frac{(\varphi_i(\mathbf{r}) - \varphi_i^b)}{N_i} - \alpha(\mathbf{r}) \\ & - \frac{1}{2} \sum_X \sum_Y \chi_{XY} (\varphi_X(\mathbf{r}) \langle \varphi_Y(\mathbf{r}) \rangle - \varphi_X^b \varphi_Y^b) + \frac{1}{2} q(\mathbf{r}) \psi(\mathbf{r}) \end{aligned} \quad (4.33)$$

The chemical potentials follow from the distribution of segments in the bulk phase:

$$\begin{aligned} \frac{\mu_i}{k_B T} = \\ \ln \varphi_i^b + 1 - N_i \sum_j \frac{\varphi_j^b}{N_j} - \frac{N_i}{2} \sum_X \sum_Y \left(\varphi_X^b - \frac{N_{Xi}}{N_i} \right) \chi_{XY} \left(\varphi_Y^b - \frac{N_{Yi}}{N_i} \right) \end{aligned} \quad (4.34)$$

where N_{Xi} is the number of segments of type X in molecule i .

4.6.4 One-gradient and Two-gradient geometries

The interfacial tension of the interface between two coexisting phases is most naturally evaluated in a one-gradient coordinate system. In such a system, the common procedure is to evaluate all quantities per unit area (that is per lattice site). We then have just one coordinate. Let's choose the z -variable for this and $\mathbf{r} = z$. The lattice layers are numbered $z = 1, \dots, M$, with a value of M sufficiently large so that the interface is far from the system boundaries. At the edge of the system, we typically implement reflecting (mirror-like) boundary conditions. This means that the volume fractions of all components on either side of the boundaries are the same: $\varphi(0) = \varphi(1)$ and $\varphi(M+1) = \varphi(M)$. In this case the grand potential is straightforwardly identified by the interfacial tension. The angular brackets are evaluated as specified in the main text.

The curvature dependence of the interfacial tension is evaluated using a spherical coordinate system. In this case we have gradients in the radial direction and $\mathbf{r} = r$, wherein the radial layers are numbered $r = 1, 2, \dots, M_r$. We apply again mirror-like boundary conditions. In the spherical lattice the number of lattice sites at coordinate r is given by $L(r) = \frac{4}{3}\pi(r^3 - (r-1)^3)$ and we see that the volume per lattice site is constant. To compute local averages we need *a priori* weights which are now depending on the coordinate r : $\langle X(r) \rangle = \sum_{r'=r-1, r, r+1} \lambda(r; r') X(r')$. It can be shown that the transition probabilities obey an internal balance equation $L(r)\lambda(r; r') = L(r')\lambda(r'; r)$. One obeys to this constraint when we use the dimensionless area between layers r and r' as follows: $\lambda(r; r') = \frac{A(r; r')}{L(r)} \lambda$, where $A(r; r') = 4\pi r^2$.

For the evaluation of the oil droplets at the air-water interface we adopt a two-gradient coordinate system. Again we use two variants. In the two-gradient flat case $\mathbf{r} = (y, z)$, which we use to consider a drop which is not curved in the x - y plane, we take the mean-field average in the x -direction. Again it is natural to normalise all quantities per unit length in the x -direction. Then, the number of sites $L(y, z) = 1$. The local average is now implemented by $\langle X(y, z) \rangle = \sum_{y'=y-1, y, y+1} \sum_{z'=z-1, z, z+1} \lambda(y, z; y', z') X(y, z)$, wherein the transition probabilities again should obey to the internal balance. This happens when $\lambda(y, z; y', z') = \lambda(y; y')\lambda(z; z')$.

A nano-scale drop is naturally curved in the x - y plane and therefore we adopt a two-gradient cylindrical coordinate system to deal with this case. The graphical illustration is presented in figure 4.2 in the main text. In this case the we have a radial coordinate r and a z -coordinate parallel to the long axis, $\mathbf{r} = (r, z)$. The

mean field averaging is done over the $L(r)$ lattice sites at each coordinate:

$$L(r, z) = L(r) = \pi (r^2 - (r - 1)^2) = \pi (2r - 1) \quad (4.35)$$

The grand potential is computed by $\Omega = \sum_z \sum_r L(r)\omega(r, z)$, and similarly the single chain partition function q_i is evaluated from the end-point distribution functions: $q_i = \sum_z \sum_r L(r)G_i(r, z, 1|N)$. The angular brackets have the following implementation;

$$\langle X(r, z) \rangle = \sum_{r'=r-1, r, r+1} \sum_{z'=z-1, z, z+1} \lambda(r, z; r', z') X(r', z') \quad (4.36)$$

The internal balance equation $L(r)\lambda(r, z; r', z') = L(r')\lambda(r', z'; r, z)$ is satisfied when $\lambda(r, z; r', z') = \lambda(z, z')\lambda(r, r')$ where the transition probabilities in the z -direction have been specified above and the ones in the radial direction are given by $\lambda(r, r - 1) = \lambda 2(r - 1)/(2r - 1)$ and $\lambda(r, r + 1) = \lambda 2r/(2r - 1)$, with $\lambda(r, r) = \lambda(z, z) = \lambda(y, y) = \lambda$. As in the one-gradient system λ is the only variable.

References

- [1] P. G. de Gennes, *Rev. Mod. Phys.*, 1985, **57**, 827–863.
- [2] D. Bonn and D. Ross, *Rep. Prog. Phys.*, 2001, **64**, 1085–1163.
- [3] L. Schimmele, M. Napiorkowski and S. Dietrich, *J. Chem. Phys.*, 2007, **127**, 164715–164743.
- [4] J. Drelich, *Colloids Surf., A*, 1996, **116**, 43 – 54.
- [5] F. Bresme and N. Quirke, *J. Chem. Phys.*, 1999, **110**, 3536–3547.
- [6] F. Bresme and N. Quirke, *J. Chem. Phys.*, 2000, **112**, 5985–5990.
- [7] A. I. Rusanov and E. N. Brodskaya, *J. Colloid Interface Sci.*, 1977, **62**, 542 – 555.
- [8] T. Werder, J. H. Walther, R. L. Jaffe, T. Halicioglu and P. Koumoutsakos, *J. Phys. Chem. B*, 2003, **107**, 1345–1352.
- [9] F. Bresme and N. Quirke, *Phys. Rev. Lett.*, 1998, **80**, 3791–3794.
- [10] Y. Djikaev, *J. Chem. Phys.*, 2005, **123**, 184704–184716.
- [11] T. Ingebrigtsen and S. Toxvaerd, *J. Phys. Chem. C*, 2007, **111**, 8518–8523.
- [12] P. N. Hurter, J. M. H. M. Scheutjens and T. A. Hatton, *Macromolecules*, 1993, **26**, 5592–5601.
- [13] P. N. Hurter, J. M. H. M. Scheutjens and T. A. Hatton, *Macromolecules*, 1993, **26**, 5030–5040.
- [14] G. J. Fleer, M. A. Cohen Stuart, J. M. H. M. Scheutjens, T. Cosgrove and B. Vincent, *Polymers at Interfaces*, Chapman & Hall, London, 1993, pp. 1–502.

- [15] F. A. M. Leermakers, J. M. H. M. Scheutjens and J. Lyklema, *Biophys. Chem.*, 1983, **18**, 353 – 360.
- [16] F. A. M. Leermakers, C. M. Wijmans and G. J. Fleer, *Macromolecules*, 1995, **28**, 3434–3443.
- [17] A. B. Jódar-Reyes, J. L. Ortega-Vinuesa, A. Martín-Rodríguez and F. A. M. Leermakers, *Langmuir*, 2002, **18**, 8706–8713.
- [18] Y. Lauw, F. A. M. Leermakers and M. A. Cohen Stuart, *J. Phys. Chem. B*, 2003, **107**, 10912–10918.
- [19] A. B. Jódar-Reyes, J. Lyklema and F. A. M. Leermakers, *Langmuir*, 2008, **24**, 6496–6503.
- [20] A. W. P. Vermeer, F. A. M. Leermakers and L. K. Koopal, *Langmuir*, 1997, **13**, 4413–4421.
- [21] P. Chen, J. Gaydos and A. W. Neumann, *Langmuir*, 1996, **12**, 5956–5962.
- [22] W. D. Harkins and A. Feldman, *J. Am. Chem. Soc.*, 1922, **44**, 2665–2685.
- [23] A. Amirfazli and A. W. Neumann, *Adv. Colloid Interface Sci.*, 2004, **110**, 121 – 141.
- [24] R. C. Tolman, *J. Chem. Phys.*, 1948, **16**, 758.
- [25] K. Koga, X. C. Zeng and A. K. Shchekin, *J. Am. Chem. Soc.*, 1998, **109**, 4063–4070.
- [26] D. Kashchiev, *J. Chem. Phys.*, 2003, **118**, 9081–9083.
- [27] A. E. van Giessen and E. M. Blokhuis, *J. Chem. Phys.*, 2002, **116**, 302–310.
- [28] A. E. van Giessen, E. M. Blokhuis and D. J. Bukman, *J. Chem. Phys.*, 1998, **108**, 1148–1156.
- [29] M. Charlaganov, P. Košovan and F. A. M. Leermakers, *Soft Matter*, 2009, **5**, 1448–1459.
- [30] F. A. M. Leermakers, J. C. Eriksson and J. Lyklema, in *Fundamentals of Interface and Colloid Science: Soft Colloids*, ed. J. Lyklema, Elsevier, Amsterdam etc., 2005, vol. V, ch. 4, pp. 4.1–4.123.
- [31] R. A. Kik, F. A. M. Leermakers and J. M. Kleijn, *Phys. Chem. Chem. Phys.*, 2005, **7**, 1996–2005.
- [32] T. F. Svitova, M. H. Randal and J. R. Clayton, *Langmuir*, 1999, **15**, 7392–7402.
- [33] A. Dussaud and M. Vignes-Adler, *Langmuir*, 1997, **13**, 581–589.
- [34] K. Stoeckelhuber, B. Radoev and H. Schulze, *Colloids Surf., A*, 1999, **156**, 323 – 333.

Chapter 5

A self-consistent field study of emulsion droplets at the air/water interface to underpin trends found for the atomisation of agricultural sprays

In this Chapter, the self-consistent field (SCF) approach is applied to underpin the recently suggested mechanism of spray formation from dilute oil-in-water emulsions based on spreading of emulsion droplets. Spray formation is a highly dynamic process which is not accessible experimentally so that we use modelling to get a better understanding of the breakup mode of the liquid sheet into spray droplets. At the same time typical agricultural spray liquids are mixtures of several components, which provides an additional challenge for experimental work. The SCF approach allows investigation of the interactions between different components in a section which is representative for the whole system and also provides access to effects of the molecular structure and concentration on the thermodynamic properties of the system.

to be submitted.

5.1 Introduction

The Scheutjens-Fleer self-consistent field (SF-SCF) approach was developed to study polymer adsorption at solid/liquid interfaces more than three decades ago^{1,2} and was further extended in various directions. Focussing on the studies that feature liquid-liquid (L-L) interfaces, we may point to an early study of polymer adsorption at a liquid-liquid interface,³ and a modelling effort to consider particles at or near the L-L interface in the context of Pickering emulsions.⁴ The formation of surfactant micelles at the L-L interface was analysed just a few years ago.⁵ More recently, we initiated the model for an oil droplet placed at the vapour/water interface.⁶ The oil in that study has a structure of a hexadecane molecule which, when placed at the air/water interface, adopts a lens-like shape with finite contact angles. Direct observations of the three-phase contact line was possible using a two-gradient cylindrical coordinate system. The line tension was found to be in the order of $\tau \approx 10^{-9}$ N. Elaborating on this model with a simple oil structure, we aim to study wetting behaviour of more complex systems including various amphiphilic components embedded in three phases of oil, vapour and water.

The motivation of this theoretical analysis is the verification of the recently suggested spray atomization mechanism based on spreading properties of emulsion droplets.⁷ When spray liquid is atomized through a hydraulic flat fan nozzle, it passes the orifice and emerges as a thin liquid sheet. The atomization of this sheet into spray droplets occurs downwards from the nozzle's outlet when the sheet first disrupts into ligaments which further on break up into spray droplets. The thickness of the liquid sheet is thereby inversely proportional to the distance from the nozzle.^{8,9} High speed photographs of the sheet breakup reveal that atomization onset is different for different spray liquids. Dilute oil-in-water emulsions disrupt by perforation and induce an earlier atomization onset, closer to the nozzle, where the liquid sheet is thicker.^{10,11} As a consequence, produced sprays are coarser and contain less fine droplets than water sprays.

In agricultural applications sprays are usually characterized by their volume median diameter (VMD) which is a measure of the mean droplet size and the fine spray fraction with droplet in diameter $< 100 \mu\text{m}$ (Chapter 2). This fine spray fraction is considered to be the most drift-prone during the application process and can lead to an unintended contamination with agrochemicals of non-target organisms and ecosystem.^{12,13} Therefore, it is of interest to reduce the percentage of these fine droplets in a spray by means of application of dilute oil-in-water emulsions.

It was observed that the magnitude of the spray coarsening effect depends on the properties of the emulsified oil, emulsion quality and concentration (Chapter 6). It was also measured that dilute emulsions of vegetable-based oils create coarser sprays than an emulsion based on mineral oil.¹⁴ Furthermore, it has been observed that changes in the dynamic air/water surface tension at the moment of sheet breakup affect the spray atomization process of dilute oil-in-water emulsions.¹⁰ In the mechanistic explanation discussed in Chapter 6 it was suggested that atomization onset is modulated by the spreading emulsion droplets which have entered the air/water interface of the liquid sheet. Fast spreading emulsion droplet may induce a liquid bulk flow and locally thin out the sheet that, reinforced by sheet perturbation, can induce the perforation onset.

The tendency of an oil to spread can be characterized by the classical spreading coefficient S , which describes the difference of interfacial energies γ at the air(vapour)/water (VW), the oil/water (OW), and the air(vapour)/oil (VO) interfaces.¹⁵

$$S = \gamma_{VW} - \gamma_{OW} - \gamma_{VO} \quad (5.1)$$

The balance of the interfacial energies allows a complete wetting for $S \geq 0$. In the case when $S < 0$, the oil forms a compact lens.

The velocity of the liquid sheet when it leaves the nozzle is in the range of 10 – 25 m/s.^{8,16} Experimentally, it is not yet possible to measure if and how an emulsion droplet spreads at the interface of the liquid sheet. The objective of this investigation is therefore to analyse molecular interactions in the three-phase systems of dilute oil-in-water emulsions by using the SCF approach. Thermodynamic properties calculated in the SCF modelling are based on the molecular structures of various compounds and their concentration in a specified volume, which is represented by a system of lattice sites organised in an appropriate geometry. The representative section of the liquid sheet shall contain a sessile droplet placed at the air/water interface so that the wetting behaviour of this droplet, which is influenced by other system components, can be studied with the theoretical model. As discussed in Chapter 6, we consider this scenario as the most probable configuration for the situation when the liquid sheet just has been formed under the nozzle outlet.

The molecular structures which are used for these calculations are inspired by the molecular compositions of "real" oils relevant for spray applications. Here we consider a triglyceride (TG), a monoglyceride (MG) and hexadecane ($C16$)

as model oils. A spacial triglyceride-ethylene oxide with a high affinity for the oil/water interface was implemented as emulsifier molecule that promotes oil spreading. Spray liquids often contain short water-soluble components that will alter the value of the air/water interfacial tension at breakup so that we introduce a second surfactant with a high affinity for the air/water interface. By decreasing the air/water interfacial tension the water-soluble surfactant builds up surface pressure which is defined as $\Pi_{VW} = \gamma_{VW}^0 - \gamma_{VW}$ with γ_{VW}^0 being the surface tension at a pristine air(vapour)/water interface. The calculations allow to make an estimation of the magnitude of the surface pressure required to inhibit the spreading of an emulsion droplet and to interlink the experimental observations with the proposed atomization mechanism.

Applying this theoretical approach we realize that the described systems are far from a full theory and describe only a section of the whole system. Ideally one would like to study the dynamics in a full scale simulation. Such an analysis however should be preceded by a detailed thermodynamic analysis of the systems of interest. The SCF theory describes a system in thermodynamic equilibrium or, in this case, the final wetting stage which the system is aiming for and thus delivers vital information onto which a dynamic theory can be constructed. We further argue that molecular detailed equilibrium theory can be used to study scenarios that are relevant for the dynamic situation, and thus already allows us to infer on what would happen in dynamic processes.

5.2 Materials and Methods

Spray liquids have been prepared with emulsions based on sunflower oil (purchased from John L. Seaton & Co. Ltd.), rapeseed oil methyl ester (trade name Synative ES ME SU purchased from Cognis) and mineral oil (trade name Exxsol D140 purchased from ExxonMobil Chemicals). Appropriate emulsifier mixtures were selected to guarantee the optimal emulsion stability and quality according to the CIPAC method MT 36.3.¹⁷ The emulsions were created by dilution of an oil/emulsifier mixture in hard CIPAC C water.¹⁸ As described in table 5.1, all dilute oil-in-water emulsions were prepared at a concentration of 0.1% w/w of the dispersed phase in water. They were homogenized by shaking and placed in a pressurized vessel that supplied the spray liquid to the nozzle. Alkyl-ethylene oxide type surfactant (trade name Synperonic A7 purchased from Croda) and sodium C8-ether sulphate (supplied by AkzoNobel) were used to modify the air/water interfacial tension of the spray liquid. All spray liquids have been prepared with materials of technical

Table 5.1: Composition of spray liquids that contain dilute emulsions with the concentration of dispersed phase 0.1% w/w.

oil	% w/w in spray liquid	emulsifier	% w/w in spray liquid	% w/w dispersed phase
mineral oil	0.09	Tanemul SO70 ^b	0.008	0.1
		Tanemul L3 ^b	0.002	
sunflower oil	0.09	Arlatone TV ^a	0.01	0.1
methyl ester	0.09	Tanemul SO70 ^b	0.004	0.1
		Emulsifier 1371A ^c	0.006	

supplier: ^a Croda, ^b Tanatex, ^c Lanxess

quality that have been used without further purification.

The sprays were produced with a flat fan TeeJet XR11003 nozzle which was operated at a pressure of 3 bar. The nozzle was mounted on a linear unit and moved 33 cm above the laser beam with a velocity of 2 cm/s along the long axis of the spray fan. The droplet size distributions were measured with a Spraytec instrument (Malvern Instruments Ltd.), equipped with a 300 mm lens. This equipment allows to measure droplet sizes in the range of 0.1–900 μm . Spraytec Software Version 3.03 was used to calculate the numerical values of the volume median diameter (VMD) and the percentage of spray liquid with diameter $< 100 \mu\text{m}$. The measurements were replicated three times for each sample. The reproducibility of the VMD values was $\pm 3 \mu\text{m}$ and that of the V_{100} values better than $\pm 1\%$. The measurements were performed at room temperature of 20–25°C. The liquid temperature was about 21°C.

To determine the spreading properties of the emulsified oil, the static interfacial tensions at the air/oil and the oil/water interfaces were measured with a Prozessor-Tensiometer K100 (Krüss GmbH) using the Wilhelmy plate method. A BP2 bubble tensiometer (Krüss GmbH) was used to obtain the dynamic surface tension at the fast expanding air/water interface at $\geq 10 \text{ ms}$ 20°C. The surface tension at breakup of the liquid sheet γ_{VW}^{br} was obtained by extrapolation to 1.5 ms as described in Chapter 6.

5.3 Self-Consistent Field Theory

Here we will only mention the underlying approximation of the SF-SCF theory and explain the various geometries used in the calculations to evaluate different

oil/water/vapour/surfactant systems. For more details we refer to our previous publication.⁶

In the self-consistent-field approach, the direct binary interactions of all molecules are replaced by interactions with an external potential field, specified by a segment potential u . The potential fields thus represent the interactions with the molecular environments that this molecule is subjected to. The target of the SCF approach is to predict the dimensionless concentration profile $\varphi_i(\mathbf{r}, s)$ of segments $s = 1, 2, \dots, N_i$ of a molecules type i (water, oil, vapour, surfactant) which may be collected into volume fraction profiles per segment type $\varphi_X(\mathbf{r})$ (X represent hydrocarbon, water, free volume, etcetera). Thus, molecules are seen as strings of segments, and according to the discretisation scheme each segment fits in a lattice site. We use two lattice geometries: (i) in a one-gradient coordinate system we consider lattice layers (in x - y plane) over which the concentration fluctuations are averaged and volume fractions are computed or a spherical coordinate system with lattice layers r consisting of spherical shells with $L(r) \propto r^2$ sites over which the densities are averaged, (ii) a two-gradient cylindrical coordinate system, with gradients both in the z -direction and in a radial direction r are accounted for, while a mean field averaging is implemented along all lattice sites within the ring of lattice sites specified by $\mathbf{r} = (z, r)$ coordinates.

The central quantity of the SCF theory is the mean field free energy which is expressed in terms of the volume fraction and corresponding potential profiles. In addition there is an incompressibility constraint imposed on the system. The latter is implemented using Lagrange parameters $\alpha(\mathbf{r})$. One can always write a SCF free energy in the following (generic) form:

$$\frac{F}{k_B T} = -\ln Q[u] - \sum_{\mathbf{r}} \sum_X u_X(\mathbf{r}) \varphi_X(\mathbf{r}) + F^{\text{int}}[\varphi] + \sum_{\mathbf{r}} \alpha(\mathbf{r}) \left(\sum_X \varphi_X(\mathbf{r}) - 1 \right) \quad (5.2)$$

in this equation Q represents the partition function of the system which can be evaluated when the potentials are known, and F^{int} specifies the interaction energy in the system, which can be evaluated when the volume fractions are known. It is important to mention that in order to be able to compute the partition function Q one has to specify a chain model. Here we use the freely jointed chain model which can efficiently be executed on a lattice using the well-documented propagator formalism. Using the propagators one also can compute the volume fractions straightforwardly and efficiently. To evaluate F^{int} one must decide what types are

included and how this is done. Here we implemented the Bragg-Williams mean field approximation which accounts for short-range nearest neighbour interactions only. These are parameterized by the Flory-Huggins parameters χ_{XY} between two segment types X and Y . When this value is positive it signals repulsion and a negative value implies attraction. Interactions between similar segment types are zero by construction, i.e. by choice of the reference state.

The output of the calculations is information on the relevant stable conformation of the system. To find this, one needs to find the saddle point of the free energy, that is, the so-called self-consistent field point which obeys to

$$\frac{\partial F}{\partial \varphi_X(\mathbf{r})} = 0 \quad (5.3)$$

$$\frac{\partial F}{\partial u_X(\mathbf{r})} = 0 \quad (5.4)$$

$$\frac{\partial F}{\partial \alpha(\mathbf{r})} = 0 \quad (5.5)$$

To obtain the most probable state of the system, implies a numerical algorithm¹⁹ wherein an initial guess for the segment potential for all segments u^i produces through calculations new volume fractions φ^n . Subsequently, the calculated volume fractions can be used as an input to obtain a new value of the segment potentials u^n as output. A fixed point of these equations implies that the input potentials are equal to the output potentials. We can formulate the SCF procedure also by specifying input volume fractions (as a guess) and computing *via* the potentials the new volume fractions as the output. Then the fixed point means that input volume fractions equal output volume fractions. Those solutions which have a fixed point and obey to the incompressibility constraint $\sum_X \varphi_X(\mathbf{r}) = 1$ can be shown to optimize the Helmholtz energy and thus represent a relevant equilibrium state of the system. Inserting these volume fraction profiles as well as the corresponding potentials in the Helmholtz energy gives the optimized Helmholtz energy. The SCF solution is routinely generated with a precision of at least seven digits.

5.3.1 Measurables

The one-gradient flat geometry was used to derive the interfacial tensions for the planar interfaces in such a way that the system encompasses two bulk phases. The system is not necessarily limited to two components. When more components are present one typically specifies the bulk volume fraction in one of the bulk phases

which may be known from complementary calculations. Then these molecules will partition between the two phases and will adsorb/deplete from the interface. The lattice has a finite number $z = 1, \dots, M$ of parallel layers with implemented reflection boundary conditions. For the current system, the interfaces created in these calculations are sharp having a thickness of a water molecule cluster with three lattice sites. The interfacial width is thus only slightly larger than the discretization length. The interfacial tensions can be identified from the grand potential Ω per unit area across the interface.

$$\Omega = F - \sum_i \frac{\theta_i}{N_i} \mu_i \quad (5.6)$$

Wherein μ_i indicates the chemical potential of component i (found by applying the Flory-Huggins equations for the homogeneous bulk phases) and $\theta_i = \sum_z \varphi_i(z)$ is the amount of segment per unit area of component i in the system, and N_i is the number of segments per molecule i and is unity for the simple case of monomers. Thus $\theta_i/N_i = n_i$ is the number of molecule per unit area in the system. It is possible to write $\Omega = \sum_z \omega(z)$, which features the grand potential density $\omega(z)$. The grand potential density gives access to various thermodynamic quantities, such as line tension of an oil droplet in the cylindrical coordinate systems. In passing we note that when the interface is curved, such as in a spherical oil droplet in water, inside such droplet the grand potential density is identified by the Laplace pressure ΔP which obeys to the Laplace equation

$$\Delta P = \frac{2\gamma}{R} \quad (5.7)$$

when the interfacial tension γ is evaluated at the so-called surface of tension defined by the radius for which the notional change of the radius of the drop does not change the interfacial tension, that this $[\partial\gamma/\partial R] = 0$. The interfacial tension as found by equation 5.7 may depend on the radius R of the drop but converges to the value of the planar interface in the limit of $R \rightarrow \infty$.

The excess amounts of each component at an interface can be computed with respect to the Gibbs plane. By defining the Gibbs plane z_{Gibbs} between two phases of A and B components, we can calculate the Gibbs excess concentration of a component X at the respective interface. When the total amount of one major component B is $\theta_B = \sum_z \varphi_B(z)$ with concentrations far from the interface $T_B(1) = \varphi_B(1)$ and $T_B(m) = \varphi_B(m)$, the Gibbs plane is assigned as

$$z_{\text{Gibbs}} = (\theta_B - T_B(m) \times m) / (T_B(1) - T_B(m)) \quad (5.8)$$

For the component X there is a pair of bulk values: $T_X(1) = \varphi_X(1)$ and $T_X(m) = \varphi_X(m)$ and the total amount $\theta_X = \sum_z \varphi_X(z)$. The Gibbs excess Γ_X can be calculated as

$$\Gamma_X = \theta_X - z_{\text{Gibbs}} \times T_X(1) - (m - z_{\text{Gibbs}}) \times T_X(m) \quad (5.9)$$

Knowing the Gibbs excess at the three interfaces and the surfactant concentration in the three bulk phases, it is possible to obtain its excess concentration at the three-phase contact line Γ^L .

A one-gradient spherical coordinate system was used to model the micellisation of surfactants. In a spherical lattice, the micelle is placed in the center of the coordinate system and is surrounded by a water-rich or an oil-rich phase in the case of inverted micelles. $r = 1, 2, \dots, M_r$ concentric layers are arranged in a shell-like manner. The mean-field approximation is applied in each of the layers r . The critical micelle concentration (*cmc*) can be derived from the grand canonical potential $\Omega(n_{agg})$ which is the function of surfactant aggregation number and has a maximum near the *cmc*.^{20,21} Macroscopically stable micelles are formed when $\partial\Omega/\partial n_{agg} < 0$ so that *cmc* conditions were identified by the case for which $\partial\Omega/\partial n_{agg} = 0$.

A two-gradient cylindrical geometry was used to study the positioning of the oil droplet at the air/water interface. The cylindrical lattice consists of $M_z = 50$ layers in z direction with and $M_r = 100$ layers in radial r direction. The resulting properties of the segments are rationally symmetric along the cylinder length axis. The segments of the oil molecules and surfactants are pinned in the middle of the M_z axis at one side of the lattice where $M_r = 0$. The remainder of the lattice is filled by vapour-rich and water-rich phases which constitute the air/water interface.

The calculated numerical values are presented in dimensionless units in magnitude of thermal energy $k_B T$. The discretisation length $b \approx 0.2$ nm is an appropriate size for a lattice cell to fit a methyl unit considering that a C-H bond length is about 0.154 nm and the angle of 109.5° gives a length of the methyl unit of 0.217 nm which is approximately 0.2 nm. The interfacial tension at the air/water interface has been evaluated in earlier studies using the SCF approximation as $\gamma_{VW} = 0.665 k_B T/b^2$ or $\gamma_{VW} = 68.9$ mN/m, which compares favourable with the known value for water.

5.3.2 Parameters

The experimentally used oils are mixtures of several compound one of which typically predominates. Our approach is to restrict the structural variety by modelling purely the main compound applying the coarse grained approach. This implies that described oils are only qualitatively linked to the oils which have been used in the experimental part and that the spreading of these oils can in the first instance be understood using the SCF approach.

All molecular structures used in the SCF modeling are collected in figure 5.1. The sunflower oil contains predominately triglyceride fatty acids of varying saturation degrees and chain lengths ranging between C_{16} and C_{18} . We use a C_{16} triglyceride to mimic the structure of sunflower oil. Synative ES ME SU which is rapeseed oil methyl ester with a chain length of predominately C_{16} to C_{18} (and about 0.2% w/w esters with a chain length $< C_{14}$). The structure of methyl ester was replaced by a C_{16} monoglyceride compound that bears structural resemblance with the triglyceride molecule. The modelled hexadecane oil is used to describe a non-aromatic mineral oil which consists of a mixture of alkanes with a similar chain length.

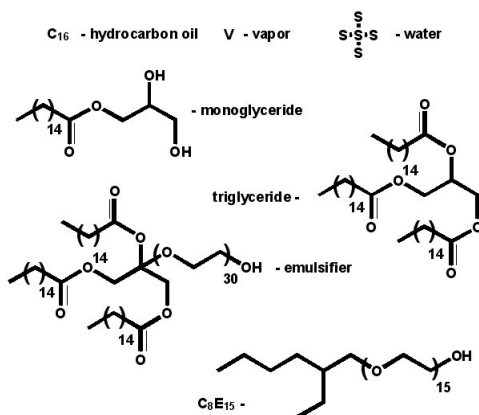


Figure 5.1: Various types of molecules used for SCF modelling.

The Flory-Huggins interaction parameters are specified in table 5.2. The vapour phase in this system is described by the free volume monomers V which are unoccupied lattice sites. A simplistic S_5 -model²² is applied to describe water molecules as a cluster structure with one central unit that is surrounded by four similar units as shown in figure 5.1. The interaction parameter $\chi_{V,S} = 2.5$ results in a strong demixing between vapour and water segments.

Table 5.2: Flory-Huggins χ -interaction parameters.

χ	V	S	C	O	O_E
V	0	2.5	2	2.5	2.5
S	2.5	0	1.1	0	-0.6
C	2	1.1	0	1	2
O	2.5	0	1	0	0
O_E	2.5	-0.6	2	0	0

Further interaction parameters were chosen such, that each of the oil phase separates with water and vapour. The CH_3 - and the CH_2 -units of the hexadecane oil and of fatty acids in the tri- and the monoglyceride structures are represented by C -segments. The hydroxyl and the carboxyl groups in both vegetable oils are described by O -segments. With $\chi_{CV} = 2$ and $\chi_{CS} = 1.1$ C -segments create a sharp interface with the vapour- and the water-rich phase favouring the formation of a third oil-rich phase. O -segments with $\chi_{OV} = 2.5$ and $\chi_{OS} = 0$ reveal a strong repulsion with vapour segments and are tolerated by the water-clusters implying an orientation of the glyceride backbone towards the water-rich phase.

Emulsifier blends listed in table 5.1 are as well mixtures of several compounds. The beneficial properties of these emulsifier blends are their good solubility in the oil phase and a high affinity for the oil/water interface; both of which guarantee a good homogeneity and a long-term stability of the produced dilute emulsions. In the modelling part we want to avoid the confusion which might be caused by the structural variety of emulsifier blends. Instead, we aim to design one molecule that reproduces the desired properties of these emulsifier blends without altering its molecular structure for each of the investigated oils. As shown in figure 5.1, the modelled emulsifier consists of a triglyceride-like part attached to a long ethylene oxide chain. The ethylene oxide groups (E-groups) contain C - and O_E -segments. O_E -segments are more hydrophilic than O -segments of the glyceride backbone. This is reflected by the corresponding χ -parameter $\chi_{O_E S} = -0.6$. This interaction parameter enables the emulsifier molecule to stretch its ethylene oxide chains into the water-rich phase what, combined with a considerable chain length of 30 E-groups and strong repulsive interaction within the chain $\chi_{CO_E} = 2$, both increase the molecular attraction towards the oil/water interface. The triglyceride part at the same time remains immersed into the oil-rich phase which makes this spacial molecule to a good emulsifier for each of the oils.

As outlined above, it is of interest to study the spreading behaviour of sessile

emulsion droplets in the presence of a further surfactant molecule that occupies the air/water interface. Approaching this goal, we introduce an alkyl-ethylene oxide C_8E_{15} . For simplification reasons this surfactant, same as the modelled emulsifier, does not reflect an exact molecular structure of the surfactants used in the experimental part of this study but possesses the desired physical properties. The rather long ethylene oxide chain and a short C_8 -tail with a side chain, both increase the affinity of the surfactant for the air/water interface. At the same time the surfactant will also be attracted by the oil/water interface which represents a realistic scenario for experimental situations.

5.4 Results and Discussion

5.4.1 Modeling

First, we characterise surfactant-free systems that contain oil, water and vapour molecules. One-dimensional flat geometry was applied to extract the grand potential at the air/water (γ_{VW}), the air/oil (γ_{VO}) and the oil/water (γ_{OW}) interfaces. Table 5.3 shows the resulting interfacial tensions γ for the hexadecane ($C16$), the triglyceride (TG) and the monoglyceride (MG) oil containing systems. In a previous study, the curvature dependence of interfacial tensions was found to be small and was therefore neglected in this study.⁶

The absence of oxygen-carrying segments in the molecular structure of the mineral oil accounts for its high oil/water interfacial tension $\gamma_{OW} = 0.478 k_B T/b^2$. The O -segments in the glyceride backbones of both MG and TG structures diminish the oil/water repulsion providing comparably low oil/water interfacial tensions $\gamma_{OW} = 0.384 k_B T/b^2$ for the triglyceride and $\gamma_{OW} = 0.249 k_B T/b^2$ for the monoglyceride oil.

Table 5.3: Calculated surface tensions γ in $k_B T/b^2$ units.

	$C16$	TG	MG
γ_{OW}	0.478	0.384	0.249
γ_{VO}	0.537	0.549	0.518
γ_{VW}	0.665	0.665	0.665

Figures 5.2a-f show the shape and the positioning of the three oil droplets at the air/water interface calculated in a two-dimensional cylindrical lattice. The volume fractions of each oil are concentrated in the middle part of the lattice in

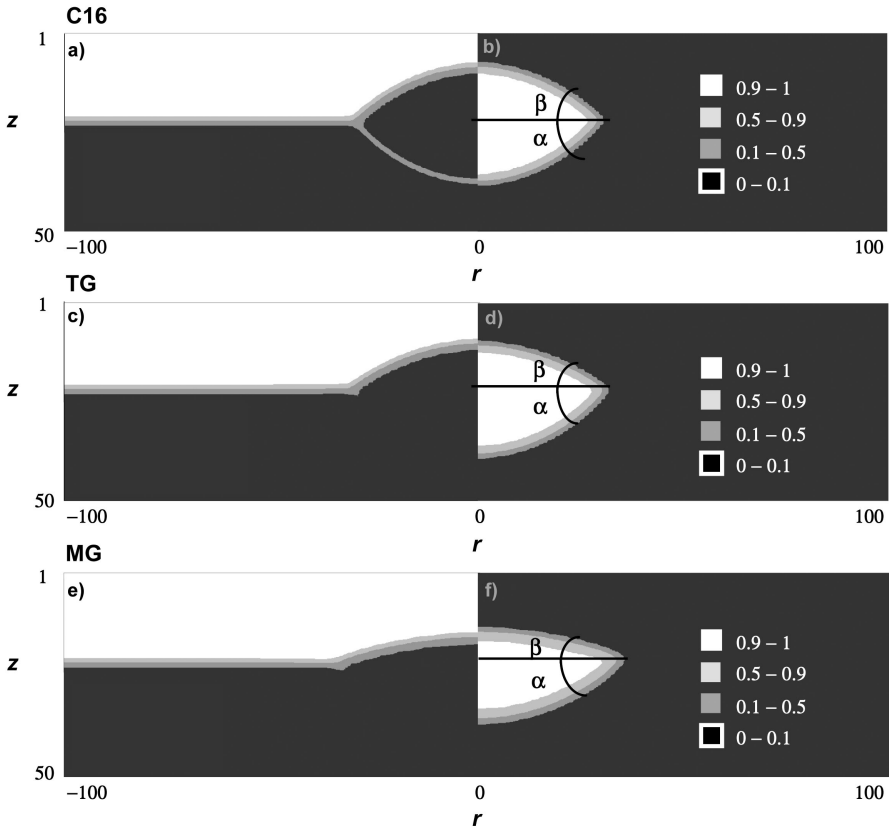


Figure 5.2: Equidensity contour plots computed in a two-gradient cylindrical geometry of a) volume fraction of the free volume units φ_V in a *C16*/water/vapour system, b) volume fraction of the hydrocarbon oil φ_{C16} , c) volume fraction of the free volume units φ_V in a *TG*/water/vapour system, d) volume fraction of triglyceride oil φ_{TG} , e) volume fraction of the free volume units φ_V in a *MG*/water/vapour system, f) volume fraction of the monoglyceride oil φ_{MG} .

the form of a compact droplet while free volume predominately occupies the upper half of the lattice allowing the water clusters to assemble in the lower part of the lattice. The volume fractions of the free volume and of the hexadecane oil in a *C16*/water/vapour system are shown in figures 5.2a and b. An accumulation of vapour-segments at the oil/water interface in figure 5.2a can be explained by the strong repulsion between the *C16* molecules and water clusters. A triglyceride oil droplet is illustrated in figures 5.2c and d and the monoglyceride droplet in figures 5.2e and f. There is no accumulation of the vapour segments between the oil-rich and the water-rich phases for both glyceride-containing oils due to a lower surface tension between the two phases.

Comparing the shape of the three sessile droplets, it becomes evident that *C16* with the highest oil/water interfacial tension forms a more compact drop than the monoglyceride oil with the lowest γ_{OW} . The calculated macroscopic interfacial tensions (table 5.3) allow the estimation of the three-phase contact angles from the Neumann triangle of interfacial forces.²³

$$\cos \alpha = \frac{\gamma_{VW}^2 + \gamma_{OW}^2 - \gamma_{VO}^2}{2\gamma_{VW}\gamma_{OW}} \quad (5.10)$$

$$\cos \beta = \frac{\gamma_{VW}^2 + \gamma_{VO}^2 - \gamma_{OW}^2}{2\gamma_{VW}\gamma_{VO}} \quad (5.11)$$

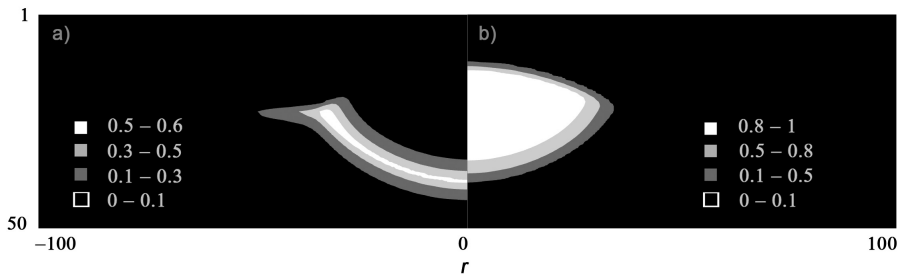
As indicated in figure 5.2, β is the contact angle at the oil/air and α at the oil/water interface. The *C16* oil droplet has contact angles $\alpha = 52.9^\circ$ and $\beta = 45.5^\circ$, triglyceride droplet has contact angles $\alpha = 55.6^\circ$ and $\beta = 35.2^\circ$. The monoglyceride droplet is more stretched at the interface than both other oil droplets which is reflected by the lowest contact angles $\alpha = 45.0^\circ$ and $\beta = 19.8^\circ$. The calculated contact angles describe well the shapes of the three oil droplets illustrated in figure 5.2.

In the next step, the emulsifier molecule is stepwise titrated to the three-phase system. Thereby, the upper concentration limit is defined by the critical micelle concentration of the emulsifier in the respective phase. The *cmc* values obtained in a spherical one-dimensional lattice are reported in table 5.4. Emulsifier forms stable micelles in the water-rich phase at a *cmc* $\approx 10^{-14}$ while its inverse micelles are stable at sufficiently higher concentrations.

Figure 5.3 shows a *C16*/water/vapour system with emulsifier concentration $\varphi_{emulsifier} = 1 \times 10^{-17}$. The surfactant molecules are located strictly at the oil/water interface and are concentrated in the vicinity of the three-phase contact

Table 5.4: Calculated *cmc* of emulsifier in the water- and the oil-rich phases.

oil	solvent	<i>cmc</i>
<i>C16</i>	water	3.8×10^{-14}
	oil	5.4×10^{-10}
<i>TG</i>	water	4.4×10^{-14}
	oil	9.9×10^{-5}
<i>MG</i>	water	2.4×10^{-14}
	oil	1.1×10^{-3}

**Figure 5.3:** Counter plot of a *C16*/water/vapour system with emulsifier at a concentration $\varphi_{emulsifier} = 1 \times 10^{-17}$. a) Volume fraction of the emulsifier molecules and b) volume fraction of the hydrocarbon oil φ_{C16} .

line. It is possible to estimate the excess amount of surfactant at the three-phase contact line Γ^L for the situation illustrated in figure 5.3. The total emulsifier concentration in the system $\theta_{emulsifier} = \Sigma_z \varphi_{emulsifier}(z)$ consists of the surfactant concentrations φ in each bulk volume (V) and the excess fractions at each of the interfaces (A).

$$\begin{aligned} \theta_{emulsifier} = & A^{OW} \Gamma_{emulsifier}^{OW} + V^{OW} \varphi_{emulsifier}^{OW} \\ & + A^{VW} \Gamma_{emulsifier}^{VW} + V^{VW} \varphi_{emulsifier}^{VW} \\ & + A^{OV} \Gamma_{emulsifier}^{OV} + V^{OV} \varphi_{emulsifier}^{OV} + L_c \Gamma_{emulsifier}^L \end{aligned} \quad (5.12)$$

The geometry of the systems was calculated as described in Chapter 4 and the resulting excess surfactant concentrations per unit area at the three interfaces are $\Gamma_{emulsifier}^{OW} = 3.5$, $\Gamma_{emulsifier}^{OV} = 1.2 \times 10^{-7}$ and $\Gamma_{emulsifier}^{VW} = 3.4 \times 10^{-5}$. With $\theta_{emulsifier} = 21517$, this gives the surfactant concentration at the contact line $\Gamma_{emulsifier}^L = 3.2$ per unit length. The computed Gibbs excess reveals that surfactant accumulates strongly at the oil/water interface and at the contact line and that this molecular distribution is required to promote oil spreading. A depletion of the emulsifier at the interface or the contact line will certainly result in a lower tendency of the oil to wet the interface.

In figure 5.4, the contact angles α and β are plotted as a function of the emulsifier concentration. The decrease of the oil/water interfacial tension first affects the contact angle β allowing the droplet to sink deeper into the water-rich phase. Both contact angles decrease further with increasing concentration of the emulsifier so that an emulsion droplet completely wets the interface at $\varphi = 2 \times 10^{-15}$ in the case of hexadecane oil, at $\varphi = 8 \times 10^{-15}$ in the case of triglyceride and at $\varphi = 3 \times 10^{-16}$ in the case of monoglyceride. The oil/water interfacial tension at these concentrations is $0.114 - 0.138 k_b T / b^2$.

MG requires less emulsifier to spread further than both other oil-rich phases. *TG* and *C16* spread completely at higher emulsifier concentrations due to their high interfacial tensions. The spreading of *TG* is counteracted by the high γ_{OV} .

Emulating small amphiphilic molecules that can be present in the aqueous bulk phase during spray applications, we add a C_8E_{15} surfactant to the systems that already contains the emulsifier molecules sufficient to wet the interface completely. The critical micelle concentrations of the C_8E_{15} in the water-rich phase and each of the oil-rich phases are collected in table 5.5.

Figure 5.5 shows the distribution of volume fraction of all components in a

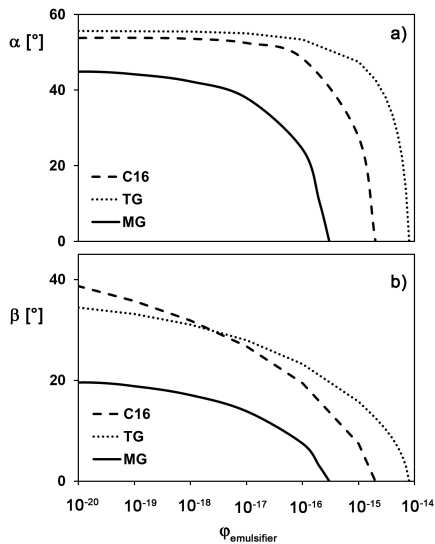


Figure 5.4: Three-phase contact angles a) α at the oil/vapour interface and b) β at the oil/water interface plotted versus the total emulsifier concentration ($\varphi_{emulsifier}$).

Table 5.5: Calculated cmc of C_8E_{15} surfactant in the water- and the oil-rich phases.

oil	solvent	cmc
$C16$	water	–
	oil	6.3×10^{-6}
TG	water	–
	oil	4.2×10^{-5}
MG	water	–
	oil	5.4×10^{-3}

flat one-dimensional geometry with 200 layers for a $C16$ /water/vapour system. The C_8E_{15} surfactant adsorbs preferentially at the air/water interface and at the oil/water interface along with the emulsifier. This has the consequences that the C_8E_{15} surfactant builds up a surface pressure at the air/water interface and at the same time it influences the oil/water interfacial tension as illustrated in figure 5.6.

Equations 5.10 and 5.11 indicate that the decrease of the air/water interfacial tension (and an increase in surface pressure) inhibits spreading and that a decrease in the oil/water interfacial tension, on the other hand, promotes it. In all investigated systems the effect of the surface pressure dominates spreading by inducing a continuous increase of both contact angles (figure 5.7). Thereby, changes in the

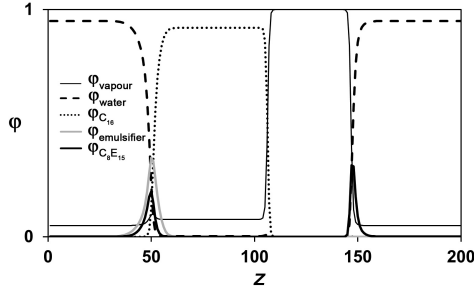


Figure 5.5: Three interfaces in a $C16$ /water/vapour system with $\varphi_{emulsifier} = 1 \times 10^{-17}$ and $\varphi_{C_8E_{15}} = 1 \times 10^{-3}$.

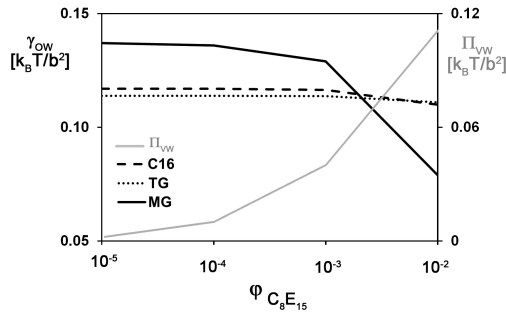


Figure 5.6: Surface pressure at the air/water interface Π_{VW} (gray) and the oil/water interfacial tension γ_{OW} as function of the concentration of the C_8E_{15} surfactant with $\varphi_{emulsifier}^{C16} = 2 \times 10^{-15}$, $\varphi_{emulsifier}^{TG} = 8 \times 10^{-15}$ and $\varphi_{emulsifier}^{MG} = 3 \times 10^{-16}$.

contact angle β are smaller because γ_{OV} remains unaffected. By altering the γ_{OW} and γ_{VW} , both surfactants force the oil droplet to sink further into the water-rich phase reducing the area that the droplet covers at the air/water interface.

Figure 5.7 shows an example for one set of concentrations. At higher and lower emulsifier concentrations the contact angles are correspondingly less or more influenced by the surface pressure. This relation is not dictated by a molecular composition of the surfactant that acts as the spreading inhibitor so that the emulsifier can also retard spreading when accumulating at the air/water interface. The modelling results show that with increasing surface pressure, each of the emulsion droplets regains its more compact lens-like shape as indicated by the increasing contact angles. It is interesting to notice that spreading is retarded in all cases at a surface pressure as low as $\Pi_{VW} = 0.01 k_B T / b^2$ (for $\varphi_{C_8E_{15}} = 1 \times 10^{-4}$) and is much pronounced at $\Pi_{VW} = 0.04 k_B T / b^2$ (for $\varphi_{C_8E_{15}} = 1 \times 10^{-3}$) that converted correspond to a surface pressure $\Pi_{VW} = 1$ mN/m and 4 mN/m.

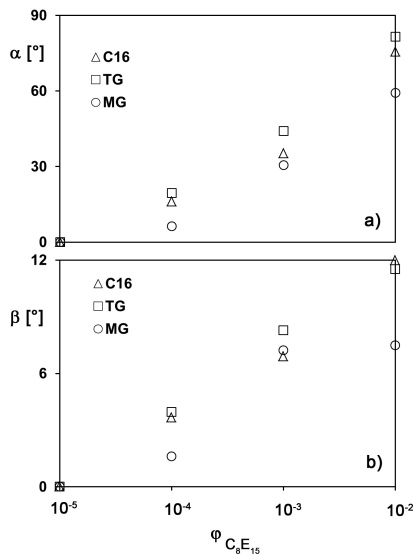


Figure 5.7: Three-phase contact angles a) α at the oil/vapour interface and b) β at the oil/water interface plotted versus the total concentration of soluble surfactant ($\varphi_{C_8E_{15}}$) with $\varphi_{emulsifier}^{C16} = 2 \times 10^{-15}$, $\varphi_{emulsifier}^{TG} = 8 \times 10^{-15}$ and $\varphi_{emulsifier}^{MG} = 3 \times 10^{-16}$.

Here we describe a static-state situation where spreading is modulated mostly by the concentration of emulsifier that completely covers the oil/water interface and the three-phase contact line. The oil/vapour interfacial tension that remains unoccupied also contributes significantly to this process and accounts for the emulsifier concentration required to achieve full spreading. Under dynamic conditions spreading velocity of an emulsion droplet will be associated with the spreading properties of pure oil because emulsifier concentration may be depleted at the oil/water interface during the spreading process. Then, the coverage of the air/water interface will strongly depend on the diffusion coefficient of the molecules dissolved in water and not only on their concentration. Using this static approach, we can anticipate the tendencies that a fast spreading oil with possibly low surface tensions will be less affected by the increase in the surface pressure than a slow spreading oil with high surface tensions.

5.4.2 Experimental results

As mentioned above, the *C16* hydrocarbon, the triglyceride and the monoglyceride structures are model systems for a typical mineral oil, sunflower oil and rapeseed oil methyl ester used in the experimental part of this study. Table 5.6 shows the

Table 5.6: The measured interfacial tensions and the derived spreading coefficient S calculated for the interfacial tension at the air/water interface $\gamma_{VW} = 72.0$ mN/m.

oil	γ_{VO} [mN/m]	γ_{OW} [mN/m]	S [mN/m]
mineral oil	28.6	43.1	0.3
sunflower oil	33.5	25.2	13.3
rapeseed oil methyl ester	31.6	11.9	28.5

measured interfacial tensions of three investigated oils and their resulting spreading coefficients. Mineral oil that contains a mixture of aliphatic hydrocarbons of different chain lengths has the highest experimental oil/water interfacial tension $\gamma_{OW} = 43.1$ mN/m and correspondingly the lowest spreading coefficient. The sunflower oil, that consists mostly of triglycerides, has a $\gamma_{OW} = 25.2$ mN/m and its spreading coefficient is higher than that of the mineral oil. The lowest oil/water interfacial tension of 11.0 mN/m and the highest spreading coefficient has the methyl ester.

The tendency of an oil droplet to spread at the pristine air/water interface defined by the spreading coefficient in the experimental part (table 5.6) is reflected by the contact angles of the three modelled systems (figure 5.2). The dependence of the calculated γ_{OW} on the molecular structure of the oil (table 5.3) is consistent with experimental data (table 5.6). The calculated coefficients of pure oils are $S_{C16} = -0.352$, $S_{TG} = -0.268$ and $S_{MG} = -0.104 k_B T/b^2$. They increase with increasing emulsifier concentration approaching zero at complete wetting.

When dilute oil-in-water emulsions based on the systems described above are sprayed through a conventional nozzle, all formed sprays are coarser than the water spray. At the same time the sprays produced by dilute emulsions differ in their mean droplet size. Water without additives creates sprays with VMD = 194 μm and 11.0% of spray droplet with diameter < 100 μm . The mineral oil-based emulsion increases the VMD of the spray to 237 μm and decreases the percentage of fine spray droplets down to 5.8% compared to water (table 5.7). As shown in table 5.8, a dilute sunflower oil emulsion creates coarser sprays with VMD = 256 μm with 3.3% of fine spray droplets. Dilute emulsion based on emulsified methyl ester leads as well to formation of coarser sprays compared to water alone with a VMD = 246 μm and 3.8% of spray droplet < 100 μm (table 5.9). Spray coarsening achieved by the mineral oil-based emulsion is weaker compared to the coarsening effect which was measured with the sunflower oil and the methyl ester emulsions.

When a water-soluble surfactant is present in the spray liquid at a sufficiently

Table 5.7: The VMD and the fine spray fraction of spray liquids that contain 0.1% w/w mineral oil emulsions and a non-ionic or an anionic surfactant. γ_{VW}^{br} is the dynamic air/water interfacial tension and Π_{VW}^{br} is the surfaces pressure at breakup.

non-ionic surfactant				anionic surfactant			
γ_{VW}^{br} [mN/m]	Π_{VW}^{br} [mN/m]	VMD [μ m]	volume % < 100 μ m	γ_{VW}^{br} [mN/m]	Π_{VW}^{br} [mN/m]	VMD [μ m]	volume % < 100 μ m
72.0	0	237	5.8	72.0	0	237	5.8
71.2	0.8	216	7.8	71.7	0.3	216	7.8
68.7	3.3	205	9.3	70.3	1.7	200	9.9
67.6	4.4	185	12.9	67.9	4.1	192	11.4

Table 5.8: The VMD and the fine spray fraction of spray liquids that contain 0.1% w/w sunflower oil emulsions and a non-ionic or an anionic surfactant. γ_{VW}^{br} is the vapour/water interfacial tension and Π_{VW}^{br} is the surfaces pressure at breakup.

non-ionic surfactant				anionic surfactant			
γ_{VW}^{br} [mN/m]	Π_{VW}^{br} [mN/m]	VMD [μ m]	volume % < 100 μ m	γ_{VW}^{br} [mN/m]	Π_{VW}^{br} [mN/m]	VMD [μ m]	volume % < 100 μ m
72.0	0	256	3.3	72.0	0	256	3.3
69.9	2.1	231	5.4	71.0	1.0	246	3.6
68.1	3.9	219	6.8	69.7	2.3	233	5.0
65.5	6.5	192	10.6	67.8	4.2	221	6.4

Table 5.9: The VMD and the fine spray fraction of spray liquids that contain 0.1% w/w rapeseed oil methyl ester emulsions and a non-ionic or an anionic surfactant. γ_{VW}^{br} is the vapour/water interfacial tension and Π_{VW}^{br} is the surfaces pressure at breakup.

non-ionic surfactant				anionic surfactant			
γ_{VW}^{br} [mN/m]	Π_{VW}^{br} [mN/m]	VMD [μ m]	volume % < 100 μ m	γ_{VW}^{br} [mN/m]	Π_{VW}^{br} [mN/m]	VMD [μ m]	volume % < 100 μ m
72.0	0	246	3.8	72.0	0	246	3.8
70.5	1.5	238	4.7	71.2	0.5	233	5.3
68.8	3.2	230	5.5	69.4	2.6	215	7.7
67.5	4.5	196	10.2	65.5	6.5	191	11.6

high concentration to affect the dynamic surface tension at the moment of break γ_{VW}^{br} , it also influences the mean droplet size of produced sprays. Experimental data for the three dilute emulsions with an anionic and non-ionic surfactant dissolved in water are collected in tables 5.7-5.9. Already small changes of the interfacial dynamic surface tension, that induce a surface pressure as low as $\Pi_{VW}^{br} = 0.8$ mN/m (table 5.7), are sometimes sufficient to achieve a measurable reduction of the spray droplet size. At a surface pressure of 3.6 - 4.4 mN/m, sprays produced by dilute emulsions become as fine as sprays produced by water with the VMD

close to 194 μm and the fine spray fraction $\approx 11.0\%$. These observations allow the conclusion that an increasing surface pressure either decreases the number of incidents that induce perforation or inhibits emulsion droplets in their mode of action.

5.5 Conclusion

Wetting behaviour of a single emulsion droplet that has entered the air/water interface is an interesting phenomena for theoretical investigation and at the same time has a high relevancy for applied sciences. In this study such a system was investigated in the light of the recently suggested spray atomization mechanism based on the spreading properties of emulsion droplets. A detailed experimental analysis of the spray atomization onset during a spray application is not possible due to the prevalent high dynamics. These systems were accessed applying a molecularly detailed concept.

Using the self-consistent field approach we set up a model that contains an oil/emulsifier phase embedded in an air/water system with a second short water-soluble surfactant. It was shown that the oil/water interfacial tension is strongly influenced by the volume fraction of the emulsifier that behaves as a spreading promoter. The air/water interfacial force was, on the other hand, modulated by the volume fraction of the water-soluble surfactant. This compound builds up surface pressure and behaves as a spreading inhibitor forcing the spread emulsion droplet to adapt a lens-like shape. Both processes were observed for oils of different chemical composition, all of which mimic compounds typically used in agricultural spray liquids.

Theoretical investigations show that, an oil-rich phase with lower interfacial tensions and a higher tendency to spread requires less emulsifier to wet the interface completely and is less affected by the surface pressure from a molecule that acts as a spreading inhibitor. As shown in the experimental part, dilute emulsions based on oils with a high positive spreading coefficient produce coarser sprays than those based on a mineral oil with a low positive spreading coefficient. Sprays formed by each of the dilute emulsions become finer with increasing surface pressure at breakup. These observations imply that spreading of emulsion droplets at the interface of the liquid sheet modulates perforation and that the spreading velocity determines the onset of the spray atomization and the final spray droplet size. Photographs of the disrupting liquid sheet reveal¹¹ that a limited number of holes developing in the liquid sheet is sufficient to induce spray atomization. For a large

number of emulsion droplet typically present in the spray liquid, some will be located at the air/water interface of the liquid sheet. Based on this observation, we analyse how emulsion droplets behave after they have entered the interface by consulting the theoretical model. Despite the fact that our experimental systems are highly dynamic while calculations describe wetting at equilibrium conditions, this comparison is possible as long as both approaches account for the changes of the derived thermodynamic parameters rather than for the absolute values of surfactant concentration or interfacial tensions.

The calculations reveal that spreading process of emulsion droplets can be slowed down or even completely inhibited by a surfactant which accumulates at the air/water interface. Thereby, surface pressure required to retard spreading is as low as 1 mN/m. This value is in good agreement with the experimentally obtained surface pressure required to affect the spray droplet size. An increase in surface pressure up to 4 mN/m is consistent with a decrease in spray droplet size during spray application and is also sufficient to inhibit significantly emulsion droplet spreading as shown in the theoretical part for the three investigated oils. The consistency of results further supports the accuracy of our hypothesis of spray atomization that dilute oil-in-water emulsions is based on the spreading properties of emulsified oils.

The tendencies described in the model are clear. Surely, relying on these results, it would be interesting to proceed the investigations and perform dynamic simulations that describe larger systems involving a full liquid sheet and a number of emulsion droplet. The theoretical considerations discussed in this study broaden the understanding of how certain physical properties of spray liquids affect the spray atomization onset and provide a basement for further investigations.

References

- [1] J. M. H. M. Scheutjens and G. J. Fleer, *J. Phys. Chem.*, 1979, **83**, 1619–1635.
- [2] J. M. H. M. Scheutjens and G. J. Fleer, *J. Phys. Chem.*, 1980, **84**, 178–190.
- [3] M. C. P. van Eijk and F. A. M. Leermakers, *J. Chem. Phys.*, 1999, **110**, 6491–6499.
- [4] J. W. O. Salari, F. A. M. Leermakers and B. Klumperman, *Langmuir*, 2011, **27**, 6574–6583.
- [5] A. B. Jódar-Reyes, J. Lyklema and F. A. M. Leermakers, *Langmuir*, 2008, **24**, 6496–6503.
- [6] E. Hilz, F. A. M. Leermakers and A. W. P. Vermeer, *Phys. Chem. Chem. Phys.*, 2012, **14**, 4917–4926.

- [7] E. Hilz, A. W. P. Vermeer, F. A. M. Leermakers and M. A. Cohen Stuart, *Aspects Appl. Biol.*, 2012, **114**, 71–78.
- [8] R. P. Fraser, P. Eisenklam, N. Dombrowski and D. Hasson, *AIChE J.*, 1962, **8**, 672–680.
- [9] N. Dombrowski and W. R. Johns, *Chem. Engin. Sci.*, 1963, **18**, 203–214.
- [10] R. W. Dexter, in *Pesticide formulations and application systems*, ed. A. K. Viets, R. S. Tann and J. C. Mueninghoff, American Society of Testing and Materials, West Conshohocken, PA, 2001, vol. 20, pp. 27–43.
- [11] M. C. Butler Ellis, C. R. Tuck and P. C. H. Miller, *Atomization Spray*, 1999, **9**, 385–397.
- [12] P. A. Hobson, P. C. H. Miller, P. J. Walklate, C. R. Tuck and N. M. Western, *J. Agr. Eng. Res.*, 1993, **54**, 293–305.
- [13] P. C. H. Miller and C. R. Tuck, *J. ASTM Int.*, 2005, **2**, 1–13.
- [14] N. M. Western, E. C. Hislop, M. Bieswal, P. J. Holloway and D. Coupland, *Pestic. Sci.*, 1999, **55**, 640–642.
- [15] W. D. Harkins and A. Feldman, *J. Am. Chem. Soc.*, 1922, **44**, 2665–2685.
- [16] M. D. Cloeter, K. Qin, P. Patil and B. Smith, Proceedings of 22nd Annual Conference on Liquid Atomization and Spray Systems (ILASS-Americas), Cincinnati, OH, USA, 2010, pp. 1–9.
- [17] CIPAC MT 36.3 Emulsion Characteristics and Re-emulsification Properties, *CIPAC MT 36.3 Emulsion Characteristics and Re-emulsification Properties*, Collaborative International Pesticides Analytical Council, 2000.
- [18] CIPAC MT 18.1.3 Standard Water C, *CIPAC MT 18.1.3 Standard Water C*, Collaborative International Pesticides Analytical Council, 2010.
- [19] O. A. Evers, J. M. H. M. Scheutjens and G. J. Fleer, *Macromolecules*, 1990, **23**, 5221–5233.
- [20] J. Sprakel, N. Besseling, M. Cohen Stuart and F. Leermakers, *Europ. Phys. J. E*, 2008, **25**, 163–173.
- [21] A. B. Jódar-Reyes and F. A. M. Leermakers, *J. Phys. Chem. B*, 2006, **110**, 6300–6311.
- [22] M. Charlaganov, P. Košovan and F. A. M. Leermakers, *Soft Matter*, 2009, **5**, 1448–1459.
- [23] U. Retter and D. Vollhardt, *Langmuir*, 1993, **9**, 2478–2480.

Chapter 6

Mechanism of perforation based on spreading properties of emulsified oils

Dilute oil-in-water emulsions create coarser sprays than water when atomized through a flat fan nozzle. The mechanism behind this process is perforation of the thin liquid sheet that is initially formed under the nozzle outlet. In this Chapter, we investigate how emulsion droplet size, concentration of emulsifier, physical properties of the dispersed phase, and the dynamic surface tension at breakup influence the perforation. Based on experimental data, a spray atomization mechanism is proposed that is based on the spreading properties of emulsified oils.

This Chapter is published as:

E. Hilz, A. W. P. Vermeer, M. A. Cohen Stuart, and F. A. M. Leermakers, Mechanism of perforation based on spreading properties of emulsified oils. *Atomization and Sprays*, **2012**, *22* (12), 1053–1075.

6.1 Introduction

During spray applications of agrochemicals, fine spray droplets can be carried by crosswind from the application site.¹ This ‘downwind movement of airborne spray droplets beyond the intender area of application originating from aerial or ground-based spraying operations’ is defined as spray drift.² The amount of spray drift is often correlated with the spray volume contained in droplets with diameter < 100 μm or V_{100} .^{3,4} As a consequence, the risk of off-target exposure decreases whenever V_{100} is reduced.

The spray droplet size distribution can be adjusted by the choice of technical equipment and spraying parameters such as spraying pressure, nozzle design and size, tractor driving speed and application height.^{5,6} Along with technical parameters and operating conditions, the physical properties of spray solutions influence size distribution, velocity and mass of spray droplets.^{5,7-9}

When sprayed through a conventional flat fan nozzle, dilute oil-in-water emulsions increase the volume median diameter (VMD) of produced sprays and decrease the fine fraction compared to water.¹⁰⁻¹⁸ For this reason, dilute emulsions are interesting for drift control purposes as tank-mix additives or as part of formulated products with spray drift reduction properties. Dilute emulsions induce spray coarsening by influencing the spray formation process.

When a spray liquid passes the nozzle body, the kinetic energy, gained from the liquid’s ejecting velocity, initiates the formation of a liquid sheet below the nozzle orifice. Surface tension counteracts the ejecting velocity and pulls the liquid towards the central fan axis. Local primary disturbances at the air/water interface of the created liquid sheet produce irregularities which grow until they overcome the surface tension forces. At this point, the liquid sheet breaks up, forming ligaments which, thereafter, disrupt into spray droplets. Usually, the liquid sheet reaches a life time of a few ms before it breaks up into spray droplets.¹⁹ Its thickness is inversely proportional to the distance from the nozzle.²⁰ If the liquid sheet breaks up at a position closer to the nozzle orifice, where its thickness is larger, the diameter of the formed spray droplets will be larger as well. In contrast, a delayed onset of sheet rupture leads to the formation of finer sprays.

Possible breakup mechanisms of the liquid sheet have been described in literature.^{21,22} Surface tension holds the sheet together and a decrease in surface tension leads to the formation of finer sprays. Viscous liquids, on the other hand, reduce the disturbances produced through air friction and form more placid, sustainable sheets and coarser sprays. The typical mode of sheet breakup induced by dilute

oil-in-water emulsions is perforation. During the perforation, holes appear in the liquid sheet, grow in size and form a network of filaments. Perforation shortens the breakup length of the liquid sheet, so that the created sprays are coarser compared to water sprays.^{14,15,23} The growth rate of the perforation radius was investigated²⁴ as well as the relation between the length of the sheet at breakup and the diameter and the number of emulsion particles.²⁵

However, the mechanism that initiates hole formation and the subsequent atomization of the liquid sheet into spray droplets is still unclear. Initially, it has been suggested that hydrophobic particles cause perforation.²² It was hypothesized that perforation occurs if an emulsion droplet or particle with a diameter that equals the thickness of the liquid sheet connects both interfaces.^{22,26} These hypotheses were contradicted by more recent studies on dilute emulsions.^{15,25} It was suggested that the breakup length of the liquid sheet and the spray droplet size are influenced by the number of emulsion droplets.²⁵ Moreover, the deformability of emulsion droplets was recognized as an important parameter and it was suggested that rapidly stretched emulsion droplets with an oil/water interface which is not at equilibrium may initiate the perforation onset,²⁵ e.g. by diffusion to the air/water interface of the liquid sheet where they act as weak points.¹⁵ In the same study, the onset of spray coarsening was observed at emulsion concentrations of $2 \times 10^{-3} - 5 \times 10^{-2}\%$ w/w and a causal relation between the initial emulsion droplet size and the emulsion concentration at the onset of spray coarsening was reported. Sprays become coarser with increasing emulsion concentration as long as the dynamic surface tension at breakup remains unchanged. At higher emulsion concentrations, the dynamic air/water interfacial tension can decrease and reduce the spray coarsening effect. Recently, the viscosity of the dispersed phase was recognized as another important parameter.¹⁸ High viscosity of the dispersed phase was correlated with a high resistance of emulsion droplets to breakup. It was hypothesized that emulsion droplets, when elongated in the shear flow within the nozzle, immediately retract thereafter. This quick retraction was claimed to redistribute the flow momentum perpendicular to the flow direction and to cause an earlier sheet breakup. It was also reported that the composition of the dispersed phase is important. Emulsions based on vegetable oils were observed to produce coarser sprays than a mineral oil-based emulsion.¹² The concentration of emulsifier showed no influence on the spray coarsening effect induced by dilute mineral oil emulsions.¹⁷

Although all these studies discuss the effect of dilute oil-in-water emulsions on spray formation, some aspects remain an open question. One of these unanswered

issues is how perforation is influenced by the decrease in the dynamic surface tension at the air/water interface of the liquid sheet. Another is why different emulsified oils produce sprays of different qualities with respect to the mean droplet size and the fine fraction.

The objective of this study is to gain further insight into the differences in spray characteristics produced by sprays containing different dilute emulsions, and to describe the mechanism that initiates perforation. For this purpose we prepared several test emulsions and investigated their physical properties. These properties are 1) the viscosity of the emulsified oil, 2) the emulsion droplet size distribution before spraying and after agitation, 3) the concentration of the emulsifier, 4) the dynamic surface tension at the air/water interface, and 5) finally, it was investigated to what extent the spreading properties of the emulsified oil influence perforation. The classical spreading coefficient S was used to characterise the spreading properties of oils. S is defined as the difference in free energy per unit area between the pristine surface and the (oil-)covered surface or the balance of the interfacial tensions at the air/water, the air/oil and the oil/water interfaces.²⁷

6.2 Material and Methods

All spray liquids were prepared with commercially available additives which are commonly used for the formulation of plant protection products. All chemicals were used as obtained without further purification. The emulsions were prepared on the basis of sunflower oil (purchased from John L. Seaton & Co. Ltd.), rapeseed oil methyl ester (trade name Synative ES ME SU purchased from Cognis), mineral oil (trade name Exxsol D140 purchased from ExxonMobil Chemicals), white oil (trade name Bayol 85 purchased from ExxonMobil Chemicals), and polydimethylsiloxanes (PDMS, trade names Tegiloxan 3, 100 and 350 supplied by Evonik Industries). Water soluble surfactants sodium ethoxylated alkyl (C8) sulphate (supplied by AkzoNobel) and polyoxyethylene C12-C15 alcohol (trade name Synperonic A7 purchased from Croda) were used to modify the dynamic air/water interfacial tension of the spray liquid. The oil/emulsifier combinations (table 6.1) were chosen to guarantee a good stability and quality of the emulsions according to the CIPAC MT 36.3 method.²⁸

Oils were first mixed with an appropriate emulsifier (table 6.1). Dilute emulsions were prepared by dilution of the prepared oil/emulsifier mixture in CIPAC C standard hard water (hardness 500 ppm)²⁹ at a concentration of 0.1% w/w of the oil/emulsifier mixture in water. Consequently, the spray solution contains 0.09%

w/w oil and 0.01% w/w emulsifier (or emulsifier blend). These dilute emulsions were homogenized by shaking and placed in a pressurized vessel that supplied spray liquid to the nozzle.

Table 6.1: Composition of spray liquids that contain dilute emulsions with the concentration of dispersed phase 0.1% w/w. γ_{AW}^{br} is the dynamic interfacial tension at sheet breakup.

oil	% w/w in spray liquid	emulsifier	% w/w in spray liquid	% w/w dispersed phase	γ_{AW}^{br} [mN/m]
sunflower oil	0.09	Arlatone TV ^a	0.01	0.1	71.8
methyl ester	0.09	Tanemul SO70 ^b Emulsifier 1371A ^c	0.004 0.006	0.1	71.6
mineral oil	0.09	Tanemul SO70 ^b Tanemul L3 ^b	0.008 0.002	0.1	71.5
white oil	0.09	Atplus 309 F-LM ^a	0.01	0.1	71.8
PDMS	0.09	Arlatone TV ^a	0.01	0.1	-

supplier: ^a Croda, ^b Tanatex, ^c Lanxess

Sprays were produced with an extended-range flat fan TeeJet XR11003 VS nozzle which was operated at a pressure of 3 bar. The extended-range flat fan nozzle has a design of a simple hemispherical column with a V shaped outlet and an elliptical cross-section at the orifice. The nozzle was mounted on a linear unit and moved above the laser beam with a velocity of 2 cm/s along the long x-axis of the spray fan. The measurements were replicated three times for each sample. The reproducibility of the VMD values was $\pm 3 \mu\text{m}$ and that of the V_{100} values better than $\pm 1\%$.

The droplet size distributions were measured with Spraytec (Malvern Instruments Ltd.), positioned at a distance of 33 cm below the nozzle outlet. Spraytec is a laser diffraction instrument equipped with a 300 mm lens that allows measuring the droplet size in the range of 0.1 – 900 μm . The working principle of a Malvern instrument is described elsewhere.³⁰ Malvern laser diffractometer is an accepted and well evaluated technique suited for measuring of agricultural sprays but there can be differences in droplet size spectra obtained with other measuring techniques especially for coarse and very coarse sprays.^{31,32} The measurements were performed at room temperature of 20-25°C. The liquid temperature was about 21°C.

Spraytec Software Version 3.03 was used to calculate the numerical values of the volume median diameter (VMD) and the % volume of liquid sprayed with drops smaller than 100 μm in diameter (V_{100}). The volume median diameter is the average droplet size, such that 50% of the volume of sprayed liquid is in droplets of smaller diameter than the VMD and another 50% is in droplets larger than the

VMD.²¹ The value of the V_{100} indicates the percentage of drift-prone droplets in the spray.^{3,4}

Emulsion droplet size in the spray liquid was measured with a diffractometer Mastersizer S (Malvern Instruments Ltd.) equipped with a Hydro G sample dispersion unit with an ultrasonic system. The ultrasonic system was used at 50 Watts and 40 kHz for 30 s to induce a measurable agitation of emulsion droplets. The accuracy of the results is $\pm 2\%$ on the emulsion mean diameter ($D_{v0.5}$). The distribution width of the emulsions was characterised by the relative Span factor. The relative Span factor is defined by $(D_{v0.9} - D_{v0.1})/D_{v0.5}$.²¹ $D_{v0.1}$, $D_{v0.5}$, $D_{v0.9}$ is a droplet diameter such that 10%, 50%, 90% of total spray liquid volume are in droplets of smaller diameter. A small Span corresponds to a narrow droplet size distribution.

The viscosity of the oil phase was measured using a HAAKE RheoWin rotational Rheometer (Haake GmbH) equipped with a concentric cylinder system at a shear rate of 100 s^{-1} . All measurements were performed at 20°C . The repeatability of the results was in the range $\pm 1 \text{ mPas}$.

Photographs of the atomization of the liquid sheet were obtained with a Nikon D200 camera equipped with a R1C1, a synchronized Wireless Close-Up Speedlight System having a flash duration of $600 \mu\text{s}$. The pictures were made with the flash installed behind the nozzle and facing the camera. The flash light was damped by a diffuser. The length of the liquid sheet at breakup, l , and the spray angle, β , were obtained from high-speed photographs of the sheet in the x -plane. Both parameters were determined from two photographs of the liquid sheet of the same solution. The spray angle was determined as the opening angle which the liquid forms at the moment when it leaves the nozzle orifice. It is the angle between both sheet edges. The sheet length at breakup was measured vertically to the nozzle tip as the length of the continuous sheet down to the first hole (similarly as shown in figure 6.2). Estimated from the photographic pictures, the length of the sheet ranges between 10 – 15 mm for pure emulsions and of maximum 30 mm for an emulsion/surfactant mixture. The sheet velocity produced by a flat fan nozzle has been measured as 20 m/s with a phase Doppler analyser, 40 mm vertically below the standard flat fan nozzle spraying water alone.¹⁹ From these data, the lifetime of the liquid sheet at breakup can be estimated as $t^{br} = 0.7 \text{ ms}$ for pure emulsions and as $t^{br} = 1.5 \text{ ms}$ for spray liquids that contain a mixture of a dilute emulsion and a surfactant.

To determine the spreading properties of the emulsified oil, the static interfacial tensions at the air/oil and the oil/water interfaces were measured with a Prozessor-

Tensiometer K100 (Krüss GmbH) using the Wilhelmy plate method. The accuracy of the experimental method is of 0.001 mN/m. The reproducibility of the results was better than ± 0.5 mN/m. The temperature of the measured liquid was 20°C.

A BP2 bubble tensiometer (Krüss GmbH) was used to obtain the dynamic surface tension at the fast expanding air/water interface at 10 – 100 ms. The accuracy of the experimental method is of 0.1 mN/m. The reproducibility of the results was about ± 1 mN/m. The surface tension at breakup was calculated by fitting the measured data to the following approximation as used in literature.¹⁹

$$\gamma_{AW} = \gamma_{AW}^0 - \alpha t^{1/2} \quad (6.1)$$

The time $t = 0$ s corresponds to $\gamma_{AW} = 72.0$ mN/m. The dynamic surface tension was calculated at sheet breakup $t^{br} = 0.7$ ms for pure emulsions and $t^{br} = 1.5$ ms for spray liquids that contain a mixture of a dilute emulsion and a surfactant. The surface tension of CIPAC C hard water was measured as $\gamma_{AW} \approx 72.0$ mN/m. The dynamic interfacial tensions of dilute emulsions at the moment of sheet breakup γ_{AW}^{br} are listed in table 6.1.

6.3 Results and Discussion

Table 6.2: Average values of the VMD and the V_{100} for sprays produced with water without additives and dilute emulsions sprayed at a concentration of 0.1% w/w of the dispersed phase.

	water	sunflower oil	methyl ester	mineral oil	white oil
VMD [μm]	194.6	256.9	246.1	237.5	231.2
V_{100} [%]	11.0	3.3	3.8	5.8	6.1

A liquid sheet formed through a flat fat nozzle breaks up into spray droplets some cm below the nozzle outlet.¹⁹ The distribution of the VMD values in a spray fan produced with the XR11003 nozzle is shown in figure 6.1a. The spray center is indicated as the zero position on the x -axis. The spray droplet size varies symmetrically around the spray center. As shown in figure 6.1b, drift-prone droplets with a diameter $< 100 \mu\text{m}$ are created predominately in the center of the spray fan. At the edges of the spray fan all droplet are $> 100 \mu\text{m}$.

As measured by other researchers, emulsions sprayed through a conventional

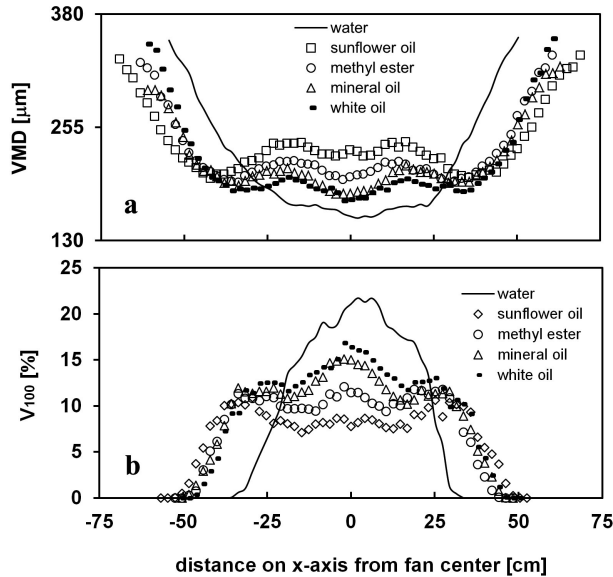


Figure 6.1: a) The VMD and b) the V_{100} along the fan x -axis of three dilute emulsions sprayed at a concentration of 0.1% w/w of the dispersed phase.

nozzle increase the velocity of the spray droplets compared to water⁸ and change the velocity profile of the liquid sheet.³³ In the case of dilute emulsions, spray liquid has a wider region of higher velocity downstream the nozzle³³ which leads to the formation of wider spray fans compared to water. Increasing the width of the spray fan (figure 6.1a), emulsions increase the spray angle. The velocity at the edges of the sheet is the lowest³³ which corresponds to the formation of larger spray droplets at the edge of the spray fan for dilute emulsions and water (figure 6.1a). All dilute emulsions also increase the spray droplet size in the middle part of the spray fan compared to water. This can be explained by the difference in the breakup mechanisms of both liquids. The liquid sheet that is formed below the nozzle orifice thins out with increasing distance from the nozzle outlet.²⁰ Water forms a longer and consequently a thinner sheet compared to a sheet formed by an emulsion.²⁵ The length of the liquid sheet created by an emulsion is shorter compared to a water sheet and therefore spray droplets formed by an emulsions are coarser in the fan center.

All emulsions increase the spray droplet size and reduce the fine spray fraction, but each to a different absolute value of the VMD and V_{100} (table 6.2). The sunflower oil-based emulsion produces the widest fan (figure 6.1a) and reduces

more efficiently the fine spray fraction (figure 6.1b). This corresponds to a higher VMD and a lower V_{100} compared to other emulsions. To understand the differences in the performance of dilute emulsions, the physical properties of spray liquids and emulsified oils were investigated as discussed in the following subsections.

6.3.1 Viscosity of the oil

As shown in table 6.3, the viscosities of the dispersed phases range between 65.0 mPas for the sunflower oil and 6.1 mPas for the rapeseed oil methyl ester. Sunflower oil has the highest viscosity and rapeseed oil methyl ester the lowest; both induce a higher increase of the VMD and a greater reduction of the V_{100} compared to the mineral and the white oil-based emulsion (table 6.2). Based on these data a first indication is given that the spray coarsening effect of an emulsion is rather weakly correlated to the viscosity of the emulsified oil.

Table 6.3: The viscosities η_d and densities ρ_d of emulsified oils.

	sunflower oil	methyl ester	mineral oil	white oil
η_d [mPas]	65.0	6.1	6.2	22.7
ρ_d [g/m ³]	0.919	0.880	0.833	0.845

Table 6.4: Properties of PDMS oils and their emulsions sprayed at a concentration of 0.1% w/w of the dispersed phase.

η_d [m Pas]	ρ_d [g/m ³]	VMD [μ m]	V_{100} [%]	γ_{AO} [mN/m]	γ_{OW} [mN/m]	S [mN/m]	$D_{v0.5}$ [μ m]	Span
3.0	0.890	252.2	3.4	18.4	36.4	17.2	7.2	4.52
100.0	0.965	252.9	3.3	20.7	28.8	22.5	30.5	2.06
350.0	0.950	248.7	3.7	20.8	32.0	19.2	68.2	2.50

The effect of the viscosity of the dispersed phase was further investigated with three polydimethylsiloxanes emulsions. Tegiloxan 3, 100 and 350 with viscosities of 3 mPas, 100 mPas and 350 mPas (as specified by the manufacturer) contain molecules of identical chemical composition but a varying length, so that their physical properties remain similar despite a significant viscosity increase from 3 to 350 mPas.

As shown in table 6.4, the three PDMS oils produce sprays of a comparable high VMD and a low V_{100} without an indication that the viscosity of the emulsified oil

or the initial emulsion droplet size affect the spray characteristics. T350 produces a spray with a slightly lower VMD compared to sprays produced by T3 and T100 probably due to a poor emulsion quality of T350 in water.

6.3.2 Emulsion droplet size

During the spray application, liquids are subjected to high shear stress within the nozzle.³⁴ An emulsion droplet can be deformed, elongated or can even break up if the forces in the nozzle surpass the Laplace pressure in an emulsion droplet.³⁵ The Laplace pressure is linked to the droplet size, so that deformation and breakup of larger droplets can be expected during agricultural applications. Therefore, this process needs to be considered for a better understanding of the interactions between emulsion droplets and the continuous phase.

The shear rates in a flat fan nozzle were reported in the literature to range between $\dot{\gamma} = 1.6 \times 10^4 \text{ s}^{-1}$ and $\dot{\gamma} = 1.2 \times 10^5 - 7.0 \times 10^5 \text{ s}^{-1}$.^{18,34} XR11003 nozzle used in this study is a flat fan nozzle with a similar design, so that we can assume the shear rates to be in the same range as reported above.

Due to high dynamics of the system, the emulsion droplet size distribution cannot be measured within the liquid sheet. Measurements of the droplet size in the collected liquid after spraying take time, so that emulsion droplets may coalesce.¹⁸ If the emulsion droplet size before spraying is similar to that after spraying, it is not possible to estimate whether the droplet size was not affected by the agitation in the nozzle or if emulsion droplets grew to their initial size within the elapsed time by coalescence. Additionally, air bubbles can be induced during the spraying process into the collected liquid. Air bubbles can interfere with the measurements of the emulsion droplets size and they take several minutes to dissipate.²⁵

To overcome these obstacles, we suggest to use ultrasound for estimation if the size of emulsion droplets is influenced by agitation. Here, it shall be emphasized that this method provides rather a measure of the "robustness" of emulsion droplets and does not indicate the emulsion droplet size in the liquid sheet. The main advantage of this approach is that there is no time delay between the agitation and the size measurements and we can deduce if emulsion droplets break up into smaller droplets by energy input.

After emulsions have been formed by shaking, they were subjected to ultrasound for 30 s at room temperature. The emulsion droplet size and the relative distribution width (Span) before and after agitation are shown in table 6.5. Before agitation, the sunflower oil-based emulsion contains larger droplets with a wider

Table 6.5: Emulsion volume mean diameter ($D_{v0.5}$) and the span before agitation and after applying ultrasound for 30 s.

	before spraying		after agitation	
	$D_{v0.5}$ [μm]	Span	$D_{v0.5}$ [μm]	Span
sunflower oil	9.6	8.21	2.7	2.77
methyl ester	1.4	1.57	1.4	1.55
mineral oil	2.5	2.59	2.4	2.50
white oil	2.6	2.67	2.5	2.30

droplet size distribution than the emulsion of the methyl ester, the mineral oil and the white oil-based emulsions. Agitation, created by ultrasound, induces breakup of large emulsion droplets in the case of sunflower oil. As anticipated, finer emulsions are hardly affected by agitation. These results indicate that in the case of coarser emulsions, the number of emulsion droplets will increase after the spray liquid has been atomized and all emulsion droplets may be of a more uniform size when they leave the nozzle. Consequently, emulsion drops in the size range of 1-10 μm are relevant for the perforation onset.

6.3.3 Spreading

Interfacial properties of emulsion droplets are typically used to describe the stability and formation of emulsions. Moreover, it is well known that these properties can change the behaviour of a system that contain multiple phases. Atomization process of dilute oil-in-water emulsions might as well be affected by the interfacial properties of emulsion droplets and, therefore, we will have a closer look at them in this subsection.

Before and after application, most emulsion droplets will remain submerged in the bulk liquid. However, some of them may enter the air/water interface. Emulsion droplets will not enter the interface by diffusion (diffusion of emulsion droplets is too slow for the time of sheet formation and breakup). However, being uniformly distributed in the spray liquid, some emulsion droplets will be present close to the interface or at the air/water interface of the newly created liquid sheet. The entering probability depends on the sheet thickness, its interfacial area, the emulsion droplet size, and the interfacial properties of the emulsion droplets. The geometry and the thickness of the liquid sheet of all investigated dilute emulsions are similar (see section Mechanism). The entering probability increases with increasing number of emulsion droplets. The number of droplet depends on the droplet size. As

Table 6.6: The static interfacial tensions γ_{AO} at the air/oil interface and γ_{OW} at the oil/water interface. S is the spreading coefficient calculated with the interfacial tension at the air/water interface $\gamma_{AW} = 72.0$ mN/m.

oil	γ_{AO} [mN/m]	γ_{OW} [mN/m]	S [mN/m]
sunflower oil	33.5	25.2	13.3
rapeseed oil methyl ester	31.6	11.9	28.5
mineral oil	28.6	43.1	0.3
white oil	30.3	36.2	5.5

indicated in table 6.5, emulsion droplets of all test liquids are of a more uniform size after agitation by ultrasound (or after these liquids are atomized through the nozzle), so that the number of emulsion droplets in each sample increases compared to the droplets number before agitation or spraying. Using the droplet size number distribution of the methyl ester emulsion obtained for a concentration of 0.1% w/w of the dispersed phase in water, the number of the emulsion droplets in the spray liquid can be calculated as 3.7×10^{11} in 1 L. Certainly, the absolute droplet number will differ for different emulsions. This a quite large number particle and at the same time, only a limited number of holes is required to induce the breakup.²⁴ Thus, only a few emulsion droplets merged with the interface will suffice to initiate this process.

After an oil droplet has entered the air/water interface, it will spread. The spreading tendency depends on the three interfacial tensions: γ_{AW} at the air/water, γ_{AO} at the air/oil and γ_{OW} at the oil/water interfaces. The measure of this tendency is the classical spreading coefficient S :²⁷

$$S = \gamma_{AW} - \gamma_{AO} - \gamma_{OW} \quad (6.2)$$

For the condition $\gamma_{AO} + \gamma_{OW} > \gamma_{AW}$, the spreading coefficient is negative and the oil droplet forms a lens at the air/water interface as shown in figure 6.3a. In the case when $\gamma_{AO} + \gamma_{OW} < \gamma_{AW}$, S becomes positive and the oil droplet spreads at the air/water interface, its radius grows until the equilibrium conditions are reached (figure 6.3b). At complete wetting and at equilibrium, the spreading tension $S_e = 0$. The equilibrium conditions are not relevant for highly dynamic systems investigated in this study. The γ_{AO} and the γ_{OW} of all tested oils and the corresponding spreading coefficients are collected in table 6.4 and 6.6.

Sunflower oil and rapeseed oil methyl ester have a high positive spreading coef-

ficient. This corresponds to a high tendency of these oils to spread when they merge with the air/water interface. The spreading coefficient of the mineral oil is 0.3 mN/m which implies a slow spreading of this oil at the air/water interface. The spreading coefficient of the white oil is 5.5 mN/m. At the same time, mineral and white oil emulsions produce finer sprays than those produced by vegetable-based oils and PDMS. A similar tendency was reported earlier by Western *et al.*¹².

Here, two groups of emulsions can be identified. One group that contains oils with a high positive spreading coefficient produces coarser sprays. Another group that contains oils with a low positive spreading coefficient produces sprays that are finer than sprays created by the first group of oils.

6.3.4 Emulsifier concentration

Table 6.7: The VMD and V_{100} of sprays that contain dilute emulsions based on sunflower oil with a varying mass fraction of emulsifier ϕ_e .

ϕ_e	0.33	0.25	0.16	0.09	0.06	0.04	0.03
VMD [μm]	256.9	258.8	257.0	256.9	258.5	258.1	243.5
V_{100} [%]	3.1	3.2	3.3	3.3	3.2	3.3	4.7

The effect of the emulsifier concentration on the spray droplet size distribution was studied by spraying emulsions prepared on the basis of sunflower oil with different mass fractions of the emulsifier ϕ_e . As show in table 6.7, the VMD and the V_{100} are similar for a wide range of ϕ_e . The VMD increases and the fine spray fraction becomes $V_{100} = 4.7\%$ for the lowest $\phi_e = 0.03$. This can be attributed to the poor emulsion quality and creaming effects observed at the lowest concentration of emulsifier.

The dynamic interfacial tension at breakup γ_{AW}^{br} of sprays in table 6.7 was estimated as ~ 71.5 mN/m, except for $\phi_e = 0.03$. In this case $\gamma_{AW}^{br} = 68.8$ mN/m.

6.3.5 Dynamic surface tension

The dynamic air/water interfacial tension of dilute emulsions was modified by water soluble non-ionic and anionic surfactants.

Photographic pictures of dilute emulsions and mixtures of an emulsion and a surfactant were taken to define the time of the sheet breakup and to visualize the spray formation process. As shown in figure 6.2a, the emerging liquid sheet of

the surfactant-free emulsion is very short. Figures 6.2b and c show that the sheet length increases with increasing concentration of the water soluble surfactant. With increasing sheet length, the dynamic surface tension at breakup decreases. This indicates that the disintegration mechanism is delayed and atomization happens at larger distances from the nozzle outlet, at a point where the liquid sheet is thinner. At a certain surfactant concentration the sheet reaches a length where it probably disrupts due to oscillation rather than by perforation. At this point the emulsion no longer contributes to the atomization process. Similar pictures were obtained for all test emulsions.

Table 6.8: Interfacial tension γ_{AW} at 1.5 ms, the VMD and the V_{100} and the resulting spreading coefficient S of 0.1% w/w sunflower oil emulsions and a surfactant at different concentrations.

non-ionic surfactant				anionic surfactant			
γ_{AW} [mN/m]	S [mN/m]	VMD [μm]	V_{100} [%]	γ_{AW} [mN/m]	S [mN/m]	VMD [μm]	V_{100} [%]
71.7	13.0	241.1	4.7	71.0	12.3	246.7	3.6
69.9	11.2	231.0	5.4	71.2	12.5	240.0	4.0
68.1	9.4	219.3	6.8	69.7	10.5	233.2	5.0
66.6	7.9	209.4	8.0	67.8	9.1	221.9	6.4
65.5	6.8	192.6	10.6	62.5	3.8	173.8	17.0

Table 6.9: Interfacial tension γ_{AW} at 1.5 ms, the VMD and the V_{100} and the resulting spreading coefficient S of 0.1% w/w mineral oil emulsions and a surfactant at different concentrations.

non-ionic surfactant				anionic surfactant			
γ_{AW} [mN/m]	S [mN/m]	VMD [μm]	V_{100} [%]	γ_{AW} [mN/m]	S [mN/m]	VMD [μm]	V_{100} [%]
71.9	0.2	222.2	6.6	71.7	0	216.0	7.8
71.2	-0.4	216.0	7.8	70.3	-1.3	200.7	9.9
68.7	-2.9	205.4	9.3	68.3	-3.3	195.8	10.7
67.9	-3.7	191.4	11.9	67.9	-3.7	192.7	11.4
67.6	-4.0	185.5	12.9	67.1	-4.5	191.2	11.5

Spray characteristics of dilute sunflower oil-based emulsion/surfactant mixtures are collected in table 6.8. The VMD and the V_{100} for sprays that contain mineral oil-based emulsion with surfactant are shown in table 6.9. Table 6.10 shows the results for sprays with emulsions based on the rapeseed oil methyl ester with both

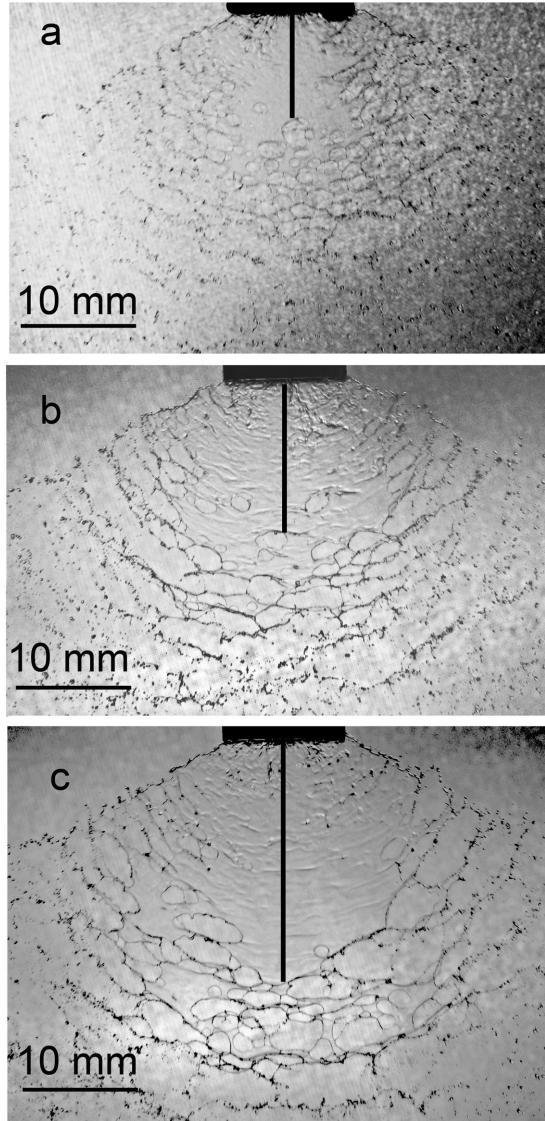


Figure 6.2: Photographic pictures of sprays that contain sunflower oil-based emulsions as a function of the dynamic surface tension at the air/water interface at breakup γ_{AW}^{br} : a) $\gamma_{AW}^{br} = 71.8$ mN/m, b) $\gamma_{AW}^{br} = 69.9$ mN/m, c) $\gamma_{AW}^{br} = 65.5$ mN/m. Black line indicates the length of the liquid sheet at breakup.

surfactant types. Table 6.11 shows spray characteristics of emulsions based on white oil with both surfactant types. In all cases a decrease of the γ_{AW} results

Table 6.10: Interfacial tension γ_{AW} at 1.5 ms, the VMD and the V_{100} and the resulting spreading coefficient S of 0.1% w/w rapeseed oil methyl ester emulsions and a surfactant at different concentrations.

non-ionic surfactant				anionic surfactant			
γ_{AW} [mN/m]	S [mN/m]	VMD [μm]	V_{100} [%]	γ_{AW} [mN/m]	S [mN/m]	VMD [μm]	V_{100} [%]
70.5	27.0	238.1	4.7	71.2	27.7	233.3	5.3
68.8	25.3	230.2	5.5	69.4	25.9	215.0	7.7
67.5	24.0	196.0	10.2	67.6	24.1	213.9	7.5
67.4	23.9	195.1	10.8	65.6	22.1	191.0	11.6
66.1	22.6	187.7	11.6	62.4	18.9	174.0	16.3

in the formation of finer sprays with a lower VMD and a higher V_{100} compared to VMD and V_{100} of pure emulsions. The spreading coefficient S decreases with increasing γ_{AW} at the moment of the sheet breakup. The V_{100} increases gradually with decreasing dynamic surface tension until the produced sprays show a droplet size distribution comparable to that of water (VMD = 194.6 μm and V_{100} = 11.0%).

Table 6.11: Interfacial tension γ_{AW} at 1.5 ms, the VMD and the V_{100} and the resulting spreading coefficient S of 0.1% w/w white oil emulsions and a surfactant at different concentrations.

non-ionic surfactant				anionic surfactant			
γ_{AW} [mN/m]	S [mN/m]	VMD [μm]	V_{100} [%]	γ_{AW} [mN/m]	S [mN/m]	VMD [μm]	V_{100} [%]
71.7	5.2	225.7	6.5	71.8	5.2	218.1	7.4
70.7	4.2	211.2	8.5	70.4	3.9	200.6	10.2
68.4	1.9	201.4	10.2	69.8	3.3	196.8	11.0
67.8	1.3	189.5	12.2	69.1	2.6	192.4	11.7
67.2	0.7	181.7	13.6	68.1	1.6	189.3	12.3

Apparently, the dynamic surface tension at breakup controls the spray droplet size of dilute oil-in-water emulsions. The decrease of the spray droplet size with increasing dynamic surface tension was observed earlier for e.g., emulsions sprayed at high concentrations.¹⁵ Our experiments show that emulsions at concentrations $> 0.5\%$ w/w induce a decrease in the dynamic interfacial tension and sprays become finer (data not shown). The mechanism behind these process seems to be similar to that reported in tables 6.8–6.11. The decrease of the dynamic surface tension for the more concentrated emulsions can occur because the excess emulsifier dissolves

in the continuous water phase and occupies air/water interface.

6.4 The Mechanism

In this section we will further discuss mechanisms proposed in literature attempting to find the most plausible explanation for the atomization onset of spray liquids that contain dilute emulsions.

It has been proposed earlier that an emulsion droplet can cause sheet disruption by puncturing both interfaces.²² To investigate the possibility of this mechanism we estimate the relation between the emulsion droplet size and the thickness of the emerging liquid sheet. The thickness of the liquid sheet at breakup, L^{br} , is calculated according to the following equation:¹⁵

$$L^{br} = A/l\beta \quad (6.3)$$

A is the area of the nozzle aperture, l the length of the liquid sheet and β the spray angle in rad. The area of the orifice of an XR11003 nozzle was calculated as $A = 8.7 \times 10^{-7} \text{ m}^2$.³⁶ The spray angles differ between $122 \pm 1^\circ$ for the methyl ester, mineral oil and white oil emulsions, and $126 \pm 1^\circ$ for the sunflower oil emulsion. The resulting sheet thickness at the moment of spray atomization is $L^{br} = 35.9 \pm 4.8 \text{ }\mu\text{m}$ for sprays with sunflower oil emulsions with $l = 11.0 \pm 1.0 \text{ mm}$; $L^{br} = 29.1 \pm 3.4 \text{ }\mu\text{m}$ for the emulsions based on the methyl ester with $l = 14.0 \pm 1.0 \text{ mm}$; and $L^{br} = 26.3 \pm 2.0 \text{ }\mu\text{m}$ for the mineral and the white oil emulsions with $l = 15.5 \pm 0.5 \text{ mm}$.

The methyl ester emulsion has a narrow droplet size distribution already before spraying whereby all emulsion droplets are of diameter $< 10 \text{ }\mu\text{m}$. Therefore, it is unlikely that one emulsion drop can puncture the liquid sheet with a thickness $L^{br} \geq 26.3 \text{ }\mu\text{m}$. Photographs of the sheet disruption show that all test emulsions influence atomization in a similar way. Thus, the puncturing mode of action is unlikely even though other emulsions include droplets $> 10 \text{ }\mu\text{m}$.

It was further suggested that the viscosity of the dispersed particles is crucial.¹⁸ Our data show a weak correlation between the viscosity of the dispersed phase and the spray coarsening effect so that the viscosity appears not to be a key parameter for the perforation onset.

It was also suggested that the hydrophobic oil/water interface of stretched emulsion droplets may interact with local sheet perturbation and induce the perforation

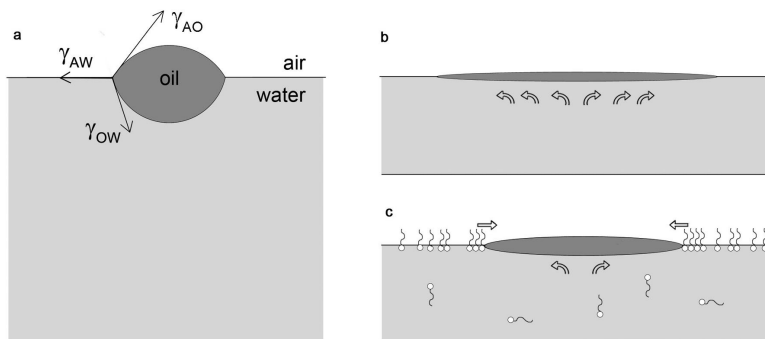


Figure 6.3: Schematic pictures of a) an emulsion droplet placed at a air/water interface, b) an emulsion droplet spreading in a thinner sheet region and inducing a subsurface flow, c) an inhibited spreading of an emulsion droplet at the air/water interface which is occupied by surfactants. The arrows indicate the direction of the subsurface flow and the counteracting forces caused by the interfacial surfactant layer. The emulsifier molecules are not shown in this schematic image.

onset.^{15,25} At the same time, solid particles were not shown to affect the spray formation mechanism.¹⁵ Furthermore, it was reported in literature that solid silica particles that have a similar wettability as emulsion droplets hardly affect the spray droplet size distribution.¹⁸ Based on these observations it was concluded that the deformability of emulsion droplets is an important factor that affects the spray formation process.^{15,18,25} However, this parameter has never been used to explain differences in spray characteristics produced with different dilute emulsion or mixtures of a dilute emulsion and a surfactant. Our data show that hydrophobicity itself does not provide an explanation for the perforation onset. On the other hand, interfacial properties and the presence of emulsion droplets at the air/water interface appear to be important.

We suggest that processes that dominate atomization of the liquid sheet happens due to fluid entrainment during the spreading of emulsion droplets at the air/water interface. Once at the interface, emulsion droplets with a positive spreading coefficient will inevitably spread, inducing a bulk flow as indicated in figure 6.3b. This subsurface flow thins out the sheet below the spreading droplet. Such sheet thinning may become a starting point for the hole formation. The spreading of an emulsion droplet can locally diminish the surfactant concentration at the oil/water interface and the resulting oil/water interfacial tension can be higher than its equilibrium value;³⁷ so that it will be closer to that of pure oil.

A similar mechanism has been established as a possible mode of action of an-

tifoams.³⁸ The direction of the subphase flow and induced film rupture were observed for oil droplets spreading over a substrate in a Petri dish.^{39,40}

Spreading of a liquid at the interface of another liquid has been described applying mathematical models.^{39,41–45} These models describe the propagation of the microscopic film of surfactant or oil. Thereby, water-insoluble spreading layer is treated as a flat plate with a constant spreading force which is independent of the film thickness. The spreading induces substrate flow that decreases asymptotically in vertical direction. The penetration depth m is described as

$$m = \sqrt{\eta t / \rho} \quad (6.4)$$

with η/ρ representing the downward diffusion or vorticity, η is the viscosity of the substrate liquid, ρ its density, and t is time. The depth of the disturbance in the sheet has to be in the order of the sheet thickness to cause thinning and possibly a consequent rupture.^{22,38} Logically, a vertically oriented liquid sheet can breakup due to thinning effects that are created by the subphase flows when an emulsion droplet spreads at its interface and the penetration depth is in the order of the sheet thickness.

For the investigated systems, the flow depth $m = 31.6 \mu\text{m}$ is calculated for water being the bulk liquid at 20°C and $t = 1 \text{ ms}$ at breakup. The flow depth m correlates well with the calculated thickness of the liquid sheet at breakup $L^{br} = 26.3 - 35.9 \mu\text{m}$. This calculation supports the breakup mechanism induced by spreading emulsion droplets as shown in figure 6.3b. However, interactions at breakup might be more complex than in figure 6.3b, when perturbations at the interface of the liquid sheet are reinforced by the spreading process, which can happen at both sides of the sheet simultaneously.

The proposed mechanism also provides an explanation why surfactants counteract an early atomization induced by dilute oil-in-water emulsions. As illustrated in figure 6.3c, surfactant molecules accumulate at the air/water interface, build up surface pressure and slow down the spreading process. A lower spreading velocity and a weaker subsurface flow may delay the perforation onset. Moreover, it takes more time to develop a back-flow (due to inertial effect),^{39,40} which counteract the subsurface flow induced by spreading droplets and stabilize the sheet. As a consequence, spray formation will occur further down from the nozzle outlet at a position where the liquid sheet is thinner, and thus finer sprays are created.

The limiting step for this mechanism is the entering of the emulsion droplet into

the air/water interface. Different characteristics have been suggested in literature to quantify the entry barrier. A positive entering coefficient E implies that the oil will penetrate the air/water interface.⁴⁶

$$E = \gamma_{AW} - \gamma_{AO} + \gamma_{OW} \quad (6.5)$$

However, a positive entering coefficient describes necessary but not sufficient conditions and the entering process may be limited by energy barrier arising from the thin liquid (pseudoemulsion) film between the emulsion droplet and the air/water interface. A generalized entering coefficient E^g was suggested to describe the entering barrier by Bergeron *et al.*⁴⁴.

$$E^g = - \int_{\Pi(h_\infty)=0}^{\Pi(h)} h d\Pi_{AWO} \quad (6.6)$$

Π_{AWO} is the disjoining pressure isotherm of the air/water/oil film and h is the water film thickness. Furthermore, energy of interaction (per unit area) f in the thin liquid film between the oil droplet and the gaseous phase has been used to quantify its stability:⁴⁷

$$f = - \int_{\infty}^{h_E} \Pi_{AWO} dh \quad (6.7)$$

with h_E the equilibrium film thickness.

All oils investigated in this study have a high positive entering coefficient. This implies that emulsion droplets will penetrate the interface under static conditions. High ejecting velocity may help to overcome the entering barrier by pushing emulsion droplets towards the air/water interface. Moreover, the mobility of emulsion droplets increases with decreasing size. This effect was estimated to decrease the frequency of drop entry events at the air/water interface.³⁸ It was also deduced that smaller emulsion droplets need to approach the interface much closer to enter.

Experimental data show that methyl ester forms emulsions with a smaller Span factor before spraying and after agitation. Although having the highest spreading coefficient, fine emulsion droplets of methyl ester can have a low entering probability. Entering seems to be the limiting step for the atomization onset of this particular emulsion.

It appears that the entering probability along with spreading properties of the

oil defines the onset of perforation. When an emulsion droplet is at the interface after the liquid leaves the nozzle, it will directly start spreading, and within few milliseconds (time at sheet breakup) it can initiate a subsurface flow which is strong enough to cause a local sheet thinning. An emulsion droplet requires a certain diameter to initiate these processes which, according to the experimental data, is in the order of a few μm . The subsurface flow can also be supported by sheet perturbations or flows induced by other emulsion droplets resulting in a combined effect. The consequence is a locally thinned region in the liquid sheet where a hole is formed.

6.5 Conclusions

In this Chapter, we investigated the mechanism of perforation onset induced by dilute oil-in-water emulsions, aiming to outline processes that lead to nucleation of holes in the liquid sheet formed by a hydraulic nozzle. For this purpose, dilute emulsions based on different oils have been analysed. The oils vary in their chemical composition and physical properties. Furthermore, the emulsifier concentration was varied in one case and the dynamic surface tension was modified through addition of water-soluble surfactants.

Emulsifier concentration has no impact on the spray quality as long as it does not influence the stability of the emulsion. Perforation of the liquid sheet is initiated by emulsion droplets with a diameter of some micrometers. Although the droplet size of different emulsions vary before spraying, it will be probably more uniform after passing the spray nozzle.

The proposed mechanism is based on the observation that dilute emulsions that contain oils with a high positive spreading coefficient induce formation of coarser sprays than those that contain oils with a low positive spreading coefficient. Emulsion droplets, that spread at the interface of the liquid sheet, may induce subsurface flow. The penetration depth of the subsurface flow is in the order of the sheet thickness at breakup, which would be sufficient to introduce formation of thin areas that easily collapse. Consequently, subsurface flow, reinforced by interfacial perturbations of the sheet, can nucleate perforation that leads sheet rupture.

It appears that the mechanism is a combination of entering and spreading events. Entering frequency will vary with size and interfacial properties of emulsion droplets but cannot be quantified from experimental data discussed here and requires further investigations.

However, the proposed mechanism provides a plausible and detailed explanation for the perforation onset of dilute emulsions alone and in mixture with water-soluble surfactants. When surfactants are added to the spray liquid, they accumulate the air/water interface and slow down or even prevent spreading. This process is concomitant with the decrease of the spreading coefficient. Thus, surfactants, that decrease the dynamic surface tension at breakup, delay the perforation onset.

From the application point of view these observations suggest that emulsions of oils with a high spreading coefficient, such as vegetable- and silicone-based oils, can more efficiently reduce the fine spray fraction than emulsions of mineral-based oils with a low spreading coefficient (when atomized through a flat fan nozzle). The effect of an emulsion on the spray droplet size can be significantly reduced by additives that decrease the dynamic surface tension at breakup.

References

- [1] FOCUS, *Landscape And Mitigation Factors In Aquatic Risk Assessment. Volume 1. Extended Summary and Recommendations. Report of the FOCUS Working Groupon Landscape and Mitigation Factors in Ecological Risk Assessment*, 2007, EC Document Reference SANCO/10422/2005 v.2.0. pp. 1-169.
- [2] G. R. Stephenson, I. G. Ferris, P. T. Holland and M. Nordberg, *Pure Appl. Chem.*, 2006, **78**, 2075–2154.
- [3] P. A. Hobson, P. C. H. Miller, P. J. Walklate, C. R. Tuck and N. M. Western, *J. Agr. Eng. Res.*, 1993, **54**, 293–305.
- [4] P. C. H. Miller, *Pesticide Outlook*, 2003, **14**, 205–209.
- [5] FOCUS, *Landscape And Mitigation Factors In Aquatic Risk Assessment. Volume 2. Detailed Technical Reviews. Report of the FOCUS Working Groupon Landscape and Mitigation Factors in Ecological Risk Assessment*, 2007, EC Document Reference SANCO/10422/2005 v.2.0. pp. 1-436.
- [6] A. S. Felsot, J. B. Unsworth, J. B. H. J. Linders, G. Roberts, D. Rautman, C. Harris and E. Carazo, *J. Environ. Sci. Heal. B*, 2010, **46**, 1–23.
- [7] A. J. Hewitt, *Environmentalist*, 2008, **28**, 25–30.
- [8] P. C. H. Miller, C. R. Tuck, S. Murphy and M. da Costa Ferreira, Proceedings of 22nd European Conference on Liquid Atomization and Spray Systems (ILASS-Europe), Como Lake, Italy, 2008, pp. 1–8.
- [9] E. Hilz and A. W. P. Vermeer, *Crop. Prot.*, 2013, **44**, 75–83.
- [10] J. H. Combellack, N. M. Westen and R. G. Richardson, *Crop Prot.*, 1996, **15**, 147–152.
- [11] H. Zhu, R. W. Dexter, R. D. Fox, D. L. Reichard, R. D. Brazee and H. E. Ozkan, *J. Agric. Engineering Res.*, 1997, **67**, 35–45.
- [12] N. M. Western, E. C. Hislop, M. Bieswal, P. J. Holloway and D. Coupland, *Pestic. Sci.*, 1999, **55**, 640–642.

-
- [13] M. C. Butler Ellis and C. R. Tuck, *Crop Prot.*, 1999, **18**, 101–109.
- [14] P. C. H. Miller and M. C. Butler Ellis, *Crop Prot.*, 2000, **19**, 609 – 615.
- [15] R. W. Dexter, in *Pesticide formulations and application systems*, ed. A. K. Viets, R. S. Tann and J. C. Mueninghoff, American Society of Testing and Materials, West Conshohocken, PA, 2001, vol. 20, pp. 27–43.
- [16] M. C. Butler Ellis and A. Bradley, *Aspects Appl. Biol.*, 2002, **66**, 251–258.
- [17] O. Nicetic, G. Dorr, N. Woods and G. A. C. Beattie, Proceedings of 7th International Symposium on Adjuvants for Agrochemicals (ISAA 2004), Cape Town, South Africa, 2004, pp. 136–142.
- [18] K. Qin, H. Tank, S. Wilson, B. Downer and L. Liu, *Atomization Spray*, 2010, **20**, 227–239.
- [19] M. C. Butler Ellis, C. R. Tuck and P. C. H. Miller, *Colloid Surface A*, 2001, **180**, 267–276.
- [20] N. Dombrowski, D. Hasson and D. E. Ward, *Chem. Engin. Sci.*, 1960, **12**, 35–50.
- [21] A. H. Lefebvre, *Atomization and Sprays*, Hemisphere publishing corporation, 1989.
- [22] N. Dombrowski and R. P. Fraser, *Philos. T. R. Soc. S. A*, 1954, **247**, 101–130.
- [23] P. C. H. Miller, M. C. Butler Ellis and C. R. Tuck, Proceedings of 4th International Symposium on Adjuvants for Agrochemicals (ISAA 1995), Melbourne, Australia, 1995, pp. 95–102.
- [24] R. P. Fraser, P. Eisenklam, N. Dombrowski and D. Hasson, *AIChE J.*, 1962, **8**, 672–680.
- [25] M. C. Butler Ellis, C. R. Tuck and P. C. H. Miller, *Atomization Spray*, 1999, **9**, 385–397.
- [26] M. C. Butler Ellis, C. R. Tuck and P. C. H. Miller, *Crop Prot.*, 1997, **16**, 41–50.
- [27] W. D. Harkins and A. Feldman, *J. Am. Chem. Soc.*, 1922, **44**, 2665–2685.
- [28] CIPAC MT 36.3 Emulsion Characteristics and Re-emulsification Properties, *CIPAC MT 36.3 Emulsion Characteristics and Re-emulsification Properties*, Collaborative International Pesticides Analytical Council, 2000.
- [29] CIPAC MT 18.1.3 Standard Water C, *CIPAC MT 18.1.3 Standard Water C*, Collaborative International Pesticides Analytical Council, 2010.
- [30] C. S. Parkin, in *Application Technology for Crop Protection*, ed. G. A. Matthews and E. C. Hislop, CAB International, 1993, pp. 57–84.
- [31] W. C. Hoffmann, A. J. Hewitt, J. B. Ross, W. E. Bagley, D. E. Martin and B. K. Fritz, *J. ASTM Int.*, 2008, **5**, year.
- [32] A. Herbst, Proceedings of 17th Annual Conference on Liquid Atomization and Spray Systems (ILASS-Europe), Zürich, Switzerland, 2001.
- [33] M. D. Cloeter, K. Qin, P. Patil and B. Smith, Proceedings of 22nd Annual Conference on Liquid Atomization and Spray Systems (ILASS-Americas), Cincinnati, OH, USA, 2010, pp. 1–9.

- [34] H. Zhu, R. D. Brazee, D. L. Reichard, R. D. Fox, C. R. Krause and A. C. Chapple, *Atomization Spray*, 1995, **5**, 343–356.
- [35] C. Dalmazzone, *Lubrication Sci.*, 2005, **17**, 197–237.
- [36] H. Guler, H. Zhu, H. Ozkan, R. Derksen, Y. Yu and C. Krause, *Trans. ASABE*, 2007, **50**, 745–754.
- [37] J. J. M. Janssen, A. Boon and W. G. M. Agterof, *AIChE J.*, 1994, **40**, 1929–1939.
- [38] V. Bergeron, P. Cooper, J. Giermanska-Kahn, D. Langevin and A. Pouchelon, *Colloid Surface A*, 1997, **112**, 103–120.
- [39] J. G. E. M. Fraaije and A. M. Cazabat, *J. Colloid Interf. Sci.*, 1989, **133**, 452–460.
- [40] D. P. Gaver and J. Grotberg, *J. Fluid Mech.*, 1992, **235**, 399–414.
- [41] O. E. Jensen, *J. Fluid Mech.*, 1995, **293**, 349–378.
- [42] N. D. DiPietro, C. Huh and R. G. Cox, *J. Fluid Mech.*, 1978, **84**, 529–549.
- [43] P. Joos and J. van Hunsel, *J. Colloid Inter. Sci.*, 1985, **106**, 161–167.
- [44] V. Bergeron, M. E. Fagan and C. J. Radke, *Langmuir*, 1993, **9**, 1704–1713.
- [45] D. W. Camp and J. C. Berg, *J. Fluid Mech.*, 1987, **184**, 445–462.
- [46] J. V. Robinson and W. W. Woods, *J. Soc. Chem. Ind.*, 1948, **67**, 361–365.
- [47] L. Lobo and D. T. Wasan, *Langmuir*, 1993, **9**, 1668–1677.

Chapter 7

Atomization mechanism of agricultural sprays based on spreading properties of emulsified oils: Effect of hydrophobic silica added to oil

Dilute oil-in-water emulsions create coarser sprays than water when atomized through a flat fan nozzle. The mechanism behind this process is perforation of the thin liquid sheet that is initially formed under the nozzle outlet. Several attempts to explain the perforation onset have been discussed in literature. Recently, it was suggested that perforation onset is initiated by entering and subsequent spreading of emulsion droplets at the air/water interface of the liquid sheet. Building on this mechanistic solution, in this Chapter we investigate how the viscosity of the emulsified oil influences the perforation onset and the characteristics of produced sprays.

Parts of this Chapter have been presented at the conference Agrochemical Formulations (Informa), 2013.

7.1 Introduction

During agricultural applications, the fine spray fraction with droplets in diameter $< 100 \mu\text{m}$ is considered to be the most drift-prone having a high environmental contamination risk.^{1,2} For this reason, it is desirable to minimize the fine fraction during an agrochemical spray application. Dilute oil-in-water emulsions produce coarser sprays than water when atomized through a flat fan nozzle and are therefore interesting for drift reduction purposes.³

When spray liquid is atomized through a flat fan nozzle, it forms a liquid sheet. From high-speed photography, perforation was identified as the typical disintegration mode of the liquid sheet induced by dilute oil-in-water emulsions.⁴ Thereby, point disturbances in the sheet occur, develop into holes which grow in size and form a network of unstable ligaments. The ligaments finally disrupt into spray droplets. The thickness of the liquid sheet is inversely proportional to the distance from the nozzle.⁵ Dilute emulsions initiate perforation of the liquid sheet at shorter distances from the nozzle, where its thickness is higher and, therefore, sprays created by perforation are typically coarser than pure water sprays. The growth rate of the perforation radius was investigated⁵ as well as the relationship between the length of the sheet at breakup and the diameter and number of emulsion particles.⁶

Hole nucleation was first explained by the puncture of a particle through the liquid sheet when its diameter equals to the sheet thickness.⁴ This hypothesis was contradicted by more recent studies on dilute emulsions.^{6,7} It was reported that solid particles such as bentonite, kaolin, hydrated silica and calcium carbonate that are not able to deform in the flow, affect neither the spray droplet size nor the shape of the spray fan.⁷ On the contrary, deformable emulsion droplets were observed to increase the spray droplet size and to decrease the fine spray fraction.^{6,7} Recently, the viscosity of the emulsified oil was recognized as an essential property that influences the perforation onset and, thus, the spray droplet size.⁸ It was suggested that emulsion droplets may elongate in the shear flow within the nozzle and immediately retract thereafter. This quick retraction was claimed to redistribute the flow momentum perpendicular to the flow direction and shorten the oscillation length of the sheet.

Our investigations show that perforation might be initiated by entering and spreading of emulsion droplets at the interface of the liquid sheet. Spreading of oil or emulsion droplets at an air/water interface induces subsurface flow that can locally thin the subphase liquid. The local thinning of the liquid sheet combined with perturbations induced by a turbulent flow can initiate nucleation of perforation

holes (Chapter 6). The penetration depth of the subsurface flow was calculated to be in the order of the thickness of the liquid sheet which is required to induce rupture of a thin liquid film.⁴ The entering event of emulsion droplets onto the air/interface appears to be the limiting step in this process. Thereby, the entering frequency decreases with decreasing hydrophobicity of emulsion droplet and decreasing emulsion droplet diameter.⁹

Different oil-in-water emulsions, however, produce sprays of different qualities with respect to the mean droplet size and the fine spray fraction. The magnitude of spray coarsening can depend on several properties of dilute emulsions such as emulsion concentration⁸ or number of emulsion droplets in the spray solution,⁶ origin of the oil,¹⁰ oil viscosity,⁸ spreading properties of emulsion droplets and presence of surfactants at the air/water interface of the liquid sheet at breakup (Chapter 6).

Spreading properties of an oil can be described by the classical spreading coefficient S which is defined as the difference in free energy per unit area between the pristine surface and the (oil-)covered surface or the balance of the interfacial tensions at the air/water γ_{AW} , the air/oil γ_{AO} and the oil/water γ_{OW} interfaces.¹¹

$$S = \gamma_{AW} - \gamma_{AO} - \gamma_{OW} \quad (7.1)$$

Interfacial tensions of emulsion droplets stretched in the flow at velocities of about 20 m/s¹² will be close to interfacial tensions of pure oils that were considered to quantify the spreading coefficient. It was observed that dilute emulsions of vegetable and silicone oils with a high positive spreading coefficient produce coarser sprays than mineral oil-based emulsions with a lower positive spreading coefficient (Chapter 6).

At sufficiently high viscosity of the oil, its spreading might be slowed down. This effect might be important and needs further analysis. Continuing investigations of the perforation mechanism, we use the same oils as in our previous study. Thereby, the viscosity of these oils is modified with hydrophobized fumed silica which is typically used for formulation of agricultural products. Fumed silica increases the viscosity of the oil and can influence the oil droplet size and the distribution width of dilute emulsions. At the same time, silica particles can induce other changes in the system which are relevant for the atomization of the liquid sheet into spray droplets. Studying all these different effects we want to quantify their relevance and impact on the spray formation process.

7.2 Material and Methods

Sunflower oil purchased from John L. Seaton & Co. Ltd., rapeseed oil methyl ester (Synative ES ME SU) purchased from Cognis, mineral oil (Exxsol D140) purchased from ExxonMobil Chemicals and white oil (Bayol 85) purchased from ExxonMobil Chemicals were used to create emulsions. Fumed silica Aerosil[®] R 812 S obtained from Evonik Industries was used to modify the viscosity of each of the oils. All chemicals were used as received without further purification. Aerosil[®] R 812 S was added to the oil at concentrations of 3% w/w, 5% w/w, and 7% w/w respectively and stirred for at least 30 minutes. Thereafter, the thickened oil was mixed with the emulsifier and diluted in water.

Emulsions were produced by dilution of an oil/emulsifier stock solution with water and homogenised by shaking. The stock solution consists of an oil with a mass fraction of an appropriate emulsifier or an emulsifier mixture as listed in table 7.1. Thereafter, dilute emulsions were placed in a pressurized vessel that supplied the spray liquid to the nozzle. All emulsions were sprayed at a concentration of 0.1% w/w of the dispersed phase in CIPAC C standard hard water (hardness 500 ppm).¹³

Sprays were produced with a flat fan TeeJet XR11003 nozzle which was operated at a pressure of 3 bar. The droplet size distributions were measured with a Spraytec (Malvern Instruments Ltd.), positioned at a distance of 33 cm below the nozzle outlet. Spraytec laser diffractometer equipped with a 750 mm lens covers the range of 2.0 - 2000 μm . The nozzle was mounted on a linear unit and moved above the laser beam with a velocity of 2 cm/s along the long axis of the spray fan. Spraytec Software Version 3.03 was used to calculate the numerical values of the volume median diameter (VMD) and the percentage of spray liquid in droplets with diameter < 100 μm (V_{100}). The VMD is the average droplet size, such that 50% of the volume of sprayed liquid is in droplets of smaller diameter than the VMD and another 50% is in droplets larger than the VMD.¹⁴ The measurements were replicated three times for each sample. The reproducibility of the VMD values was $\pm 3 \mu\text{m}$ and that of the V_{100} values better than $\pm 1\%$. The measurements were performed at room temperature of 20-25°C. The liquid temperature was about 21°C.

The emulsion droplet size in the spray liquid was measured with a Mastersizer S (Malvern Instruments Ltd.) equipped with a Hydro G sample dispersion unit that contains an ultrasonic system. The width of the emulsion droplet size distribution is characterised by the dispersion index Span. The relative Span factor is defined

Table 7.1: Dilute oil-in-water emulsions prepared at the concentration of 0.1% w/w of dispersed phase in water.

oil	% w/w in spray liquid	emulsifier	% w/w in spray liquid	% w/w dispersed phase
sunflower oil	0.09	Arlatone TV ^a	0.01	0.1
methyl ester	0.09	Tanemul SO70 ^b	0.004	0.1
		Emulsifier 1371A ^c	0.006	
mineral oil	0.09	Tanemul SO70 ^b	0.008	0.1
		Tanemul L3 ^b	0.002	
white oil	0.09	Atplus 309 F-LM ^a	0.01	0.1

supplier: ^a Croda, ^b Tanatex, ^c Lanxess

as $(D_{v0.9} - D_{v0.1})/D_{v0.5}$.¹⁴ $D_{v0.1}$, $D_{v0.5}$, $D_{v0.9}$ is a droplet diameter such that 10%, 50%, 90% of total spray liquid volume are in droplets of smaller diameter. A small Span corresponds to a narrow droplet size distribution.

The viscosity of the oil phase was measured using a HAAKE RheoWin rotational Rheometer (Haake GmbH) equipped with a concentric cylinder system at a shear rate of 100 s^{-1} . All measurements were performed at 20°C . The repeatability of the results was in the range $\pm 1 \text{ mPas}$.

After emulsions have been formed, they were subjected to ultrasound within the Hydro G sample unit. The ultrasonic system was used at 50 Watts and 40 kHz for 30 seconds to induce a measurable agitation of the emulsion droplets. The emulsion droplet size and width of the size distribution were detected before and after agitation by ultrasound. The purpose of this agitation is to provide a measure of the "robustness" of emulsion droplets and allow to investigate if emulsion droplet size will be affected by agitation induced by shear stress in a nozzle.

Shear rates in a flat fan nozzle can reach $1.2 \times 10^5 - 7.0 \times 10^5 \text{ s}^{-1}$.¹⁵ Alternative measurements of the emulsion droplet size in the collected spray liquid can be disturbed by incorporated air bubbles.⁶ At the same time, the probability of droplet's coalescence increases with elapsed time so that delayed measurements may cause an increase of the emulsion droplet size.⁸ Thus, agitation by ultrasound represents a reliable method to estimate if the emulsion droplet size distribution is affected by agitation induced in the nozzle.

To determine the spreading properties of the emulsified oil, the static interfacial tensions γ_{AO} at the air/oil and γ_{OW} at the oil/water interfaces were measured with a Prozessor-Tensiometer K100 (Krüss GmbH) using the Wilhelmy plate method. The accuracy of the experimental method is of 0.001 mN/m . The reproducibility of the results was less than $\pm 0.5 \text{ mN/m}$. The temperature of the measured liquid

was 20°C.

7.3 Results and Discussion

7.3.1 Viscosity of the dispersed phase

When atomized through a flat fan XR11003 nozzle, CIPAC hard water produces spray with a VMD = 189.0 μm and the fine spray fraction is $V_{100} = 12.7\%$. Dilute oil-in-water emulsions sprayed at a concentration of 0.1% w/w produce coarser sprays than water (tables 7.2-7.5). Thereby, sunflower oil and methyl ester emulsions produce sprays with a larger mean droplet size than the mineral and white oil-based emulsions. This effect was correlated with the spreading properties of these oils described by the classical spreading coefficient (Chapter 6).

As shown in table 7.2, the viscosity of sunflower oil increases with increasing concentration of fumed silica. At the same time, an about threefold viscosity increase induces only small changes in the mean spray droplet size and in the fine spray fraction. Fumed silica slightly increases the oil/water interfacial tension γ_{OW} so that the hydrophobicity of the oil described by the sum of the oil/water and the oil/air interfacial tensions ($\gamma_{AO} + \gamma_{OW}$) increases as well. It was not possible to measure the interfacial properties at 7% w/w of the fumed silica due to a high viscosity of the oil/thickener mixture.

Table 7.2: The VMD and the V_{100} of sunflower oil emulsions sprayed at a concentration of 0.1% w/w. η_d is the viscosity of the dispersed phase, γ_{AO} and γ_{OW} are the interfacial tensions at the air/oil and the oil/water interfaces.

oil thickener [% w/w]	VMD [μm]	V_{100} [%]	η_d [mPas]	γ_{AO} [mN/m]	γ_{OW} [mN/m]	$(\gamma_{AO} + \gamma_{OW})$ [mN/m]
0	234.7	5.3	65	33.5	25.2	58.7
3	238.0	5.2	119	34.3	26.7	61.0
5	238.5	5.1	147	33.9	27.4	61.3
7	241.7	5.2	174	—	—	—

The viscosity of the rapeseed oil methyl ester with increasing concentration of fumed silica is summarized in table 7.3. The absolute viscosity of the methyl ester is lower compared to sunflower oil. However, sprays produced by emulsions of methyl ester with a modified viscosity become coarser and the fine spray fraction decreases with increasing concentration of fumed silica. Again, the oil becomes

Table 7.3: The VMD and the V_{100} of rapeseed oil methyl ester emulsions sprayed at a concentration of 0.1% w/w. η_d is the viscosity of the dispersed phase, γ_{AO} and γ_{OW} are the interfacial tensions at the air/oil and the oil/water interfaces.

oil thickener [% w/w]	VMD [μm]	V_{100} [%]	η_d [mPas]	γ_{AO} [mN/m]	γ_{OW} [mN/m]	$(\gamma_{AO} + \gamma_{OW})$ [mN/m]
0	222.1	6.8	6	31.6	11.9	43.5
3	226.1	6.4	18	31.3	12.3	43.6
5	230.1	6.0	32	31.5	12.6	44.1
7	232.0	5.9	59	31.5	13.0	44.5

Table 7.4: The VMD and the V_{100} of mineral oil emulsions sprayed at a concentration of 0.1% w/w. η_d is the viscosity of the dispersed phase, γ_{AO} and γ_{OW} are the interfacial tensions at the air/oil and the oil/water interfaces.

oil thickener [% w/w]	VMD [μm]	V_{100} [%]	η_d [mPas]	γ_{AO} [mN/m]	γ_{OW} [mN/m]	$(\gamma_{AO} + \gamma_{OW})$ [mN/m]
0	215.2	8.0	6	28.6	43.1	71.7
3	217.8	7.8	18	29.1	43.7	72.8
5	220.1	7.5	51	31.1	45.0	76.1
7	222.9	7.2	116	–	–	–

Table 7.5: The VMD and the V_{100} of white oil emulsions sprayed at a concentration of 0.1% w/w. η_d is the viscosity of the dispersed phase, γ_{AO} and γ_{OW} are the interfacial tensions at the air/oil and the oil/water interfaces.

oil thickener [% w/w]	VMD [μm]	V_{100} [%]	η_d [mPas]	γ_{AO} [mN/m]	γ_{OW} [mN/m]	$(\gamma_{AO} + \gamma_{OW})$ [mN/m]
0	208.3	8.9	23	30.3	36.2	66.5
3	225.0	6.7	74	31.0	39.7	70.7
5	229.7	6.3	90	31.5	48.7	80.2
7	232.0	6.0	105	–	–	–

more hydrophobic with the addition of oil thickener. Similar tendencies were obtained when fumed silica was added to the mineral oil (table 7.4). In the case of white oil, the increasing concentration of fumed silica significantly increases the mean spray droplet size and at the same time decreases the fine spray fraction, as shown in table 7.5. Thereby, two properties of dilute white oil emulsions change significantly: the viscosity of the oil and the hydrophobic properties of the dispersed phase expressed as $(\gamma_{AO} + \gamma_{OW})$.

7.3.2 Emulsion droplet size

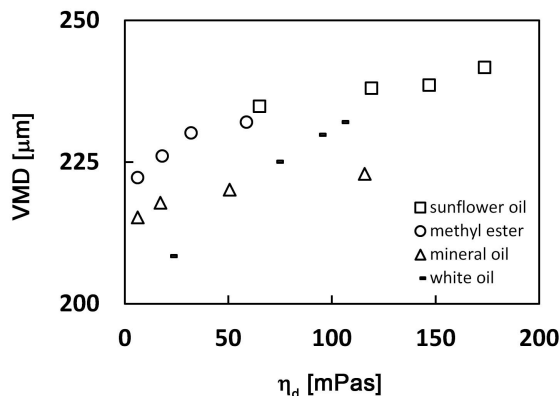


Figure 7.1: The VMD of dilute oil-in-water emulsions sprayed at a concentration of 0.1% w/w sprays plotted as a function of the viscosity of the dispersed phase η_d .

In figure 7.1 the mean spray droplet size is plotted as a function of the oil viscosity. It appears, that there is a general tendency that oils with a higher viscosity produce coarser sprays. At the same time, dilute emulsions based on oils with a similar viscosity produce sprays with very different mean sizes. *E.g.*, plain white oil emulsion, mineral oil emulsion with 3% w/w of Aerosil[®] R 812 S and methyl ester emulsion with 3% w/w of Aerosil[®] R 812 S; all have a similar oil viscosity of $\eta_d = 23$ mPas, $\eta_d = 18$ mPas and $\eta_d = 18$ mPas. The mean droplet size of created sprays is $208.3 \mu\text{m}$, $217.8 \mu\text{m}$ and $226.1 \mu\text{m}$. It is also remarkable that the viscosity increase can be almost twentyfold (as in the case of the mineral oil), while the concomitant increase in the spray droplet size is rather moderate.

The viscosity of the dispersed phase affects the size of emulsion droplets in the spray liquid. The width of the droplet size distribution of sunflower oil emulsions before spraying increases with increasing concentration of the oil thickener (table 7.6). The mean emulsion droplet size and the distribution width decrease after agitation with ultrasound. Generally, oils of higher viscosity produce emulsions with a larger droplet size and a broader distribution width before and after agitation (tables 7.7-7.8). This correlation is less pronounced for emulsions produced with white oil (table 7.9).

In figure 7.2 the VMD of sprays produced by dilute oil-in-water emulsions is plotted as a function of emulsion droplet size before spraying and after agitation. The VMD increases with increasing emulsion droplet size before spraying (figure

Table 7.6: Emulsion mean diameter ($D_{v0.5}$) and the Span of sunflower oil emulsions before agitation and after applying ultrasound.

oil thickener [%w/w]	η_d [mPas]	before spraying		after agitation	
		$D_{v0.5}$ [μm]	Span	$D_{v0.5}$ [μm]	Span
0	65	9.6	8.21	2.7	2.77
3	119	8.9	8.41	3.1	2.86
5	147	8.7	9.72	3.5	2.86
7	174	5.4	19.25	2.8	8.07

Table 7.7: Emulsion mean diameter ($D_{v0.5}$) and the Span of rapeseed oil methyl ester emulsions before agitation and after applying ultrasound.

oil thickener [%w/w]	η_d [mPas]	before spraying		after agitation	
		$D_{v0.5}$ [μm]	Span	$D_{v0.5}$ [μm]	Span
0	6	1.4	1.57	1.4	1.55
3	18	3.7	3.17	4.0	2.86
5	32	3.2	3.61	2.9	2.25
7	59	4.4	4.37	3.3	2.59

Table 7.8: Emulsion mean diameter ($D_{v0.5}$) and the Span of mineral oil emulsions before agitation and after applying ultrasound.

oil thickener [%w/w]	η_d [mPas]	before spraying		after agitation	
		$D_{v0.5}$ [μm]	Span	$D_{v0.5}$ [μm]	Span
0	6	2.5	2.59	2.4	2.50
3	18	3.1	10.7	2.8	7.02
5	51	3.9	17.53	3.05	5.50
7	116	8.4	3.59	6.1	3.68

Table 7.9: Emulsion mean diameter ($D_{v0.5}$) and the Span of white oil emulsions before agitation and after applying ultrasound.

oil thickener [%w/w]	η_d [mPas]	before spraying		after agitation	
		$D_{v0.5}$ [μm]	Span	$D_{v0.5}$ [μm]	Span
0	23	2.6	2.67	2.5	2.30
3	74	3.2	3.89	3.3	3.24
5	90	3.2	2.52	2.9	1.97
7	105	3.7	7.50	3.0	1.96

7.2a). This correlation is less pronounced for sprays produced by dilute emulsions based on the same oil such as mineral or sunflower oil. This shows that it is not possible to establish a simple relation between oil viscosity and the spray droplet size produced by dilute emulsions.

Larger emulsion droplets may break into smaller ones due to high shear and elongational rates in the nozzle. Ultrasound was applied to dilute emulsions for 30 seconds to estimate if emulsion droplet size is influenced by agitation. As illustrated in figure 7.2b, the emulsion droplet size decreases after sonication towards a more uniform value. This observation implies that the viscosity of the dispersed phase does not control the number of emulsion droplets after spraying due to break-up of larger emulsified particles in the nozzle.

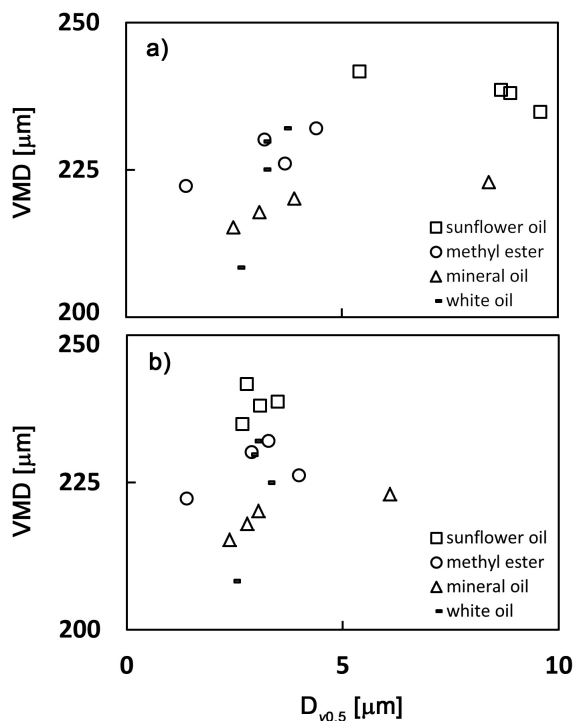


Figure 7.2: The VMD of dilute oil-in-water emulsions sprayed at a concentration of 0.1% w/w sprays plotted as a function of the mean emulsion droplet size $D_{v0.5}$ a) before spraying, b) after agitation with ultrasound for 30 seconds.

7.3.3 Mechanism

According to the recently suggested mechanism, spray formation from dilute oil-in-water emulsion is induced by emulsion droplets entering and subsequently spreading at the air/water interface of the liquid sheet. A sufficiently high viscosity might suppress spreading of emulsion droplets, delay perforation onset and cause formation of finer sprays. The data reveal that by tendency sprays of thickened emulsions become coarser than sprays produced by emulsions without thickening agent. This indicates that Aerosil[®] influences other properties of emulsion droplet which are crucial for the perforation onset.

The understanding of this observation can be gained by considering similar systems used for other applications. It is a well known effect that mixtures of oils and hydrophobic particles are more effective antifoams than the same oils without solid particles.^{9,16} Hydrophobic particles were observed to adhere to the oil/water interface and to facilitate the emerging of oil droplets at the air/water interface of a foam lamella.^{16,17} This occurs when hydrophobic particles of irregular shape bridge the thin water film between the oil droplet and the air/water interface. This effect was shown, for instance, for liquid paraffin that has a negative spreading coefficient¹⁶ and polydimethylsiloxanes⁹ that have a positive spreading coefficient in mixtures with hydrophobised silica particles.

The hydrophobic silica particles used in this study resemble the particles that are applied to enhance the antifoam efficiency. Although, conditions during the atomization process are significantly more dynamic than those during the foam rupture, we suggest that clusters of hydrophobic silica particles facilitate the entry of emulsion droplets during the spray atomization process. Before spraying, clusters of hydrophobic particles will be located in the oil phase within the emulsion droplet while its oil/water interface is occupied by emulsifier molecules. During spraying, larger emulsion droplets may break up in the nozzle or be deformed and rapidly change their shape. During these breakup and deformation processes, silica clusters will be exposed to the oil/water interface of emulsion droplets. The clusters at the interface can pierce through the pseudo-emulsion film between the emulsion droplet and the air/water interface of the liquid sheet if a droplet is located close enough to the interface.

Moreover, experimental data reveal that the addition of fumed silica particles increases the hydrophobicity of the emulsion droplets, and thus, their affinity to merge with the air/water interface. The hydrophobicity increases especially in the case of white oil where a significant spray coarsening was measured for thickened

dilute emulsions.

The entering event appears to be the limiting step in the mechanism of the perforation onset discussed in Chapter 6. The presence of hydrophobic clusters at the oil/water interface of emulsion droplets and an increase of the hydrophobicity of the oil; both these effects will increase the entering probability at the interface of the liquid sheet formed during the spraying process. As a consequence, entering of emulsion droplets at an earlier point, closer to the nozzles outlet, when the liquid sheet is thicker, will induce formation of coarser sprays.

7.4 Conclusions

In this Chapter, spray formation of dilute oil-in-water emulsions based on pure oils and mixtures of oil and fumed silica was investigated. Dilute emulsions produces coarser sprays than water when atomized through a flat fan nozzle. An additional spray coarsening can be achieved when a viscosity modifier Aerosil® R 812 S, which is based on hydrophobised fumed silica, is added to the dispersed phase. Hydrophobic silica primary increases the viscosity of the oil. Earlier, it was concluded that the viscosity increase of the dispersed phase induces formation of coarser sprays.⁸ Our data show that oils of comparable viscosities produce spray of the same quality with respect to the spray mean droplet diameter and that a viscosity increase with oil thickener induces sometimes an only moderate spray coarsening.

Aerosil® R 812 S particles also influence interfacial properties of oils when located at the oil/water interface as indicated by a small increase in the oil/water interfacial tension. Discussing this effect in the light of the recently proposed mechanism of spray formation based on spreading of emulsion droplets at the air/water interface of the liquid sheet, it appears that addition of fumed silica may increase the entering probability of emulsion droplets. We suggest that silica particles may go to the oil/water interface of emulsion droplets when these break up or deform due shear stress in the nozzle. Located at the interface, hydrophobic particles can bridge between the iteface of the liquid sheet and the emulsion droplet and thus increase its entering probability.

For agricultural application these findings imply that emulsified mixtures of oils with hydrophobic silica may produce even coarser sprays than those without silica. However, the magnitude of this effect differs for different oils and the fraction of fine spray droplets is sometimes hardly influenced by addition of a viscosity modifier.

References

- [1] P. A. Hobson, P. C. H. Miller, P. J. Walklate, C. R. Tuck and N. M. Western, *J. Agr. Eng. Res.*, 1993, **54**, 293–305.
- [2] P. C. H. Miller, *Pesticide Outlook*, 2003, **14**, 205–209.
- [3] E. Hilz and A. W. P. Vermeer, *Crop. Prot.*, 2013, **44**, 75–83.
- [4] N. Dombrowski and R. P. Fraser, *Philos. T. R. Soc. S. A*, 1954, **247**, 101–130.
- [5] R. P. Fraser, P. Eisenklam, N. Dombrowski and D. Hasson, *AIChE J.*, 1962, **8**, 672–680.
- [6] M. C. Butler Ellis, C. R. Tuck and P. C. H. Miller, *Atomization Spray*, 1999, **9**, 385–397.
- [7] R. W. Dexter, in *Pesticide formulations and application systems*, ed. A. K. Viets, R. S. Tann and J. C. Mueninghoff, American Society of Testing and Materials, West Conshohocken, PA, 2001, vol. 20, pp. 27–43.
- [8] K. Qin, H. Tank, S. Wilson, B. Downer and L. Liu, *Atomization Spray*, 2010, **20**, 227–239.
- [9] V. Bergeron, P. Cooper, J. Giermanska-Kahn, D. Langevin and A. Pouchelon, *Colloid Surface A*, 1997, **112**, 103–120.
- [10] N. M. Western, E. C. Hislop, M. Bieswal, P. J. Holloway and D. Coupland, *Pestic. Sci.*, 1999, **55**, 640–642.
- [11] W. D. Harkins and A. Feldman, *J. Am. Chem. Soc.*, 1922, **44**, 2665–2685.
- [12] M. C. Butler Ellis, C. R. Tuck and P. C. H. Miller, *Colloid Surface A*, 2001, **180**, 267–276.
- [13] CIPAC MT 18.1.3 Standard Water C, *CIPAC MT 18.1.3 Standard Water C*, Collaborative International Pesticides Analytical Council, 2010.
- [14] A. H. Lefebvre, *Atomization and Sprays*, Hemisphere publishing corporation, 1989.
- [15] H. Zhu, R. D. Brazee, D. L. Reichard, R. D. Fox, C. R. Krause and A. C. Chapple, *Atomization Spray*, 1995, **5**, 343–356.
- [16] P. Garrett, J. Davis and H. M. Rendall, *Colloid Surface A*, 1994, **85**, 159–197.
- [17] K. G. Marinova and N. D. Denkov, *Langmuir*, 2001, **17**, 2426–2436.

Chapter 8

Atomization of agricultural sprays from mixtures of a polymer solution with a dilute oil-in-water emulsion

In this Chapter, the spray formation of mixtures that contain a dilute oil-in-water emulsion and a polymer liquid is investigated. Polymer liquids and dilute oil-in-water emulsions create coarser sprays than water when atomized through a flat fan nozzle. The mode of action of polymer liquids is due to the increase in shear or elongational viscosity of the spray liquid. Furthermore, we use the hypothesis that emulsion droplets induce spray formation by spreading at the air/water interface of the liquid sheet. By analysing spray droplet size spectra, elongational properties of spray liquids, and breakup patterns of the liquid sheet, it is possible to identify the dominant properties driving spray formation in those mixtures and to investigate interactions at breakup.

Parts of this Chapter have been presented at the conference SuproFruit, 2011.

8.1 Introduction

Spray applications of agricultural products carry a risk of pesticide losses *via* spray drift. Spray drift is defined as ‘downwind movement of airborne droplets from the application area during aerial or ground-based applications’.¹ It has been demonstrated that drift risk correlates well with the amount of fine spray droplets with diameter $< 100 \mu\text{m}$ (V_{100}).^{2,3} These fine droplets remain air-borne longer than droplets with a larger diameter and thus can be more easily carried away by crosswind from the application area. In order to manipulate the spray droplet size distribution and to decrease the formation of drift-prone fine droplets, the use of drift retardants in the form of tank-mix additives became common practice in some European and non-European countries.^{4–6} Drift retardants usually contain polymeric material or an oil-based polymer formulation.^{7,8}

When spray liquid is atomized through a hydraulic flat fan nozzle, the liquid velocity provided by pressure leads to the formation of a flat sheet under the nozzle outlet. Spray atomization therefore depends on the physical properties of the spray liquid and the ambient gas, and on the ejecting velocity.⁹ The sheet expands against the counteracting surface tension of the liquid and its length decreases with increasing relative velocity, between the liquid and the ambient gas. Finally, the sheet becomes unstable and oscillations disrupt it into ligaments and then into spray droplets. If emulsion droplets are present in the spray liquid, the breakup mode is perforation.^{10,11} In this mode, atomization onset occurs closer to the nozzle outlet through hole formation. These holes rapidly grow in size and form a network of ligaments that finally break up into spray droplets.

Physical properties of spray liquids that are known to influence droplet size distribution are viscosity, surface tension, and the presence of emulsion droplets in the spray liquid.¹² In some cases, polymers can marginally decrease the static surface tension.¹³ The dominating effect of polymer solutions is the change in viscous properties of the spray liquid.^{14–16} Viscosity increase reduces the oscillation so that the spray sheet produced is more placid and can sustain greater perturbations before breakup. Atomized polymer liquids increase the spray droplet size over the whole fan width compared to pure water sprays. Thereby, the distribution width either remains unchanged¹³ or increases compared to water.⁴

For Newtonian liquids, a good correlation was observed between the shear viscosity and the increase in spray droplet size.¹⁶ This correlation is weaker for non-Newtonian viscoelastic solutions. Polymer solutions that exhibit a low increase in shear viscosity but a measurable increase in apparent elongational viscosity were

found to influence the mean spray droplet size.¹³ Elongational viscosity is the magnitude of the resistance to stretching forces.¹⁷ Three parameters were outlined that influence the extensional properties of spray liquids: 1) the rigidity of the polymer chain; 2) the molecular weight of the polymer; and 3) its concentration.^{14,16} Extensional viscosity can decrease or increase with strain rate.^{16,18} Dilute solutions of rigid-rod polymers have a constant extensional viscosity.¹⁴ In solutions of flexible polymers, the extensional viscosity strongly increases with increasing stretching rate. The behaviour of elongational viscosity of semi-rigid polymers can be placed in-between. As a consequence, polymer solutions with a constant or an increasing elongational viscosity achieve a significant spray coarsening.¹⁶

Dilute oil-in-water emulsions are known to increase the mean droplet size and to reduce the fine spray fraction when sprayed through a convectional flat fan nozzle.^{19–21} Emulsion concentrations required to achieve spray coarsening range between $2 \times 10^{-3} - 5 \times 10^{-2}\%$ w/w.²¹ At higher concentrations ($> 1\%$ or sometimes even at $> 0.01\%$), emulsions have been observed to decrease the dynamic surface tension of the spray liquid.²¹ Recently, it has been suggested that spreading emulsion droplets that are located at the air/water interface of the liquid sheet can induce a flow in the bulk liquid and a subsequent local thinning of the liquid sheet which may interact with local perturbations at the interface and initiate perforation onset (Chapter 6). Emulsions based on oils with a high spreading coefficient were observed to create coarser sprays than those based on oils with a low spreading coefficient.

The atomization modes of spray liquids that contain either an emulsion or a polymer solutions have been discussed in the literature and the crucial physical properties for both spray formation mechanisms have been outlined.¹² The objective of this research was to investigate mixtures of dilute polymer liquids in combination with an emulsion and to study the interactions between the viscosity increase of polymer solutions and the spreading that drives perforation onset. Mixtures of polymers and emulsions are of a particular interest for spray drift retardants that contain an oil-based polymer formulation, as well as for spray liquids where a polymer and a dilute emulsion are mixed in the tank.

8.2 Material and Methods

Drift control additives Ag-Rho DEP 775 and Ag-Rho DV 27 are guar-based spray drift retardants supplied by Rhodia. Ag-Rho DEP 775 contains water soluble granules with 75% modified guar gum whereas Ag-Rho DV 27 is a 20% formulation

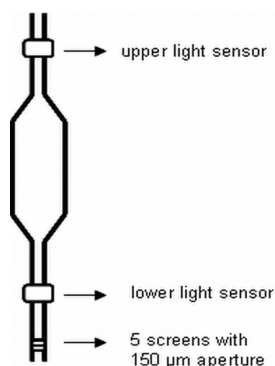


Figure 8.1: A schematic of a screen viscometer. A pack of five fine-meshed screens with an aperture of $150\ \mu\text{m}$ was incorporated at the tip of a glass pipette. Both light sensors detect the efflux time of a liquid.

of modified guar gum based on rapeseed oil. A non-ionic polyacrylamide derivative (PAMS) was provided by CIBA Speciality Chemicals. The spray solutions were prepared in hard CIPAC C water ($500\ \text{ppm}$)²² and stirred for two hours at low speeds to prevent polymer degradation.

Sunflower oil purchased from John L. Seaton & Co. Ltd. was emulsified with Arlatone TV purchased by Croda. The fraction of emulsifier in the spray liquid was 0.01% w/w and the concentration of the oil was 0.09% w/w giving an emulsion concentration of 0.1% w/w. The emulsion was created by adding the oil/emulsifier mixture in CIPAC C water and homogenized by shaking. All substances were used as supplied without further purification.

All sprays were produced with a TeeJet XR11003 flat fan nozzle which was operated at a pressure of 3 bar. The droplet size distributions were measured with a laser diffraction instrument (Spraytec, Malvern Instruments Ltd.), equipped with a 300 mm lens, at a distance of 33 cm below the nozzle outlet. The nozzle was mounted on a linear unit and moved above the laser beam at a velocity of 2 cm/s across the x -axis of the spray fan. The Spraytec Software Version 3.03 was used to derive the numerical values of the volume median diameter (VMD) and the percentage of spray liquid in droplets with diameter $< 100\ \mu\text{m}$ (V_{100}). The measurements were replicated three times for each sample. The reproducibility of the VMD values was $\pm 3\ \mu\text{m}$ and that of the V_{100} values better than $\pm 1\%$. The measurements were performed at room temperature of $20\text{-}25^\circ\text{C}$. The liquid temperature was about 21°C .

Photographs of the liquid sheet were made with a Nikon D200 camera equipped with a R1C1, a synchronized Wireless Close-Up Speedlight System ($600\ \mu\text{s}$ flash

light duration). The flash light was installed behind the nozzle and opposite to the camera. It was additionally damped by a diffuser.

As shown in figure 8.2, a ‘screen viscometer’ was built according to the ASTM standard for agricultural spray liquids.²³ The viscometer was filled by applying suction to the pipette body above the screen pack so that the liquid is filled up to the upper light sensor. Thereafter, the liquid was allowed to flow through the screen pack under gravity. The efflux time of the test liquid through the ‘screen viscometer’ was detected with two light sensors and compared to the efflux time of water. The derived screen factor is very sensitive to the increase in elongational properties of dilute polymer solutions and provides a relative comparison between different spray liquids. It also gives an estimate of the elongational properties of a spray liquid (or the relative elongational viscosity).²³

A BP2 bubble tensiometer (Krüss GmbH) was used to obtain the dynamic surface tension at the air/water interface of the spray liquid at surface age of 10 ms.

8.3 Results and Discussion

For these investigations, two polymer types were chosen that differ in their elongational and shear behaviour. Guar gum is a semi-rigid polymer that increases the shear viscosity without a significant increase in elongational viscosity.¹⁶ Flexible polyacrylamide derivatives (PAM), on the other hand, significantly increase the elongational viscosity of the spray liquid above a critical strain rate.¹⁵

Sprays produced with CIPAC C hard water using an XR11003 flat fan nozzle gave a VMD = 194.6 μm and a fine spray fraction of $V_{100} = 11.0\%$. Both guar-based Ag-Rho DEP 775 and the PAM solutions increase the VMD and decrease V_{100} with increasing concentration, as summarized in tables 8.1 and 8.2. The increase of the screen factor was moderate for the semi-rigid guar polymer which indicates a relatively low increase in elongational viscosity. PAM solutions exhibit high elongational viscosity as indicated by the steep increase of the screen factor already at a polymer concentrations as low as 0.001% w/w (table 8.2). In both cases, the polymers affinity for the air/water interface is low as indicated by the dynamic surface tension, ranging between 71.2 -71.9 mN/m.

Dilute emulsion of sunflower oil created sprays with a VMD = 256.9 μm and $V_{100} = 3.3\%$ when atomized through an XR11003 flat fan nozzle. The screen factor of the emulsion was measured as zero and the dynamic surface tension at 10 ms was 69.7 mN/m.

Table 8.1: The volume median diameter (VMD) and the fine spray fraction (V_{100}) of sprays produced with Ag-Rho DEP 775. SF is the screen factor and DST is the dynamic surface tension at 10 ms.

guar gum % w/w	VMD [μm]	V_{100} [%]	SF	DST [mN/m]
0.0075	198.7	11.6	1.14	71.7
0.0225	217.2	9.9	1.34	71.9
0.0750	297.5	6.2	2.36	71.2

Table 8.2: The volume median diameter (VMD) and the fine spray fraction (V_{100}) of sprays produced with PAM. SF is the screen factor and DST is the dynamic surface tension at 10 ms.

PAM % w/w	VMD [μm]	V_{100} [%]	SF	DST [mN/m]
0.0010	204.4	10.2	2.71	71.7
0.0025	216.2	8.9	4.08	71.5
0.0050	246.3	7.5	6.41	71.6
0.0100	308.0	4.6	9.53	71.7

Figure 8.2 shows the effect of different spray liquids on the width of the spray fan and the distribution of the mean droplet sizes across the fan x -axis. The center of the spray cloud is indicated by the zero coordinate on the fan x -axis, and the edges of the expanded fan are at 80 cm from the center in both directions. Water sprayed through a flat fan nozzle creates a spray that is finer in the middle section, and becomes significantly coarser at both edges. Guar gum as well as PAM narrow the spray width and shift the whole spectrum to higher droplet size. The sunflower oil emulsion specifically diminishes the fine spray fraction in the central part of the spray fan. The increase of the droplet sizes at the fan edges is lower than in the case of both polymers liquids.

Ag-Rho DV 27 is a combination of both a polymer and an emulsion, provided

Table 8.3: The volume median diameter (VMD) and the fine spray fraction (V_{100}) of sprays produced with Ag-Rho DV 27. SF is the screen factor and DST is the dynamic surface tension at 10 ms.

guar gum % w/w	VMD [μm]	V_{100} [%]	SF	DST [mN/m]
0.002	231.9	6.1	1.02	71.9
0.006	212.6	7.8	1.09	72.0
0.020	213.4	7.3	1.32	72.2
0.060	265.0	5.38	2.50	72.3

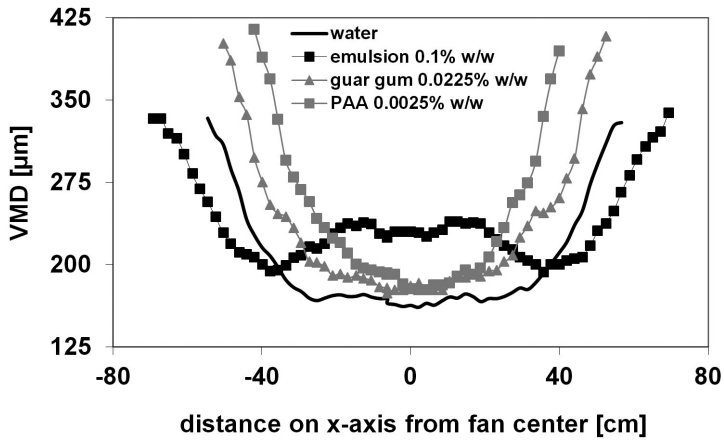


Figure 8.2: The VMD of different spray liquids across the fan width (x -axis).

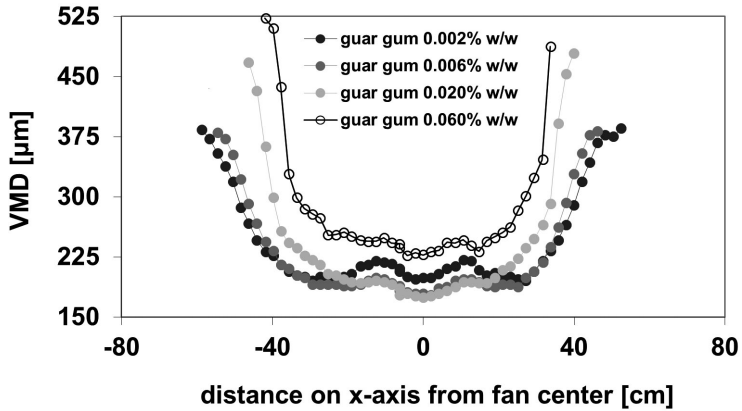


Figure 8.3: Effect of the Ag-Rho DV 27 on the VMD distribution across the fan width (x -axis).

as a ready-to-use formulation for drift reduction purposes. As shown in table 8.3, Ag-Rho DV 27 achieved a significant spray coarsening at the lowest concentration with 0.002% w/w of the guar gum content. The corresponding screen factor is 1.15. This indicates that at this concentration the elongational viscosity does not contribute to the size increase of the spray droplets. Product concentrations with 0.006% w/w and 0.02% w/w of the guar gum content produced finer sprays while their screen factor remained low. The highest concentration of 0.06% w/w induced the formation of significantly coarser sprays, consistent with an increase of the screen factor.

Figure 8.3 shows the spray patterns for each Ag-Rho DV 27 concentration. At a concentration of 0.002% w/w, the produced spray was coarser in the middle section, similar to spray of the dilute emulsion. The highest Ag-Rho DV 27 concentration with 0.06% w/w guar gum showed development of a viscosity-driven pattern. Patterns produced by the solutions with 0.006% w/w and 0.02% w/w guar content were in-between the oil-dominated and the viscosity driven regimes. These observations are consistent with the measurement of the screen factor which increased at the highest Ag-Rho DV 27 concentration (table 8.3). As shown in table 8.3, the dynamic surface tensions of these polymer liquids are all virtually similar and they do not influence the spray formation process.

Photographic pictures in figure 8.4 show disintegration patterns of the investigated spray liquids. The length of the liquid sheet is indicated by the black line. The sheet in figure 8.4a is disrupted by perforations formed close to the nozzle (encircled). This disintegration pattern is most likely dominated by emulsion droplets. Figure 8.4b shows similar disruption patterns as in figure 8.4a but with a slightly longer breakup length. Figure 8.4c displays a mixed disintegration pattern with a more smoother sheet compared to figure 8.4a, but with a delayed perforation onset. The breakup length increased with increasing polymer concentration. Figure 8.4d shows a completely different breakup scheme. Here, a long smooth sheet is formed that expands, remaining intact for a relatively long time, and then disrupts at a greater distance from the nozzle. Oscillation and hole formation are visible at the disintegrating rim. Formation of a long smooth sheet is typical for high viscosity spray liquids.

A low screen factor of 1.02, and the typical perforation patterns at a short disintegration distance for guar gum content of 0.002% w/w of Ag-Rho DV 27, lead to the conclusion that at this concentration spray coarsening is dominated by the presence of emulsion droplets. As indicated by the $SF = 2.5$ and illustrated by the disintegration patterns in figure 8.4c, the concentration of 0.06% w/w guar gum

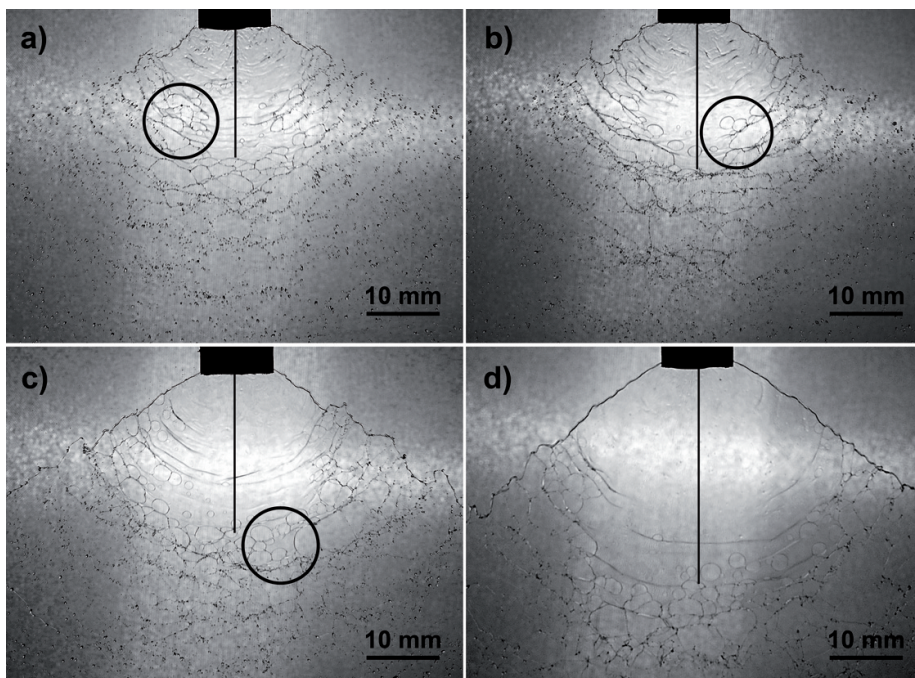


Figure 8.4: Photographs of the sheet breakup of Ag-Rho DV 27 spray liquid. The concentrations are referred to the content of the guar gum: a) 0.002% w/w, b) 0.006% w/w, c) 0.02% w/w, d) 0.06% w/w. Black line indicates the sheet length. The circles highlight perforation holes.

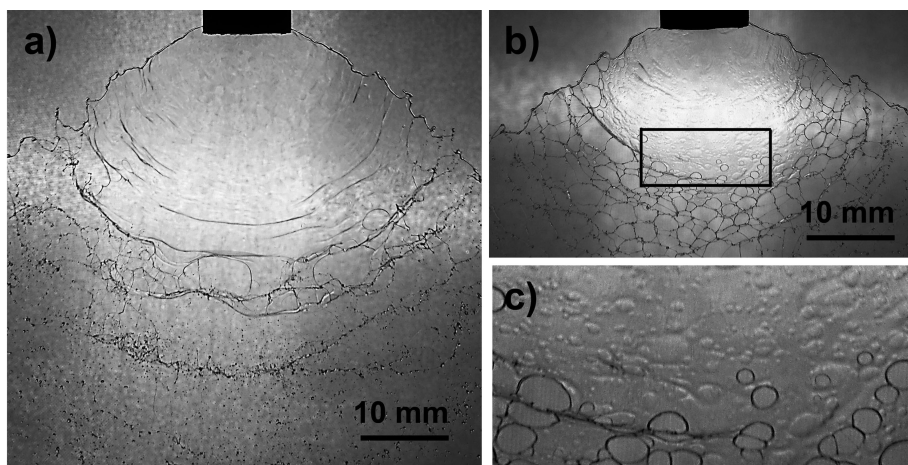


Figure 8.5: Photographs of the sheet breakup of a) Ag-Rho DEP 775 (0.03% w/w guar gum), b) a mixture of a sunflower oil emulsion at a concentration of 0.5% w/w and Ag-Rho DEP 775 (0.03% w/w guar gum), c) magnified section from picture b).

sufficiently increased the viscosity of the spray liquid such that viscosity dominates the disintegration mode of the sheet.

The hypothesis that perforated-sheet disintegration mode is induced by the spreading of emulsion droplets is suggested to explain these observations. Mathematical models have been developed to describe the dynamics of spreading oils (or a surfactant layer) on the surface of another liquid.^{24–29} During the spreading of an oil drop, formation of a microscopic leading film is often considered. The velocity of this film depends on the classical spreading coefficient $S = \gamma_{AW} - \gamma_{AO} - \gamma_{OW}$.³⁰ S is defined as the difference in free energy per unit area between the pristine surface and the (oil-)covered surface, or the balance of interfacial tensions between air (A), water (W) and oil (O) phases. Oils with a positive initial spreading coefficient spread at the interface while oils with $S < 0$ form a lens. In a simplified steady-state situation with a uniform spreading velocity and a constant film thickness, the spreading velocity is balanced by the shear stress exerted by the substratum flow τ .

$$\nabla\gamma + \tau = 0 \quad (8.1)$$

$\nabla\gamma$ is the surface tension gradient along the spreading film. The local shear stress induced by the velocity gradient at the surface ($z = 0$) is $\tau = \eta(du_x/dz)_{z=0}$. η is the viscosity of the underlying liquid and u_x is the velocity gradient along the interface in x direction. The radius of the spreading film R at time t is^{25,27,28}

$$R = K \left(\frac{S^2 t^3}{\eta \rho} \right)^{1/4} \quad (8.2)$$

K is a constant and ρ the density of underlying fluid. As implemented in equation 8.2, the spreading rate decreases with increasing bulk viscosity of the underlying liquid. Consequently, spreading velocity decreases with increasing viscosity of the bulk liquid due to greater friction between the oil phase and the underlying aqueous layer. During spray formation from a liquid sheet, these conditions may occur at high polymer concentrations. To analyse this dependence, we looked at the breakup patterns in the liquid sheet induced by the investigated emulsion/polymer mixtures.

Photographs of sheet breakup shown in figure 8.4 illustrate that perforation holes are formed at each concentration of the guar gum (less visible in figure 8.4d). However, with increasing polymer concentration, hole nucleation occurs further down from the nozzle outlet at a position where the liquid sheet is disrupted by

oscillation. This observation indicates that above a certain polymer concentration, spray formation is completely controlled by viscosity. At a low polymer concentration, the spreading emulsion droplets apparently dominate the onset of spray formation.

Moreover, with increasing viscosity of the spray liquid, the liquid sheet will probably become thicker. This assumption is based on calculations that show that the thickness of a film formed through an airblast atomizer increases with the viscosity of the spray liquid.³¹ Furthermore, ‘die-swelling’ occurs in viscous liquid jets.³² Consequently, a similar effect is likely to occur during the formation of liquid sheets through a flat fan nozzle. These considerations can be used to explain the sheet atomization of a polymer/emulsion mixture. The subphase flow inserted by a spreading layer has a depth $m = \sqrt{\eta t / \rho}$ that follows from the mathematical models describing the kinetics of spreading layers. The flow depth has to be of the same order as the film thickness to induce perturbations large enough to induce film rupture.^{11,33} Consequently, with increasing substrate thickness, the induced bulk flow becomes too weak to initiate film disturbances or film breakup. Similar observations have also been made under experimental conditions. A droplet of oleic acid placed at the interface of a liquid with a sufficiently low substrate thickness causes rupture of the substrate film so that the drop is surrounded by a kind of ‘dry halo’ for a short period of time.^{24,34} Thereafter, back-flow develops and restores the film.

A suggestion that similar interactions occur during spray atomization is given by the shape of by the liquid sheet and sheet disruption patterns. Figure 8.5a shows disintegration of a smooth and long spray sheet produced by a solution of Ag-Rho DEP 775. As shown in figure 8.5b, a sunflower oil-based emulsion added to the polymer solution of Ag-Rho DEP 775 shortens the breakup length of the liquid sheet by perforation. The magnified part of the photographs in figure 8.5c shows a rough region above the disintegration holes. The roughness is caused by ‘bumps’ or thin islands in the sheet. These ‘islands’ might be caused by spreading emulsion droplets whose spreading velocity is reduced by the friction with the viscous spray liquid. Similar pictures were obtained for PAM/emulsion mixtures (not shown). This roughness was not observed in sheets formed by Ag-Rho DV 27, probably due to the low emulsion concentration.

The interactions between emulsion droplets and the polymer liquid analysed in this Chapter appear to scale with the viscosity of the spray liquid, and are therefore independent of the polymer type.

8.4 Conclusions

Spray formation of mixtures of dilute emulsion and a polymer solutions have been investigated in this Chapter, applying the recently proposed atomization hypothesis based on spreading properties of emulsion droplets. Screen factor measurements were used to estimate the relative elongational viscosity of polymer solutions. Polyacrylamide derivatives with long flexible chains resulting in a high resistance to elongational flow significantly increased the screen factor. The increase of the screen factor is consistent with spray coarsening achieved at comparably low polymer concentrations. The increase of the screen factor by spray liquids that contain the semi-rigid guar gum polymer was lower, so that higher concentrations of this polymer are required.

In a mixture of a dilute emulsion and a polymer solution, the effects depend on polymer concentration. At low polymer concentration spray coarsening is dominated by the emulsion droplets. Under these conditions the viscosity is low and an emulsion droplet can spread uninterrupted at the air/water interface initiating perforation onset. At higher polymer concentration, spray atomization is controlled by increased viscosity of the spray liquid. In this case, the viscosity increase of the spray liquid slows down spreading, so that the induced subphase flow is insufficient to cause an early sheet disintegration by perforation. There is a region in-between where neither the emulsion nor the viscosity dominated mechanism has sufficient traction to dominate atomization.

Results given in this Chapter demonstrate the interaction of polymer liquids with emulsion droplets during spray atomization on a somewhat qualitative basis. However, this discussion covers new aspects of a long-investigated subject that had not yet been accounted for in earlier studies. These aspects suggest a direction for future research on the atomization of agricultural spray liquids which are of a more complex nature.

References

- [1] G. R. Stephenson, I. G. Ferris, P. T. Holland and M. Nordberg, *Pure Appl. Chem.*, 2006, **78**, 2075–2154.
- [2] P. A. Hobson, P. C. H. Miller, P. J. Walklate, C. R. Tuck and N. M. Western, *J. Agr. Eng. Res.*, 1993, **54**, 293–305.
- [3] P. C. H. Miller, *Pesticide Outlook*, 2003, **14**, 205–209.
- [4] N. B. Akesson, W. E. Steinke and W. E. Yates, *J. Environ. Sci. Health, B.*, 1994, **29**, 785–814.

-
- [5] FOCUS, *Landscape And Mitigation Factors In Aquatic Risk Assessment. Volume 2. Detailed Technical Reviews. Report of the FOCUS Working Group on Landscape and Mitigation Factors in Ecological Risk Assessment*, 2007, EC Document Reference SANCO/10422/2005 v.2.0. pp. 1-436.
- [6] SDRT, *Spray Drift Reduction Technology: A European Database*, <http://www.sdrt.info/>, 2012, (2 October 2012).
- [7] H. Zhu, R. W. Dexter, R. D. Fox, D. L. Reichard, R. D. Brazee and H. E. Ozkan, *J. Agric. Engineering Res.*, 1997, **67**, 35–45.
- [8] M. Schmidt, *Grundl. Landtechnik*, 1980, **30**, 126–134.
- [9] A. H. Lefebvre, *Atomization and Sprays*, Hemisphere publishing corporation, 1989.
- [10] M. C. Butler Ellis, C. R. Tuck and P. C. H. Miller, *Atomization Spray*, 1999, **9**, 385–397.
- [11] N. Dombrowski and R. P. Fraser, *Philos. T. R. Soc. S. A*, 1954, **247**, 101–130.
- [12] E. Hilz and A. W. P. Vermeer, *Crop. Prot.*, 2013, **44**, 75–83.
- [13] R. P. Mun, B. W. Young and D. V. Boger, *J. Non-Newtonian Fluid Mech.*, 1999, **83**, 163–178.
- [14] G. M. Harrison, R. Mun, G. Cooper and D. V. Boger, *J. Non-Newton. Fluid Mech.*, 1999, **85**, 93–104.
- [15] P. A. Williams, R. J. English, R. L. Blanchard, S. A. Rose, L. Lyons and M. Whitehead, *Pest Manag. Sci.*, 2008, **64**, 497–504.
- [16] R. W. Dexter, *Atomization Spray*, 1996, **6**, 167–191.
- [17] A. Lindner, J. Vermant and D. Bonn, *Physica A*, 2003, **319**, 125–133.
- [18] S. L. Ng, R. P. Mun, D. V. Boger and D. V. James, *J. Non-Newton. Fluid Mech.*, 1996, **65**, 291–298.
- [19] N. M. Western, E. C. Hislop, M. Bieswal, P. J. Holloway and D. Coupland, *Pestic. Sci.*, 1999, **55**, 640–642.
- [20] P. C. H. Miller and C. R. Tuck, *J. ASTM Int.*, 2005, **2**, 1–13.
- [21] R. W. Dexter, in *Pesticide formulations and application systems*, ed. A. K. Viets, R. S. Tann and J. C. Mueninghoff, American Society of Testing and Materials, West Conshohocken, PA, 2001, vol. 20, pp. 27–43.
- [22] CIPAC MT 18.1.3 Standard Water C, *CIPAC MT 18.1.3 Standard Water C*, Collaborative International Pesticides Analytical Council, 2010.
- [23] ASTM International, *Designation: E2408 - 04. Standard test method for relative extensional viscosity of agricultural spray tank mixes*, 2006.
- [24] J. G. E. M. Fraaije and A. M. Cazabat, *J. Colloid Interf. Sci.*, 1989, **133**, 452–460.
- [25] O. E. Jensen, *J. Fluid Mech.*, 1995, **293**, 349–378.
- [26] N. D. DiPietro, C. Huh and R. G. Cox, *J. Fluid Mech.*, 1978, **84**, 529–549.
- [27] P. Joos and J. van Hunsel, *J. Colloid Inter. Sci.*, 1985, **106**, 161–167.

- [28] V. Bergeron, M. E. Fagan and C. J. Radke, *Langmuir*, 1993, **9**, 1704–1713.
- [29] D. W. Camp and J. C. Berg, *J. Fluid Mech.*, 1987, **184**, 445–462.
- [30] W. D. Harkins and A. Feldman, *J. Am. Chem. Soc.*, 1922, **44**, 2665–2685.
- [31] N. K. Rizk and A. H. Lefebvre, *T. ASME*, 1980, **102**, 706–710.
- [32] A. Mansour and N. Chigier, *J. Non-Newton. Fluid Mech.*, 1995, **58**, 161–194.
- [33] V. Bergeron, P. Cooper, J. Giermanska-Kahn, D. Langevin and A. Pouchelon, *Colloid Surface A*, 1997, **112**, 103–120.
- [34] D. P. Gaver and J. Grotberg, *J. Fluid Mech.*, 1992, **235**, 399–414.

Chapter 9

Formulation types with spray drift reduction potential

In this Chapter, spray additives and commercial crop protection products are analysed for their ability to reduce the amount of fine spray droplets (*e.g.*, with diameter $< 100 \mu\text{m}$) when atomized through a flat fan nozzle. Spray coarsening is correlated with the formulation type, the dynamic surface tension at 10 ms, the emulsion stability, and the type of the emulsified oil. Furthermore, one data set is discussed where droplet size spectra have been used to calculate the downwind deposition using the Silsoe arable crop drift model. A small-scale field experiment is performed to verify the calculated downwind deposition of two selected spray liquids. In a second small-scale field trial, the droplet size spectra are directly compared with field deposits.

Parts of this Chapter are published in conference proceedings of International Advances in Pesticide Application (Aspects of Applied Biology) E. Hilz, A. W. P. Vermeer, *Effect of formulation on spray drift: a case study for commercial imidacloprid products*, **2012**, *114*, 445-450; E. Hilz, A. W. P. Vermeer, F. A. M. Leermakers, M. A. Cohen Stuart, *Spray drift: How emulsions influence the performance of agricultural sprays produced through a conventional flat fan nozzle*, **2012**, *114*, 71-78.

9.1 Introduction

During spray application of agrochemicals, fine spray droplets can be carried away from the treated area by air currents and contaminate sensitive ecological resources, non-target crops, bystanders, residents, and livestock. This off-target deposition of spray droplets is referred to as spray drift.¹ The drift risk, or the spray fraction displaced downwind as airborne spray, is influenced by operation variables and weather conditions.² Spray droplet size is recognized as the most significant factor which determines the transport and deposition of spray droplets.³⁻⁶ Fine spray droplets can more easily be carried away by crosswinds due to their low sedimentation velocity (droplet diameter 10 μm with 0.003 m/s, droplet diameter 200 μm with 1.2 m/s).⁷ Fine spray fractions that contain spray droplet in diameters $< 100 \mu\text{m}$ (V_{100}) are often considered to be most drift-prone.⁸⁻¹¹ Consequently, off-target losses can be reduced when the fine spray fraction is minimized.

One way to manipulate the spray droplet size distribution is by choice of the spraying parameters *e.g.*, use of low-drift nozzles, or reduction of spray pressure.¹² Another approach is to modify the physical properties of spray liquids *etc.*¹³ Drift retardants and deposition control agents are successfully used in some non-European countries, the UK, and recently in the Netherlands;^{12,14} their purpose is to coarsen sprays during agrochemical applications. These tank-mix additives contain polymers, emulsifiable oils (or concentrated emulsions), or a mixture of both.^{9,15-18} Some chemical compounds can be incorporated into a formulated pesticide product, or are already part of common formulation types. However, the use of formulations for drift reduction purposes is not yet generally accepted because the induced effects are complex and have not yet been sufficiently evaluated.¹²

Butler Ellis and Bradley¹⁹ investigated the effect of different formulation types on spray droplet size and drift risk in wind tunnel experiments. It was shown that the effect of spray liquid on drift risk depends upon the extent of spray drift, and on nozzle design. It was also observed that emulsions are likely to reduce spray drift while water-soluble formulations mostly increase drift risk.

It is known from earlier investigations, that polymer-based drift retardants increase the spray droplet size by increasing the viscosity of the spray liquid.² In this context, polymeric materials typically used for drift reduction purposes can be split into two groups.²⁰ The first group contains flexible high-molecular-weight polymers ($M_w > 5 \times 10^6$) that can already increase the spray droplet size at concentrations of a few ppm. A disadvantage is, however, that these polymers are often sensitive to degradation by agitation through sprayer pump, and to pH changes.^{15,21,22}

For these reasons, it is challenging to incorporate these polymers into a formulated product and at the same time guarantee the drift-reducing effect in the spray liquid. The second group consists of more robust low-molecular-weight polymers (such as polysaccharides) which are less sensitive to salt concentration and shear. However, these products require a relatively high concentrations to achieve a desired degree of spray coarsening.²⁰ At these concentrations they are difficult to include in a usable formulated product.

Dilute oil-in-water emulsions also create coarser sprays compared to pure water, when atomized through a conventional nozzle.^{9,17,23} Emulsion concentrations needed for the onset of spray coarsening are in the range $10^{-2} - 10^{-3}\%$ w/w.¹⁷ Moreover, a dilute emulsion remains unaffected by recirculation through a sprayer pump.²⁴ However, the spray coarsening effect induced by dilute emulsions is nozzle type dependent.²⁵ The concentration and the type of the emulsified oil have an influence on the droplet size distribution of produced sprays.^{9,17} Recently, it has been claimed that emulsified oils with a high viscosity²³ or a high positive spreading coefficient (Chapter 6) can more efficiently reduce the fine spray fraction when applied through a flat fan nozzle. Concentrated emulsions or emulsifiable oils are often part of a formulated product and appear to be well suited for the purposes of spray drift reduction. Formulated products usually contain surface active material. Water-soluble surfactants that reduce the dynamic surface tension of the spray liquid are known to create finer sprays compared to water.²

The deposition drift at short distances is usually filtered by the no-spray buffer zones. The calculations of the buffer zone width in Germany and some other countries²⁶ are up to now based on the measurements according to the data collected by Ganzelmeier and Rautmann in 1989-1999.^{27,28} The use of accepted drift reducing equipment can reduce the buffer zone width. According to developed classification schemes, appropriate equipment can provide drift reduction up to $\leq 90\%$.¹⁴ These classification schemes, however, do not account for the effects of formulated products. Many formulation types, as we will show, affect the quality of produced sprays so that the resulting spray deposition often varies with the formulation type.

In this study, we investigate the impact of a formulation(type) on the spray droplet size distribution under laboratory conditions and we compare the results with spray deposition in the field. The measured droplet size spectra are analyzed in terms of the content and the concentration of additives in a formulated product. Moreover, relevant physical properties of spray liquids are characterised. The final goal of this analysis was the classification of common formulation types according to their ability to reduce the fine spray fraction, that is the fraction with droplets

in diameter $< 100 \mu\text{m}$. Additional, blank EC formulations were used to analyse the combined effect of a dilute emulsion with a water-soluble surfactant that decreases the dynamic surface tension of the spray liquid at 10 ms.

To estimate the drift risk under field conditions, two products (two different formulation types) were sprayed out in a small-scale drift trial. The droplet size spectra of these commercially available Bayer CropScience formulations were measured earlier within the scope of a study performed at the Silsoe Spray Application Unit.²⁹ Moreover, these data have been fitted into the Silsoe arable crop drift model developed³⁰ to calculate arable boom spraying drift risk.³¹ A direct comparison between the droplet size spectra and the deposition at the downwind edge of a field was made in a second small scale drift trial where three formulation types were sprayed simultaneously.

Small-scale drift trials, such as those performed, have several advantages. They require less time and less human resources, smaller application areas, and carry a lower contamination risk. At the same time, sampling is easier to handle than in extensive field experiments. It seems that such trials can be used to estimate the drift deposition simultaneously for several products and to verify the modelling output.

9.2 Material and Methods

Table 9.1: Formulation types according to the international classification scheme.³²

Term	Code	Spray liquid
Capsule suspension	CS	suspension
Emulsifiable concentrate	EC	(micro)emulsion
Emulsion, oil in water	EW	(micro)emulsion
Oil dispersion	OD	emulsion
Suspension concentrate	SC	suspension
Suspo-emulsions	SE	suspension/emulsion
Soluble concentrate	SL	liquid
Water dispersible granules	WG	suspension
Wettable powder	WP	suspension
A mixed formulation of CS and EW	ZW	suspension/emulsion

Common formulation types of crop protection products are summarized in table 9.1. Next to the formulation type, the product label usually refers to the in-can content of the active ingredient (a.i.) in g/L (liquid) or % w/w (solid) as a number

that follows an international abbreviation code.

EW, SE, ZW formulation types contain some organic solvents. OD and EC formulations contain an organic solvent that is used as a "filler" liquid, so that an emulsion is formed by the dilution of the formulated product in water. Consequently, the content of emulsifiable oil in OD and EC formulation types is usually higher than in EW, SE, ZW formulations.

Most of the analysed products are commercially available from Bayer CropScience. Products provided by other manufacturers are labelled with the company name. Additives that were used to prepare spray liquids are summarized in table 9.2. All of them were of technical grade and were used as obtained without further purification. All spray liquids were prepared in CIPAC C standard hard water (500 ppm).³³

Four emulsions (blank ECs) were prepared to study the physical properties of dilute oil-in-water emulsions and their effect on the spray droplet size distribution. In these emulsions the dispersed phase consists of an oil with a mass fraction of the appropriate emulsifiers as listed in table 9.3. The investigated emulsions were prepared in CIPAC C standard hard water and homogenized by shaking. The emulsifiers were selected to guarantee optimal emulsion stability according to the CIPAC method MT 36.3.³⁴ Non-ionic and anionic spray additives (table 9.2) were added to modify the dynamic surface tension of the spray liquid.

We restricted our investigations to an extended range flat fan nozzle TeeJet XR11003VS, representing a common nozzle type for ground-boom applications in Europe. The droplet size distributions were measured by laser diffraction (Spraytec, Malvern Instruments Ltd.), 33 cm below the nozzle outlet. The Spraytec was equipped with a 300 mm lens that measures droplet sizes in the range of 0.1 – 900 μm . The nozzle was operated at a pressure of 3 bar and moved above the laser beam with a velocity of 2 cm/s across the long axis of the spray fan. The Software Version 3.03 was used to derive the numerical values of the volume median diameter (VMD) and the percentage of spray liquid in droplets with diameter < 100 μm (V_{100}) that was considered as the drift-prone spray fraction. The VMD defines a mean droplet diameter whereby 50% of spray volume are in smaller and the remaining 50% are in larger spray droplets than the VMD.³⁵

Table 9.2: Adjuvants used for investigations.

trade name	supplier	type	function
Sunflower oil	John L. Seaton & Co. Ltd.	sunflower oil	emulsifiable oil
Synative ES ME SU	Cognis	rapeseed oil methyl-ester	emulsifiable oil
Exxsol D140	ExxonMobil	mineral oil	emulsifiable oil
Bayol 85	ExxonMobil	white oil	emulsifiable oil
Arlatone TV	Croda	polyoxyethylene sorbitol oleate	emulsifier
Atplus 309 F-LM	Croda	alkylaryl sulfonate	emulsifier
Tanemul SO70	Tanatex	fatty acid polyethylene glycol ether ester	emulsifier
Tanemul L3	Tanatex	fatty alcohol polyglycol ether	emulsifier
Emulsifier 1371A	Lanxess	preparation of alkylarylsulfonates	emulsifier
Synperonic A7	Croda	alkyl-ethylene oxide	non-ionic spray additive
Agral	Syngenta	nonyl phenol ethylene oxide	non-ionic spray additive
—	AkzoNobel	sodium C8-ether sulphate	anionic spray additive
Mero	Bayer CropScience	81.4% rapeseed oil methyl ester	coformulant
Induce	Bayer CropScience	oleic, linoleic, stearic acids	coformulant

The measurements were performed at least three times for each sample. The reproducibility of the VMD values was $\pm 3 \mu\text{m}$ and that of the V_{100} values better than $\pm 2\%$. The measurements were performed at room temperature of 20-25°C.

A BP2 bubble tensiometer (Krüss GmbH) was used to obtain the dynamic surface tension at the air/water interface of the spray liquid. The dynamic interfacial tension was measured at a surface age of 10 ms.

Two small-scale drift trials were done to compare the measured droplet size spectra with the downwind deposition in field. The experiments were done with bicycle-plot sprayers equipped with a 2.5 m spray boom and applying a volume rate of 200 l/ha. Five TeeJet XR11003VS nozzles were mounted on the boom with an inter-nozzle distance of 50 cm, and operated at a pressure of 3 bar, 50 cm above the grassland as schematically shown in figure 9.1. Petri dishes were placed at 3 m, 5 m, 10 m, and 20 m distance downwind from the application line. Twenty Petri dishes were placed in one row with a separation distance of 50 cm in-between. A 20 m distance between the application areas remained untreated to prevent cross-contamination between plots. After spraying, the Petri dishes were covered, collected and analysed for a.i in g/ha.

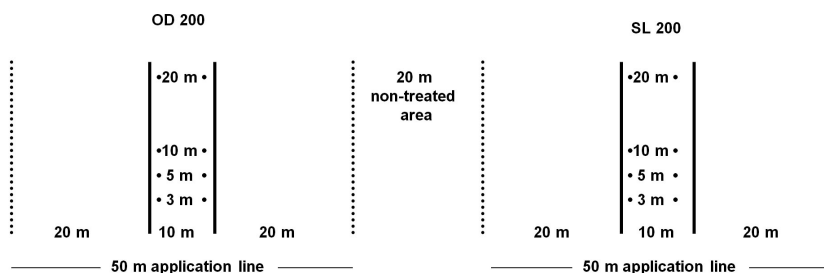
In the first experiment, two bicycle-plot sprayers were run simultaneously with three replicas spraying an OD 200 and an SL 200 formulation of imidacloprid. The sprayer velocity was 7.2 km/h. The wind direction was $90^\circ - 11.7^\circ$ in the first run, $90^\circ - 32.7^\circ$ in the second run and $90^\circ - 27.2^\circ$ in the third run. The average wind velocity at 2 m was 4.2 m/s (3.1 m/s at 1 m, 4.8 m/s at 5 m) in the first, 4.9 m/s (3.6 m/s at 1 m, 5.8 m/s at 5 m) in the second and 4.5 m/s (3.7 m/s at 1 m, 5.1 m/s at 5 m) in the third run. The relative humidity was 59% and the air temperature was 7.4°C.

The spray liquids were prepared at a concentration of 1 ml/l. Plastic Petri dishes had a diameter 14.5 cm giving a area of 0.0165 m². After application, Petri dishes were collected and the residues were dissolved in 7 ml acetonitrile/water (1/1) mixture by shaking for 10 minutes at 40 rpm. Imidacloprid content was analysed using reversed phase liquid chromatography (HPLC with an external standard). The percentage of spray drift was calculated as the average percentage of a.i. in each row of samplers. The spray drift reduction was calculated relative to content of the a.i. in the spray liquid.

A second field experiment was performed using the same equipment whereby three bicycle-plot sprayers were run simultaneously. The application area (figure 9.1) was extended by a third application block. Three formulations were sprayed: prothioconazole + spiroxamine EC 160+300, fluopyram + spiroxamine

Table 9.3: Composition of dilute emulsions.

oil	% w/w in spray liquid	emulsifier	% w/w in spray liquid	total % w/w dispersed phase
sunflower oil	0.09	Arlatone TV	0.01	0.1
rapeseed oil methyl ester	0.09	Tanemul SO70 Emulsifier 1371A	0.004 0.006	0.1
mineral oil	0.09	Tanemul SO70 Tanemul L3	0.008 0.002	0.1
white oil	0.09	Atplus 309 F-LM	0.01	0.1

**Figure 9.1:** A schematic picture of the field trial dimensions.

SE 66.7+266.6 and an imidacloprid SL 200 as the reference. The spray liquids were prepared at a concentration of 2.5 ml/l for the SL 200, 3.0 ml/l for the EC 160+300 and 1.1 ml/l for the SE 66.7+266.6.

The relative humidity during the field experiment was 88% and the air temperature 14°C. The average wind velocity was 2.6 m/s (at 2 m height) for the first, 3.5 m/s for the second and 4.5 m/s for the last run. The application line was set 90° to the wind direction; the deviations of the wind direction during the application were not directly measured but were not above 30°. Glass Petri dishes were used in this trial with a diameter of 9 cm giving a deposition area of 0.0063 m². The imidacloprid residues were dissolved in 4 ml acetonitrile/water (1/1) mixture and analysed as described above. Spiroxamine residues were dissolved in 3 ml acetone with an internal standard when shaking for 5 minutes at 40 rpm and analysed using a GC-MS.

The Silsoe arable crop drift model³⁰ was used to model the off-target deposition based on the droplet size spectra for a set of formulation types sprayed through different agricultural nozzles.³¹ The spray droplet spectra for these formulations

were measured with a “Visisizer” instrument (Oxford Laser Ltd.) at the Silsoe Spray Applications Unit.²⁹ The measurements were made 35 cm below the nozzle outlet. The nozzle was mounted on a computer controlled x-y transporter and traversed the laser at a speed of 2 cm/s. TeeJet XR11003VS, Lumark 03F110, TeeJet DG11003VS, and TeeJet AI 11003VS flat fan nozzles were operated at a spray pressure of 3 bar. Bayer CropScience formulations of imidacloprid OD 200, SC 350, and SL 200 were atomized through all tested nozzles at a concentration of 100 g a.i. in 300 l. A 0.1% w/w solution of a non-ionic spray additive Agral was used as a reference spray liquid as recommended by the international standard ISO Standard 22856.³⁶

9.3 Spray characteristics

9.3.1 Formulated products

In this section, different formulated products were investigated to determine what physical properties of the spray liquids have an effect on spray characteristics such as VMD and V_{100} . Water was used as the reference liquid.

Water produced a VMD = 194.6 μm and a fine spray fraction of $V_{100} = 11.0\%$ when atomized through a flat fan nozzle XR11003 VS. As shown in table 9.4, spray liquids of different fungicide formulations prepared at concentrations recommended by the manufacturer influenced spray characteristics with respect to VMD and V_{100} .

EW and SE formulation types that produce an emulsion increased the VMD of the spray and significantly reduced the drift-prone spray fraction. The water-based SC and the solid WG formulations produced sprays with a VMD and a V_{100} similar to sprays produced using water alone. These observations indicate that the presence of emulsion droplets influences the spray droplet size distribution. The type and the concentration of the a.i. apparently do not alter spray characteristics.

Spray characteristics of different deltamethrin products are shown in table 9.5. EC and EW formulations increased the VMD and decreased the V_{100} compared to ZW and SC products. Applying the common dilution concept based on the content of the a.i. in the spray liquid, the concentration of the product (and thus the concentration of the emulsified oil) in spray liquid is higher for products with a lower a.i. content. Consequently, the emulsion concentration of the EC 15 is higher than the emulsion concentration of the EC 100 for the same content of the a.i. in the spray liquid. As shown in table 9.5, the decrease of the fine spray fraction down to 3.4% is most significant for the EC with the lowest a.i. content of 15 g/L.

Table 9.4: Spray characteristics of fungicide products.

formulation type	active ingredient	conc.	VMD	V_{100}
EW 450	prochloraz	5.5 ml/l	242.0	5.0
EW 66.7+266.6	fluopyram, spiroxamine	4.0 ml/l	258.5	3.0
SE 125+125	fluopyram, prothioconazol	2.5 ml/l	257.5	4.1
SE 200	tebuconazole	1.2 ml/l	249.5	4.7
SE 200	fluopyram	1.2 ml/l	256.6	3.3
SC 500	fluopyram	2.5 ml/l	199.2	10.6
SC 250+250	fluopyram, trifloxystrobin	2.5 ml/l	207.6	9.5
SC 250+250	fluopyram, trifloxystrobin	1.6 ml/l	199.2	11.2
SC 500 ^a	fluazinam	2.0 ml/l	206.4	10.5
SC 250 ^a	mandipropamid	3.0 ml/l	198.1	11.1
WG 4.5+68 ^b	mancozeb, cymoxanil	10.0 g/L	194.6	11.3
WG 1.75+70 ^c	benthiavalicarb, mancozeb	10.0 g/L	197.7	11.2

manufacturer: ^a Syngenta, ^b DuPont, ^c Certis

EW products featured a mixed behaviour without a clear dominant tendency of either the dilution factor or the increase in spray droplet size. EW products are ready-to-use emulsions and their content of emulsifiable oil tend to be lower than that in EC and OD formulations. The dynamic surface tension of all spray liquids measured at 10 ms ranged between 72.1 – 68.2 mN/m.

Fungicide ECs were sprayed at a dilution rate of 0.1 g/L of the a.i. The VMD, the V_{100} of produced sprays along with the effective diameter of the emulsion droplets in the spray liquid are summarized in table 9.6. Table 9.6 shows that some ECs produced coarser sprays than water alone. Some, on the other hand, hardly influenced spray characteristics. These observations can be explained by the quality of the emulsions produced on dilution in the carrier volume. The diameter of emulsion droplets varies from micro- to nano-size among different products. Spray liquids that contain diluted macroemulsions increased the VMD and decreased the V_{100} of the spray. Spray liquids that produce finer emulsions hardly influenced the spray droplet size distribution and formed sprays with a comparably low VMD and a relative high fine spray fraction. These observations indicate that spray formation is influenced by dilute oil-in-water emulsions only when they are "cloudy" and contain micrometer-size droplets. Diluted nanoemulsions, which do not scatter light, also have no impact on spray formation.

Some EC formulations decreased the dynamic surface tension at the relevant concentration; e.g. down to 61.4 mN/m by the prothioconazole EC 200. This may

Table 9.5: Spray characteristics of deltamethrin formulations 6.25 g/L a.i.

formulation type	VMD [μm]	V_{100} [%]	DST [mN/m]
EC 100	218.7	7.4	71.4
EC 25	240.9	4.4	68.9
EC 25	242.1	4.1	71.6
EC 15	251.8	3.4	68.2
EW 50	216.0	7.8	71.8
EW 25	215.3	8.2	70.1
EW 20	220.0	7.2	72.0
EW 15	214.1	8.2	68.5
ZW 75	191.5	11.7	72.1
SC 26.25	197.3	10.4	72.0

Table 9.6: Spray characteristics of fungicide formulations sprayed at a concentration of 0.1 g/L a.i. D_{eff} is the effective diameter of the emulsion droplets. DST denotes the dynamic surface tension measured at 10 ms.

formulation type	active ingredient	VMD [μm]	V_{100} [%]	D_{eff}	DST [mN/m]
EC 200	tebuconazole	249.8	3.4	6.1 μm	71.0
EC 133+67	tebuconazole, trifloxystrobin	250.1	3.3	3.0 μm	64.4
EC 250	prothioconazole	226.5	6.1	1.5 μm	61.4
EC 167+107	bromuconazole, tebuconazole	233.5	5.4	1.0 μm	71.0
EC 300	bitertanol	207.3	9.3	142.3 nm	70.9
EC 200	cyproconazole	190.3	12.0	68.2 nm	56.8
EC 125+125	prothioconazole, trifloxystrobin	204.3	9.5	35.2 nm	71.0
EC 100+100	fluoxastrobin, prothioconazole	193.1	11.3	31.8 nm	70.4

induce formation of finer sprays and reduce the spray coarsening effect of emulsion droplets.² The same set of EC products was sprayed at a dilution concentration of 0.25% w/w. Tendencies to altering droplet spectra relative to the water standard and for different formulated products, were very similar to those reported in table 9.6. For a dilution concentration of 0.25% w/w, the deviation from the absolute VMD values reported in table 9.6 was $\leq 10 \mu\text{m}$. The deviations on V_{100} were measured to be $\leq 1\%$ except for the EC 250 and the EC 100+100 for which the V_{100} increases to $\sim 2\%$.

Table 9.7 shows spray characteristics of different OD formulations sprayed at a concentration of 0.1 g/L of a.i. The content of the vegetable oil in the formulation decreases from the top row down. All spray liquids decreased the drift-prone frac-

Table 9.7: Spray characteristics of insecticide OD formulations sprayed at a concentration of 0.1 g/L a.i. The products are listed in order of increasing content of the emulsified oil. The content of vegetable-based oil ranges between 45% - 25%. DST denotes the dynamic surface tension measured at 10 ms.

formulation type	active ingredient	VMD [μm]	V_{100} [%]	DST [mN/m]
OD 75+10 ^a	imidacloprid, deltamethrin	233.0	5.2	64.4
OD 100+75 ^a	flubendiamide, spirotetramat	244.1	4.6	71.5
OD 240 ^a	thiacloprid	232.1	5.6	71.6
OD 200 ^a	imidacloprid	239.6	4.8	71.6
OD 100+10 ^a	thiacloprid, deltamethrin	230.0	5.7	64.6
OD 180 ^a	thiacloprid	233.7	5.3	70.6
OD 150+20 ^a	thiacloprid, deltamethrin	229.5	5.8	71.4
OD 150+40 ^a	imidacloprid, deltamethrin	209.0	8.7	69.4
OD 210+90 ^b	imidacloprid, betacyfluthrin	220.5	7.2	71.8
OD 100 ^c	spirotetramat	217.8	7.8	71.1

oil content: ^a vegetable-based oil (45% - 25%), ^b oil mixture, ^c mineral-based oil

tion compared to water. The absolute values of the VMD and the V_{100} scaled with the concentration of the solvent. Evidently, products that contain vegetable oils achieve larger spray coarsening than products that contain mineral oils. ODs with the highest oil content reduced the fine spray fraction down to 5.2 – 4.6%. The OD 75+10 produced more fine droplets than the OD 100+75, probably due to the decrease in dynamic surface tension down to 64.4 mN/m. The lowest concentration of the vegetable oil in the product resulted in a smaller decrease of the V_{100} . OD that contained an oil mixture, or was mineral oil-based, produced fine sprays with $V_{100} = 7.2 - 7.8\%$.

Summarizing these data, three parameters can be identified that seem to be crucial for the coarsening effect achieved by oil-based liquid formulations: the concentration of the emulsifiable oil, its type and the dynamic surface tension of the spray liquid. This set of data shows that those formulated products that produce a dilute oil-in-water emulsion in the spray liquid reduced the drift-prone spray fraction and increased the volume median diameter of the spray compared to water. Formulation types without oil produced similar or even finer sprays than water alone.

A mesoscopic size of emulsion droplets (cloudy emulsions) is required to achieve spray coarsening. The data showed no evidence for a correlation between the presence of solid particles in the spray liquid and the spray coarsening effect. Solid

particles of the a.i. are usually $< 10 \mu\text{m}$ in size and are part of OD and SC formulations. Even larger particles can be part of WG and WP products. The measured droplet size spectra lead to the conclusion that solid particles in the spray liquid do not influence spray formation.

9.3.2 Tank-mix spray additives

The effect of the emulsion concentration and the oil chemistry on the spray droplet size distribution was investigated for a concentration series of dilute oil-in-water emulsions (blank ECs).

Four oils were selected such that two of them were mineral oils (Exxsol D140 and Bayol 85) and other two were of vegetable type: sunflower oil and rapeseed oil methyl ester. As shown in figure 9.2, the VMD increased and the V_{100} decreased with increasing concentration of each emulsion, following a power law relationship. Figure 9.2 illustrates that spray coarsening is greater for the two vegetable oil-based than for the two mineral oil-based emulsions. The VMD increased and the V_{100} decreased in a similar way when an emulsion is stabilized by a polymer (data not shown). This leads to the conclusion that the type of emulsifier is not essential for the spray coarsening effect as long as the stability of the emulsion is not affected.

The vegetable-based sunflower oil and the methyl ester achieved spray coarsening already from a concentration of $10^{-4}\%$ w/w. Generally, a higher concentration of the mineral and white oil-based emulsions was required to achieve a similar spray coarsening as with emulsified oils of vegetable origin.

At a concentration of 0.1% w/w, the dynamic surface tension (DST) of the investigated emulsions was ~ 71.0 mN/m. At a concentration of 0.5% w/w, the DST was measured as 59.7 mN/m for the sunflower oil and 65.5 mN/m for the methyl ester emulsion. The dynamic surface tension of Bayol 85 and Exxsol D140 emulsions at a concentration of 0.5% w/w remained at ~ 71.0 mN/m.

An anionic sodium sulphate and a non-ionic alkyl-ethylene oxide were used to study the effect of the dynamic surface tension on the spray droplet size distribution. Figure 9.3 shows the VMD and the V_{100} of sprays produced with both additives plotted as a function of the dynamic surface tension. The dynamic surface tension decreases with increasing concentration of the additive. A decrease of the dynamic surface tension induced formation of finer sprays.

In the next step, the effect of the dynamic surface tension was investigated for a mixture of an emulsion and a surfactant. The sunflower oil emulsion was sprayed at a concentration of 0.1% w/w. At this concentration, the sunflower

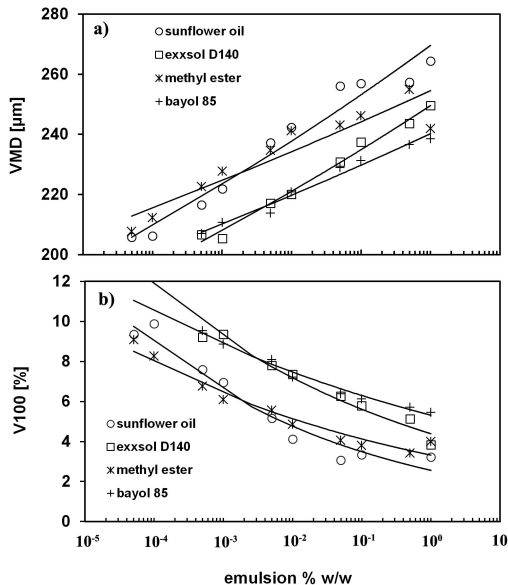


Figure 9.2: a) VMD, b) V_{100} as a function of emulsion concentration.

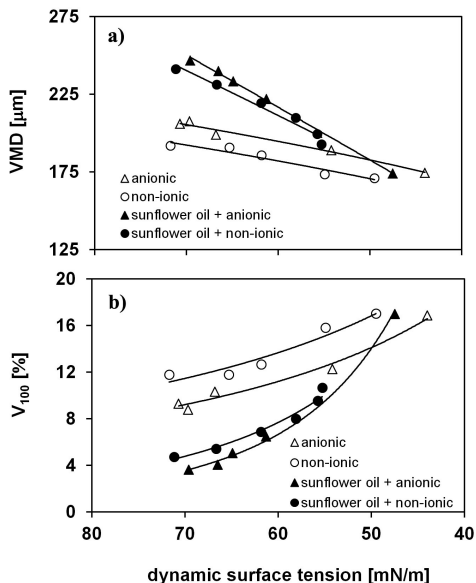


Figure 9.3: a) the VMD, b) the V_{100} of sunflower oil emulsions sprayed at a concentration of 0.1% w/w and anionic, non-ionic spray additives.

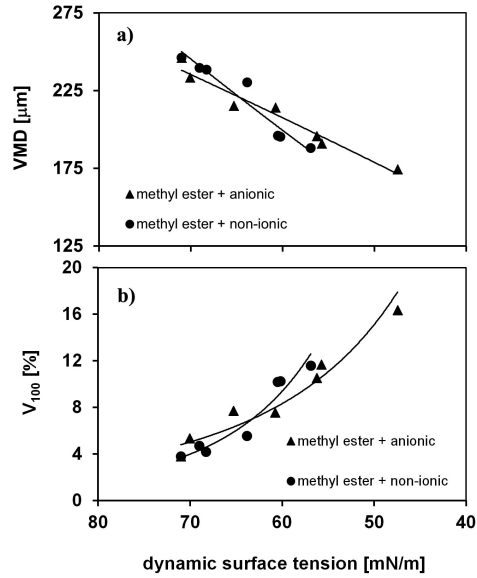


Figure 9.4: a) VMD, b) V_{100} of methyl ester emulsions sprayed at a concentration of 0.1% w/w and anionic, non-ionic spray additives.

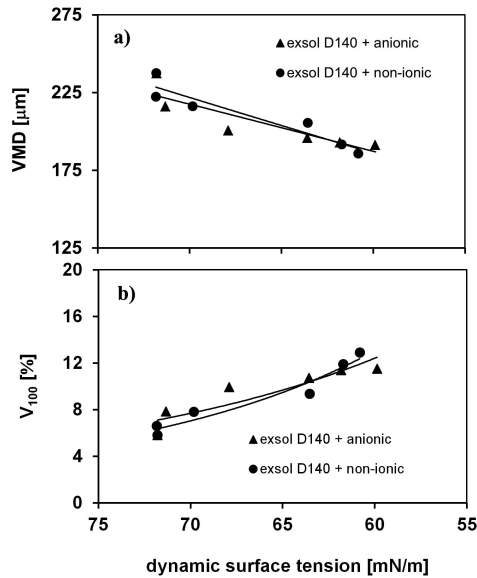


Figure 9.5: a) VMD, b) V_{100} of Exxsol D140 emulsions sprayed at a concentration of 0.1% w/w and anionic, non-ionic spray additives.

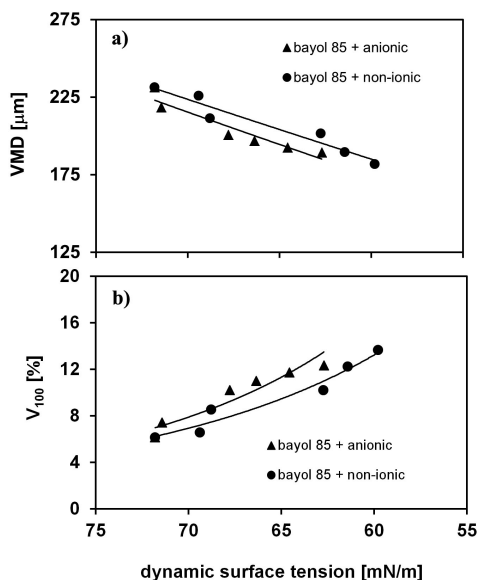


Figure 9.6: a) VMD, b) V_{100} of Bayol 85 emulsions sprayed at a concentration of 0.1% w/w and anionic, non-ionic spray additives.

oil-based emulsion achieved a measurable spray coarsening without a decrease in surface tension. As shown in figure 9.3, in mixtures of a dilute emulsion with an additive, the VMD of the produced sprays decreased and the V_{100} increased with decreasing dynamic surface tension. A further decrease of the dynamic surface tension induced formation of sprays which were finer than sprays produced by water. Similar correlations were obtained for all other dilute emulsions as shown in figures 9.4-9.6.

Further, the investigated emulsions were applied as spray additives for a flubendiamide SC 480. The SC when sprayed at a concentrations of 5.0 g/L produced sprays with VMD = 201.6 μm and V_{100} = 10.5%. With respect to the VMD and the V_{100} , the spray produced by the SC 480 was similar to the reference water spray (VMD = 194.6 μm and V_{100} = 11.0%). The dynamic surface tension of this spray liquid was 71.7 mN/m.

Two vegetable oil-based and two mineral oil-based emulsions were added at a concentration of 0.1 g/L to the diluted flubendiamide formulation. As shown in table 9.8, all diluted emulsions increased the VMD and decreased the V_{100} of the produced sprays. The spray coarsening effect was greater for vegetable-based oils than for mineral-based oils and the tendencies were similar to those for diluted

Table 9.8: Spray characteristics of flubendiamide SC 480 with spray additives added at a concentration 0.1 g/L.

formulation	additive 0.1 g/L	VMD [μm]	V_{100} [%]	DST [mN/m]
	-	201.6	10.5	71.7
	rapeseed oil methyl ester	252.8	4.2	71.4
SC 480	sunflower oil	247.0	4.6	71.8
flubendiamide	Bayol 85	222.8	7.1	71.1
5.0 g/L	Exxsol D140	221.5	7.1	71.6
	Induce	252.5	4.2	68.3
	Mero	249.0	4.4	70.2

emulsions without the SC product (figure 9.2). Oil-based co-formulants Mero and Induce also achieved spray coarsening and significantly reduced the fine spray fraction down to 4.4% and 4.2% when added as tank-mix additives (table 9.8).

In conclusion, dilute emulsions that are used as tank-mix additives increase the VMD and reduce the fine spray fraction in a similar way as formulated in-can products.

9.4 Modelling and drift trials

To establish a connection between the droplet size spectra and the spray drift measured in the field, we will first discuss a set of data measured at the Silsoe Spray Application Unit in 2009 for differently formulated products of imidacloprid.²⁹ This set of data used to parametrise a model and to calculate the trajectories of spray droplets and their downwind deposition.³¹

The droplet size distributions from four nozzles of different designs were measured for an SL 200, an OD 200 and a SC 350 imidacloprid formulations. The four nozzles were: a Lurmark 03F110 conventional flat fan nozzle; a TeeJet XR10003VS extended range flat fan nozzle; a TeeJet DG pre-orifice nozzle; and a TeeJet AI11003VS air-inclusion nozzle that produces a mid-range droplet size spectra. The measurements were made for a concentration of 100 g a.i. per 300 litres of water. Agral additive was sprayed at a concentration 0.1 % w/w as a reference spray liquid.

As shown in table 9.9, the SL and the SC formulation types produce sprays with a V_{100} and a VMD that were similar to those of the water spray. The Agral reference spray solution increased the V_{100} and decreased the VMD compared to

Table 9.9: The volume median diameter and the percentage of spray volume in droplets smaller than 100 μm (V_{100}) measured for different imidacloprid formulations.²⁹

	TeeJet		Lurmark		TeeJet		TeeJet	
	XR11003VS		03F110		DG11003VS		AI11003VS	
	VMD	V_{100}	VMD	V_{100}	VMD	V_{100}	VMD	V_{100}
	[μm]	[%]						
water	204.1	11.3	185.2	13.2	262.5	6.0	563.7	1.6
SC 350	197.5	12.8	179.6	14.8	257.9	7.0	558.7	1.5
SL 200	202.7	12.1	187.4	12.9	259.3	6.8	548.4	1.1
Agral	185.8	15.4	175.5	14.7	246.4	7.3	522.2	1.1
OD 200	243.3	6.0	222.3	7.0	316.2	2.8	533.0	0.8

Table 9.10: Spray drift reduction of different types of formulation types in % relative to the reference Agral solution.³¹

nozzle type	water	Agral 0.1% w/w	SL 200	OD 200	SC 350
Lurmark F110	2.2		18.9	53.6	1.9
TeeJet DG	29.9	reference	29.1	81.7	9.6
Teejet AI	29.3	spray liquid	28.1	80.2	9.5
TeeJet XR	29.8		29.2	56.9	26.9

water for all tested flat fan nozzles except for the TeeJet AI. The OD formulation significantly reduced the V_{100} and increased the VMD for each nozzle design.

Table 9.10 shows the relative spray drift reduction for each product compared to the Agral reference solution. The relative spray drift reduction of water and the SL 200 are comparable, except for sprays produced through the Lurmark F110 nozzle. The SC 350 produced finer sprays than water for all tested nozzles. The calculated data indicate that the OD formulation reduces the percentage of drift-prone fines in a most efficient way with a minimum of 53.6% drift reduction compared to the Agral solution. A substantially higher spray drift reduction of 81.7% is obtained when the OD is atomized through a low-drift TeeJet DG nozzle.

These data illustrate the effect of the physical properties of the spray liquid on spray droplet size. Sprays produced through the same nozzle resulted in different droplet size distributions depending on the different formulation types. The OD formulation that created an emulsion in the spray liquid increased the VMD and decreased the fine spray fraction compared to water and to the Agral reference solution. Formulation types that did not contain emulsified oils created sprays

Table 9.11: Modelled drift reduction in % relative to the reference Agral solution at various downwind distances calculated for a TeeJet 11003 DG nozzle.³¹

distance [m]	water	Agral 0.1% w/w	SL 200	OD 200
1	30.3		29.3	81.3
2	30.5		29.8	83.8
3	30.1		29.8	85.0
4	29.8	reference	29.8	85.6
5	29.6	spray liquid	29.7	86.1
10	29.3		29.5	87.0
15	29.1		29.2	87.4
20	28.8		28.9	87.6

with a similar droplet size to water, or even finer sprays, indicating a greater drift risk potential. Although the absolute values of the VMD and the V_{100} differ for different flat fan nozzles, the formulation-dependent trends are mostly similar.

The downwind deposition calculated for this data set for distances of 1 – 20 m are summarized in table 9.11. The deposition was modelled for one TeeJet DG nozzle type. As shown in table 9.11, water and the SL 200 produced at all distances approximately 29% less spray drift compared to the reference solution. The obtained off-target deposition for the OD formulation is relatively consistent over all distances with drift reduction of 81.3% at 1 m and 87.6% at the 20 m. Spray drift reduction calculated for the OD formulation was about a factor of three larger for all distances, compared to the SL formulation or pure water.

A small drift trial was performed to verify the predictions from the droplet size spectra and deposition modelling. The data obtained in the field trial are shown in table 9.12. The results were calculated for an average value in each row as the percentage of the applied dose. The relative reduction in deposition drift anticipated by the droplet size spectra in table 9.10 and predicted by the modelling output in table 9.11 was achieved by the OD formulation at short distances of 3 m and 5 m. At 20 m distance, the absolute deposition concentration was similar for both tested formulation types. The deposition concentrations at 20 m were close to the sensitivity limits of the analytical measurement. Hence, they might not be meaningful for this experiment.

The experimental data obtained for the downwind deposition at distances < 20 m are comparable with the relative drift reduction predicted by the droplet size spectra and supported by calculations based on the Silsoe arable crop drift model.

A second field experiment was done to compare the downwind deposition of an

Table 9.12: Downwind deposition of spray liquids that contain the OD 200 and the SL 200 formulations, applied three times at a rate of 200 l/ha. The spray drift reduction was calculated relative to the a.i. content in the spray liquid with SL (198 mg/L) and OD (195 mg/L).

		OD 200		
spray liquid	[mg/L]	[mg/m ²]	[% applied]	
	585	11.7	100	
Distance [m]	[mg/collector]	[mg/m ²]	[% of applied dose]	
3	1.0×10^{-3}	0.061	0.52	
5	3.3×10^{-4}	0.020	0.17	
10	1.2×10^{-4}	0.008	0.06	
20	9.1×10^{-5}	0.006	0.05	
		SL 200		
spray liquid	[mg/L]	[mg/m ²]	[% applied]	
	595	11.9	100	
Distance [m]	[mg/collector]	[mg/m ²]	[% of applied dose]	
3	3.4×10^{-3}	0.207	1.74	
5	1.3×10^{-3}	0.082	0.70	
10	2.1×10^{-4}	0.013	0.11	
20	9.0×10^{-5}	0.005	0.05	

EC 160+300 and a SE 66.7+266.6 formulation. The drift experiment was done to verify the drift reduction potential of the sprays with the droplet size data shown in table 9.13.

The recommended application rates were 1.6 ml EC and 3.0 ml SE formulation in 1 L water. The SE reduced the fine spray fraction down to 3.0%. Spray characteristics of the EC product differed with its concentration in spray liquid. Sprays produced at a concentration of 7.5 ml/l were finer than those produced at 0.5 ml/l. The EC product contained a high loading of surface active material which affected the dynamic surface tension. Consequently, the V_{100} and the VMD of produced differ as a function of the dynamic surface tension.

In this field trial, the SL 200 of imidacloprid was sprayed as the reference liquid. As shown in table 9.14, both the EC and the SE formulations decreased the off-target deposition over all distances compared to the SL 200 reference spray liquid. As anticipated from the droplet size spectra, both EC and SE formulations generated less off-target depositions than the SL 200. Although the SE formulation created coarser spray than the EC formulation (table 9.13), it produced about the same deposition (percentage) at 3 m and 5 m; and more off-target deposits than

Table 9.13: Spray characteristics for prothioconazole+spiroxamine EC 160+300 and fluopyram+spiroxamine SE 66.7+266.6.

formulation type	concentration [ml/l]	VMD [μm]	V_{100} [%]	DST [mN/m]
water	–	196.4	11.0	72.0
SE 66.7+266.6	1.6	258.8	3.0	68.3
	0.5	234.8	4.7	63.7
EC 160+300	3.0	219.3	5.3	44.6
	7.5	218.9	6.2	39.7

Table 9.14: Downwind deposition for the EC 160+300 and SE 66.7+266.6 and the reference imidacloprid SL 200 sprayed at 200 g/ha. The spray drift reduction was calculated relative to the spray liquid content of imidacloprid (539 mg/L) or spiroxamine (SE 120 mg/L and EC 390 mg/L).

SL 200			
spray liquid	[mg/L]	[mg/m ²]	[% applied]
	1618	32.2	100
Distance [m]	[$\mu\text{g}/\text{collector}$]	[$\mu\text{g}/\text{m}^2$]	[% of applied]
3	2.334	367.0	1.134
5	0.715	112.4	0.347
10	0.120	20.2	0.062
20	0.100	17.4	0.054
EC 160+300			
spray liquid	[mg/L]	[mg/m ²]	[% applied]
	1170	23.4	100
Distance [m]	[$\mu\text{g}/\text{collector}$]	[$\mu\text{g}/\text{m}^2$]	[% of applied]
3	1.106	177.0	0.756
5	0.360	54.4	0.233
10	0.042	6.6	0.029
20	0.013	2.0	0.009
SE 66.7+266.6			
spray liquid	[mg/L]	[mg/m ²]	[% applied]
	360	7.2	100
Distance [m]	[$\mu\text{g}/\text{collector}$]	[$\mu\text{g}/\text{m}^2$]	[% of applied]
3	0.346	54.3	0.755
5	0.084	13.1	0.183
10	0.029	4.6	0.064
20	0.006	0.9	0.014

the EC at 10 m and 20 m (table 9.14).

The difference in the relative deposition values obtained for the SL 200 in both drift trials may be explained by different weather conditions.

These trials show that spray droplet sizes measured with a laser-based technique can be used as a relative measure for the potential off-target deposition or as a tool to identify formulations that are capable of reducing drift of agricultural sprays, or both.

9.5 Conclusions

In the first section of this Chapter, we analysed spray characteristics and showed that spray droplet size distributions are influenced by the formulation type of an agrochemical product. Providing a more general interpretation of the results, it can be stated that reduction of the fine spray fraction can be achieved with formulations that induce formation of a macroscopic emulsion in the spray liquid. The exact values of the mean spray droplet size and the fine spray fraction depend on the concentration and the composition of co-formulants. The correlation of a formulation type with the spray droplet size is often not straightforward and requires additional information about the dynamic surface tension of the spray liquid, the emulsion concentration, and the type of the emulsified oil. Despite differences in absolute values of the VMD and V_{100} , all tested OD and SE formulations produced coarser sprays than water, and in some cases significantly reduced the fine spray fraction. It was shown that EC and EW formulation types can also induce spray coarsening. This effect, however, strongly depends on the composition of the formulated EC and EW products and the concentration of co-formulants.

In a similar way, dilute emulsions added as tank-mix additives can also significantly reduce the fine spray fraction. From these observations, it appears that the desired drift reduction properties can be systematically formulated into a liquid product by incorporating an emulsifiable oil or an emulsion concentrate. As discussed in the introduction, polymers with the required robustness or at a required concentration are difficult to include in a formulated product: hence, the simplest way to achieve drift reduction with a formulation is to use dilute oil-in-water emulsions. Moreover, additives that decrease the dynamic surface tension of the spray liquid counteract the spray coarsening effect induced by a dilute emulsion. At the same time, the surfactant concentration in a formulated product has not necessarily to be kept low. The results reveal that an OD formulation with a high surfactant concentration,³¹ can quite well induce spray coarsening and significantly reduce

the fine spray fraction (table 9.9).

Without going into details of the composition of any particular formulated product, its drift reduction potential can be identified at an early development stage by measuring the spray droplet size distribution of sprays produced at a relevant concentration. It is shown that a formulated product that on dilution produces an emulsion can efficiently reduce the deposition drift during field application. The correlation was tested only for one nozzle design and the values in deposition drift did not always reflect differences in spray droplet size between two oil-based formulation over several distances. However, the principal tendencies are evident and they are supported by results of spray deposition modelling. The obtained droplet size spectra are easy to determine and can be used to calculate the downwind deposition by computational or mathematical models, avoiding the necessity of conducting extensive and time-consuming field experiments for each new product.

When discussing drift reduction achieved with modified physical properties of spray liquids, it is necessary to address other possibilities of drift reduction such as nozzle design. It is often claimed that the use of low-drift or air-induction nozzle can achieve a more significant spray drift reduction than the use of a formulation or a tank-mix drift retardant. The droplet size spectra in table 9.9 show that the drift reducing effect of a low-drift nozzle is greater compared to the effect of a formulation. The best reduction of the fine spray fraction, however, was obtained for a combination of a drift reduction TeeJeet AI nozzle and the OD 200 formulation. The AI nozzle decreased the fine spray fraction of the water spray from 11.3% for the spray produced with an XR flat fan nozzle down to 1.6%. The OD 200 decreases the volume of fine droplets additionally by a factor of two relative to water for each of the nozzles: from 11.3% to 6.0% for the standard flat fan nozzle and from 1.6% to 0.8% for the corresponding AI nozzle. The factor of two reduction of the drift-prone fraction was obtained for all investigated nozzle designs and seems to be nozzle-independent. These results indicate that the most efficient mode of spray drift management is the combination of a low-drift nozzle with a formulation which possesses drift-reduction potential.

As a summary of all results discussed in this study, it appears that a classification scheme, similar to those used for different spraying equipment,¹⁴ can be developed for formulated agrochemical products. Such a scheme could describe ranges of drift reduction connected to a formulation type and concentration but not absolute values in deposits or airborne spray. For this, methods have to be established for evaluation of drift reduction properties of formulation types and

products have to be specified which can be used as a standard for a certain formulation type. The most interesting situation would possibly be the classification with regard to a simple nozzle design (conventional flat fan nozzle) where a significant reduction of fine spray fraction could be achieved when a certain formulation type is used. To complete the picture, other nozzle designs have to be considered as well. This approach could become part of drift risk mitigation scenarios and can improve the precision of the calculations for the buffer zone widths towards more realistic values.

References

- [1] G. R. Stephenson, I. G. Ferris, P. T. Holland and M. Nordberg, *Pure Appl. Chem.*, 2006, **78**, 2075–2154.
- [2] E. Hilz and A. W. P. Vermeer, *Crop. Prot.*, 2013, **44**, 75–83.
- [3] J. H. Combellack, *Weed research*, 1982, **22**, 193–204.
- [4] S. L. Bird, D. M. Esterly and S. G. Perry, *J. Environ. Qual.*, 1996, **25**, 1095–1104.
- [5] S. C. K. Carlsen, N. H. Spliid and B. Svensmark, *Chemosphere*, 2006, **64**, 778–786.
- [6] A. J. Hewitt, *Atomization Sprays*, 1997, **7**, 235–244.
- [7] H. Holterman, *Kinetics and evaporation of water drops in air*, 2003, IMAG Report 2003-12.
- [8] H. De Ruiter, H. J. Holterman, C. Kempenaar, H. G. J. Mol, J. J. de Vlieger and J. van de Zande, *Influence of adjuvants and formulations on the emission of pesticides to the atmosphere. A literature study for the Dutch Research Programme Pesticides and the Environment (DWK) theme C-2*, 2003, Plant Research International B.V., Wageningen, Report 59.
- [9] N. M. Western, E. C. Hislop, M. Bieswal, P. J. Holloway and D. Coupland, *Pestic. Sci.*, 1999, **55**, 640–642.
- [10] P. C. H. Miller, *Pesticide Outlook*, 2003, **14**, 205–209.
- [11] M. C. Butler Ellis, P. C. H. Miller, D. E. Baker, J. D. Lane and C. R. Tuck, Proceedings of 5th International Symposium on Adjuvants for Agrochemicals (ISAA 1998), Memphis, Tennessee, 1998, pp. 389–394.
- [12] FOCUS, *Landscape And Mitigation Factors In Aquatic Risk Assessment. Volume 2. Detailed Technical Reviews. Report of the FOCUS Working Groupon Landscape and Mitigation Factors in Ecological Risk Assessment*, 2007, EC Document Reference SANCO/10422/2005 v.2.0. pp. 1-436.
- [13] A. J. Hewitt, *Environmentalist*, 2008, **28**, 25–30.
- [14] SDRT, *Spray Drift Reduction Technology: A European Database*, <http://www.sdrt.info/>, 2012, (2 October 2012).
- [15] H. Zhu, R. W. Dexter, R. D. Fox, D. L. Reichard, R. D. Brazee and H. E. Ozkan, *J. Agric. Engineering Res.*, 1997, **67**, 35–45.

- [16] P. C. H. Miller and C. R. Tuck, *J. ASTM Int.*, 2005, **2**, 1–13.
- [17] R. W. Dexter, in *Pesticide formulations and application systems*, ed. A. K. Viets, R. S. Tann and J. C. Mueninghoff, American Society of Testing and Materials, West Conshohocken, PA, 2001, vol. 20, pp. 27–43.
- [18] M. Schmidt, *Grundl. Landtechnik*, 1980, **30**, 126–134.
- [19] M. C. Butler Ellis and A. Bradley, *Aspects Appl. Biol.*, 2002, **66**, 251–258.
- [20] R. W. Dexter, *Atomization Spray*, 1996, **6**, 167–191.
- [21] H. Hoffmann, M. L. Turco Liveri and F. P. Cavasino, *J. Chem. Soc., Faraday Trans.*, 1997, **93**, 3161–3165.
- [22] D. L. Reichard, H. Zhu, R. A. Downer, R. D. Fox, R. D. Brazee, H. E. Ozkan and F. R. Hall, *Trans. ASAE*, 1996, **39**, 1993–1999.
- [23] K. Qin, H. Tank, S. Wilson, B. Downer and L. Liu, *Atomization Spray*, 2010, **20**, 227–239.
- [24] A. C. Chapple, R. A. Downer and R. H. Franklin, *ASTM STP 1112*, 1992, **12**, 193–205.
- [25] P. C. H. Miller, C. R. Tuck, S. Murphy and M. da Costa Ferreira, Proceedings of 22nd European Conference on Liquid Atomization and Spray Systems (ILASS-Europe), Como Lake, Italy, 2008, pp. 1–8.
- [26] A. S. Felsot, J. B. Unsworth, J. B. H. J. Linders, G. Roberts, D. Rautman, C. Harris and E. Carazo, *J. Environ. Sci. Heal. B*, 2010, **46**, 1–23.
- [27] H. Ganzelmeier, D. Rautmann, R. Spagenberg, M. Streloke, M. Hermann, H. J. Wenzelburger and H. F. Walter, *Mitt. Biol. Bundesanst. Land Forstwirtschaft., Berlin-Dalem*, 1995, **305**, 1–111.
- [28] D. Rautmann, M. Streloke and R. Winkler, *Mitt. Biol. Bundesanst. Land Forstwirtschaft.*, 2001, **383**, 133–141.
- [29] P. C. H. Miller, C. R. Tuck, C. M. O’Sullivan and M. C. Butler Ellis, *Measurements of droplet size distributions from different designs of agricultural spray nozzle operating with different liquids*, 2009.
- [30] P. C. H. Miller, Proceedings of the North American Conference on Pesticide Spray Drift Management, Portland, Maine, 1998, pp. 229–244.
- [31] R. Vermeer, A. C. Chapple and R. Friessleben, *Use of oil based suspension concentrates for reducing drift during spray application*, Patent WO 2011147766.
- [32] CropLife International, *Catalogue of pesticide formulation types and international coding system*, 2008, Technical Monograph n2, 6th Edition, Brussels.
- [33] CIPAC MT 18.1.3 Standard Water C, *CIPAC MT 18.1.3 Standard Water C*, Collaborative International Pesticides Analytical Council, 2010.
- [34] CIPAC MT 36.3 Emulsion Characteristics and Re-emulsification Properties, *CIPAC MT 36.3 Emulsion Characteristics and Re-emulsification Properties*, Collaborative International Pesticides Analytical Council, 2000.
- [35] W. C. Hoffmann, A. J. Hewitt, J. B. Ross, W. E. Bagley, D. E. Martin and B. K. Fritz, *J. ASTM Int.*, 2008, **5**, year.
- [36] ISO Standard 22856, *Equipment for crop protection - Methods for the laboratory measurement of spray drift - Wind tunnels*, 2008, Switzerland.

Summary and General Discussion

This Chapter summarizes the results of the dissertation. It provides a discussion about implementation of these results in processes related to application of crop protection products in a wider perspective. Moreover, the Chapter contains suggestions for further investigations on the mechanism of spray formation induced by dilute oil-in-water emulsions.

Application of crop protection products often carries risk of spray drift, which is associated with unintended contamination of surface water, aquatic organisms and the environment,¹⁻³ or exposure of workers, bystanders and residents.⁴ Spray drift is defined as the ‘downwind movement of airborne spray droplets beyond the intender area of application originating from aerial or ground-based spraying operations’.⁵ The drift risk is most often related to the fine spray fraction that contains spray droplets with diameter $< 100 \mu\text{m}$.⁶⁻⁸ In recent years, the European regulation on non-target contamination with agrochemicals, which can also be caused by spray drift, has become stricter^{1,3} and, thus, demands for efficient and simple methods for drift mitigation during agricultural applications are rising.

In this thesis, we explore a method of drift risk reduction through use of formulated “ready-to-use” products which, when diluted in water, can induce changes in the physical properties of the respective spray liquid. It is known that the physical properties of spray liquids influence spray droplet size, droplet velocity, and spray sheet structure.⁹⁻¹³ To be more precise, the fine drift-prone spray fraction can be significantly reduced by adding polymer-based thickeners or dilute oil-in-water emulsions. Spray liquids that contain polymeric material produce coarser sprays due to increase in the viscosity. The mechanism behind the effect induced by dilute oil-in-water emulsions is not yet completely understood. At the same time, dilute emulsions provide an interesting approach for drift reduction purposes because emulsions or emulsified oils are part of many common formulation types. Different emulsions are known to influence the spray characteristics to different extents. Investigations into the mechanism of spray formation initiated by dilute emulsions provides an understanding of the differences in the mean droplet size of sprays produced by different emulsions.

Dynamic conditions during spray formation determine limitations for the experimental analysis. In this context, experimental studies can be done under static conditions and then related to processes during spray formation. Another way to gain insights into these highly dynamic systems is by performing theoretical investigation based on experimental outcome. Computational fluid dynamics (CFD) simulations and a self-consistent field (SCF) approach with coarse-gradient approximation have been used in this project.

As outlined above, spray drift is a multifaceted phenomenon that encompasses environmental and regulatory aspects and involves mechanisms of spray formation which are of interest for fundamental investigations. To cover all these facets, we have used a variety of methods and techniques, performed experimental studies

under dynamic and static conditions, computational simulations of representative systems, done small-scale outdoor trials, produced an extensive literature research. As a consequence, the project has produced a manifold outcome. It provides a suggested mechanism explaining spray formation induced by dilute emulsions. The proposed mechanism accounts for different physico-chemical properties of oils and interactions in mixtures with additives such as polymers and water-soluble surfactants. Moreover, the knowledge of possible interactions and relevant properties during spray formation enables classification of formulation types with respect to their spray drift reducing potential. These aspects can be further considered for development of new, innovative commercial products and give a more detailed picture of physical properties of spray liquids that can be used to manipulate the spray droplet size distribution.

Mechanism of perforation

When a spray liquid is atomized through a conventional flat fan nozzle, it emerges under the nozzle outlet in the form of a liquid sheet. The liquid sheet disrupts into ligaments and finally into spray droplets. Spray formation can occur through oscillation of the sheet. The second breakup mode is perforation which is shown in figure 1 and is the typical spray formation mechanism for dilute oil-in-water emulsions. Perforation onset or the mechanism of hole formation is not yet well understood and represents an interesting research area which is investigated in this thesis.

The droplet size distribution of a spray produced by a dilute emulsion depends on emulsion quality and concentration and on the properties of the dispersed phase. Chapter 2 contains a review where relevant physical properties of emulsified oils are listed. These are the type of the oil (mineral- or vegetable-based),¹⁴ the number and possibly the size of emulsion droplets,¹⁵ the concentration of the dispersed phase,¹⁰ as well as its viscosity,¹⁶ and the dynamic surface tension of the spray liquid at breakup.¹⁰

Building on these investigations, we constructed up an approach to characterise emulsions based on oils of different chemistry. As described in Chapter 6, these oils are sunflower oil, rapeseed oil methyl ester, white oil, and mineral oil. When sprayed through a flat fan nozzle, all of these emulsions produce coarser sprays than water and the magnitude of spray coarsening is closely associated with the physical properties of the dispersed phase. Moreover, emulsions of polydimethylsiloxanes which represent oils of same chemical structure with different molecular

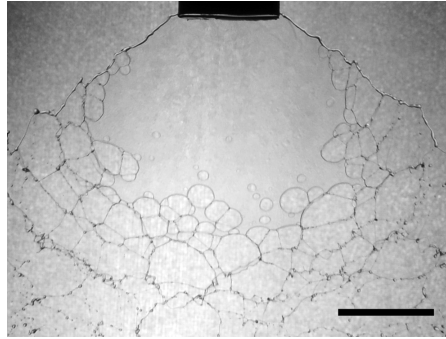


Figure 1: Photograph of the breakup of a liquid formed by a mixture of 0.1% w/w emulsion of rapeseed oil methyl ester and 0.1% w/w of Guar gum based thickener (Kelzan S) sprayed at a pressure of 1 bar through a XR11003 flat fan nozzle. The black bar indicates 10 mm.

chain lengths and, thus, different viscosities, have also been considered.

Experimental results show that emulsion droplet size, the content of emulsifier, and the viscosity of the dispersed phase have no significant influence on the spray formation process as long as they do not alter the stability of the produced emulsion. On the other hand, the concentration of the emulsified oil or number of emulsion droplets in the spray liquid, the dynamic surface tension at breakup, and the spreading properties of the emulsified oil have all been identified as important parameters. Based on these observations, a mechanism for the perforation onset is proposed in Chapter 6. In this hypothesis, we consider the possibility of the emulsion droplets being present at the air/water interface after the spray liquid leaves the nozzle, as schematically shown in figure 2a. The presence of emulsion droplets at the interface may initiate the sheet breakup through subsurface flow induced by the spreading emulsion drop as shown in figure 2b.

The tendency of an oil to spread at the interface is defined by its spreading coefficient $S = \gamma_{AW} - \gamma_{OW} - \gamma_{AO}$.¹⁷ γ is the interfacial tension and the subscripts A , O and W describe the air, water and the oil phases. Vegetable-based oils with a high positive spreading have a greater tendency to spread over a pristine air/water interface than mineral-based oils with a low spreading coefficient. The spreading properties are not affected by the viscosity of the oil but depend on its chemical structure; hence, all investigated polydimethylsiloxanes produced sprays with a very similar mean spray droplet size. There is a clear tendency that dilute emulsions based on oils with a high positive spreading coefficient form coarser sprays with an earlier sheet breakup than emulsions based on oils with a low spreading

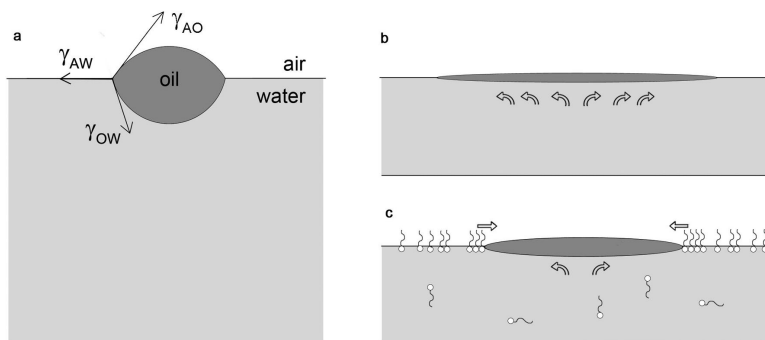


Figure 2: Schematic pictures of a) an emulsion droplet placed at a air/water interface, b) an emulsion droplet spreading in a thinner sheet region and inducing a subphase flow, c) an inhibited spreading of an emulsion droplet at the air-water interface which is occupied by surfactants. The arrows indicate the direction of the subphase flow and the counteracting forces caused by the interfacial surfactant layer. Emulsifier molecules are not shown in this schematic image.

coefficient. However, this tendency cannot be described alone by the spreading energy. Apparently, there is another important factor that also influences sheet breakup.

The mechanism as proposed in Chapter 6 is used to explain interactions in mixtures of dilute emulsions with water-soluble surfactants and provides an explanation as to why a decrease in surface tension at breakup influences spray formation. By decreasing the air/water interfacial tension the water-soluble surfactants build up surface pressure with is defined as $\Pi_{AW} = \gamma_{AW}^0 - \gamma_{AW}$ which γ_{AW}^0 being the surface tension at a pristine air/water interface. Induced surface pressure can retard spreading and minimize the velocity and the depth of the subsurface flow, delaying the perforation onset (figure 2c).

It appears that the entering incident, which is poorly investigated in this thesis, can be the crucial step in the proposed mechanism. Figure 1 shows a photograph of a liquid sheet at breakup. Holes appear in the liquid sheet, develop, and lead to its disintegration. It becomes evident that only a limited number of incidents is sufficient to initiate the breakup. This implies that for 3.7×10^{11} emulsion droplets in 1 L spray liquid that contains 0.1% w/w of emulsified rapeseed oil methyl ester, only a limited number of emulsion drops is required to initiate the breakup process.

A pseudo-emulsion film formed between the oil droplet and the air/water interface prevents an emulsion droplet from entering. The entering probability depends on the emulsion droplet size, its mobility, and its interfacial properties.¹⁸

Moreover, the entering incident can be facilitated by the presence of hydrophobic silica particles located at the interface of the droplet which can pierce through the pseudo-emulsion film. Such hydrophobised silica particles are often used in commercial products as oil thickeners.¹⁶ Results discussed in Chapter 7 suggest that these particles, when dispersed in the oil phase of the dilute emulsion, initiate an additional spray coarsening which is attributed to the increased frequency of entering incidents rather than to the viscosity increase of the oil phase. The hydrophobised particles tend to stay with the oil phase of the emulsion droplet but when an emulsion is rapidly deformed in the nozzle, the silica particles can stick to the newly created oil/water interface of the droplet.

The mechanism based on the combined effect of entering and spreading developed in this thesis provides a plausible explanation for experimental results accounting for a wide range of possible interactions in the spray liquid. However, entering probability of emulsion droplets requires further investigations for a definite verification of this hypothesis.

The scenario shown in figure 2a is considered as the most probable at perforation onset and was used to construct a model system for theoretical investigations. In Chapter 3, CFD simulations were applied to investigate the dynamics of a liquid lamella when an oil droplet is placed at the interface. The results shows that a droplet at the interface can induce significant perturbation of the liquid sheet that leads to necking of the lamella and its subsequent breakup. Furthermore, it was observed that physical properties of the oil influence the magnitude of the induced perturbation and, in a consequence, the time scale of breakup. These results provide a second possible scenario at perforation onset: the flow induced by an oil drop may reinforce interfacial perturbations of the liquid sheet and, thus, lead to the perforation onset.

In Chapters 4 and 5 the self-consistent field approach was used to study what happens to an oil/emulsion droplet after it has entered the air/water interface. It is shown that a pure oil adopts a lens-like shape, which becomes more elongated with decreasing γ_{OW} . Thereby, emulsifier molecules promote spreading by accumulating at the oil/water interface. As shown in Chapter 5, spreading can be retarded by the increase in the surface pressure caused by water-soluble surfactants that predominately occupy the air/water interface. These results support well the observations made in the experimental part of the thesis, discussed in Chapter 6.

In Chapter 8, mixtures of dilute emulsions with polymer solutions were investigated and the results are explained by consulting the proposed breakup mechanism. Both polymer solutions and dilute emulsions induce spray coarsening. The data

show that at a low polymer concentration, spray coarsening is dominated by emulsion droplets while at high polymer concentrations, sheet breakup is controlled by the viscosity increase of the spray liquid. Evidently, at higher concentrations polymer solutions retard the action of emulsion droplet at breakup. Two explanations are possible in this context. The spreading of emulsion droplets might be slowed down due to the viscosity increase of the spray liquid. It is also conceivable that the increase in the viscosity may lead to the formation of thicker sheets so that the subsurface flow and perturbations initiated by spreading emulsion droplets do not reach the depth and the magnitude sufficient to induce breakup.

Formulations that can reduce spray drift

The practical objective of this thesis was the classification of existing formulation types of crop protection products according to their ability to reduce the fine spray fraction. This effect can be used as a measure to minimize drift risk during agricultural spray application. Moreover, based on the results of these investigations, recommendations can be established for the development of formulated products with drift reducing properties.

Chapter 2 is a review that highlights the manifold aspects related to the spray drift phenomenon. In the conclusion to this Chapter, we made an attempt to classify the most common liquid formulation types. Formulation types that can achieve drift risk reduction when atomized through a conventional hydraulic nozzle are those, that contain emulsifiable oil or a concentrated emulsion. The effect of some formulation types such as EC (emulsifiable concentrate) and EW (emulsion, oil in water) depends upon the content and the composition of formulated additives. Such products as SL (soluble concentrate) and SC (suspension concentrate) and solid formulation types probably will not alter spray characteristics. OD (oil dispersion) and SE (suspo-emulsions), on the other hand, have a high potential for drift reduction purpose when applied through a flat fan nozzle. These formulation types can also contribute to drift risk reduction when sprayed with an air-induction nozzle by producing spray droplets with higher velocities than surfactant loaded spray liquids. Finally, it has to be noted that the formulation type does not necessarily state if an emulsifiable oil is a part of the respective product. If an SC product contains oil-based adjuvants, it can also induce desired changes of the spray droplet size and velocity which are not predictable from the product type.

Chapter 9 shows experimental evidence for the classification scheme anticipated in Chapter 2. Several commercial products, mostly supplied by Bayer CropScience

AG, were sprayed at appropriate concentrations. The project was set up by this company which allowed studying the recipes of these products and to relate changes in the spray droplet size to the composition of the recipe. It was observed that changes in spray droplet size are consistent with the composition of a formulation and can be well described by the physical properties of spray liquids. This outcome has a straightforward implication, namely a systematic development of crop protection products with drift reducing properties. Dilute oil-in-water emulsions based on oils of vegetable origin or silicone oils appear to be well suited for these purposes. The drift reduction potential of a product can be identified at an early development stage by measuring the droplet size distribution of sprays produced at a relevant concentration, compared to a standard spray liquid.

At the same time, large-scale drift trials are considered as an essential procedure to collect sufficient experimental proof and to support the evidence provided by the laboratory measurements. As suggested in this thesis, supporting data can be obtained with small-scale drift trials which have several advantages. They require less time and human resources, smaller application areas, and carry a lower contamination risk. At the same time, sampling is easier to handle than in extensive field experiments. It seems that such trials can be used to estimate the drift deposition and to verify the modelling output generated by simulation programs for spray deposition.

Drift trials performed in this thesis display similar tendencies in spray deposition with respect to a formulation type as predicted by the laboratory measurements. However, the tendencies are not always consistent at different deposition distances and among the two oil-based formulations considered here. This implies, that along with the spray droplet size distribution, other spray characteristics (such as *e.g.* mean liquid velocity, velocities of spray droplets, spray angle, and structure) are important to predict spray deposition patterns during agricultural applications.

Outlook

In course of this project, a unique approach was developed to analyse the perforation onset induced by dilute oil-in-water emulsions. This approach is based on spreading properties of emulsion droplets after they have entered the interface of the liquid sheet. The proposed mechanism was used to describe interactions between different components in a spray liquid and at the same time it was used to explain changes in the spray droplet size induced by dilute emulsions based on different oils.

Overall, the mechanism covers systems which are interesting for drift reduction purposes. However, the mechanism is not yet fully elaborated so that some aspects require further research and further detailed investigations. The entering probability is one of these aspects. It would be very interesting to quantify the entering frequency in relevant systems and to investigate how it is influenced in mixtures of different polymer solutions and through addition of hydrophobic particles into the oil phase of emulsion droplets.

To reduce complexity, we focused in this thesis on sprays produced with a simple flat fan nozzle. At the same time, it is known that the effect on spray droplet size induced by physical properties of spray liquids is closely linked to the nozzle design. In general, dilute oil-in-water emulsions produce coarser sprays than water when atomized through a conventional flat fan nozzle and finer sprays than water when sprayed through an air-induction nozzle. An air-induction nozzle incorporates air bubbles into the spray liquid and spray droplets. Dilute emulsion prevent air intake so that the spray droplets produced contain less air compared to spray droplets of pure water and, thus, are smaller in size. In future, it would be interesting to extend the proposed mechanism for other nozzle designs such as air-induction nozzles and to investigate why dilute emulsions prevent air inclusion.

In the long term, the results presented in this thesis can be used as a source for the development of a classification scheme for commercial products with respect to their ability to reduce drift risk. Following this development, the acceptance of formulated products with drift reducing properties in Europe will lead to the adjustment of the width of no-spray buffer zones with and without the use of special risk mitigation equipment. This is advantageous for agricultural practice in several ways: the spray risk can be minimized without additional effort or acquisition of (sometimes costly) equipment and at the same time larger land areas can be cultivate and less organisms and weeds can develop resistance in the immediate off-crop area. From a commercial perspective, with such a regulatory development, highly qualitative and innovative products can be offered to the market and (re)registration process of agrochemicals can possibly be facilitated.

References

- [1] FOCUS, *Landscape And Mitigation Factors In Aquatic Risk Assessment. Volume 1. Extended Summary and Recommendations. Report of the FOCUS Working Group on Landscape and Mitigation Factors in Ecological Risk Assessment*, 2007, EC Document Reference SANCO/10422/2005 v.2.0. pp. 1-169.
- [2] FOCUS, *Landscape And Mitigation Factors In Aquatic Risk Assessment. Volume 2. Detailed Technical Reviews. Report of the FOCUS Working Group on Landscape and*

- Mitigation Factors in Ecological Risk Assessment*, 2007, EC Document Reference SANCO/10422/2005 v.2.0. pp. 1-436.
- [3] Directive 2009/128/EC, *Official Journal of the European Union*, 2009.
- [4] M. C. Butler Ellis and P. C. H. Miller, *Biosystems Eng.*, 2010, **107**, 169–177.
- [5] G. R. Stephenson, I. G. Ferris, P. T. Holland and M. Nordberg, *Pure Appl. Chem.*, 2006, **78**, 2075–2154.
- [6] P. A. Hobson, P. C. H. Miller, P. J. Walklate, C. R. Tuck and N. M. Western, *J. Agr. Eng. Res.*, 1993, **54**, 293–305.
- [7] H. Holterman, *Kinetics and evaporation of water drops in air*, 2003, IMAG Report 2003-12.
- [8] P. C. H. Miller, *Pesticide Outlook*, 2003, **14**, 205–209.
- [9] R. W. Dexter, *Atomization Spray*, 1996, **6**, 167–191.
- [10] R. W. Dexter, in *Pesticide formulations and application systems*, ed. A. K. Viets, R. S. Tann and J. C. Mueninghoff, American Society of Testing and Materials, West Conshohocken, PA, 2001, vol. 20, pp. 27–43.
- [11] M. C. Butler Ellis, C. R. Tuck and P. C. H. Miller, *Crop Prot.*, 1997, **16**, 41–50.
- [12] P. C. H. Miller and C. R. Tuck, *J. ASTM Int.*, 2005, **2**, 1–13.
- [13] P. C. H. Miller, C. R. Tuck, S. Murphy and M. da Costa Ferreira, Proceedings of 22nd European Conference on Liquid Atomization and Spray Systems (ILASS-Europe), Como Lake, Italy, 2008, pp. 1–8.
- [14] N. M. Western, E. C. Hislop, M. Bieswal, P. J. Holloway and D. Coupland, *Pestic. Sci.*, 1999, **55**, 640–642.
- [15] M. C. Butler Ellis, C. R. Tuck and P. C. H. Miller, *Atomization Spray*, 1999, **9**, 385–397.
- [16] K. Qin, H. Tank, S. Wilson, B. Downer and L. Liu, *Atomization Spray*, 2010, **20**, 227–239.
- [17] W. D. Harkins and A. Feldman, *J. Am. Chem. Soc.*, 1922, **44**, 2665–2685.
- [18] V. Bergeron, P. Cooper, J. Giermanska-Kahn, D. Langevin and A. Pouchelon, *Colloid Surface A*, 1997, **112**, 103–120.

Samenvatting

De laatste decenia zijn wereldwijd verschillende trends zichtbaar geworden die een intensivering van de voedselproductie noodzakelijk maken. Een stijgende wereldbevolking, een teruglopend areaal dat voor commerciële landbouw beschikbaar is en een hogere vleesconsumptie in met name Azie zijn slechts enkele voorbeelden hiervan. Om deze stijging in de voedselproductie te garanderen is het gebruik van gewasbeschermingsmiddelen onvermijdelijk. Naast de voordelen die gewasbeschermingsmiddelen met zich meebrengen zijn er echter ook risico's met deze producten verbonden. Om deze risico's op een voor de samenleving acceptabel niveau te brengen gelden voor de toelating van gewasbeschermingsmiddelen strenge toelatingsnormen. Zo moet steeds aangetoond worden dat het toepassen van deze producten voor mens en omgeving veilig is. Hiertoe moet gegarandeerd worden dat de blootstelling voor omwonenden, aangrenzende natuurgebieden en oppervlakte water onder vastgelegde grenzen blijft. Het mag duidelijk zijn dat deze grenzen afhangen van het potentiële risico van de betreffende actieve stoffen.

In het algemeen worden gewasbeschermingsmiddelen toegepast door vernevelen van een verdunde waterige spuitoplossing. Hierbij wordt de oplossing onder druk door een spuitdop geperst waarbij een nevel ontstaat met een bepaalde druppelgrootteverdeling. Na het verlaten van de spuitdop wordt eerst een vloeïstofilm (lamel) gevormd die na een bepaalde afstand in druppels opbreekt. In het algemeen geldt dat hoe langer de lamel intact blijft, des te kleiner zijn de druppels die hieruit gevormd worden. De druppelgrootteverdeling hangt af van het type spuitdop dat wordt gebruikt, de druk waarbij gespoten wordt en van diverse fysisch-chemische eigenschappen van de spuitoplossing. Afhankelijk van de grootte van de druppels zal een deel van de nevel met de wind meegevoerd en zodoende in de omgeving verdeeld worden, een proces dat drift genoemd wordt. Naast de bovengenoemde aspecten hangt de intensiteit van drift ook af van de weersomstandigheden, snelheid van het voertuig waarmee gespoten wordt, de hoogte van de spuitbalk boven het te behandelen gewas en bijvoorbeeld het groeistadium van het gewas.

In de jaren tachtig zijn door Ganzelmeier en Rautmannn experimentele onderzoeken uitgevoerd die de toepassingsomstandigheden van gewasbeschermingsmiddelen korreleren met de afstand waarover drift plaatsvindt. Wanneer deze

gegevens in verband worden gebracht met de potentiële risico's van een bepaald middel kan men een afstand tot de grens van het te behandelen perceel vastleggen waarbinnen niet gespoten mag worden om te voorkomen dat de gewasbeschermingsmiddelen buiten het te behandelen oppervlak terechtkomen. De uitkomst van deze onderzoeken beschrijft het effect van waterige oplossingen, zonder het effect van veranderingen in de fysisch-chemische eigenschappen, welke door het toedienen van een gewasbeschermingsmiddel (formulering) worden veroorzaakt, in de evaluatie te betrekken.

Het doel van het onderzoek beschreven in dit proefschrift was om het effect van deze produkteigenschappen op de mate van drift te beschrijven. Er werd een methode ontwikkeld waarmee op een eenvoudige manier deze eigenschappen in laboratorium experimenten kunnen worden bepaald. Met die methode is nagegaan welk verband er bestaat tussen druppelgrootteverdeling en samenstelling van de spuitvloeistof. Tenslotte is onderzocht of het mogelijk is producten te ontwikkelen welke de mate van drift kunnen reduceren.

In hoofdstuk 2 wordt op basis van een literatuuronderzoek beschreven welke fysisch-chemische eigenschappen van de spuitoplossing, en dus indirect van de formulering waaruit deze wordt gemaakt, de druppelgrootteverdeling van de spuitnevel kunnen beïnvloeden. Hierbij is gebleken dat naast eigenschappen als viscositeit en dynamische oppervlakte spanning de aanwezigheid van emulsies in de spuitoplossing een positief effect kan hebben op de druppelgrootteverdeling. Afhankelijk van de eigenschappen van de geëmulgeerde olie dan wel oplosmiddel zijn deze effecten meer of minder dominant. De achterliggende mechanismen voor deze wisselwerking waren echter nog niet beschreven.

Om deze mechanismen beter te kunnen begrijpen zijn in hoofdstuk 3, 4 en 5 modelberekeningen beschreven. In hoofdstuk 3 is onderzocht hoe de dynamische eigenschappen van een emulsiedruppel die zich in het water-lucht grensvlak van een vloeistoffilm bevindt turbulenties in de aangrenzende vloeistof kan induceren. Hiertoe is gebruik gemaakt van vloeistofdynamicsimulaties. Middels deze berekeningen kon geconcludeerd worden dat geringe veranderingen in de vorm van een „olie“ druppel in het water-lucht grensvlak leidt tot beweging in de waterfase rond de druppel, wat op zijn beurt tot sterke turbulentie in de vloeistoffilm voert. Het uiteindelijke gevolg is dat lamellen sneller opbreken en daardoor grotere druppels voortbrengen. In hoofdstuk 4 wordt een zelf-consistente-veldtheorie methode besproken waarbij de structuur en thermodynamische eigenschappen van een emulsiedruppel in een grensvlak worden berekend. Met behulp van deze modelberekeningen kon aangetoond worden dat de spreidingscoëfficiënt, welke afhangt

van de oppervlaktespanningen tussen de water-lucht en olie fase een belangrijke eigenschap is om het opbreken van een lamel in druppels te beschrijven. In hoofdstuk 5 worden deze modelberekeningen vergeleken met een experimenteel systeem en wordt onderzocht wat de invloed van surfactants op de spreidingscoëfficiënt van geselecteerde olies is.

In hoofdstuk 6 worden experimenten beschreven waarbij gericht bepaalde eigenschappen van de spuitoplossing worden gevarieerd, en het effect van deze veranderingen op de druppelgrootte verdeling wordt onderzocht. Hierdoor was het mogelijk een aantal variabelen uit te sluiten en werd een mechanisme voorgesteld dat op basis van de beschikbare experimenten en de ondersteunende modelberekeningen het opbreken van een lamel waar zich emulsiedruppeltjes in bevinden goed beschrijft.

Afhankelijk van de eigenschappen van de geëmulgeerde fase in de spuitoplossing heeft een emulsiedruppel een bepaalde kans om in het grensvlak te komen (uitgedrukt als „entering coefficient“), die afhangt van verschillen in de oppervlaktespanning van het water-olie, olie-lucht en water-lucht grensvlak. Wanneer een druppel zich in het water-lucht grensvlak begeeft zal hij zich, afhankelijk van zijn spreidingscoëfficiënt op het oppervlak uitspreiden. Hierdoor worden in de bulkfase van de lamelle in de nabijheid van de emulsiedruppel stromingen veroorzaakt. Wanneer deze stromingen sterk genoeg zijn kunnen deze turbulenties veroorzaken wat tot een sneller opbreken van de lamelle en dus grotere druppels leidt. Verder kon worden aangetoond dat wanneer de spuitoplossing behalve de geëmulgeerde fase ook nog surfactants bevat, die bij voorkeur aan het lucht-water grensvlak absorberen, het spreiden van de oliedruppels daardoor wordt afgeremd, waardoor het opbreken van de lamellen vertraagd wordt. Hetzelfde effect kon worden bereikt door de rekviskositeit van de waterfase te verhogen. Om een beter inzicht te verkrijgen in de mate waarop de entering- and spreidings coëfficiënt de genoemde processen beïnvloeden werd de viscositeit van de oliefase gevarieerd. In hoofdstuk 6 wordt beschreven dat wanneer de oppervlakte eigenschappen van de oliefase (voor emulsies met een toenemende viscositeit) niet verandert, dit geen invloed heeft op het mechanisme waarmee de lamel breekt. Wanneer echter als verdikker silicadeeltjes gekozen werden die de grensvlakeigenschappen van de emulsie beïnvloeden (hoofdstuk 7) werden effecten zichtbaar. Het kon worden aangetoond dat dit veroorzaakt wordt doordat deze deeltjes met name de entering coefficient verbeterden waardoor meer mogelijke startpunten werden gecreëerd en dus sneller een turbulente film ontstond.

Naast emulsies worden polymeren als drift reducerende toevoeging gebruikt. De werking berust op verhoging van de rekviskositeit van de spuitoplossing. Daarom

werd in hoofdstuk 8 onderzocht in hoeverre twee verschillende toevoegingen (emulsies en polymeren) elkaar beïnvloeden wanneer ze gelijktijdig worden toegepast. Hierbij is gebleken dat emulsies al bij zeer geringe concentraties in de spuitoplossing een groot effect hebben. Polymeren laten pas goede werking zien bij hoge concentraties. Bij tussenligende concentraties van zowel emulsies als polymeren was het in hoofdstuk 6 beschreven remmende effect van het polymeer op het door de emulsie geïnduceerde opbreken goed meetbaar. Hieruit kan geconcludeerd worden dat bij het ontwikkelen van produkten met een ingebouwde mechanisme voor driftreductie het niet voldoende is een te emulgeren fase toe te voegen, maar dat ook alle verdere componenten van de formulering in overweging genomen moeten worden.

Nadat in de voorafgaande hoofdstukken onderzocht is door welke fysisch-chemische eigenschappen van de spuitvloeistof het opbreken van een lamel in druppels beschreven en begrepen kan worden, is in hoofdstuk 9 geanalyseerd in hoeverre de verkregen kennis toepasbaar is op reële systemen. Hiertoe is van verschillende model-emulsies en commerciële formuleringen die in de spuitoplossing een emulsie vormen een druppelgrootteverdeling gemeten en is onderzocht hoe deze correleren met de in de voorafgaande hoofdstukken beschreven eigenschappen. Verder is op basis van deze druppelgrootteverdelingen uitgerekend in hoeverre hierdoor drift gereduceerd wordt. Vervolgens zijn deze voorspellingen vergeleken met experimentele drift waarden verkregen uit in de praktijk uitgevoerde vernevelingsproeven.

Concluderend kan worden gezegd dat het in dit proefschrift beschreven onderzoek ertoe heeft bijgedragen dat meer inzicht is verkregen in het mechanisme dat het effect van emulsies op de druppelgrootte verdeling bij het versproeien van een spuitoplossing beschrijft. Hierdoor is het mogelijk gericht produkten te ontwikkelen die minder drift veroorzaken in vergelijking tot de waterige oplossingen die op dit moment nog als basis dienen bij het vastleggen van spuitvrije zones, zoals die bepaald worden in het registratieproces voor nieuwe gewasbeschermingsmiddelen. In een volgende stap zou, in overleg met registreerinstanties, ervoor gekozen kunnen worden om voor formuleringen die voor driftreductie geoptimaliseerd zijn niet de standaardtabellen als basis te nemen, maar in plaats daarvan de met de desbetreffende formulering gemeten waarden.

Acknowledgements

First of all, I would like to thank the organizer of this project, Ronald Vermeer, for giving me the opportunity to work on this interesting and manifold subject and for unlimited support at each step and in each situation. Thank you for your visionary and global ideas and also for inspiring coffee breaks and warm intake into the INNO-lab family at Bayer CropScience.

Special thanks are due to my supervisor at Wageningen, Frans Leermakers, for your scientific support and for the training on theoretical thermodynamics and modelling. Thank you for being patient with me in so many situations and for never being tired to explain same things repeatedly. Thanks for your creative input in moments, when the subject gained complexity, and for your always positive attitude.

I am very grateful to my other supervisor at Wageningen, Martien Cohen Stuart, for your guidance, support and for reviewing my manuscripts. Thank you for constructive remarks and advices which immensely helped to improve this work.

A very special thank to my former Bayer colleges Manuela Eberhard and Nicole Enders, for the help at my first time in the company, for teaching how everything works and who is responsible for what, where to go and whom to ask. Thank you for the great fun we had together and for your help with the organization of formulations-related experiments.

Many thanks to Josie Zeevat-van Homelen for taking care for my enrolment and submission documents, for giving me shelter on my theoretical week in Wageningen. Without your help it would have cost me much more time and effort to organize things.

I would like to express the gratitude to my Bayer colleges who helped me in many ways on various occasions. Your input and contributions provided this work with variety and gave it more substance. Thanks to Jürgen Minet, Dirk Berkemeier and Arne Kohnen for the engineering work you performed to make my experiments work. Many thanks to Ulf Steffens for allowing me to use the photographic equipment. Thanks to Peter Mansour for instructions on the handling of the high speed camera. Thanks also to Stefan Armborst, Sascha Teitscheid and Rudolf Tonn for your help with different analytical instruments and methods. Thanks to Burkhard

Wiese, Rolf Pontzen, Malcolm Faers, Erika Seidel, Martin Steinbeck, Johan Kijlstra and Peter Baur who kindly allowed me to use the analytical equipment in their laboratories, provided products and interesting samples developed in their teams and for the sheared knowledge of formulation technology. Reinhard Friessleben, Andrew Chapple, and Armin Lind, I would like to thank you for the organization of the field experiments. Thanks to Sabine Hennig-Gizewski for keeping me company in the office.

Thanks to the FYSKO people for the great time we had together in South-East Asia and on my short visits to Wageningen. Soumi Banerjee, Lennart Beun, Dmitry Ershov, Huanhuan Feng, Monika Golinska, Armando Hernandez Garcia, Yuan Li, Liyakat Mujawar, Harke Pera, Thao Pham, Yunus Saricay, Evan Spruijt, Junyou Wang, I hope, we won't lose track of each other in future.

Thanks to the former PhD and diploma students in Monheim Julia Jasak, Johannes Glaubitz, Petra Lange, Julia Wilde, Alexander Müller, Dana Ziv, Fabrice Magne, John Aponte, Diana Moran Puente and Claudia Selbach. You enriched my experience during the three years at Bayer with your always positive thinking and through shearing your knowledge from different scientific areas.

I would like to thank my friends Alja Berlina, Pasha Sirotkin, Olja Titarenko, Evelin Schmitte and Ivanka Koleva for your interest, your cheering up and fruitful discussions on manifold subjects which were mostly unrelated to this thesis.

Finally, I would like to thank my family who believed in me from the beginning to the end. Спасибо вам большое, мои дорогие мама и бабушка, за постоянную поддержку и за то, что вы никогда не сдаёте, что придаёт мне сил справляться с собственными трудностями. Алла, Саша и Саши, спасибо вам за участие и за вашу готовность помочь в любой ситуации. Dima, I am infinitely happy to have you by my side. Writing this thesis would not be possible without you and I could not thank you enough for all your support and encouragement.

List of publications

Journals

E. Hilz, F.A.M. Leermakers and A.W.P. Vermeer, **A self-consistent field study of a hydrocarbon droplet at the air-water interface.** *Physical Chemistry Chemical Physics*, 2012, 14, 4917-4926. (Chapter 4)

E. Hilz and A.W.P. Vermeer, **Spray drift review: The extent to which a formulation can contribute to spray drift reduction.** *Crop Protection*, 2013, 44, 75-83. (Chapter 2)

E. Hilz, A.W.P. Vermeer, M.A. Cohen Stuart and F.A.M. Leermakers, **Mechanism of perforation based on spreading properties of emulsified oils.** *Atomization and Sprays*, 2012, 22(12), 1053–1075. (Chapter 6)

E. Hilz, F.A.M. Leermakers and A.W.P. Vermeer, **A self-consistent field study of emulsion droplets at the air/water interface to underpin trends found for the atomisation of agricultural sprays.** *to be submitted*. (Chapter 5)

Conference Proceedings

E. Hilz, A.W.P. Vermeer, F.A.M. Leermakers and M.A. Cohen Stuart, **Spray drift: How emulsions influence the performance of agricultural sprays produced through a conventional flat fan nozzle.** *Aspects of Applied Biology*, 2012, 114, 71-78.

E. Hilz and A.W.P. Vermeer, **Effect of formulation on spray drift: a case study for commercial imidacloprid products.** *Aspects of Applied Biology*, 2012, 114, 445-450.

R. Vermeer and E. Hilz, **The use of adjuvanted formulations for drift control.** *International Symposium on Adjuvants for Agrochemicals (ISAA 2013)*, Foz do Iguaçu, Brazil, 22-26 April 2013, 323-329.

Overview of completed training activities

Discipline specific activities

Courses

Bioavailability Workshops at BCS, Monheim am Rhein, Germany, 2009-2011

Formulation Technology Workshop, Monheim am Rhein, Germany, 2009

Winter School: Physical Chemistry, Han-sur-Lesse, Belgium, 2010

Particle Technology, Malvern & Hosokawa Alpine, Düsseldorf, Germany, 2011

Analytics training at BCS, Monheim am Rhein, Germany, 2009

Modelling (MD/SCF) course, 2011

Application Technology at BCS, Monheim am Rhein, Germany, 2010

Meetings

ISAA 2010, Freising, Germany, 2010

Workshop on Sustainable Plant Protection Techniques, Bergerac, France, 2011 ¹

International Advances in Pesticide Application, Wageningen, 2012 ^{1,2}

General Courses

English competence training, Monheim am Rhein, Germany, 2010

Presentation techniques at BCS, Monheim am Rhein, Germany, 2010

Scientific writing, Monheim am Rhein, Germany, 2011

Optionals

Preparation PhD research proposal

Laboratory meetings at BCS, Monheim am Rhein, Germany, 2009-2011

Department meetings at BCS, Monheim am Rhein, Germany, 2010-2012

PhD conference South-east Asia, Fysko, 2011

Literature study spray drift, Monheim am Rhein, Germany, 2009

Long term innovation meetings at BCS, Monheim am Rhein, Germany, 2009-2011

¹ oral presentation, ² poster

BCS (Bayer CropScience)

Curriculum Vitae

Emilia Hilz was born on the 25th of February, 1984, in Prypiat, former Soviet Union, now Ukraine. In the time period of 1986-1997 she lived in Kaluga, Russia, where she attended primary and middle school. In 1997, her family moved to Düsseldorf, Germany, where she attended the municipal Gymnasium Gerresheim and graduated from it in 2003.

Thereafter, she studied chemistry at Heinrich Heine University, Düsseldorf. After receiving the small diploma in 2006, she continued her education at the Technical University Dortmund and specialised in physical chemistry and colloid science. In spring of 2008 she participated in an educational program at Kungliga Tekniska Högskolan, Stockholm. Upon return to the Technical University Dortmund, she joined the research group of Prof. H. Rehage, where she worked on her diploma thesis investigating the formation of catanionic vesicles. The diploma project was a collaboration with the research group of Prof. M. Gradzielski at Technical University Berlin.

From April 2009 to May 2012, she worked as a PhD student on a spray drift project at Bayer CropScience AG, Germany, in collaboration with the Laboratory for Physical Chemistry and Colloid Science at Wageningen University, the Netherlands. The results of this project are presented in this thesis.

The research described in this thesis was financially supported by Bayer CropScience AG.

Cover image: A liquid sheet formed by an “Agrotop” AIRMIX NoDrift 110-03 nozzle spraying Kelzan S solution of 0.1% w/w at a pressure of 3 bar.

Printing: GVO drukkers en vormgevers B.V./ Ponsen en Looijen, Ede, NL